(1)

DIGITAL TROPOSCATTER PERFORMANCE MODEL
FINAL REPORT

Contract No. DCA100-80-C-0030
SIGNATRON Reference A288-17

December 1983

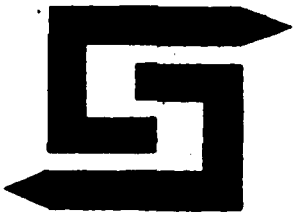

SIGNATRON®

SIGNATRON®
SIGNATRON, Inc. • 12 Hartwell Avenue • Lexington, Massachusetts 02173
(617)861-1500

DIGITAL TROPOSCATTER PERFORMANCE MODEL: FINAL REPORT

Contract No. DCA100-80-C-0030
SIGNATRON Reference A288-17
December 1983

Prepared By:

SIGNATRON, Inc.
12 Hartwell Avenue
Lexington, MA 02173

Submitted To:

Defense Communications Agency
Defense Communications Engineering Center
1860 Wiehle Avenue
Reston, Virginia 22090

UNCLASSIFIED

SECURITY CLASSIFICATION OF THIS PAGE (When Data Entered)

REPORT DOCUMENTATION PAGE		READ INSTRUCTIONS BEFORE COMPLETING FORM
1. REPORT NUMBER	2. GOVT ACCESSION NO.	3. RECIPIENT'S CATALOG NUMBER
4. TITLE (and Subtitle) Digital Troposcatter Performance Model: Final Report		5. TYPE OF REPORT & PERIOD COVERED Final Report June 1980 - November 1983 6. PERFORMING ORG. REPORT NUMBER A288-17
7. AUTHOR(s) P. Monsen, S. Parl, A. Malaga, S. Tolman J. Fetteroll		8. CONTRACT OR GRANT NUMBER(s) DCA100-80-C-0030
9. PERFORMING ORGANIZATION NAME AND ADDRESS SIGNATRON, Inc. 12 Hartwell Avenue Lexington, MA 02173		10. PROGRAM ELEMENT, PROJECT, TASK AREA & WORK UNIT NUMBERS
11. CONTROLLING OFFICE NAME AND ADDRESS Defense Communications Agency Washington, DC 20305 , Attn: Code 680		12. REPORT DATE December 1983 13. NUMBER OF PAGES 291
14. MONITORING AGENCY NAME & ADDRESS(if different from Controlling Office) Defense Communications Agency Defense Communications Engineering Center Attn: R-220 1860 Wiehle Ave., Reston, VA 22090		15. SECURITY CLASS. (of this report) Unclassified 15a. DECLASSIFICATION/DOWNGRADING SCHEDULE N/A

16. DISTRIBUTION STATEMENT (of this Report)

Approved for public release; distribution unlimited.

17. DISTRIBUTION STATEMENT (of the abstract entered in Block 20, if different from Report)

18. SUPPLEMENTARY NOTES

19. KEY WORDS (Continue on reverse side if necessary and identify by block number)

Troposcatter	Propagation Prediction
Diffraction	Multipath Prediction
MD-918 Modem	Error Rate Prediction
AN/TRC-170	Link Analysis

20. ABSTRACT (Continue on reverse side if necessary and identify by block number)

The development of a computer prediction model for digital troposcatter communication system design is described. Propagation and modem performance are modeled. These include Path Loss and RSL distributions for troposcatter propagation and mixed troposcatter/diffraction propagation conditions, multipath delay spread and relative delay between the scatter and diffraction component. The modem performance models are for the MD-918 and (Over)

DD FORM 1 JAN 73 1473 EDITION OF 1 NOV 65 IS OBSOLETE

UNCLASSIFIED

SECURITY CLASSIFICATION OF THIS PAGE (When Data Entered)

20. Abstract (continued)

AN/TRC-170 modems and include the effects of transmitter and receiver filters as well as co-channel and adjacent channel interference.

ORIGINATOR - SUPPLIED KEY WORDS INCLUDE:

FOREWORD

This document is the Final Report for Contract DCA100-80-C-0030 prepared by SIGNATRON, Inc. for the Defense Communications Agency. The report covers work performed during the period June 1980 through November 1983. It details the analysis, modeling and development of a computer prediction model for use as a tool in designing digital troposcatter systems. A User's Manual Report discusses the use of the computer program TROPO. The description of the structure and logical organization of the software is contained in the Software Documentation Report.

TABLE OF CONTENTS

TABLE OF CONTENTS (continued)

TABLE OF CONTENTS (continued)

TABLE OF CONTENTS (concluded)

LIST OF FIGURES

LIST OF FIGURES (continued)

LIST OF FIGURES (concluded)

LIST OF TABLES

SECTION 1
SUMMARY AND RECOMMENDATIONS

This document is the Final Report for Contract DCA100-80-C-0030 entitled Digital Troposcatter Performance Model. The purpose of this effort is to modify and extend the capabilities of a digital troposcatter performance prediction and analysis computer program developed under a previous contract [Monsen and Parl, 1980]. The digital troposcatter performance computer program TROPO developed under this present effort models the troposcatter channel for all types of diversity configurations used in the Defense Communications System (DCS) and gives a prediction of digital modem performance under realistic operating conditions such as RF bandwidth constraints and co-channel or adjacent channel interference. This troposcatter performance prediction model will be useful as a tool for performing link design trade-off studies for troposcatter systems which operate in the frequency range between 100 MHz and 35 GHz. A detailed description of the computer program and guidelines for its use are given in the User's Manual Report. Detailed descriptions of the structure and logical organization of the TROPO software are given in the Software Documentation Report.

1.1 BACKGROUND

The Defense Communications Engineering Center (DCEC) is responsible for the specification of transmission system performance parameters for DCS. Performance criteria for digital voice and data communications over microwave LOS and troposcatter channels are currently based on DCEC TR 12-76 [Kirk and Osterholz, 1976]. In 1976 the US Army Communications System Agency (CSA), Project Manager for DCS (Army) Communications Systems,

began a research program in support of the DCS entitled Adaptive Antenna Control (AAC) under contract ECOM DAAB07-76-C-8085. The intent of that effort was to develop an antenna system to provide an alternative diversity configuration and to improve performance on DCS diffraction and troposcatter links by angle diversity, mechanical or electronic antenna beam steering methods. Under the AAC contract, SIGNATRON developed a detailed analytical model of troposcatter progagation to aid in the design of angle, space and frequency diversity systems. By utilizing recent work of other researchers [Tatarskii, 1971], a new model of troposcatter propagation was developed for frequencies above 1 GHz. SIGNATRON also developed an analytic form of the layer theory model for frequencies below 1 GHz which agrees well with the NBS Technical Note 101 model [Rice, et al., 1967]. SIGNATRON was also the major subcontractor to GTE Sylvania for the development of a Megabit Digital Troposcatter Subsystem (MDTS) nomenclatured MD-918( )/GRC. Under the MDTS program, SIGNATRON developed a software computer model (for internal use) to predict modem performance under Rayleigh fading and multipath propagation conditions.

Noting that the two computer programs developed by SIGNATRON, were a powerful tool for troposcatter path prediction and digital modem performance prediction, DCA requested that the "AAC computer program" be made a deliverable under the AAC Contract and that the performance criteria for DCS digital troposcatter links in DCEC TR 12-76 be used in the AAC program. The AAC computer program was delivered to the Army and distributed to several other government users, including DCEC, who have responsibility for engineering troposcatter paths.

After some use of the AAC computer program at DCEC, it was realized that it would be a more useful design tool if several other capabilities were added. The purpose of this effort is to improve the existing AAC computer prediction program, and to extend it so that it is applicable to the full range of DCS troposcatter link engineering applications.

1.2 SUMMARY

The AAC computer program performs the calculations of troposcater link path loss distribution for one climatic zone and predicts the corresponding yearly average performance of the MD-918 modem from user-supplied path geometry and equipment parameters.

In this present effort the following analyses, modeling and modifications of the AAC computer program have been performed and are included in the computer program, TROPO, delivered under contract DCA100-80-C-0030.

1. Path Loss and RSL distributions for all 8 climatic zones in NBS Technical Note 101 and the 8 climate zones in MIL-HDBK-417 are calculated. Provision has also been made for the user to specify path loss variability data for a new or existing climate type. The path loss and RSL distribution calculations for NBS Technical Note 101, MIL-HDBK-417 or user specified climates are discussed in Sections 2.5 and 2.6 of this report.

2. The program computes horizon elevation angles, antenna take-off angles and effective antenna heights above average terrain elevation if the data is not supplied by the user. The calculation of the horizon elevation angles is discussed in Section 2.5.2 and the calculation of the effective antenna heights is discussed in Section 2.5.4.7.

3. TROPO predicts the RSL distribution and diversity receiver correlations for troposcatter link configurations which use dual space (2S), dual frequency (2F), dual angle (2A), quad space/frequency (2S/2F), quad space/angle (2S/2A), quad space (4S or 2S/2P), and 8th order diversity. The diversity correlation calculations are discussed in Section 2.5.6.

4. As part of the propagation and path geometry modeling for quad space (4S), also referred to as dual space/dual polarization (2S/2P) diversity, engineering guidelines to optimize system perfor-

mance have been developed. These guidelines include the selection of antenna spacing at each end of the link in order to achieve uncorrelated receive signals and are discussed in detail in Section 4.

5. TROPO calculates and prints out the coherence bandwidth of the troposcatter channel and the minimum frequency separation required to obtain uncorrelated frequency diversity reception. Frequency diversity and coherence bandwidth are discussed in Section 3.

6. TROPO models and predicts the path loss distribution and modem performance under mixed troposcatter/diffraction propagation conditions. The program has the capability to handle single, double and triple knife-edge or rounded obstacle diffraction conditions. Path loss, RSL and differential time delay between the diffracted and troposcatter received signals are calculated. The diffraction model is discussed in Section 2.6. The MD-918 modem performance under mixed troposcatter/diffraction conditions is discussed in Section 2.8.

7. TROPO includes waveguide and transmission line losses in the link RSL calculations.

8. TROPO has the capability of predicting the performance of the AN/TRC-170 modem in addition to the MD-918 modem. The analysis and modeling of the AN/TRC-170 modem performance is discussed in Appendices A through E. AN/TRC-170 modem performance calculations for dual space (2S) or quad space/frequency (2S/2F) diversity configurations assuming pure troposcatter propagation are performed in TROPO. The AN/TRC-170 modem performance for quad space (4S or 2S/2P) diversity configurations is the same as for 2S/2F when the antenna spacings at each end of the link are optimized according to the guidelines discussed in Section 4.

9. The MD-918 modem performance calculations are performed for pure troposcatter and mixed troposcatter/diffraction propagation conditions. Under pure troposcatter propagation conditions, MD-918 performance calculations for all of the dual, 4th-order and 8th-order diversity configur-

ations described in item 3 are performed. Under mixed troposcatter/diffraction propagation conditions, MD-918 performance calculations for all dual and quad order diversity configurations are performed.

10. The MD-918 and AN/TRC-170 performance calculations account for transmitter RF filtering effects to meet either a 99% power bandwidth or FCC 19311 bandwidth constraints and receiver filtering to reject out of band interference. The modem performance includes the degradations caused by intersymbol interference introduced by the filters and the peak-to-average of the transmitted waveform. The program calculates the number of poles and the 3-dB cut-off frequency (half of 3-dB bandwidth) of the Butterworth bandpass filter required at the output of the transmitter to achieve the specified bandwidth constraint. The filter parameter calculations are discussed in Section 2.7.

11. In order to determine modem performance under hostile conditions and for frequency planning purposes, TROPO can predict performance in the presence of co-channel or adjacent channel RF interference*. The RF interference may be an FDM/FM or digital QPSK signal with its own 99% power bandwidth or FCC 19311 bandwidth constraint. The frequency separation between the desired and unwanted signals can be specified arbitrarily. The interference may be in the mainbeam or the sidelobes. The interference power calculations are discussed in Section 2.7. When RF interference is specified the MD-918 modem performance calculations are performed only for 2S/2F diversity configurations.

12. Special Numerical techniques are used which allow calculation of the modem performance when two or more implicit diversity eigenvalues are nearly equal.

* NOTE: The MD-918 predictions for RFI conditions are purely theoretical. This was done to keep the software unclassified.

13. TROPO allows the user to have the option of specifying the input data in either metric or English units with the output data being in the corresponding input units.

14. TROPO provides a detailed output of the propagation and modem performance calculations and a simplified output containing a summary of the path input and program calculated performance.

15. The TROPO software source code is written in FORTRAN IV. Two versions have been delivered. One for use with PDP-11/70 computers with an F4P compiler and the other for use with IBM-370 compatible systems. The differences in the FORTRAN language for both versions are discussed in the User's Manual Report. The two versions of the program yield the same output for identical input data.

1.3 RECOMMENDATIONS

TROPO is a powerful tool for digital troposcatter link design. However a number of features can be aded to make it easier to use and allow the program to incorporate more up-to-date information as it becomes available. These are:

1. Most PDP-11/70 systems use F77 compilers. The present version cannot be used with such systems. An updated version with more streamlined software is needed for use with PDP-11/70 computers with F77 compilers.

2. The present version requires that the input data be in a particular format and that all data be supplied whether it is relevant to the desired calculations or not. A computer program which accepts only the relevant data and creates an input file in the format expected by TROPO would simplify the use of TROPO.

3. TROPO allows the user to specify path loss variability data for a new climate zone. However the path loss variability must be expressed in terms of the same effective path distance parameter

used in NBS Technical Note 101 and MIL-HDBK-417. Physically the path loss variability of troposcatter paths results from variations in the structure constant of the atmospheric turbulence while variability in diffraction paths occurs as a result of variations of the mean refractivity gradient (or effective earth radius factor). Long term predictions based on meteorological data have the potential to improve the accuracy of the predictions. Efforts are under way to obtain year round meteorological data in various climate zones. A feature which allows TROPO to use long term meteorological data is recommended.

4. The modem calculations assume that the delay spread of the troposcatter signal does not exhibit much variability. However year round data obtained on two RADC links [Sherwood, et al., 1977] indicate that the delay spread may vary by factors of 2 or 3 over the course of a year. Means of predicting the year round variability of the multipath spread and its effect on modem performance need to be modeled.

5. The modem performance measures used are those defined in DCEC-TR 12-76. A new performance criterium, error free-seconds, has been proposed for digital DCS systems in Draft MIL-STD-188-323. The addition of this performance measure to the modem calculations is recommended.

6. The modem performance calculations are based on the received signal level (RSL) distribution and delay spread predicted by TROPO. However the user may have one or both of these data from path measurements. Therefore a feature which allows the user to input these data to obtain modem performance predictions is recommended.

7. The use of minicomputers (e.g., HP-9826/36) for scientific applications is becoming increasingly common at many facilities. The feasibility of simplifying (scaling down) or dividing the TROPO software into modules (path loss, modem, etc.) for use with minicomputers should be investigated.

1.4 REPORT ORGANIZATION

Section 2 of this report gives an overview of the calculations performed by TROPO. Section 3 discusses the calculation of coherence bandwidth and space diversity correlation for troposcatter channels. Engineering guidelines for the optimization of quad space diversity systems are discussed in Section 4. The concept of service probability to account for path prediction errors is discussed in Section 5. Section 6 compares the propagation path predictons obtained using TROPO with measured data provided by DCEC. This section also discusses some of the MD-918 and AN/TRC-170 short-term (~ 1 hour) performance predictions. The analysis and development of a model of the AN/TRC-170 modem performance is discussed in Appendices A through E.

REFERENCES

Kirk, K.W. and J.L. Osterholz (1976), "DCS Digital Transmission System Performance", DCEC TR-12-76.

Military Handbook, "Facility Design for Tropospheric Scatter (Transhorizon Microwave System Design)", MIL-HDBK-417, November 1977.

Monsen, P. and S. Parl (1980), "Adaptive Antenna Control (AAC) Program", Final Report CSA-76-8085-6, Contract DAAB07-76-C-8085, US Army Communications Systems Agency, Ft. Monmouth, NJ.

Rice, P.L., A.G. Longley, K.A. Norton and A.P. Barsis (1967), "Transmission Loss Predictions for Tropospheric Communication Circuits", Revised NBS Technical Note 101, National Bureau of Standards, Washington, DC.

Sherwood, A. and I. Suyemoto (1977), "Multipath measurements over troposcatter paths", Technical Report ESD-TR-77-252, Electronic Systems Division, Air Force Systems Command, U.S. Air Force, Hanscom Air Force Base, Bedford, MA.

Tatarskii, V.I. (1971), "The Effects of the Turbulent Atmosphere on Wave Propagation", National Technical Information Service, Springfield, VA.

Draft MIL-STD-188-323, "System Design and Engineering Standards for Long Haul Digital Transmission System Performance", 4 May 1983, Defense Communications Engineering Center, Code R220, Reston, VA.

SECTION 2
OVERVIEW OF TROPO PROGRAM CALCULATIONS

In this section we present a top level description of the TROPO computer program, so that the user will have some understanding of what goes on during a typical run. The treatment here includes a description of the main calculations performed by the TROPO Program in order to assist the user with the interpretation of the output. A description of the input data required is given in the User's Manual Report. Sample outputs for different combinations of input parameters are also given in the User's Manual. For a detailed description of the structure and logical organization of TROPO software, the user is referred to the software documentation report.

Figure 2-1 is a top level flowchart of the TROPO computer program at a functional level. The blocks of Figure 2-1 typically correspond to one or more modules (subroutines). The functions performed by these blocks are described below. Not shown is the detailed Path/Modem output, which is to unit LOUT. Output to this unit occurs from various program modules, including tropo and diffraction calculation modules and the modem evaluation routines.

2.1 MAIN PROGRAM FUNCTIONS

The routines in TROPO can be grouped into nine major functions performed by the program: (1) data input and unit conversion, (2) data checking, and error diagnostics; (3) troposcatter propagation mode parameter calculations; (4) diffraction mode propagation parameter calculations; (5) climate variability calculations; (6) transmitter and receiver filter parameter calculations; (7) MD-918 modem performance calculations; (8) AN/TRC-170-DAR Modem performance calculations; and (9) summary output data.

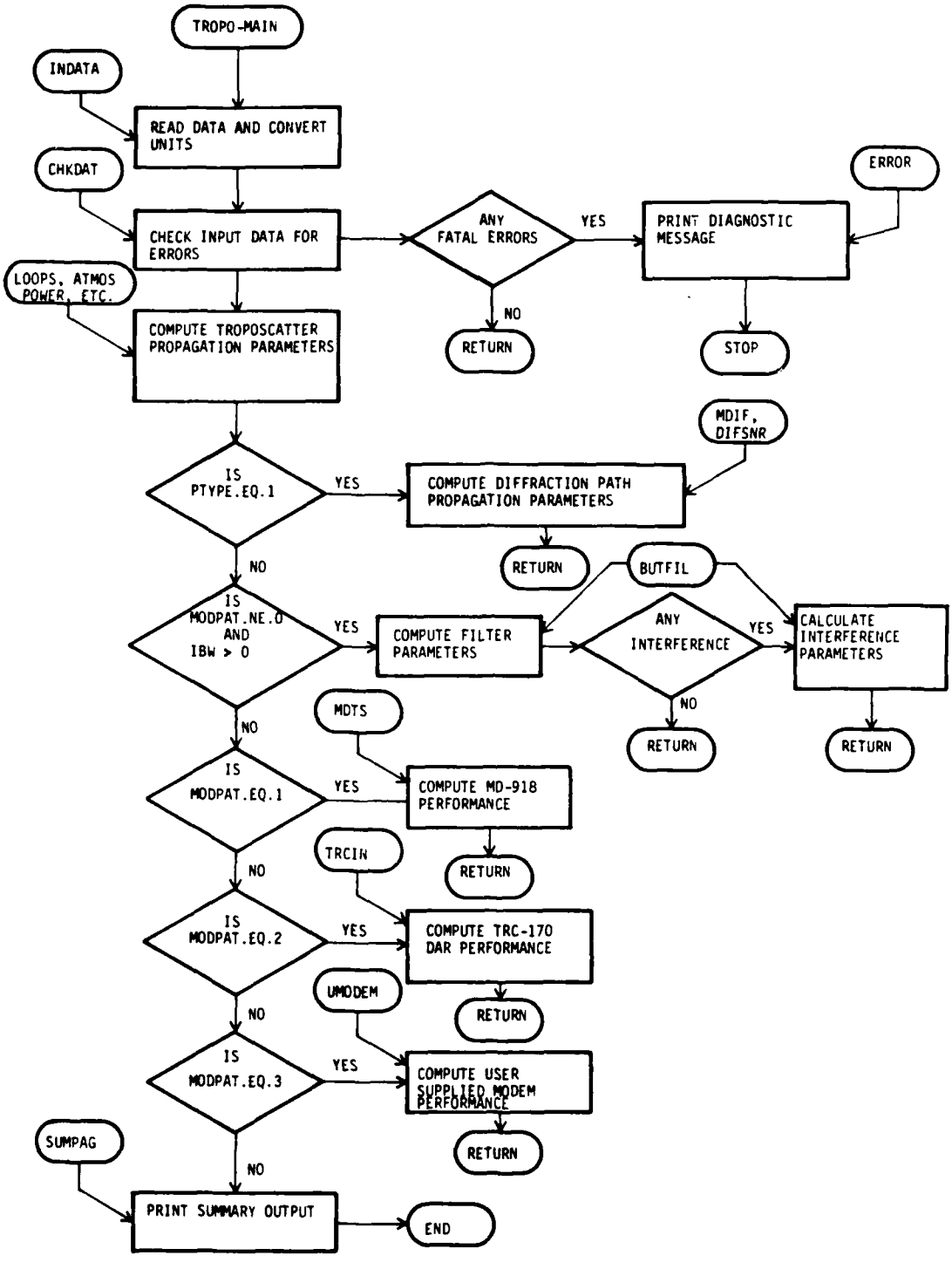

Figure 2-1 Top Level Functional Flow Chart for TROPO Program Calculations

The user can choose to have TROPO perform propagation calculations only or both modem performance and propagation calculations by the appropriate specification of the input parameter MODPAT.

When MODPAT = 0 is selected, the program performs only propagation calculations such as path loss and RSL long term (yearly) distribtions, multipath spread and diversity correlations. If MODPAT = 1 is selected, the program performs the propagation calculations and uses them to predict the performance (average bit error rate, 1000 bit block error rate, fade outage per call minute and fade outage* probability) of the MD-918 modem taking into account the effects of bandwidth constraints and interference as specified by the user. When MODPAT = 2 is selected, the program uses the propagation calculations to predict the performance of the AN/TRC-170 modem (two-frequency) for TRCTYP = 1, or the single frequency DAR modem for TRCTYP = 0. The user can also opt to the use of the propagation calculations to predict the performance of a modem other than the MD-918 or TRC-170 modems by specifying MODPAT = 3 and supplying the modules (routines) needed to calculate the performance of the modem.

* NOTE: Fade outage is defined as a short term fade (~1 second) below an 'instantaneous' bit error rate (BER) threshold (e.g., 10^{-3}, 10^{-4}, or 10^{-5}).

2.2 DATA INPUT AND CHECKING

The data which specify the parameters of the link to be evaluated are input from a disk file. The file must have a specific format, described in and illustrated by examples in the User's Manual Report.

The input file is processed line by line (subroutine INDATA) with checking for possible errors (subroutine CHKDAT) where feasible. Comment lines in the file (lines beginning with *) serve both to identify to the user what each line of data means and to enable the program to verify that data records are in the proper sequence. Therefore, each block of comment lines must occur in the proper location in the file, must agree verbatim with the required file format (at least in the columns checked by the program), and must contain exactly the number of lines expected by the program.

Depending on the selection of units made for a given TROPO run, the program converts the input units, where necessary, to the standard units used by the program, which are standard MKS units. This conversion is performed by subroutine UNITCV.

2.3 DATA INPUT ERROR DIAGNOSTICS

When something goes wrong with the input file (and experience has shown that this is a major source of difficulty with TROPO), the program sooner or later detects an error. If the error is a data inconsistency, an explanatory error message is printed to the terminal. If the error is an input syntax error the operating system will issue a system error message and terminate.

2.4 PROPAGATION MODES

Two types of propagation conditions can be selected by the user: (1) tropospheric-scatter propagation (PTYPE = 0), or (2) mixed troposcatter-diffraction propagation (PTYPE = 1). In the next two sections we discuss these two propagation modes. The standard MKS system of units is used in all mathematical expressions unless otherwise noted.

2.5 TROPOSCATTER PROPAGATION MODE

The TROPO program calculates the yearly distribution of the troposcatter path loss and the corresponding RSL (received signal level) for the user specified link geometry and climate zone (subroutine POWER). Errors in the prediction of the yearly median and standard deviation of the RSL are accounted for using the service probability concept described in detail in Section 5. TROPO also calculates the multipath spread (yearly median) of the channel and if diversity reception is used, it calculates the correlation between the various diversity signals (subroutine LOOPS). A flow chart of the routines involved in the troposcatter propagation calculations is shown in Figure 2-2.

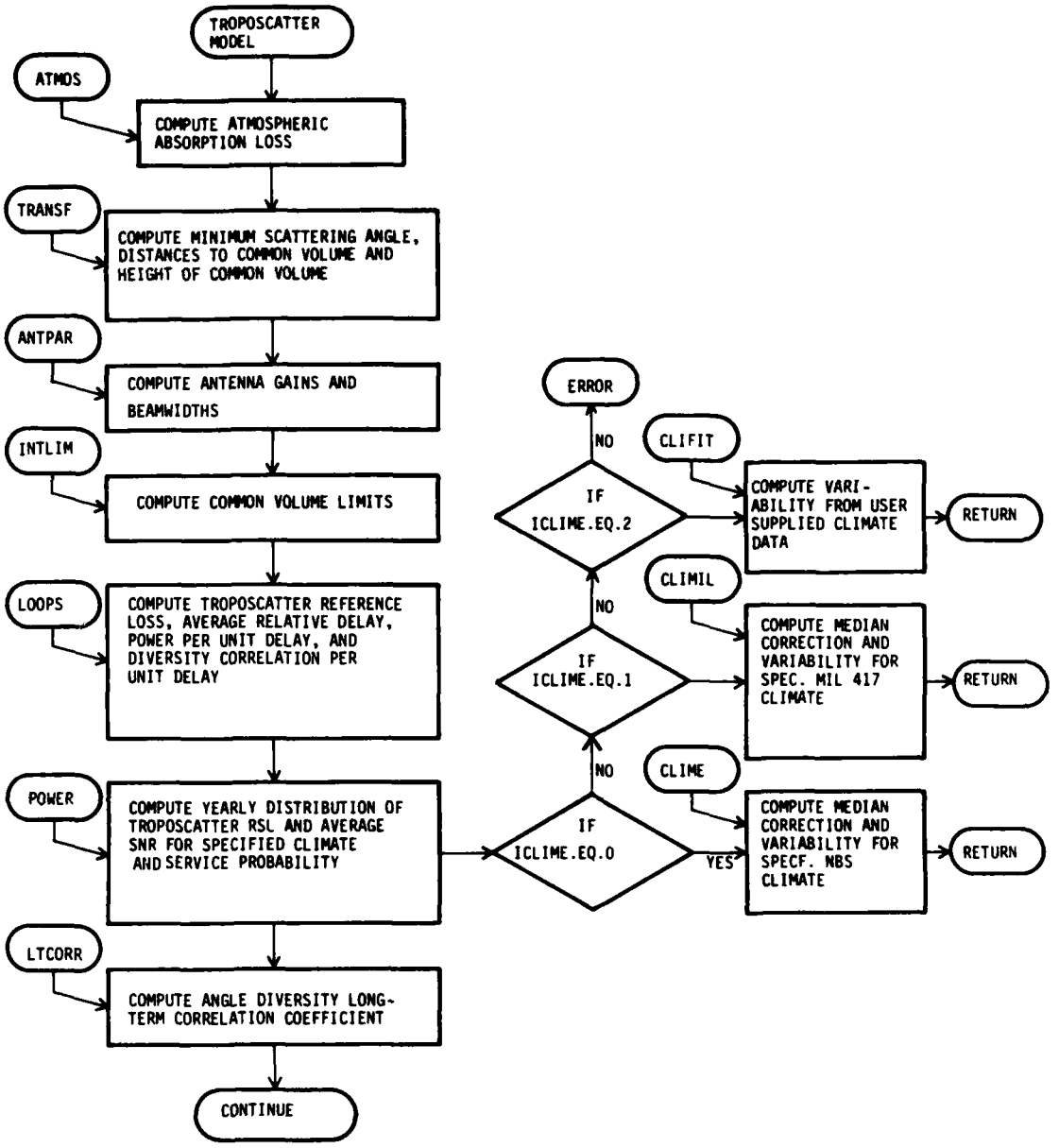

Figure 2-2 Flow Chart for Troposcatter Propagation Parameter Calculations

2.5.1 RSL and Path Loss Distributions

The received troposcatter signal is a Rayleigh fading signal which exhibits rapid short-term fluctuations and long-term power fading. The hourly median of the short-term Rayleigh fading is defined as the RSL*. The RSL exceeded q% of the time, P(q), which corresponds to the path loss not exceeded q% of the year, L(q), is defined as

$$P(q) = P(50) + Y_0(q) \quad \text{dBW or dBm}$$

and

$$L(q) = L(50) - Y_0(q) \quad \text{dB} \qquad (2.1)$$

where L(50) is the yearly median of the path loss, P(50) is the yearly median of the RSL and $Y_0(q)$ is the variability in the RSL and the path loss about the median.

The median RSL and path loss are related by

$$P(50) = P_t + G_t + G_r - L(50) \qquad (2.2a)$$

where P_t is the transmitted power in dBW or dBm, and G_t and G_r are the gains of the transmitting and receiving antennas in dBi. The median path loss (i.e., loss exceeded by half-of-all hourly medians) is defined as

$$L(50) = L_r - V(d_e) \qquad (2.2b)$$

---

* The average signal level for a Rayleigh fading signal is 1.6 dB above the median.

where L_r is the long-term (yearly) reference path loss and $V(d_e)$ is a correction factor which depends on the climate zone and a link geometry parameter called the effective path distance d_e to be defined later.

Prediction errors are accounted for by defining the RSL not to exceed q% of the year with (service) probability t as

$$P(q,t) = P(q,,0.5) - T\sqrt{12.73 + .12\ Y_0^2(q)} \qquad (2.3)$$

where P(q,0.5) is given by Equation (2.1) and T is related to the service probability t by

$$t = 0.5 + 0.5\ \mathrm{erf}(T/\sqrt{2})$$

$$\mathrm{erf}(x) = \frac{2}{\sqrt{\pi}} \int_0^x \exp(-y^2)dy \quad .$$

2.5.2 The Reference Path Loss

The reference troposcatter path loss is defined as the long-term (yearly) median path loss in continental temperate climate zones during periods of <u>minimum</u> signal strength (winter afternoons).

The calculation of the long-term reference path loss takes into account the effects of path geometry, and ray bending in a standard atmosphere. It requires calculation of the transmitter and receiver horizon elevation angles, THET and THER respectively, from the following user-supplied path geometry data: (a)

transmitter and receiver horizon distances, DLT and DLR, (b) transmitter and receiver horizon elevation above sea level, HLT and HLR, (c) transmit and receive site elevation above sea level HTO and HRO, (d) transmit and receive antenna heights above local ground, HT and HR, and (e) either the refractivity at sea level SEAN as in NBS Technical Note 101 [P.L. Rice, et al., 1967] or the effective earth radius factor ERFAC but not both. Effective antenna heights and/or average terrain elevation data are not needed to calculate the horizon elevation angles THET and THER (and hence the reference path loss), but will be needed if the user wishes to calculate the median correction factors $V(d_e)$ and the variability about the median $Y_0(q)$ for a specific climate. The horizon elevation angles THET and THER* are then used to calculate the minimum scattering angle θ_s (coded THETA0) from

$$\theta_s = \text{THET} + \text{THER} + d/R_e \qquad (2.4)$$

where d is the great circle path length and R_e (coded A) is the effective earth radius. This angle along with the antenna patterns determine the path loss.

The refractivity at sea level SEAN and/or the effective earth radius factor ERFAC are used to take into account the bending of the rays as they propagate through the lower atmosphere in the calculation of THET and THER (and the scattering angle). The user has the option of selecting either SEAN or ERFAC, but not both, for the calculation of ray bending effects because they are

* NOTE: THET and THER are often referred to as antenna take-off angles. However this is not quite correct and can lead to confusion. The antenna take-off angle is the elevation angle at which the antenna (boresight) is pointing and is not necessarily always equal to the horizon elevation.

not independent parameters. Ray bending is determined for the most part by the gradient of the refractivity within the first kilometer above the surface of the earth. In order to represent rays as straight lines, an effective earth radius R_e is defined in terms of the refractivity gradient, ΔN, as

$$\text{ERFAC} = \frac{R_e}{R} = \frac{1}{1 + R \cdot \Delta N \times 10^{-6}} \qquad (2.5)$$

where R is the true radius of the earth (R = 6373 Km).

The refractivity gradient has, in turn, been found to be empirically related to the surface refractivity, N_S, by [P.L. Rice, et al., 1967]

$$\Delta N/\text{km} = -7.32 \exp(0.005577\ N_S) \quad . \qquad (2.6)$$

The surface refractivity N_S is related to the refractivity at sea level N_0 (coded SEAN) as follows [P.L. Rice, et al., 1967]

$$N_S = N_0 \exp(-.1057\ h_s) \qquad (2.7)$$

where h_s is the elevation of the surface above sea level in km. In beyond-the-horizon paths, h_s is determined at the two radio horizons along the great circle path between the antennas, and N_S is taken as the average of two values calculated from the above relationship. The minimum monthly mean value of N_0 (referred to hereafter as SEAN) has been chosen by NBS Technical Note 101 and

the MIL-HDBK-417 for the calculation of the refractive bending effects on the reference path loss L_r because they are representative of winter conditions (i.e., weak signal periods).

If the user specifies both SEAN and ERFAC, the program ignores the value supplied for ERFAC and calculates a new effective earth radius factor according to the above relationships. The reason for choosing SEAN as the independent parameter is because the median correction factor, $V(d_e)$ (coded VDE), and variability about the median $Y_0(q)$, defined in NBS Technical Note 101 and the MIL-HDBK-417 are predicated on the use of the minimum monthly mean sea level refractivity SEAN for the calculation of the reference path loss L_r. Typical values for SEAN are shown in Figure 2-3. They range from 290 (Antarctica) to 390 (equatorial over sea paths) with values around 300 for continental temperate regions.

Some users may wish to use ERFAC as the independent variable however. If a user chooses the effective earth radius factor ERFAC for the calculation of refractive bending effects, then he must enter a value of zero for SEAN. However in this case justification of the use of a median correction factor $V(d_e)$ is required.

A typical value often used for the effective earth radius factor is ERFAC = 4/3. This value is normally regarded as the median for most regions of the world. Since we have established that there is a one-to-one correspondence between the refractivity at sea level SEAN, and ERFAC, then an effective earth radius of 4/3 corresponds to the median of the monthly mean refractivity at sea level SEAN, not the minimum monthly mean surface refractivity relative to which $V(d_e)$ is defined. However, a study of the dependence of the troposcatter path loss on the effective earth radius factor (see Figure 2-4) for a typical 100 mile link (all other conditions being equal) reveals that

MINIMUM MONTHLY SURFACE REFRACTIVITY VALUES REFERRED TO MEAN SEA LEVEL

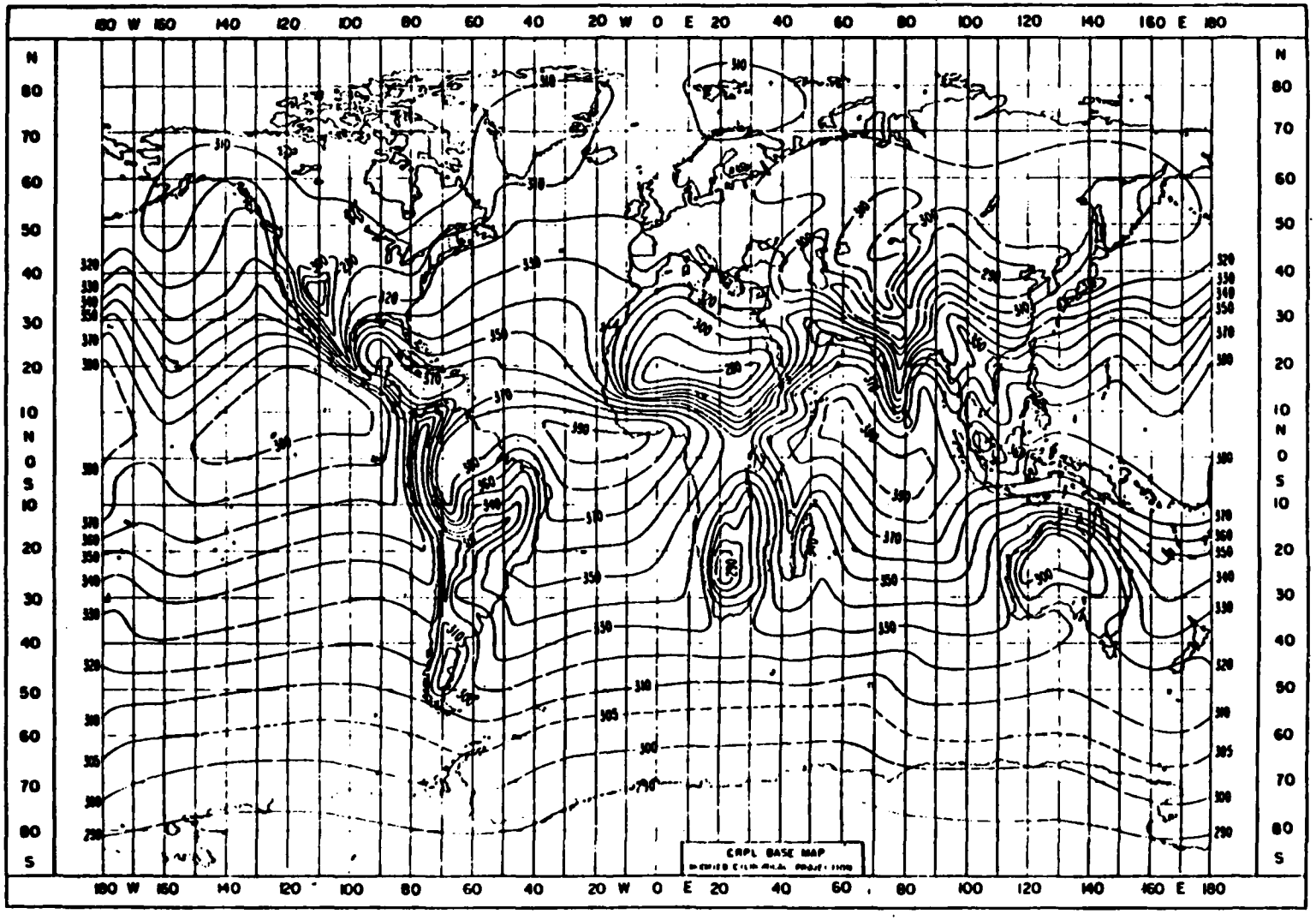

Figure 2-3 (From Rice, et al., 1967)

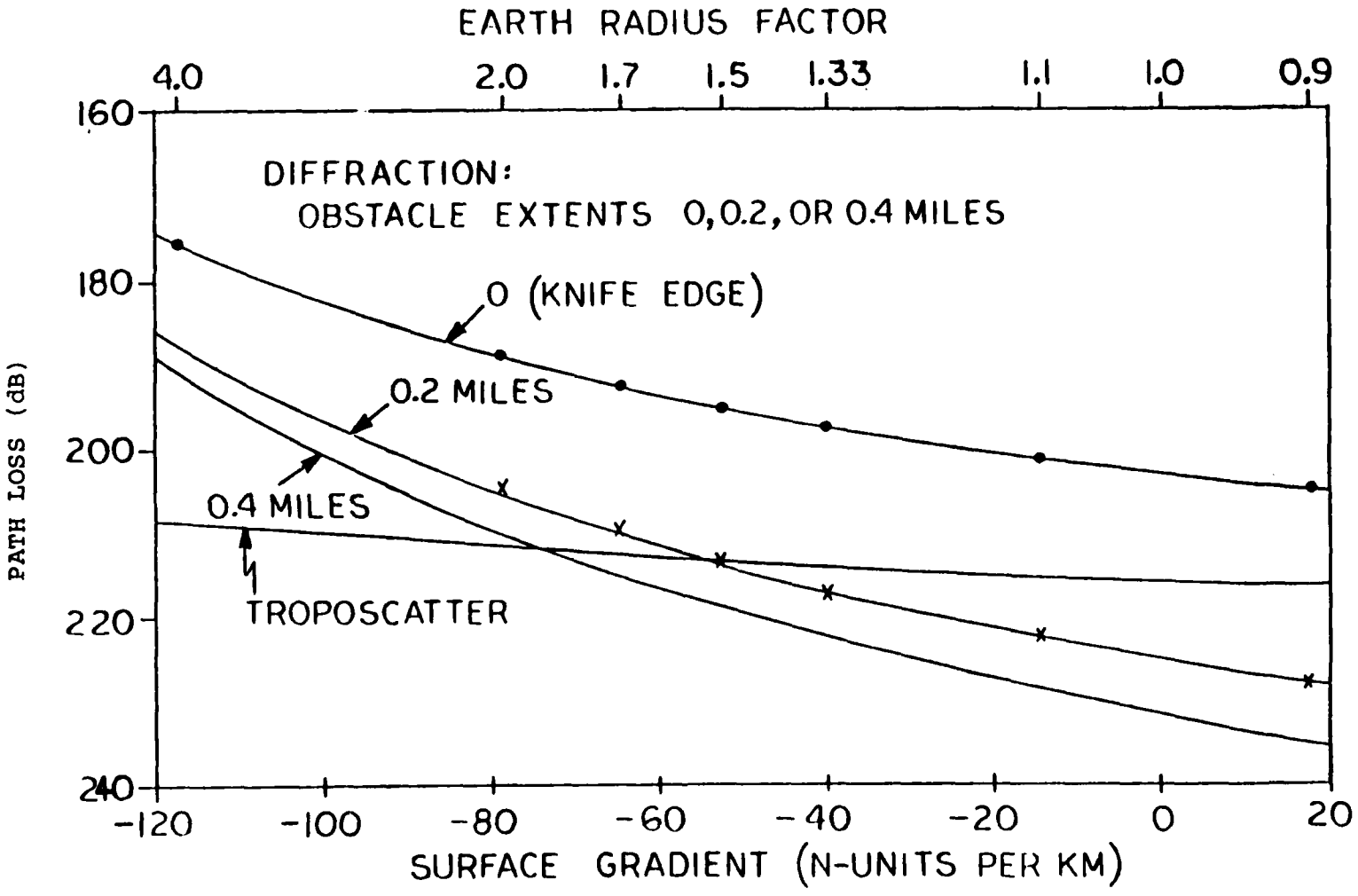

Figure 2-4 Predicted Troposcatter and Diffraction Path Losses on the Jackson Butte-Stanford Link

there is little variation (less than 1 dB) of the path loss for values of ERFAC between 1 and 2 which correspond to typical ranges in the refractivity gradients between -80 N-units/km and 0 N-units/km. Certainly the range of variation in the path loss with changes in the effective earth radius (and hence the surface refractivity N_S) is much smaller than the median correction factor, $V(d_e)$, which can be as large as ±8 dB for some climates.

These arguments lead us to conclude that for troposcatter paths the correction factor, $V(d_e)$, accounts for effects other than variations in monthly mean refractivity at sea level (or equivalently the effective earth radius factor).* In fact most of the variability in the troposcatter signal is caused by changes in the humidity and temperature within the common volume which affect the fraction of power scattered towards the receiver.

The reference troposcatter path loss is calculated from numerical evaluation of the triple integral (subroutine LOOPS)

$$P_R = P_T G_T G_R A_b \iiint C(m) \frac{|g_T(\underline{r})\ g_R(\underline{r})|^2}{R_T^2(\underline{r})\ R_R^2(\underline{r})} \theta(\underline{r})^{-m} dV \qquad (2.8)$$

where

P_R = received power (Watts),

P_T = transmitted power (Watts) (coded WLT)

G_T, G_R = transmit and receive antenna gain on boresight (dimensionless ratio),

* This is not true for diffraction paths however as seen from the curves of Figure 2-4.

g_T, g_R = transmit and receive antenna voltage gain patterns normalized to unity gain (calculated by functions TGAIN and RGAIN)

R_T, R_r = distances from transmitter and receiver to the point $\underline{r}$ in the common volume,

$\theta(\underline{r})$ = scattering angle at the point $\underline{r}$ in the scattering volume,

m = wavenumber spectrum slope of refractive index fluctuations (determines dependence of the scattering cross section on the scattering angle) (coded SCPARM),

C(m) = a proportionality constant which depends on frequency, height of the scattering volume and the choice of the wavenumber spectrum slope,

A_b = atmospheric attenuation due to oxygen and water vapor absorption (coded AA),

L_r = $P_T G_T G_R / P_r$ (dimensionless reference path loss).

The integrand of the triple integral in (2.8) is negligible outside the common volume intersected by the transmit and receive antenna patterns, g_T and g_R. Hence (2.8) includes the aperture-to-medium coupling loss.

2.5.2.1 Antenna Patterns

The gain and directional voltage pattern of the transmit and receive antennas are computed (subroutine ANTPAR) from the operating frequency and antenna diameter, assuming that each antenna is a parabolic dish with 55% area efficiency.

The gain is computed as

$$G = 6.4\ (D/\lambda)^2 \qquad (2.9)$$

where D is the antenna diameter and λ is the wavelength. The voltage gain pattern (calculated in GPATT) is assumed to be of the form

$$g(\phi) = \frac{2J_1(a \sin \phi)}{a \sin \phi} \qquad (2.10)$$

where $J_1(x)$ is the first order Bessel function of the first kind, ϕ is the off-boresight angle, and

$$a = \frac{\pi D}{1.2\lambda} \quad . \qquad (2.11)$$

The 3 dB beamwidth is calculated from

$$\phi_3 = 1.22(\lambda/D). \qquad (2.12)$$

2.5.2.2 Common Volume Geometry

The geometry and boundaries of the common volume are then determined from the intersection of the transmit and receive antenna patterns. First, a modified form of the effective Earth's radius transformation is performed in subroutine TRANSF. When the refractivity of sea level is not specified (SEAN = 0), the effective earth radius factor ERFAC specified in the input file is used; otherwise ERFAC is calculated from the specified refractivity SEAN and this value of ERFAC is used instead of the value in the input file. The effective earth radius accounts for the mean curvature of the beams due to atmospheric refraction. In the transformed coordinate system, the beams follow straight lines, simplifying the calculation of the region of intersection ("common volume").

Using the calculated patterns as well as the assumed dependence of the scattering cross section upon scattering angle, the limits of integration to be used in the propagation calculations are determined (subroutine INTLIM). Points which are outside the 3-dB beamwidth, or which involve such a large scattering angle that their contribution would be negligible, delimit the preliminary bounds on the integration. From these bounds, and the input parameter ERR, the integration step size is determined. A typical value of ERR is 0.001. The integration is terminated when the contribution to the integral falls below a number proportional to 1/NACCU. Typically NACCU = 30-500 is used. During familiarization with the program a new user should determine the effect of these accuracy parameters by typing several values and comparing the results. Decreasing ERR and/or increasing NDELB improves accuracy at the expense of increased computation time.

2.5.2.3 Atmospheric Structure Constant and Spectrum Slope

The scattering angle and frequency dependence of the troposcatter path loss depend on the choice of the slope m (coded SCPARM) of the wavenumber spectrum of the atmospheric refractive index fluctuations (turbulence).

The frequency dependence is found from the definition of C(m), i.e.,

$$C(m) = C_N^2 \, r_0^{11/3-m} \, k^{2-m} \, \frac{\Gamma(m/2)}{2\sqrt{\pi}\,\Gamma\left(\frac{m-3}{2}\right)} \cdot \frac{\Gamma(4/3)}{2^{1/3}\Gamma(2/3)} \qquad (2.13)$$

where $k = 2\pi/\lambda = 2\pi f/c$, f is the frequency, λ is the wavelength, c is the speed of light, C_N^2 is the 'structure constant' (dimensions of meters to the -2/3 power and coded CN2 (•)) of the turbulence when the spectrum slope is m = 11/3 (it is a measure of the 'strength' of the refractive index fluctuations and their 'size'), $\Gamma(X)$ is the Gamma function and r_0 is a constant with dimensions of length to be determined later.

The scattering angle dependence can be found by noting that the reference path loss, L_r, can be expressed as the product of the path loss assuming isotropic antenna patterns also called the basic path loss, L_b, and a factor called the aperture-to-medium coupling loss, L_c, which accounts for the additional loss due to the fact that a non-isotropic antenna does not illuminate all the the potential scatterers in the atmosphere.

When the antenna patterns are assumed to be isotropic (i.e., $g_T = g_r = 1$), the triple integral in (2.8) can be evaluated analytically to obtain the following expression for the basic path loss [Parl, 1979]

$$\frac{1}{L_b} = C_N^2 \, r_0^{11/3-m} \, (k\Theta_S)^{2-m} \, \frac{m-3}{4(m-1)(m-2)d} \cdot \frac{\Gamma(4/3)}{2^{1/3}\Gamma(2/3)} \qquad (2.14)$$

where Θ_S is the (minimum) scattering angle at the bottom of the common volume, and d (coded D) is the great-circle path length. This expression shows that the basic path loss has identical frequency and scattering angle dependence, i.e.,

$$L_b \sim (f\Theta_s)^{m-2} \quad . \qquad (2.15)$$

Experimental evidence [Tatarskii, 1971; Gossard, 1977] indicates that the slope m of the refractive index frequency (or wavenumber) spectrum at microwave frequencies is m = 11/3. The NBS Technical Note 101 model, however, predicts a cubic dependence on frequency and scattering angle, i.e., m = 5. The cubic type of frequency and scattering angle dependence may be justifiable at frequencies below 1 GHz (UHF and VHF) where the troposcatter signal is a combination of specular reflections and turbulent scatter [Rottger, 1980].

Since the reference path loss is the median path loss in continental temperate climates during periods of weak signal strength (winter afternoons). We use a conservative model for the structure constant C_N^2 . This constant completely determines the reference path loss when m = 11/3 and is given by [Fried, 1967]

$$C_N^2 = 8 \times 10^{-14} \, h^{-1/3} \exp(-h/3200) \qquad (2.16)$$

where h is the height of a scatter within the common volume above the surface of the earth in meters. This model assumes very dry weather conditions and it may be too pessimistic an estimate of median conditions encountered in continental temperate and more humid climates. Some short-term measurements of the vertical profile of the structure constant, C_N^2 , at a few locations in the U.S. have been published in the literature [Gossard, 1977]. Long-term distributions of C_N^2 at fixed altitudes have also been measured in Colorado [Chadwick and Moran, 1980]. The prediction accuracy of the troposcatter receive signal strength as well as the multipath spread will be greatly improved when long-term measurements of the entire vertical profile of C_N^2 at altitudes between 0-4 Km become available for all climate zones. In the meantime we use the pessimistic, dry weather, model (Equation (2.16)) to calculate the reference path loss (continental temperate climate - winter afternoons). Correction factors to estimate the median path loss in other climates are based on the NBS 101 or MIL-HDBK-417 guidelines.

The cubic frequency and scattering angle dependence of the NBS Technical Note 101 model can be obtained by specifying an m = 5 (or SCPARM = 5) spectrum slope. The parameter r_0 in (2.14) has been fixed so that (2.14) will yield the same basic path loss, L_b, as that predicted by NBS Technical Note 101 to within .5 dB. It should, however, be pointed out that the reference path loss, $L_r = L_b L_c$, calculated by the TROPO program for m = 5 may differ from the actual NBS Technical Note 101 prediction by a greater amount because of the manner in which the aperture-to-medium coupling loss, L_c, is calculated. While NBS Technical Note 101 calculates the basic path loss, L_b, and the aperture-to-medium, coupling loss, L_c, separately using semi-empirical formulas, the TROPO program calculates the reference path loss, L_r, directly according to (2.8) which includes both effects directly. The aperture-to-medium coupling loss may be determined from L_c =

L_r/L_b where L_r is given by (2.18) and L_b is the reference path loss calculated by TROPO according to Equation (2.14). Some analytical approximations for the coupling loss may be found in [Parl,1979].

2.5.2.4 Atmospheric Absorption Loss

The loss due to oxygen and water vapor absorption is calculated by subroutine ATMOS. This loss is printed out in the output data file and is negligible at frequencies below 1 GHz but can be significant at frequencies above 5 GHz.

The loss $(1/A_b)$ in dB is calculated from

$$-10 \log A_b = (\gamma_0 + \gamma_W)d \qquad (2.17)$$

where γ_0 is the specific attenuation (dB/km) of oxygen, γ_W is the specific attenuation of water vapor and d is the path length in km.

The specific attenuation of water vapor is due to both the 22 GHz absorption line and the so called residual absorption. It is given by [Liebe, 1969]

(2.18)

$$\gamma_W = 2.1 \times 10^{-5} f_G^2 + \frac{2.69 \times 10^{-3} f_G^2}{9 + (f_G - 22.235)^2} + \frac{2.69 \times 10^{-3} f_G^2}{9 + (f_G + 22.235)^2}$$

where f_G is the frequency in GHz.

The specific attenuation of oxygen is due to the 60 GHz absorption line and is calculated from

(2.19)

$$\gamma_0 = \frac{6.4 \times 10^{-3} f_G^2}{f_G^2 + .32} + \frac{1.9 \times 10^{-2} f_G^2}{5.07 + (f_G - 60)^2} + \frac{1.9 \times 10^{-2} f_G^2}{5.07 + (f_G + 60)^2} \quad .$$

This form of the specific attenuation of oxygen is similar to that proposed by Van Vleck [1947]. The line width's and line strengths have been chosen to give a good fit to the curves of specific attenuation of oxygen published by CCIR [1978] for frequencies up to 35 GHz. TROPO will give an warning message when the specified frequency is greater than this upper limit.

The absorption loss calculation (2.17) assumes the specific attenuation of water vapor and oxygen do not vary significantly with altitude. This is only true for short paths. Therefore TROPO will give a warning message when path lengths greater than 500 km are specified. This limitation could be relaxed by using an effective distance in (2.17), such as those presented graphically in NBS Technical Note 101, rather than the true distance.

2.5.3 The Median Correction Factors

The long-term reference path loss, L_r, is the median path loss in continental temperate climates during winter afternoons (time block 2). The correction factor $V(d_e)$ accounts for differences between yearly median meteorological conditions in a given climate zone and those existing during winter afternoons in continental temperate climates. The program calculates the appropriate median correction factor for the climate zone specified by the user. The user can select one of eight climate zones

defined in NBS Technical Note 101 (ICLIME = 0) [P.L. Rice, et al., 1967]: (1) continental temperate, (2) maritime temperate overland, (3) maritime temperate over sea, (4) maritime subtropical over land, (5) continental temperate time block 2 (winter afternoons), (6) desert, Sahara, (7) equatorial, and (8) continental subtropical. The user also select one of nine climate zones defined in MIL-HDBK-417 (ICLIME = 1): (1) continental temperate, (2) maritime temperate over land, (3) maritime temperate over sea, (4) maritime subtropical, (5) desert, Sahara, (6) equatorial, (7) continental subtropical, (8) mediterranean, and (9) polar. The user can also specify his own climate zone (ICLIME = 2). However in this case it is assumed that no median correction factor is needed (i.e., $V(d_e) = 0$). Curves of the median correction factor as a function of the effective distance parameter d_e for each of the climate zones defined above may be found in the appropriate references mentioned earlier.

2.5.3.1 Median Correction for NBS Climates

The median correction factor $V(d_e)$ for all climate zones except for continental temperate, maritime temperate overland and maritime temperate oversea is calculated from the analytic representation

$$V(d_e) = [c_1 d_e^{n_1} - f_2(d_e)]e^{-c_3 d_e^{n_3}} \qquad (2.20a)$$

$$f_2(d_e) = f_8 + (f_m - f_8)e^{-c_2 d_e^{n_3}} \qquad (2.20b)$$

where the values of the coefficients c_1, c_2 and c_3, exponents n_1, n_2, and n_3 and limiting values f_8 and f_m are given in Table 2-1. The median correction factor for continental temperate time block 2 is zero by definition as this is reference time/climate. The median correction factor for continental temperate, maritime temperate overland and maritime time temperate oversea are calculated by interpolating between points tabulated at 50 km intervals. The reason for this is that the values of c_1, c_2, c_3, n_1, n_2, n_3, f_m and f_8 given in NBS Technical Note 101 do not reproduce the curves plotted in the same reference.

2.5.3.2 Median Correction for MIL-HDBK 417 Climates

The median correction factor $V(d_e)$ for all Mil-Handbook 417 climate zones except mediterranean is calculated using the analytic representation of Equation (2.20). The values of the constants c_1, c_2, c_3, n_1, n_2, n_3, f_m and f_8 are given in Table 2-2 for each climate zone. The correction for mediterranean climates is calculated as the average of the correction factors for maritime temperate oversea and maritime subtropical.

2.5.4 Variability About the Median

The variability about the median, $Y_0(q)$, also depends on the climate zone, frequency and effective distance parameter d_e. It can be written as

$$Y_0(q) = g(q,f)\ Y(q,d_e) \qquad (2.21)$$

where $Y(q,d_e)$ is the variability at a reference frequency and $g(q,f)$ is a correction factor for frequencies other than the reference.

Table 2-1

Constants for Calculation of $V(d_e)$ for NBS Climates

CLIMATE	c_1	c_2	c_3	n_1	n_2	n_3	f_m	f_8
1. Continental Temperate	Interpolation							
2. Maritime Temperate Overland	Interpolation							
3. Maritime Temperate Oversea	Interpolation							
4. Maritime Subtropical	1.09×10^{-4}	5.89×10^{-8}	2.21×10^{-7}	2.06	6.81	2.97	5.8	2.2
5. Continental Temperate Time Block 2	0	0	0	0	0	0	0	0
6. Desert Sahara	-8.85×10^{-7}	2.76×10^{-4}	2.25×10^{-12}	2.8	4.82	4.78	-8.4	-8.2
7. Equatorial	3.45×10^{-7}	3.74×10^{-12}	6.97×10^{-8}	2.97	4.43	3.14	1.2	8.4
8. Continental Subtropical	1.59×10^{-5}	1.56×10^{-11}	2.77×10^{-8}	2.32	4.08	3.25	3.9	0

Table 2-2

Constants for Calculation of $V(d_e)$ for MIL-Handbook 417 Climates

CLIMATE	c_1	c_2	c_3	n_1	n_2	n_3	f_m	f_8
1. Continental Temperate	1.59×10^{-5}	1.56×10^{-11}	2.685×10^{-5}	2.32	4.08	2.0	4.2	2.0
2. Maritime Temperate Overland	1.12×10^{-4}	1.26×10^{-20}	1.17×10^{-11}	1.68	7.30	4.41	2.05	2.0
3. Maritime Temperate Oversea	1.09×10^{-4}	2.31×10^{-15}	3.82×10^{-9}	2.06	5.50	3.75	6.8	3.6
4. Maritime Subtropical	1.09×10^{-4}	1.02×10^{-13}	2.21×10^{-7}	2.06	5.0	2.97	6.2	1.5
5. Desert Sahara	-4.79×10^{-9}	5.93×10^{-7}	5.14×10^{-15}	3.67	2.41	6.21	-4.8	-8.8
6. Equatorial	9.79×10^{-17}	3.8×10^{-7}	6.97×10^{-8}	7.21	3.18	3.14	2.0	-8.8
7. Continental Subtropical	1.59×10^{-5}	1.56×10^{-5}	2.685×10^{-5}	2.32	4.08	2.0	4.2	2.0
8. Mediterranean	Average of 3 and 4							
9. Polar	Same as for Continental Temperate							

Curves of $Y(q,d_e)$ as a function of the effective distance parameter for each of the NBS Technical Note 101 and MIL-HDBK-417 can be found in these references. The reference frequency for both the NBS Technical Note 101 and MIL-HDBK-417 climates is 1 GHz for all climates except the NBS Technical Note 101 continental temperate, and continental temperate time block 2 (winter afternoons) for which the reference frequency is 100 MHz. There is no frequency correction factor (i.e., $g(q,f) = 1$) for the following NBS climates: maritime temperate over land, maritime temperate over sea, maritime subtroptical over land, and equatorial. Similarly there is no frequency correction for the following MIL-HDBK-417 climates: equatorial, maritime subtropical, mediterranean, maritime temperate over land, maritime temperate over sea and polar. Curves for the frequency correction factors for all other climates can be found in the above references. The TROPO computer program uses analytic approximations to these curves.

2.5.4.1 Variability for NBS Climates

The path loss distribution (variability) about the median at a reference frequency of 1 GHz, $Y(q,d_e)$, is calculated as

$$\begin{aligned} Y(.01,\ d_e) &= 3.33\ Y(10,\ d_e) \\ Y(.1,\ d_e) &= 2.73\ Y(10,\ d_e) \\ Y(1.,\ d_e) &= 2.0\ \ Y(10,\ d_e) \\ Y(99,\ d_e) &= 1.82\ Y(90,\ d_e) \\ Y(99.9,\ d_e) &= 2.41\ Y(90,\ d_e) \\ Y(99.99,\ d_e) &= 2.9\ \ Y(90,\ d_e) \end{aligned} \qquad (2.22)$$

The 10 percentile, $Y(10,\ d_e)$, and 90 percentile, $Y(90,d_e)$, variability factors for all NBS climates except maritime temperate overland and maritime temperate oversea are calculated using the analytic expression of Equation (2.20). The constants c_1, c_2,

c_3, n_1, n_2, n_3, f_m and f_8 for the calculation of $Y(10,d_e)$ are given in Table 2-3 and the constants for the calculation $-Y(90,d_e)$ are given in Table 2-4. The variability factors for maritime temperate overland and maritime temperate oversea are calculated by interpolating between values tabulated in increments of 50 km.

2.5.4.2 Frequency Correction Factors for NBS Climates

Four of the NBS climates require the use of a correction factor to calculate the path loss distribution at a frequency other than the reference frequency. These are continental temperate all year, continental temperate time block 2 (winter afternoons), desert (Sahara) and continental subtropical. There is no frequency correction factor for the other climates.

The frequency correction factors for the continental temperate and continental temperate time block 2 climates for percentiles $q < 50$ are approximated by

$$g(q < 50, f) = \begin{cases} 1.27 + 0.22 \sin(X), & 100 \text{ MHz} < f < 2 \text{ GHz} \\ 1.05, & f > 2 \text{ GHz} \end{cases} \quad (2.23a)$$

and for percentiles $q > 50$ by

$$g(q > 50, f) = \begin{cases} 1.23 + 0.18 \sin(X), & 100 \text{ MHz} < f < 2 \text{ GHz} \\ 1.05, & f > 2 \text{ GHz} \end{cases} \quad (2.23b)$$

Table 2-3

Constants for Calculation of $Y(10, d_e)$ for NBS Climates

CLIMATE	c_1	c_2	c_3	n_1	n_2	n_3	f_m	f_8
1. Continental Temperate	3.56×10^{-2}	9.85×10^{-8}	1.5×10^{-11}	1.13	2.8	4.85	10.5	5.4
2. Maritime Temperate Overland	Interpolation							
3. Maritime Temperate Oversea	Interpolation							
4. Maritime Subtropical	4.33×10^{-2}	7.13×10^{-11}	1.19×10^{-12}	1.09	3.89	4.93	17.5	13.6
5. Continental Temperate Time Block 2	1.04×10^{-5}	4.28×10^{-8}	3.51×10^{-8}	2.71	2.91	3.41	9.15	2.8
6. Desert Sahara	6.02×10^{-2}	1.36×10^{-5}	3.18×10^{-11}	1.08	1.84	4.69	15.1	6.0
7. Equatorial	5.22×10^{-3}	1.57×10^{-4}	5.22×10^{-17}	1.39	1.46	6.78	8.5	3.2
8. Continental Subtropical	1.01×10^{-2}	2.26×10^{-7}	3.9×10^{-9}	1.46	2.67	3.78	16.0	9.1

Table 2-4

Constants for Calculation of $-Y(90, d_e)$ for NBS Climates

CLIMATE	c_1	c_2	c_3	n_1	n_2	n_3	f_m	f_8
1. Continental Temperate	9.42×10^{-3}	5.7×10^{-11}	5.56×10^{-6}	1.33	3.96	2.44	8.2	3.0
2. Maritime Temperate Overland	Interpolation							
3. Maritime Temperate Oversea	Interpolation							
4. Maritime Subtropical	7.24×10^{-3}	4.26×10^{-15}	1.12×10^{-6}	1.35	5.41	2.56	12.7	8.4
5. Continental Temperate Time Block 2	1.0×10^{-5}	7.0×10^{-13}	7.64×10^{-9}	2.59	4.8	3.68	7.05	2.8
6. Desert Sahara	3.19×10^{-2}	5.66×10^{-8}	7.39×10^{-11}	1.14	2.76	4.4	11.4	3.3
7. Equatorial	6.51×10^{-3}	2.53×10^{-4}	2.61×10^{-16}	1.36	1.36	6.55	8.4	2.7
8. Continental Subtropical	3.49×10^{-3}	1.08×10^{-9}	9.15×10^{-11}	1.55	3.49	4.48	10.1	3.5

where

$$X = 4.495 \log_{10} (f_{MHz}/180) \tag{2.24}$$

and where f_{MHz} is the frequency in MHz.

The frequency correction factor for NBS Technical Note 101 desert (Sahara) climate is calculated for all percentiles from

$$g(q,f) = \begin{cases} 1.05 + 0.74 \sin(X) & , \ 250 \text{ MHz} < f < 2 \text{ GHz} \\ .976 & , \ f > 2 \text{ GHz} \end{cases} \tag{2.25}$$

Similarly, the frequency correction factor for NBS Technical Note 101 continental subtropical climate is calculated for all percentiles q from

$$g(q,f) = \begin{cases} 1.082 + .212 \sin(X) & , \ 200 \text{ MHz} < f < 2 \text{ GHz} \\ .976 & , \ f > 2 \text{ GHz} \end{cases} . \tag{2.26}$$

The lowest frequency for which these analytic expressions are good approximations to the correction factors shown graphically in NBS Technical Note 101 [P.L. Rice, et al., 1967] are given next to each expression.

2.5.4.3 Variability for MIL-Handbook 417 Climates

The path loss distribution (variability) about the median at a reference frequency of 1 GHz, $Y(q,d_e)$ is calculated as

$$\begin{aligned} Y(.01,\ d_e) &= a_1\ Y(10,\ d_e) \\ Y(.1,\ d_e) &= a_2\ Y(10,\ d_e) \\ Y(1.,\ d_e) &= a_3\ Y(10,\ d_e) \\ Y(99,\ d_e) &= 1.82\ Y(90,\ d_e) \\ Y(99.9,\ d_e) &= 2.41\ Y(90,\ d_e) \\ Y(99.99,\ d_e) &= 2.9\ \ Y(90,\ d_e) \end{aligned} \qquad (2.27)$$

where the proportionality constants a_1, a_2 and a_3 are climate zone dependent and are given in Table 2-5.

The 10 percentile, $Y(10,\ d_e)$, and 90 percentile, $Y(90,\ d_e)$, variability factors are calculated according to the following analytic expression

$$\left.\begin{matrix} Y(10,\ d_e) \\ -Y(90,\ d_e) \end{matrix}\right\} = \begin{cases} c_1 d_e^{\,2} e^{-d_e^{\,2}/d_m^{\,2}} & \text{if } d_e < d_c \\ c_f + c_2 e^{-\beta d_e} & \text{if } d_e > d_c \end{cases} \qquad (2.28)$$

where the constants d_m, d_c, c_1, c_2, c_f and β are climate zone dependent. Table 2-6 gives the constants for the calculation of $Y(10,\ d_e)$ and Table 2-7 gives the constants for the calculation of $-Y(90,\ d_e)$.

Table 2-5

Proportionality Constants for MIL-Handbook 417
Variability Factors

CLIMATE	a_1	a_2	a_3
1. Continental Temperate	3.33	2.73	2.0
2. Maritime Temperate Overland	3.8	3.08	2.2
3. Maritime Temperate Oversea	3.8	3.08	2.2
4. Maritime Subtropical	3.7	3.3	2.22
5. Desert Sahara	2.88	2.4	1.82
6. Equatorial	3.33	2.73	2.0
7. Continental Subtropical	2.64	2.27	1.8
8. Mediterranean	Average of 3 and 4		
9. Polar	Same as 1		

Table 2-6

Constants for Calculation of $Y(10, d_e)$ for MIL-Handbook 417 Climates

CLIMATE	c_1	c_2	c_f	β	d_m	d_c
1. Continental Temperate	11.48×10^{-4}	27.43	6.	8.03×10^{-3}	170	200
2. Maritime Temperate Overland	6.41×10^{-4}	29.02	10.8	10.94×10^{-3}	233	255
3. Maritime Temperate Oversea	7.95×10^{-4}	35.64	10.8	9.09×10^{-3}	225	255
4. Maritime Subtropical	6.64×10^{-4}	37.90	13.	7.57×10^{-3}	267	300
5. Desert Sahara	12.87×10^{-4}	64.56	6.	9.76×10^{-3}	178	225
6. Equatorial	5.44×10^{-4}	16.12	3.	5.38×10^{-3}	200	235
7. Continental Subtropical	14.16×10^{-4}	49.90	10.	10.48×10^{-3}	178	210
8. Mediterranean	Average of 3 and 4					
9. Polar	Same as 1					

Table 2-7

Constants for Calculation of $-Y(90,d_e)$ for MIL-Handbook 417 Climates

CLIMATE	c_1	c_2	c_f	β	d_m	d_c
1. Continental Temperate	6.29×10^{-4}	22.54	3.5	5.28×10^{-3}	210	250
2. Maritime Temperate Overland	6.53×10^{-4}	88.51	8.8	15.4×10^{-3}	216	250
3. Maritime Temperate Oversea	8.74×10^{-4}	41.18	10.	9.03×10^{-3}	216	250
4. Maritime Subtropical	4.24×10^{-4}	8.65	8.3	2.48×10^{-3}	283	300
5. Desert Sahara	7.69×10^{-4}	42.11	3.6	6.92×10^{-3}	206	260
6. Equatorial	5.9×10^{-4}	25.79	3.5	8.17×10^{-3}	192	235
7. Continental Subtropical	6.8×10^{-4}	33.08	3.2	7.03×10^{-3}	200	250
8. Mediterranean	Average of 3 and 4					
9. Polar	Same as 1					

2.5.4.4 Frequency Correction Factors for MIL-HDBK-417 Climates

Three of the MIL-Handbook 417 climates require correction factors to calculate the path loss distribution at a frequency other than the reference frequency of 1 GHz. These are continental temperate, continental subtropical and desert, Sahara climates. The other climates do not require a frequency correction factor.

The frequency correction factors for the MIL-HDBK-417 climates are different than those for NBS climates. The correction factor for the continental temperate and continental subtropical climates for $q < 50$ is calculated from

$$g(q<50,f) = \begin{cases} 1.105 + 1.35 \sin(X_0), & 150 \text{ MHz} < f < 1.5 \text{ GHz} \\ .97 & , f > 1.5 \text{ GHz} \end{cases} \quad (2.29a)$$

where

$$X_0 = 5.473 \log_{10}(f_{MHz}/215) \quad . \quad (2.29b)$$

The correction factor for the continental temperate climate only and percentiles $q > 50$ is calculated from

$$g(q > 50,f) = \begin{cases} 1.045 + .075 \sin(X_0), & 150 \text{ MHz} < f < 1.5 \text{ GHz} \\ .97 & , f > 1.5 \text{ GHz} \end{cases} \quad (2.29c)$$

The correction factor for continental subtropical and desert (Sahara) climates and percentiles $q > 50$ is equal to unity. However the correction factor for desert (Sahara) climates and percentiles $q < 50$ is approximated by

$$g(q < 50, f) = \begin{cases} 1.07 + .1 \sin(X_0), & 150 \text{ MHz} < f < 1.5 \text{ GHz} \\ .97 & , f > 1.5 \text{ GHz} \end{cases} \quad . \quad (2.30)$$

The lowest frequency of applicability for the MIL-HDBK-417 climate frequency correction factors approximations is 150 MHz.

2.5.4.5 User Specified Climate Variability

When the user specifies his own climate type (ICLIME = 2) the TROPO program calculates $Y_0(90) = g(f)\ Y(90, d_e)$ from the following input values supplied by the user: (a) the value $Y(90, d_e = 0)$, (b) the value of $d_e = d_{min}$ at which $Y(90, d_{min})$ has its minimum value, (c) the absolute value of $Y(90, d_{min})$, (d) the value $Y900 = Y(90, d_e > 900 \text{ km})$, and (e) the frequency correction factor g(f) if other than its default value of one.

The program computes the coefficients of a curve of the form

$$-Y(90, d_e) = \begin{cases} c_0 + c_1 d_e^2 \exp(-\alpha\, d_e^2) & , d_e < 1.316\ d_{min} \\ c_f + c_2 \exp(-\beta d_e) & , d_e > 1.316\ d_{min} \end{cases} \quad (2.31)$$

and prints out the values of c_0, c_1, c_2, c_f, α and β which fit the data supplied by the user. This curve is similar to that used in NBS Technical Note 101 except that the NBS coefficients n_1, n_2 and n_3 have been fixed, i.e., $n_1 = n_3 = 2$ and $n_2 = 1$. The reason for fixing these coefficients is that only four independent coefficients can be computed from the data supplied by the user. Nonetheless, a curve of this type will provide a good fit to all $Y(90,d_e)$ curves for the NBS Technical Note 101 and MIL-HDBK-417 curves.

The variability at other percentiles is calculated from

$$\begin{aligned} Y_0(99) &= 1.82\ Y_0(90) \\ Y_0(99.9) &= 2.41\ Y_0(90) \\ Y_0(99.99) &= 2.9\ Y_0(90) \end{aligned} \qquad (2.32a)$$

and

$$\begin{aligned} Y_0(10) &= -Y_0(90) \\ Y_0(1) &= 2.0\ Y_0(10) \\ Y_0(.1) &= 2.73\ Y_0(10) \\ Y_0(0.1) &= 3.33\ Y_0(10). \end{aligned} \qquad (2.32b)$$

These relationships between $Y_0(q)$ and $Y_0(90)$ and $Y_0(10)$ are also used in the NBS Technical Note 101 climates. Somewhat different proportionality constants for the low percentile events are used in the MIL-HDBK-417 climates. They are climate zone dependent.

2.5.4.6 Effective Distance Parameter

The parameter d_e used for calculating the median correction factor $V(d_e)$ and the variability about the median $Y(d_e)$ is a function of the effective antenna height and frequency. It is defined as [P.L. Rice, et al., 1967]

$$d_e = \begin{cases} 130\ d/(d_L + d_{S1}) & \text{km, if } d < d_L + d_{S_1} \\ 130 + d - (d_L + d_{S1}) & \text{km, if } d > d_L + d_{S_1} \end{cases} \quad (2.33)$$

where d is the great circle path length, and d_L is the sum of the effective transmitter and receiver radio horizon distances, i.e.,

$$d_L = 3\sqrt{2h_{te}} + 3\sqrt{2h_{re}} \text{ km} \quad (2.34)$$

with the effective antenna heights h_{te} and h_{re} in meters.

The remaining parameter d_{S1} is the distance at which diffraction and forward-scatter losses are approximately equal over a smooth earth of effective radius R_e = 9000 km so that

$$d_{S1} = 9000\ \theta_{A1} = 65(100/f)^{1/3} \quad (2.35)$$

where f is the frequency in MHz.

This definition of the effective distance parameter indicates that a great deal of the variability in over-the-horizon propagation at microwave frequencies is caused by mixed tropo-

scatter-diffraction propagation and that the median correction and variability curves for the climate types defined in NBS Technical Note 101 and MIL-HDBK-417 take mixed propagation conditions into account. This is perfectly satisfactory for narrowband systems where any delay differences between the troposcatter and diffraction signals are negligible. However this is not necessarily the case for high data rate digital communications systems where the delay difference between the troposcatter and diffraction signals may exceed the symbol duration. In order to avoid this problem, the TROPO program has the flexibility of calculating the medians of the troposcatter and diffraction signals explicitly if the user chooses to specify mixed-mode propagation conditions (PTYPE = 1). The program also calculates the variability of each of these modes about their respective medians according to the methods recommended in NBS Technical Note 101 and/or MIL-HDBK-417. However one has to reconsider the applicability of the median correction factors and variability curves when troposcatter and diffraction distributions are calculated explicitly (i.e., separately). In this case, it is likely that the NBS Technical Note 101 and MIL-HDBK-417 variability curves will overestimate the variability of the individual troposcatter and diffraction modes.

2.5.4.7 Effective Antenna Height

The calculation of the effective distance parameter d_e requires that the effective antenna heights, h_{te} and h_{re}, be either calculated by the program (NTERR = 1,2) or supplied by the user (NTERR = 0).

The effective transmit and receive antenna heights* are defined as

$$HTE = HT + HT0 - AVETX$$
$$HRE = HR + HR0 - AVERX \qquad (2.36)$$

where HT (HR) is the transmit (receive) antenna height above ground, HT0 (HR0) is terrain elevation above sea level at the transmit (receive) antenna site, and AVETX (AVERX) is the average foreground terrain elevation above sea level at the transmit (receive) antenna site. The user can choose to specify HT, HT0 and AVETX and HR, HR0 and AVERX (if NTERR = 1) for the calculation of the effective transmit and receive antenna heights or he can have the program calculate the average terrain elevation AVETX and AVERX (when NTERR = 2) from terrain elevation data he supplied.

The average foreground terrain elevation AVETX (or AVERX) is calculated by fitting a curve of the form

$$h(X) = \bar{h} + m(X - \bar{X}) \qquad (2.37)$$

to NP <u>evenly spaced</u> terrain elevation data points $h_i(X_i)$ between the antenna site and its radio horizon. The point X_1 must be the actual transmit site (or receive antenna radio horizon) while X_{NP} must be the transmit radio horizon (or the receive site).

* NOTE: These effective antenna heights are relative to average terrain elevation and should not be confused with effective heights above sea level which are used to take into account ray bending effects on the scattering angle. The latter are defined in Appendix B.1.

In order to get a good fit to the terrain data, NP must be greater than 5. The terrain elevation data points near the antenna and its radio horizon are excluded in the calculation of the best fit curve h(x). Thus

$$\bar{h} = \frac{1}{N} \sum_{i=IMIN}^{IMAX} h_i \quad , \quad N = IMAX - IMIN + 1$$

$$\bar{X} = \frac{X_1 + X_{NP}}{2} \tag{2.38}$$

$$m = \frac{12}{N(N+1)(X_{NP} - X_1)} \sum_{i=IMIN}^{IMAX} h_i \, (i-I_0), \quad I_0 = \frac{N-1}{2}$$

where IMIN and IMAX are chosen so as to exclude the terrain data nearest the antenna and the radio horizon as follows

$$IMIN = \begin{cases} 2 & \text{if} \quad 5 < NP < 11 \\ 3 & \text{if} \quad 11 < NP < 21 \\ 4 & \text{if} \quad 21 < NP \end{cases} \tag{2.39a}$$

and

$$IMAX = \begin{cases} NP-1 & \text{if} \quad 5 < NP < 11 \\ NP-2 & \text{if} \quad 11 < NP < 21 \\ NP-3 & \text{if} \quad 21 < NP \end{cases} \quad . \tag{2.39b}$$

The average terrain elevation at the transmit site is then calculated in subroutine AVTER as

$$\text{AVETX} = h(X_1) + m(X_1 - \bar{X}) \qquad (2.40)$$

provided that the terrain data supplied is between the transmitter and its radio horizon.

If the terrain data is between the receive radio horizon* and the receive site, then the average terrain elevation at the receive site is calculated as

$$\text{AVERX} = h(X_{NP}) + m(X_{NP} - \bar{X}) \quad . \qquad (2.41)$$

The effective antenna heights are then calculated as indicated earlier.

2.5.5 Multipath Spread

The predicted multipath spread of the troposcatter signal is calculated simultaneously with the reference path loss calculation, i.e., Equation (2.8) (subroutine LOOPS). This is done by noting that the received power P_r can be written as

* NOTE: Note that the terrain data must be both equidistant and in the proper sequence in order for the above calculations to be valid.

$$P_r = \int_{\tau_{min}}^{\tau_{max}} Q(\tau)d\tau \qquad (2.42)$$

where $Q(\tau)$ (coded $Q(.,.)$) is the received power per unit delay (delay power impulse response profile), τ_{min} is the delay of the path to the lowest point in the scattering volume, and τ_{max} is the delay to the highest point in the scattering volume.

The power per unit delay profile, $Q(\tau)$, is calculated by summing up the contributions to the total received power (see Equation (2.8)) from all those points $\underline{r}$ in the scattering volume with delay

$$\tau = \frac{R_T(\underline{r}) + R_R(\underline{r})}{c} \quad . \qquad (2.43)$$

The rms delay spread (or 2-sigma delay spread) τ_{rms} is then obtained from the definition

$$\tau_{rms}^2 = \frac{4}{P_r} \int_{\tau_{min}}^{\tau_{max}} (\tau - \tau_{AV})^2 \, Q(\tau)d\tau \qquad (2.44)$$

where the average delay τ_{AV} is defined as

$$\tau_{AV} = \frac{1}{P_r} \int_{\tau_{min}}^{\tau_{max}} \tau \, Q(\tau)d\tau \quad . \qquad (2.45)$$

The rms delay spreads (or 2-sigma delay spreads) calculated by TROPO are yearly median delay spreads. There is some evidence that the rms multipath spread exhibits long-term variability [Sherwood, et al., 1977]. However the data is not comprehensive enough to establish a correlation between link geometry, climate zone and atmospheric conditions and multipath spread. Nonetheless, the variability of the multipath spread can be sufficiently large that it cannot be ignored.

There are two major mechanisms which can cause variability in multipath spread: one is the variability of the effective earth radius factor (ERFAC) which causes the size of the effective scattering volume (i.e., that part of the common volume which contributes significantly to the total received power) to vary, and the other is variability in the height profile of the atmospheric structure constant C_N^2 . There is considerable evidence that significant layering of the turbulence and variability in the layering exists in the atmosphere so that in some cases C_N^2 may actually increase with height within the scattering volume a fraction of the time. In fact this is the only mechanism which can explain the large rms multipath spreads measured on some links [Sherwood, et al., 1977]. The distribution of multipath spread including layering effects has not been modelled yet for lack of information regarding the long-term distribution of C_N^2 as a function of height. Instead TROPO calculates and prints out the maximum delay spread τ_M that can be expected* from scatterers within the common volume, i.e.,

* NOTE: This maximum delay spread can only be exceeded whenever strong scatterers, such as airplanes, are within the volume intersected by a sidelobe of one of the antennas.

$$\tau_M = \tau_{max} - \tau_{min} \approx \frac{d}{2c} (\alpha_1 \beta_1 - \alpha_0 \beta_0) \qquad (2.46)$$

where d is the path length, c is the speed of light, α_0 and α_1 are take-off angles at the transmit site measured from the straight line bisecting the transmitter and receiver to the lowest and highest points in the scattering volume, respectively, and β_0 and β_1 are the corresponding take-off angles at the receive site as shown in Figure 2-5. This is the upper bound on the delay spread of the troposcatter signal. The value of τ_M is not used in the calculation of MD-918, AN/TRC-170 or DAR Modem performance; only the 2-sigma delay delay spread is used. τ_n is calculated and supplied to the user to warn that this value of multipath spread may occur on the path with some small probability.

2.5.6 Diversity Correlations

The types of diversity correlation calculations performed in TROPO depend on the choice of the parameter DIVTYP. If DIVTYP = 0 is specified, the program assumes a single transmitting antenna and two spaced receiving antennas (Figure 2-6, top), each of which has two angle diversity feeds. The correlation coefficients (short-term Rayleigh fading) and correlation vs. delay profiles for the following diversity configurations are then computed: (a) dual space (2S) diversity, (b) dual space/dual frequency (2S/2F) diversity, (c) dual space/dual angle (2S/2A) diversity, and (d) dual space/dual angle/dual frequency (2S/2A/2F) diversity. If DIVTYP = 1 is selected, the program assumes a single transmitting antenna and a single receiving antenna (Figure 2-6, middle) with two angle diversity feeds. Correlation

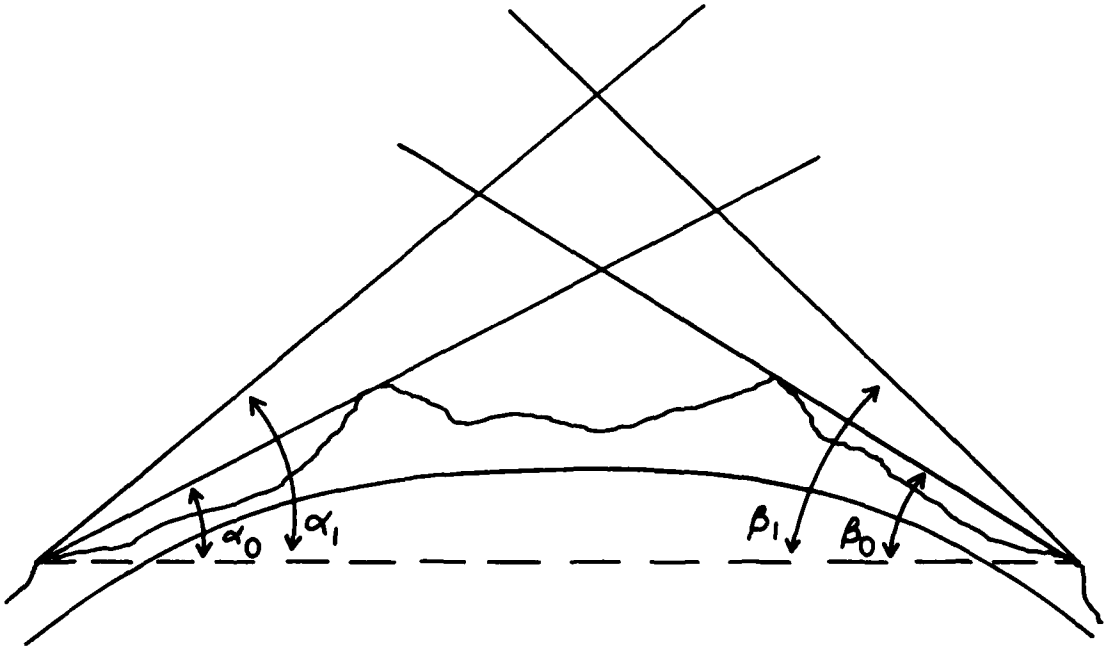

Figure 2-5 Scattering Volume Geometry

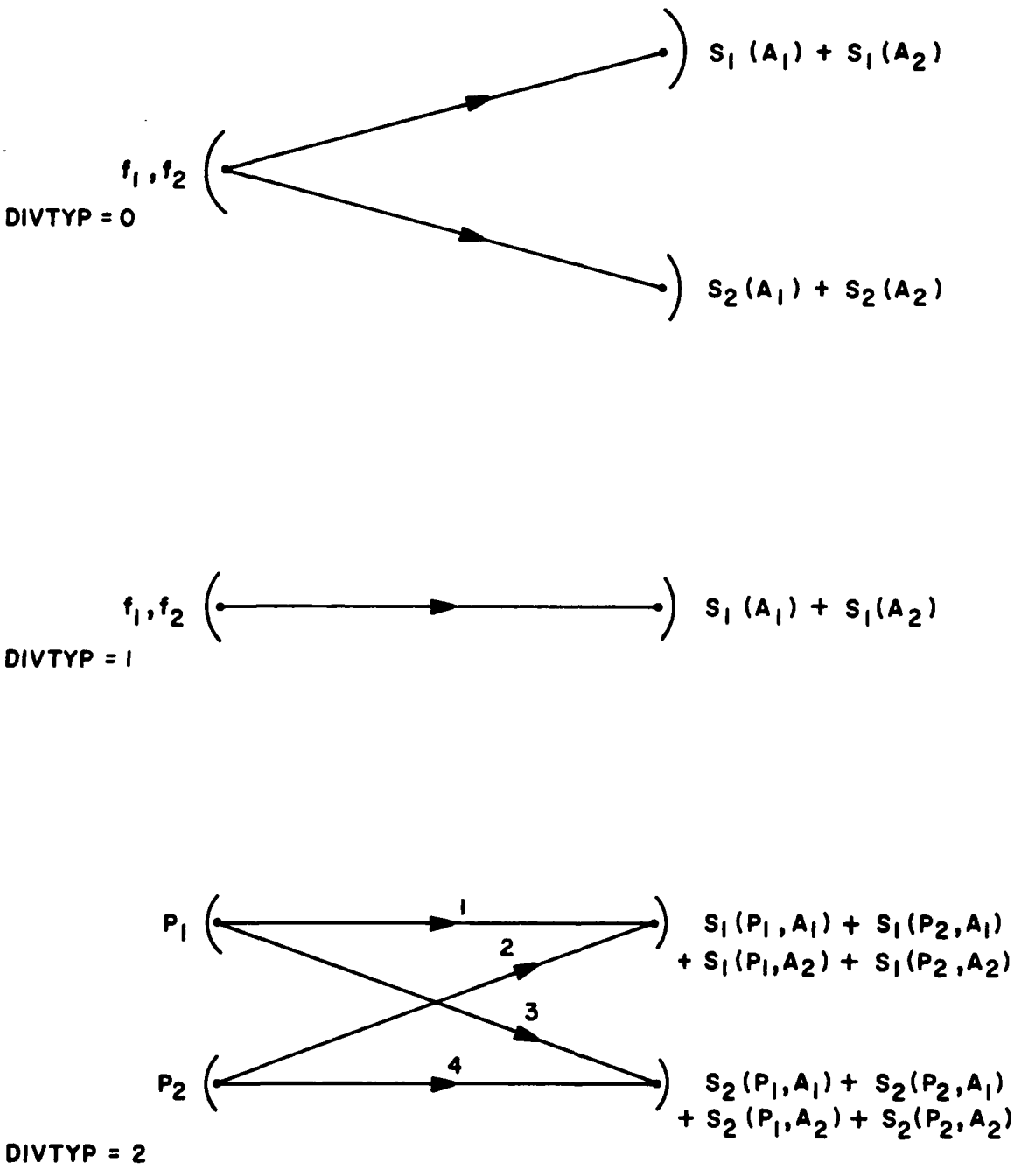

Figure 2-6 Diversity Configurations

coefficients and correlation profiles for the following diversity configurations are then calculated: (a) dual angle(2A) diversity, (b) dual frequency (2F) diversity and (c) dual frequency/dual angle (2F/2A) diversity. If DIVTYP = 2 is selected, the program assumes two spaced transmitting antennas and two spaced receiving antennas (Figure 2-6, bottom). The two transmitting antennas are assumed to transmit the same information but on orthogonal polarizations. Each of the receiving antennas is assumed to be capable of receiving both polarizations as well as having angle diversity feeds. The correlation coefficients and correlation delay profiles for the following diversity configurations are then computed: (a) dual space/dual polarization (2S/2P) also referred as quadruple space and (b) dual space/dual polarization/dual angle (2S/2P/2A) diversity.

Table 2-8 summarizes the types of correlation coefficients that are calculated for each of the standard diversity configurations that can be selected by specifying DIVTYP = 0, 1, or 2. Note that there are three types of space diversity correlation coefficients: (a) convergent/divergent path correlation (e.g., the two paths in Figure 2-6, top), (b) cross path correlation (e.g., paths 2 and 3 in Figure 2-6, bottom) and (c) parallel path correlation (e.g., paths 1 and 4 in Figure 2-6, bottom). The angle diversity correlation coefficient is the correlation between the lower and upper beams received at each antenna. The frequency diversity correlation is the correlation between the signals received at two different frequencies. TROPO assumes that when frequency diversity is used, the frequency separation is greater than the coherence bandwidth of the channel so that the frequency diversity correlation coefficient is negligible. The minimum frequency separation required is calculated and supplied in the summary printout SUMPAG.OUT (see paragraph 2.5.6.3).

Table 2-8

CORRELATION COEFFICIENTS CALCULATED

DIVERSITY CONFIGURATION	DIVTYP	SPACE DIVERSITY CORRELATION COEFFICIENT			ANGLE DIVERSITY CORRELATION COEFFICIENT	FREQUENCY DIVERSITY CORRELATION COEFFICIENT
		DIVERGENT- OR CONVERGENT PATHS	CROSS PATHS	PARALLEL PATHS		
2S	0	X				
2S/2F	0	X				X
2S/2A	0	X			X	
2S/2A/2F	0	X			X	X
2A	1				X	
2F	1					X
2F/2A	1				X	X
2S/2P	2	X	X	X		
2S/2P/2A	2	X	X	X	X	

Whenever modem performance calculations are desired, the user must specify DIVTYP = 0, 1, or 2. The modem performance for all of the possible diversity configurations (listed above for each value of DIVTYP) is then computed using the correlation coefficients and correlation profiles calculated by TROPO. A non-standard diversity configuration involving more than two antennas at one or both terminals can be specified by the user by selecting DIVTYP = 4. TROPO will then calculate the correlation coefficients specified by the user for the non-standard diversity. However no modem performance calculations are allowed.

The non-standard diversity configuration may consist of one transmitting antenna and up to four spaced receiving apertures.

In addition to specifying the diversity type configuration, i.e., DIVTYP = 0, 1, 2, or 4, the user must specify the center-to-center separation distance betwen the antennas. The antennas may be spaced either horizontally or vertically (TSEP or RSEP) on the plane perpendicular to the great circle path, but not both. This restriction allows TROPO to exploit the symmetry of the configuration to compute a real correlation coefficient. The present version of the program does not allow non-symmetrical (e.g., horizontal and vertical separation or longitudinal separation) antenna configurations about the great circle plane because the correlation coefficients would then be complex. The computation time for evaluation of the correlation coefficient (see Equation (2.45) below) using complex notation would be at least double that required for the real case.

2.5.6.1 Space Diversity Correlation Calculations

The correlation coefficient ρ_{12} between the signals received at two spaced antennas (or equivalently the correlation between two signals transmitted using two spaced antennas) is

calculated simultaneously with the reference path loss and power per unit delay calculations (subroutine LOOPS) from the definition

$$\rho_{12} = \frac{P_T G_T G_R A_b}{\sqrt{P_{r1} P_{r2}}} \iiint \frac{C(m) g_{T1}(\underline{r})\ g^*_{T2}(\underline{r})\ g_{R1}(\underline{r})\ g^*_{R2}(\underline{r})}{R_T^2(\underline{r})\ R_R^2(\underline{r})}\ \theta^{-m} dV \quad (2.47)$$

where P_{r1} is the average power of received signal 1, P_{r2} is the average power of received signal 2, g_{T1} and g_{T2} are the voltage patterns of the transmitting apertures (normalized to unit power gain), and g_{R1} and g_{R2} are the voltage patterns (normalized to unity gain) of the receiving apertures.

Note that if the correlation between the signals received with two spaced receiving apertures is desired, $g_{T1} = g_{T2}$ while the magnitudes of g_{R1} and g_{R2} are also equal. However due to the separation between the receiving apertures the phases of g_{R1} and g_{R2} differ by an amount proportional to the difference in distance from each aperture to the scatterer at a point $\underline{r}$ in the scattering volume which is assumed to be identical for both receiving apertures. The combined effect of the difference in phase path lengths from the two antennas to each element in the common volume is the primary cause of decorrelation between the signals received at two spaced antennas.

2.5.6.2 Angle Diversity Correlation Calculation

The correlation coefficient between two angle diversity signals is also computed using the definition in (2.47). However in this case the two receive antenna patterns illuminate different common volumes. The correlation between the two signals is determined by the amount of overlapping between the two receive antenna patterns.

2.5.6.3 Frequency Diversity Correlation and Coherence Bandwidth Calculations

The correlation coefficient $\rho(f_1-f_2)$ between the signals at two different frequencies f_1 and f_2 is calculated in subroutine FRQSEP by performing the Fourier transformation

$$\rho(f_1-f_2) = \int_{-\infty}^{\infty} Q(\tau)e^{-j2\pi(f_1-f_2)\tau}d\tau \qquad (2.48)$$

where $Q(\tau)$ is the power per unit delay function defined in Equation (2.42) if the two frequencies are transmitted and received using the same apertures. If the two frequencies are received on two spaced apertures, $Q(\tau)$ is replaced by the cross-correlation delay profile obtained from (2.47) using similar methods as those used in the calculation of the delay power impulse response.

The coherence bandwidth B_c of the channel is determined by searching for the frequency separation f_1-f_2 for which the correlation $\rho(f_1-f_2)$ defined in (2.48) is equal to 1/2. The minimum frequency separation FSEP for which two frequency diversity signals are uncorrelated is then defined as

$$FSEP = B_c + BW \qquad (2.49)$$

where BW is the bandwidth of the transmitted signal.

2.5.7 Long-Term Variability Correlation Coefficient for Angle Diversity

The correlation coefficients defined in the previous section are ensemble averages over the short-term Rayleigh fading. The long-term power fading (variability) for the space and frequency diversity signals is assumed to be identical, i.e., correlation of unity, since they all share the same scattering volume and hence are all subject to the same long-term fluctuations. The same is not true however for angle diversity signals whose beams illuminate different scattering volumes.

It has been found that the long-term variability about the median for the upper and lower beams in an angle-diversity system is not always perfectly correlated. This is accounted for in TROPO by computing (subroutine LTCORR) an estimate of the correlation coefficient CORRLT for long-term variability as

$$\text{CORRLT} = \exp(\text{HDIF}*\text{CONST1})$$

where

HDIF = difference in heigh of bottoms of common volumes for upper and lower beams and CONST1 is an empirical constant.

From CORRLT, a correction factor CORFAC is computed according to

$$\text{CORFAC} = \left(\frac{1 + \text{CORRLT}}{2}\right)^{1/2} . \qquad (2.49)$$

This factor is then used multiplicatively to reduce the effective standard deviation of the long-term power fading of the angle diversity beams within the routine BERCAL.

2.6 DIFFRACTION PROPAGATION MODE

When mixed troposcatter-diffraction propagation is specified (PTYPE = 1), the program calculates all of the troposcatter propagation parameters described in Section 2.5 as well as the RSL and path loss yearly distribution of the diffraction signal. The program also calculates the relative delay between the earlier arriving diffraction signal and the troposcatter signal. However, no correlation calculations are needed because the diffraction signal is not a fading signal and hence the diffraction components of the signals received on space diversity antennas are perfectly correlated.

The diffraction path is assumed to be a multiple edge diffraction path such as that shown in Figure 2-7. The maximum number of edges allowed (NOBS) is three (3). The diffraction loss for paths with more than 3 edges will be much greater than the troposcatter loss and hence these paths can be treated as pure troposcatter paths. The analytical diffraction model is valid, however, for an arbitrary number of obstacles (i.e., edges). The obstacles can be treated as either knife-edge or rounded edges. Diffraction over a smooth or slightly irregular earth can be treated as diffraction over a single rounded obstacle. However at microwave frequencies the diffraction loss over the bulge of the earth is so large compared to the troposcatter loss that such paths should be treated as pure troposcatter paths.

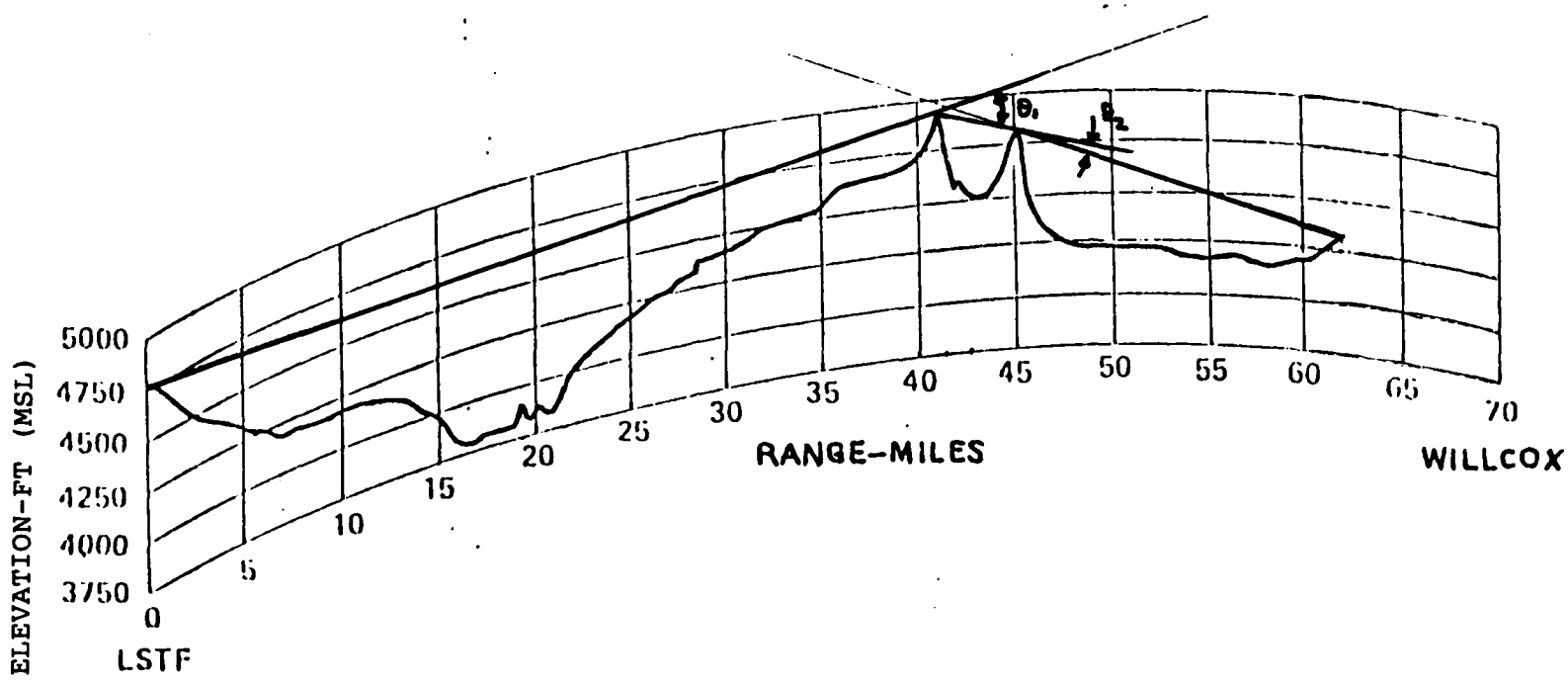

Figure 2-7 Path Profile: LSTF to WILLCOX

To calculate the diffraction path propagation parameters, the user must specify the number of diffracting edges (NOBS), their elevations above sea level (coded HL(1), ..., HL(NOBS)), their distances from the transmitter (coded DL(1), ..., DL(NOBS)) and a parameter called the 'effective horizontal extent' of the obstacle (coded DS(1), ..., DS(NOBS)) along the great circle plane which is used to determine whether the obstacle is a knife-edge or a rounded edge. The effective horizontal extent of the obstacle is defined as the distance between the points at which the diffraction ray path is tangent to the obstacle. If this distance DS is specified as zero the obstacle is a knife-edge. When DS is not zero, the obstacle is treated as a rounded edge with radius of curvature (coded RC (.) in subroutin MDIF) given by

$$R_c = DS/\theta_d \qquad (2.51)$$

where θ_d (coded ANG(.) in MDIF) is the angle of diffraction which is calculated in the program from the terrain data provided by the user. The diffraction loss can vary by as much as 15 dB/obstacle when the horizontal extent of the obstacle is varied from 0 (knife-edge) to 0.4 miles as seen from the curves of Figure 2-4 (double edge diffraction path) which indicates the importance of providing an accurate estimate of this parameter. Plotted path profiles such as that of Figure 2-7 are not detailed enough to allow us to get a good estimate of DS for each obstacle. Detailed topographic maps are needed to do so. However they may not always be available. If that is the case, a reasonable value for DS should be provided anyway keeping in mind that at microwave frequencies, most obstacles do not behave as knife-edges, and that horizontal extents greater than .4 miles may result in an overestimate of the path loss especially when the obstacles appear to be knife-edges on maps such as that of Figure 2-7.

The above terrain data as well as the great circle path distance D, transmit and receive site elevation above sea level, HTO and HRO respectively, transmitting and receiving antenna nominal heights, HT and HR respectively, and either the refractivity at sea level, SEAN, or an effective earth radius factor, ERFAC, provide sufficient information to calculate a reference path loss. The terrain between the obstacles is assumed to be rough so that ground reflections are not included in the calculation. It must not, however, have any prominent peaks which either obstruct or just touch the ray path. If that is the case, they should be treated as additional obstacles. Terrain features which do not obstruct the path should not be entered as obstacles as their effect on the path loss is considered statistically in the calculation of the long term variability of the diffraction path loss.

In order to determine the variability of the path loss about the reference value, the following additional terrain information is needed: average terrain elevation above sea level at the transmit and receive sites, AVETX and AVERX respectively, and the average terrain elevation above sea level at each obstacle site, HLAV(1), ..., HLAV(NOBS) respectively. These values need only be approximate and may be estimated from topographical data such as that obtained from Figure 2-7. However if accuracy is desired, the program can calculate the average terrain elevation at each obstacle site as well as at the transmit and receive sites from evenly-spaced terrain data between each obstacle, and between the first and last obstacle and the two terminals. The details of the calculation have been discussed earlier in Section 2.5.4. More details about the format of the terrain data to be supplied are given in the User's Manual Report. The program structure of the diffraction calculations is shown in Figure 2-8.

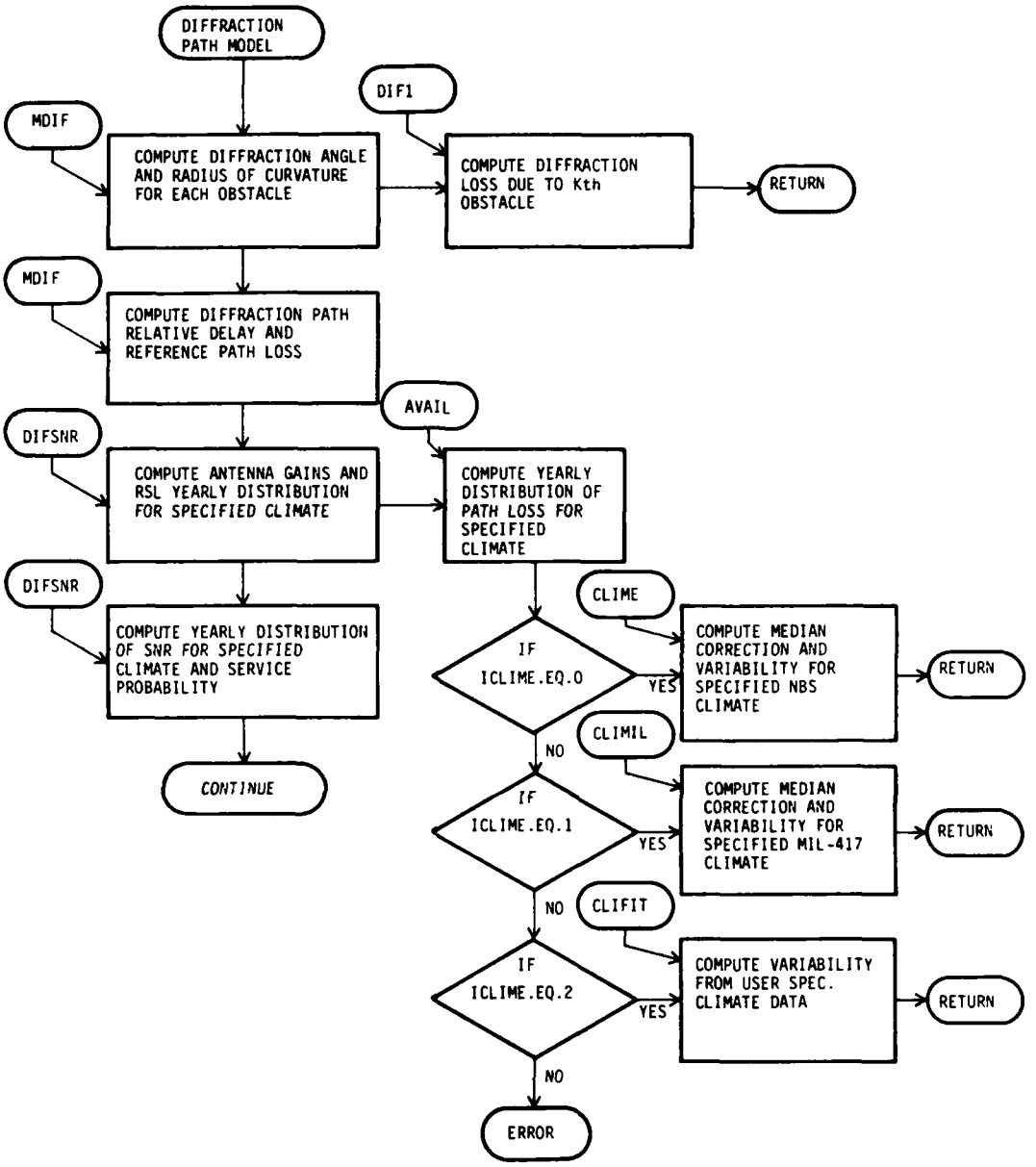

Figure 2-8 Flow Chart for Diffraction Propagation Parameter Calculations

2.6.1 RSL and Path Loss Distributions

Although the diffraction signal is not a fading signal, it exhibits long-term (yearly) variations.

The RSL exceeded q% of the year, P(q), which corresponds to the diffraction path loss not exceeded that same q% of the time, L(q), is defined as

$$P(q) = P_r + V(q) \quad \text{dBW}$$
$$L(q) = L_r - V(q) \quad \text{dB} \qquad (2.52)$$

where P_r and L_r are the reference RSL and reference path loss respectively, and V(q) is the variability of the diffraction signal about the reference. The variability V(q) can also be expressed as

$$V(q) = V(50) + Y_0(q) \quad \text{dB} \qquad (2.53a)$$

where V(50) is the median correction factor which, as in the troposcatter case, is climate zone and path length dependent, and $Y_0(q)$ is the variability about the median.

The variability of the diffraction signal is calculated by considering the diffraction path as a succession of line-of-sight paths, each of which exhibits independent long-term variations since the variations are terrain dependent and the terrain differs for each section of the path. The variability of each section of the diffraction path is calculated in the same manner as for the troposcatter path. Thus if the ray path is a double edge diffraction path as in Figure 2-7, the variability for each section of the path is given by

$$V_1(q) = V_1(50) + Y_1(q) \quad dB$$

$$V_2(q) = V_2(50) + Y_2(q) \quad dB$$

$$V_3(q) = V_3(50) + Y_3(q) \quad dB$$

where $V_1(50)$, $V_2(50)$ and $V_3(50)$ are median correction factors for each section of the path and $Y_1(q)$, $Y_2(q)$ and $Y_3(q)$ are the variability about the median. All of these parameters depend on the climate zone and an effective distance parameter, d_e, which depends on the terrain below the path and hence differs for each section of the path. The parameter d_e was defined earlier in Section 2.5.4.6.

The variability V(q) for the entire path is found by noting that the fraction of the year q for which the variability does not exceed V dB is by definition

$$q = Pr\{v < V\} = Pr\{v_1 + v_2 + v_3 < V\} \qquad (2.53b)$$

where v is a random variable whose distribution is q(V) and the inverse of the distribution V(q) is called the variability. Similarly v_1, v_2 and v_3 are random variables whose distributions are the inverse of the variabilities defined above for each section of the path. Thus it can be seen from (2.53b) that the distribution q(V) is found by convolving the distributions (actually by convolving the probability densities) $q(V_1)$, $q(V_2)$ and $q(V_3)$. The convolution of the densities is performed in subroutine CONVOL.

Prediction errors are accounted for in the same way as for the troposcatter signal by defining the diffraction RSL not exceeding q% of the year with (service) probability t as

$$P(q,t) = P(q,0.5) - T\sqrt{12.73 + .12\ Y_0^2(q)}$$

where P(q,0.5) is given by (2.52) and T is related to the service probability t by Equation (2.3b).

2.6.2 The Reference Diffraction Path Loss

As in the troposcatter propagation mode, the path loss L_r for diffraction paths is the loss in continental temperate climates during weak signal periods (winter afternoons). The diffraction signal is weakest when the sea level refractivity N_0 or the effective earth radius factor ERFAC reaches a minimum value. This can be seen from the diffraction loss curves as a function of the effective earth radius shown in Figure 2-4. Therefore in order to determine the reference path loss the user must ideally specify <u>either</u> the <u>minimum</u> monthly refractivity at sea level (SEAN) <u>or</u> the effective earth radius ERFAC corresponding to this value. The two parameters SEAN and ERFAC, are not independent as shown in Section 2.5.2. A world map of the minimum monthly sea level refractivity, SEAN, is shown in Figure 2-3. On the other hand, maps of the <u>minimum</u> monthly effective earth radius factor <u>are not</u> available. The user may however have knowledge of the yearly <u>median</u> value of the effective earth radius factor for the desired climate. Therefore TROPO assumes that either the <u>minimum</u> monthly value of the surface refractivity, SEAN, or the yearly median value of the effective earth radius factor, ERFAC, is supplied by the user. If both are specified, ERFAC is ignored and a

new value is computed from SEAN according to the relationships given in Section 2.5.2. Whenever SEAN is used to calculate the reference diffraction loss, climate dependent correction factors are required to estimate the yearly median path loss. The user may choose to use the yearly median value of the effective earth radius factor ERFAC for the climate of interest as a reference by specifying this value and specifying SEAN = 0. However, when the median value ERFAC is used as the basis for the reference path loss calculation no median correction factors are necessary because a great deal of the yearly variability in the diffraction loss is due to variability in the effective earth radius factor. This is clearly evident from the diffraction path loss curves for a double edge diffraction path shown in Figure 2-4 as a function of the effective earth radius factor.

The reference path loss $L_r = P_T G_T G_R / P_R$ is calculated in subroutine MDIF. When the path is a double diffraction path the received signal level P_R is calculated from

(2.54)

$$P_R = P_T G_T(\theta_T) G_R(\theta_R) A_b \left(\frac{\lambda}{4\pi d_1}\right)^2 \frac{|D_1(\theta_1)|^2}{kd_2} \frac{|D_2(\theta_1)|^2}{kd_3} \left(\frac{d_1}{d_1+d_2+d_3}\right)$$

where P_T is the transmitted power, $G_T(\theta_T) = G_T|g_T(\theta_T)|^2$ and $G_R(\theta_T) = G_R|g_R(\theta_R)|^2$ are the transmit and receive antenna gains at the transmit and receive horizon elevation angles, θ_T (i.e., THET) and θ_R (i.e., THER) respectively, $1/A_b$ is the atmospheric absorption loss defined earlier, d_1 is the great circle distance between the transmitter and the first obstacle, d_2 is the distance between obtacles, d_3 is the distance between the second obstacle and the receiver, $k = 2\pi f/c$, $D_1(\theta_1)$ and $D_2(\theta_2)$ are edge diffraction coefficients to be defined and which depend on the diffraction angles at the first obstacle, θ_1, and at the second

obstacle, θ_2, respectively. The factor proportional to d_1^{-2} accounts for the spherical spreading loss between the transmitter and the first obstacle. The factor proportional to D_1^2 accounts for the diffraction loss at the first obstacle and the factor d_2^{-1} accounts for the cylindrical spreading loss (elevation plane) from the first to the second obstacle. Similarly, the factor proportional to D_2^2 accounts for the diffraction loss due to the second obstacle and the factor d_3^{-1} accounts for the cylindrical spreading between the second obstacle and the receiver. The last term d_1/d where $d = d_1 + d_2 + d_3$ is a factor which accounts for the azimuthal spreading from the first obstacle to the receiver. The extension of (2.54) to an arbitrary number of obstacles should be obvious from the above description.

The diffraction coefficients D_1 and D_2 are dimensionless quantities which depend on the diffraction angles, θ_1 and θ_2, and the radii of curvature of the obstacles, R_1 and R_2, if modelled as rounded edges. They are given by

$$D_1(\theta_1) = \sqrt{\frac{kd_1(d_2+d_3)}{d_1+d_2+d_3}}\, f(\nu_1, \rho_1) \qquad (2.55a)$$

$$D_2(\theta_2) = \sqrt{\frac{kd_2d_3}{d_2+d_3}}\, f(\nu_2, \rho_2) \qquad (2.55b)$$

with

$$\nu_1 = |\theta_1| \sqrt{\frac{2d_1(d_2+d_3)}{\lambda(d_1+d_2+d_3)}} \qquad (2.55c)$$

$$\nu_2 = |\theta_2| \sqrt{\frac{\lambda d_2 d_3}{\lambda(d_2+d_3)}} \qquad (2.55d)$$

$$\rho_1 = \left(\frac{\lambda}{\pi} \frac{d_1+d_2+d_3}{d_1(d_2+d_3)}\right)^{1/2} \left(\frac{\pi R_1}{\lambda}\right)^{1/3} \qquad (2.55e)$$

$$\rho_2 = \left(\frac{\lambda}{\pi} \frac{d_2 + d_3}{d_2 d_3}\right)^{1/2} \left(\frac{\pi R_2}{\lambda}\right)^{1/3} \qquad (2.55f)$$

and $f(\nu,\rho)$ is the well known diffraction loss (loss above free-space loss) due to a single isolated rounded edge [Dougherty and Maloney, 1964], that is

$$A(\nu,\rho) = -20 \log|f(\nu,\rho)| = A(\nu,0) + A(0,\rho) + U(\nu\rho) \qquad (2.56a)$$

where

$$A(\nu,0) = -10 \log\{\tfrac{1}{2}\,[f^2(\nu) + g^2(\nu)]\}, \quad \nu > 0 \qquad (2.56b)$$

$$f(\nu) = \frac{1 + .926\nu}{2 + 1.792\nu + 3.104\nu^2}$$

$$g(\nu) = \frac{1}{2 + 4.142\nu + 3.492\nu^2 + 6.67\nu^3}$$

$$A(0,\rho) = 6.02 + 7.192\ \rho - 2.018\ \rho^2 + 3.63\ \rho^3 - 0.754\ \rho^4 \text{ dB} \qquad (2.56c)$$

$$U(\nu\rho) = \begin{cases} -6.02 - 6.7\ \nu\rho + (43.6 + 23.5\ \nu\rho)\log(1+\nu\rho), & \nu\rho < 2 \\ -14.13 + 22\ \nu\rho - 20 \log \nu\rho\ , & \nu\rho \geq 2 \end{cases}$$

(2.56d)

The first term in (2.56a), i.e., $A(\nu,0)$ (coded AV in subroutine DIF1), is the diffraction loss due to an ideal knife-edge. The second term, $A(0,\rho)$ (coded ARH0 in DIF1) is the diffraction loss due to a rounded edge at grazing incidence. The last term, $U(\nu\rho)$ (coded UVR in DIF1), accounts for the additional losses due to propagation along the surface of the rounded edge. The polynomial approximations for the diffraction loss due to a rounded edge are similar but differ from those used in NBS Technical Note 101 [P.L. Rice, et al., 1967] in that they incorporate newer more accurate approximations obtained by Dougherty and Wilkerson [1967].

If we substitute (2.55) into (2.54), we can express the reference path loss L_r in terms of the diffraction losses $f_1 = f(\nu_1, \rho_1)$ and $f_2 = f(\nu_2, \rho_2)$ as

$$\frac{1}{L_r} = \frac{P_R}{P_T G_T G_R} = A_b \left(\frac{\lambda}{4\pi d_1}\right)^2 \left(\frac{d_1(d_2+d_3)}{d_2(d_1+d_2+d_3)}\, f_1^2\right)\left(\frac{d_2}{d_2+d_3}\, f_2^2\right)\left(\frac{d_1}{d_1+d_2+d_3}\right)$$

$$= A_b \left(\frac{\lambda}{4\pi d}\right)^2 f_1^2\, f_2^2 \qquad (2.58)$$

where $d = d_1 + d_2 + d_3$. The factor $(\lambda/4\pi d)^2$ in (2.57) is the free-space loss, while f_1^2 and f_2^2 are the diffraction losses due to each obstacle. The above expression is in agreement with the Fresnel-Kirchoff theory for double knife-edge diffraction [Millington, et al., 1962] when at least one of the diffraction angles is large. When both diffraction angles are small, the diffraction loss predicted by (2.57) is slighty pessimistic by less than 3 dB. The results presented here are valid for the case of diffraction by two rounded edges but can be generalized in a straightforward manner to an arbitrary number of edges. Since the Fresnel parameters ν_1 and ν_2 (arguments of f_1 and f_2) are defined as positive quantities (see Equation (2.55)), it should be pointed out that (2.54) and (2.57) apply only when the diffraction angles are positive (Figure 2-9a).

If one or more of the diffraction angles is negative (e.g., Figure 2-9b), the expression for the received signal consists of the sum of a number of rays some of which have undergone single scattering (from the first or second edge), double scattering

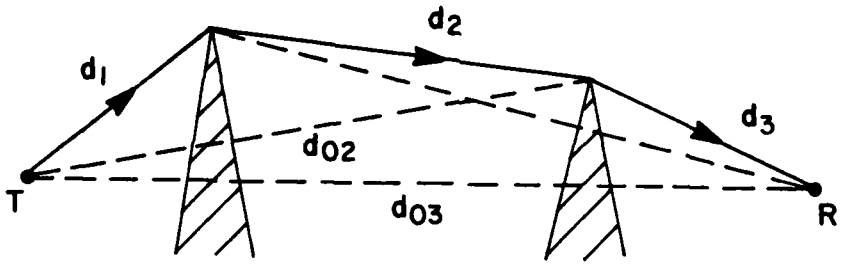

(A)

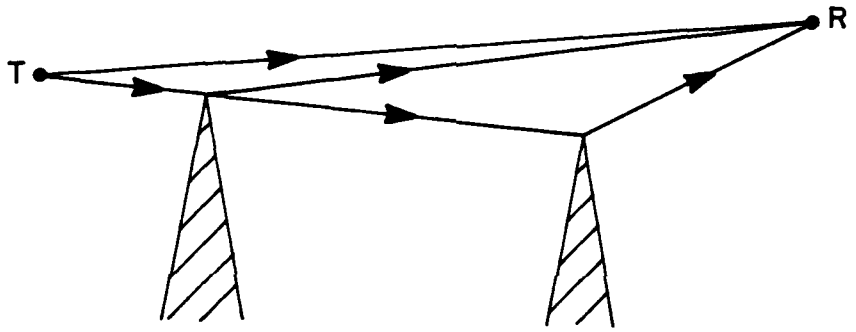

(B)

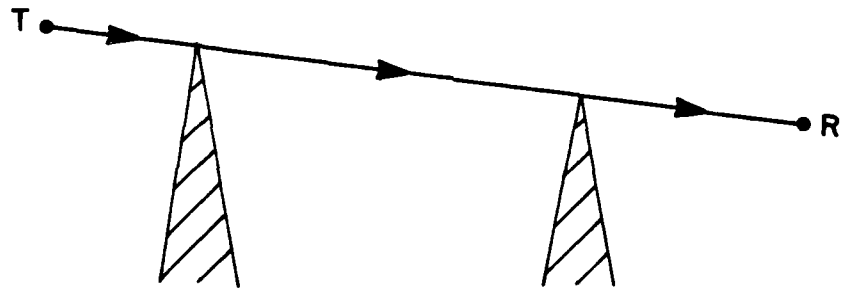

(C)

Figure 2-9 Double Edge Diffraction Path

(from the first and second edge) or no scattering at all (direct ray). The TROPO program does not consider situations such as this where there is a line-of-sight path.

2.6.3 The Diffraction Path Delay

The delay of the diffraction path $t_r = (d_1+d_2+d_3+...)/c$, where c is the speed of light, is calculated using purely geometric considerations (subroutine MDIF) by summing the lengths of the segments of the ray path the signal must traverse to be diffracted over the obstacles. However in order to avoid round-off errors the delay relative to the slant path (straight line connecting transmitter and receiver) is calculated and this value is printed out along with the short-path delay. More specifically TROPO calculates the distances (See figure 2.9a)

$$S_1 = d_1 + d_2 - d_{02}$$

$$S_2 = d_{02} + d_3 - d_{03}$$

.
.
.

$$S_k = d_{0,k} + d_{k+1} - d_{0,k+1}$$

where k is the number of edges, d_{0k} is defined as the slant path range and the delay relative to the slant path delay is defined as

$$t_r = \frac{1}{c} \sum_{i=1}^{k} S_k = \frac{1}{c} \left[\sum_{i=1}^{k} d_i - d_{0,k+1} \right]. \qquad (2.58)$$

The delay calculation of the diffraction path accounts for the free-space travel time between the transmitter and the obstacles and the receiver and does not account for the slower propagation velocity when the signal propagates over a rounded obstacle. The latter effect is small relative to the delay difference between the diffracted signal and the average delay of the troposcatter signal. The average delay of the troposcatter signal relative to the diffraction path delay is printed out in the summary output.

2.7 TRANSMITTER AND RECEIVER FILTER CALCULATIONS

TROPO provides the facility for predicting the performance of the MD-918 and AN/TRC-170/DAR modems or any user supplied modem taking into account the effects of the transmitter and receiver filters. Prior to calculating the performance of the MD-918 or AN/TRC-170/DAR Modems, TROPO calculates all the transmitter and receiver parameters required for the calculation of the modem performance in subroutine BUTFIL. A block diagram of the filter calculations performed is shown in Figure 2-10. Filter calculations are performed only when the parameter IBW > 0.

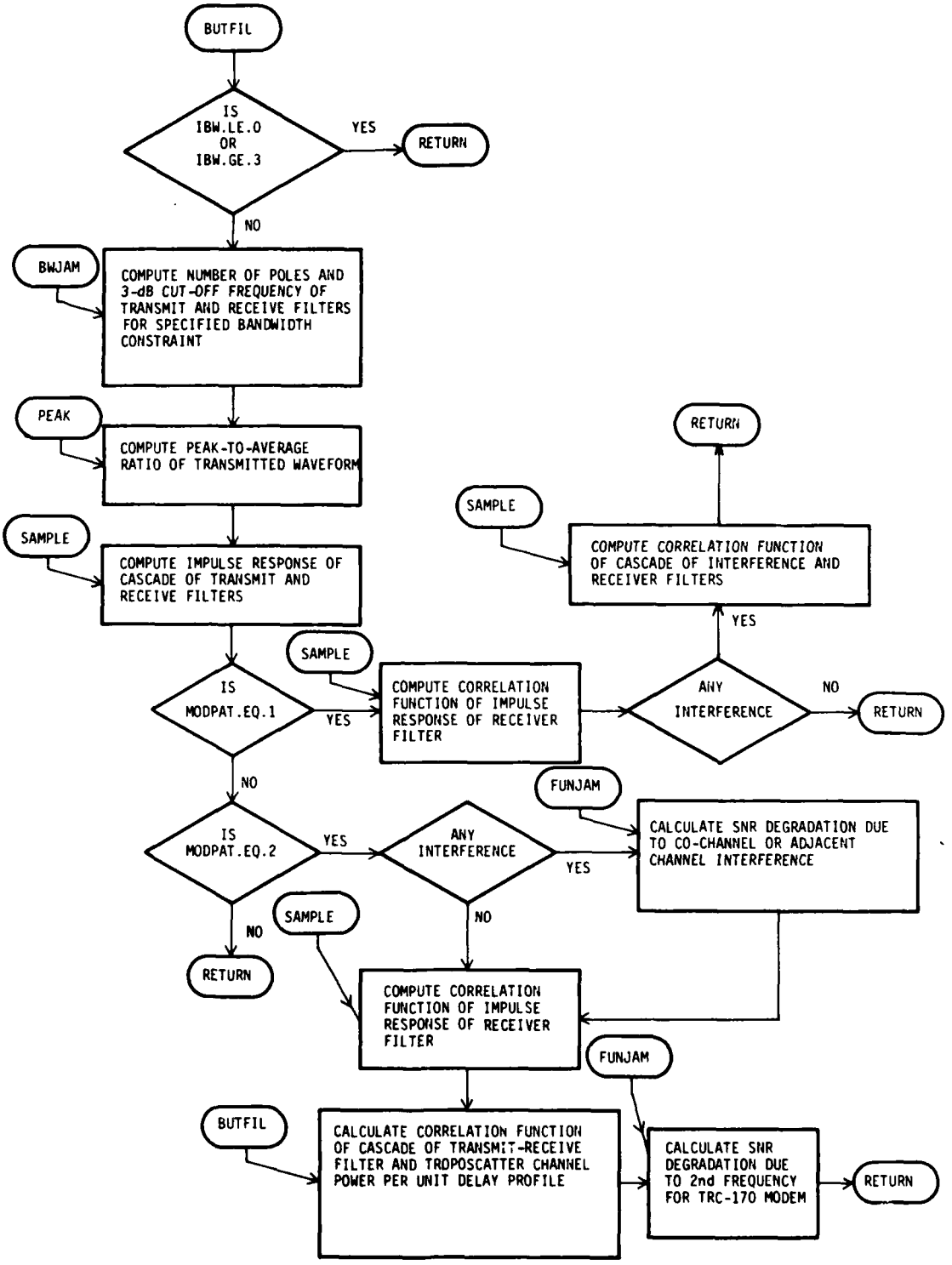

Figure 2-10 Flow Chart for Filter and Interference Effects Calculations

The transmitter filters for the MD-918 and AN/TRC-170/DAR modems consists of the cascade of the intermediate frequency (IF) filter with the baseband pulse shaping filters (rectangular impulse response with duration equal to T).* The RF filter is an N-pole Butterworth filter so that the baseband power spectrum of the transmitted signal is given by

$$S(f) = \left|B_N(f/f_c)\right|^2 \text{ sinc}^2 \text{ Tf} \qquad (2.59)$$

where $B_N(f/f_c)$ is the baseband transfer-function of the N-pole Butterworth filter with 3 dB cut-off frequency f_c (half of 3-dB bandwidth), i.e.,

$$B_N(f/f_c) = \frac{1}{1 + j(f/f_c)^N} \qquad (2.60)$$

and

$$\text{sinc}(Tf) = \frac{\sin(\pi Tf)}{\pi Tf} \quad . \qquad (2.61)$$

The number of poles and the 3 dB cut-off frequency can be specified by the user (IBW = 3) or be calculated by the program to achieve the necessary filtering so that either 99% of the power is within the specified bandwidth (IBW = 1), or to meet the

* NOTE: TROPO only accounts for the IF spectrum constraint filtering in the modem. No degradation effects of radio upconverter/downconverter or Klystron power amplifier nonlinearity are modeled.

FCC-19311 mask for the specified bandwidth (IBW = 2). If IBW = 0 is specified, the program assumes that there is no RF filtering in the transmitter. The baseband pulse duration T is defined as

$$T = \begin{cases} 2/R_c & \text{for MD-918 Modem} \\ 1/R_c & \text{for AN/TRC-170 and DAR Modems} \end{cases} \qquad (2.62)$$

where R_c is equal to the data rate for the AN/TRC-170 and DAR modems. For the MD-918 modem,

$$R_c = K_c R, \; K_c > 1$$

where R is the data rate and K_c is the integer part of the ratio of the bandwidth, B, to the data rate, R. That is, K_c is the number of chips per data bit. TROPO assumes that when the data rate specified by the user is less than one-half the specified bandwidth, the MD-918 uses a PN sequence to expand the bandwidth and exploit the implicit diversity of the troposcatter channel. The present version of TROPO calculates the performance of the AN/TRC-170 for bandwidths not greater than four times the data rate.

The impulse response of the transmitted waveform is given by

$$h_T(t) = \int_{-\infty}^{\infty} B_N(f/f_c)\text{sinc } Tf \; e^{-j2\pi ft} df \qquad (2.63)$$

and the peak-to-average ratio is defined as

$$\text{PEAKAV} = \max_{0<t<T} \frac{|h(t)|^2}{\int_{-\infty}^{\infty} |h(t')|^2 dt'} \quad . \tag{2.64}$$

2.7.1 Receiver Filtering

The receiver filters for the MD-918 consist of the cascade of a Butterworth filter and a filter matched to the baseband pulse shape of the transmitted waveform (rectangular impulse response of duration T). The number of poles and the 3-dB cut-off frequency, f_c, of the receiver Butterworth filter are specified by the user when IBW = 3. Otherwise (IBW = 1 or 2) the Butterworth filter is a 4 pole filter with 3-dB cut-off frequency given by

$$f_c = 0.5B \tag{2.65}$$

where B is the bandwidth specified by the user.

The receiver filtering for the DAR modem consists of a 4-pole Butterworth filter and 3-dB cut-off frequency $f_c = B$ while the receiver filtering for the AN/TRC-170 modem consists of a 6-pole Butterworth filter with 3-dB cut-off frequency equal to that of the transmitter filter.

When adjacent channel interference calculations are desired the number of poles and 3-dB cut-off frequency of the receiver Butterworth filter for the MD-918, DAR and AN/TRC-170 modems are calculated so that the SNR degradation of the adjacent channel interference is less than 1 dB.

The impulse response of the cascade of the transmitter and receiver filters is defined as

$$f(t) = \int_{-\infty}^{\infty} H_T(f)\, H_R(f) e^{-j2\pi ft} df \qquad (2.66)$$

where $H_T(f)$ and $H_R(f)$ are the baseband transfer functions (Fourier transform of impulse response) of the transmitter and receiver filters.

The correlation function of the receiver filter is defined as

$$f_R(t) = \int_{-\infty}^{\infty} |H_R(f)|^2 e^{-j2\pi ft} df \qquad (2.67)$$

2.7.2 *Interference Correlation Calculations*

The correlation function of the cascade of the interfering signal and the receiver filters is defined as

$$g(t) = \int_{-\infty}^{\infty} |H_R(f)|^2 [P_I(f-f_s) + P_I(f+f_s)] e^{-j2\pi ft} df \qquad (2.68)$$

where $H_R(f)$ is the baseband transfer function of the receiver filter, $P_I(f)$ is the baseband power spectrum of the interfering signal, and f_s is the frequency separation between the center frequencies (carrier) of the transmitted signal and the interfering signal.

When the interfering signal is an FDM/FM signal (MODSIG=0), the baseband power spectrum of the interferring signal is assumed to be of the form

$$P_I(f) = \frac{1}{\sqrt{\pi}\, f_0} e^{-f^2/f_0^2} \tag{2.69}$$

with

$$f_0 = \frac{B_I}{2.577\sqrt{2}} \tag{2.70}$$

and where B_I is the 99% bandwidth of the interfering signal.

When the interfering signal is a QPSK signal (MODSIG=1), the baseband power spectrum of the interfering signal is assumed to be of the form

$$P_I(f) = \frac{1}{1 + (f/f_c)^{2N}} \operatorname{sinc}^2(2f/B_I) \tag{2.71}$$

where the number of poles N=2 and the 3-dB cut-off frequency f_c are calculated so that 99% of the interference power is within the bandwidth B_I.

2.8 MD-918 MODEM PERFORMANCE

When the MD-918 modem is selected (MODPAT = 1 in the input file), TROPO calculates the short-term average bit error rate, 1000 bit block error rate, fade outage probability and fade outage per call minute* (coded BERAV, SUM2, PFD and FOMIN in subroutine BERCAL), given the troposcatter power per unit delay profiles and the correlation between diversity branches, as a function of the average (short-term) signal-to-noise ratio $\overline{E}_b/N_0$ (i.e., energy per bit/noise spectral noise). A numerical integration over the long term variability in average signal-to-noise ratio then gives the yearly average fade outage probability and the yearly average fade outage per call minute, assuming log-normal long-term fading statistics for the troposcatter signal and the diffraction signal (if mixed mode propagation is indicated).

The MD-918 employs an adaptive Decision Feedback Equalizer (DFE) to process the received signal. The DFE consists of an Adaptive Forward Equalizer (AFE) filter for each diversity input and an Adaptive Backward Equalizer (ABE) filter, both of which are tapped delay lines. A block diagram of the MD-918 is shown in Figure 2-11. The ABE filter has 3 taps with spacing equal to a QPSK symbol duration (twice the inverse of the data rate) while each of the AFE filters has 3 taps with spacing equal to 1/2 of the QPSK symbol duration. The ABE filter removes the intersymbol interference (ISI) due to the past 3 symbols. The TROPO program assumes that the ISI due to all the other past symbols is negligible when the received signal consists of a pure troposcatter signal. When mixed troposcatter/diffraction paths are specified,

* NOTE: The fade outage probability and fade outage per call minute are defined later in this section.

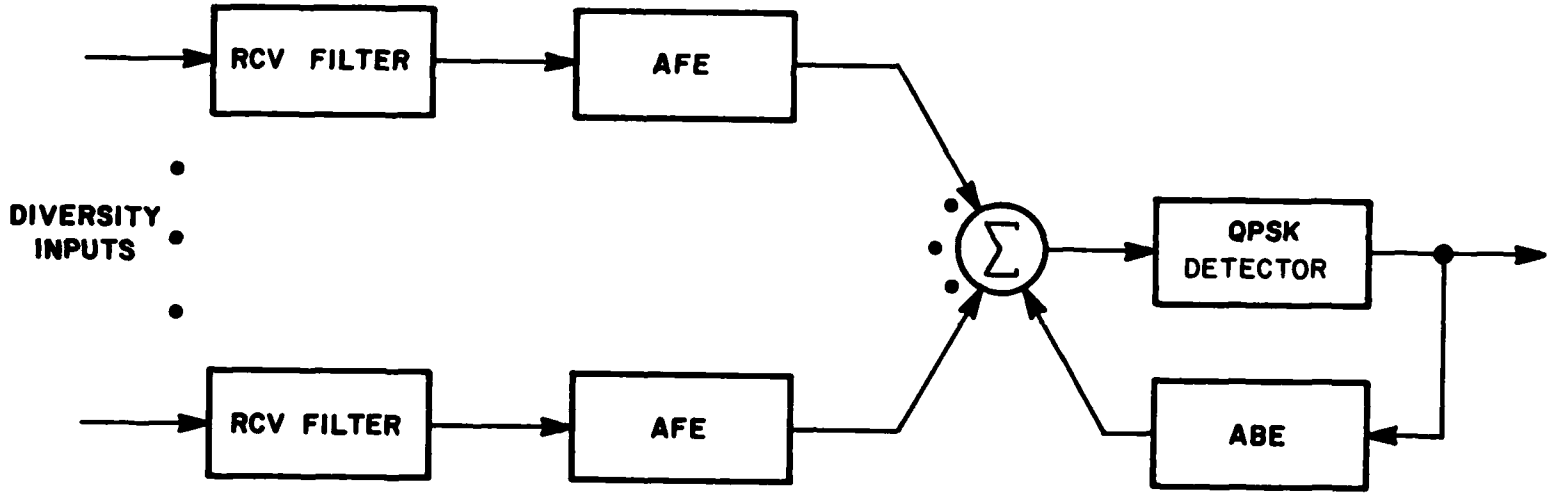

Figure 2-11 MD-918 Receiver Structure

the TROPO program accounts in the calculations for the ISI due to the fourth and fifth past symbols, which are not cancelled by the backward equalizer, in addition to the ISI due to a specified number (LISI) of future symbols. The AFE filters combine the explicit diversity branches, remove ISI due to future symbols and provide some implicit diversity gain when the tap outputs are uncorrelated. The modem performance depends on the number of (explicit) diversity branches (space, frequency, angle, etc.), number of AFE filter taps (fixed equal to 3) the tap spacing and the ratio of the data rate to the bandwidth. Although the tap-spacing is fixed in the MD-918, the user has the option of specifying the normalized tap spacing (default = 0.5) as well as the number of future symbols which are to be included in the ISI calculation (default = 2) and the diversity configuration (see Section 2.5.6). The data rates DRATE (in bits per second) for which modem performance calculations are allowed must satisfy

$$\frac{BW}{30} < DRATE < 2BW$$

where BW is the bandwidth in Hz. In the remainder of this section we present an overview of the analytical models used to calculate the various performance measures. The main routine for the calculation of the MD-918 performance is subroutine MDTS. A block diagram of the main calculations performed is shown in Figure 2-12.

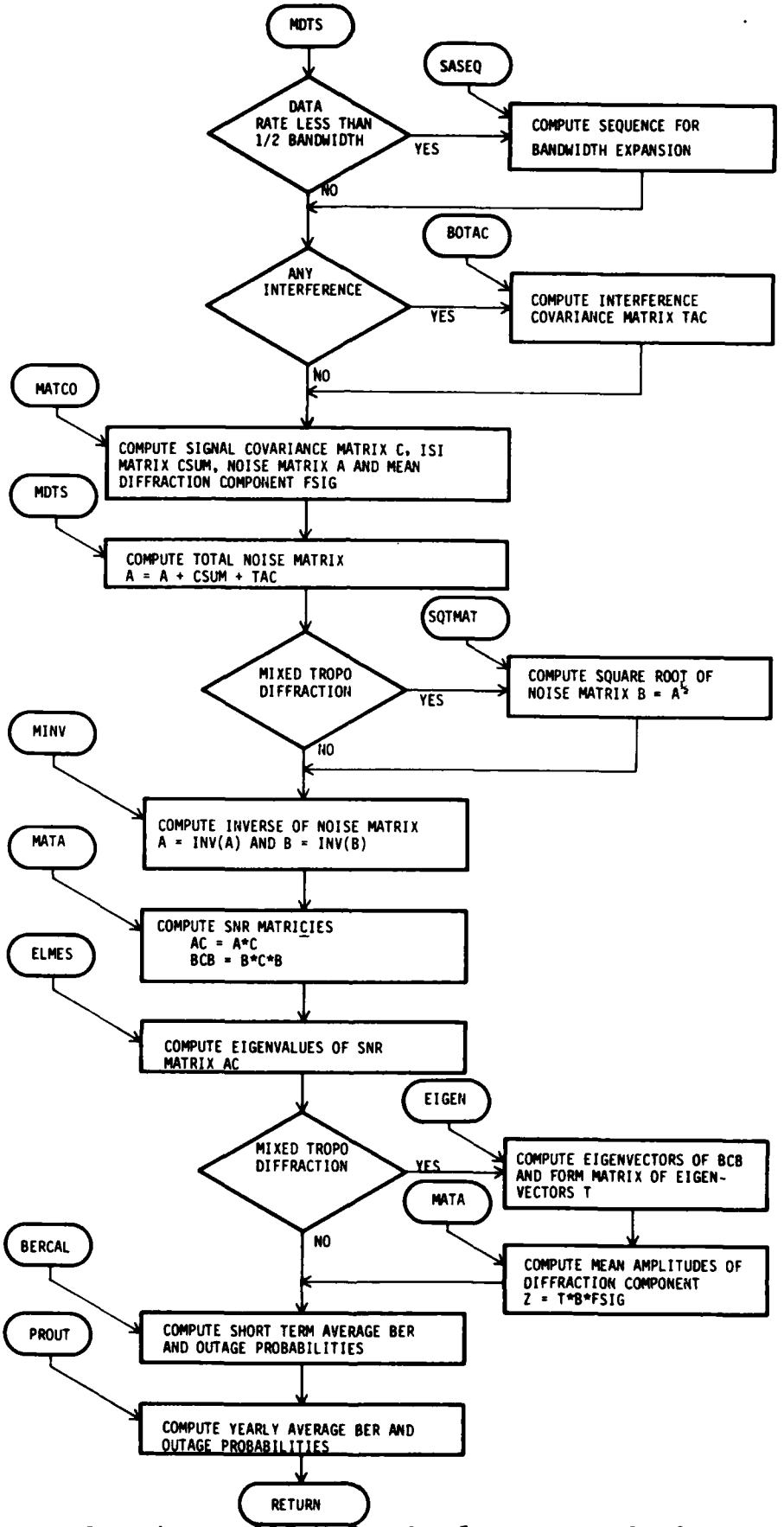

Figure 2-12 Flow Chart for the MD-918 Modem Performance Calculations

2.8.1 Short-Term Performance

2.8.1.1 Short-Term Average Bit Error Rate, Troposcatter Propagation

When the received signal is a pure troposcatter signal, the short-term average bit error rate is calculated by averaging the instantaneous bit error rate over the Rayleigh statistics of the troposcatter signal.

At a particular instant of time, the instantaneous bit error rate of the MD-918 modem is well approximated by* [Monsen, 1977]

$$P_e = \frac{1}{2} e^{-\rho} \tag{2.72}$$

where ρ is the effective instantaneous signal-to-noise ratio after equalization.

The effective signal-to-noise ratio is a random variable given by the sum [Equations 19 and 33, Monsen, 1977]

$$\rho = \frac{\overline{E_b}}{N_0} \sum_{i=1}^{N} |\alpha_i|^2 \tag{2.73}$$

* The DPSK error rate characteristic is a good approximation to the MD-918 BER performance at low error rates.

where N = IxK, I is the number of implicit diversity channels (i.e., number of taps in the adaptive-forward-equalizer) and K is the number of explicit diversity channels (i.e., space, frequency or angle diversity channels), $\overline{E_b}/N_0$ is the average signal-to-noise ratio per bit per explicit diversity branch and the α_i are independent zero-mean complex Gaussian random variables with variance

$$\overline{|\alpha_i|^2} = \lambda_i \quad , \quad i = 1, \ldots, N \tag{2.74}$$

where the λ_i are eigenvalues of the non-symmetric SNR matrix $A^{-1}C$. The matrix C is the received signal covariance matrix whose diagonal elements represent the average signal power per diversity (implicit and/or explicit) branch and the off-diagonal elements are proportional to the correlation between the implicit (taps) and explicit diversity branches [Monsen, 1977]. The covariance matrix C is normalized so that the total power per explicit diversity is unity. The matrix A is the total noise covariance matrix and is equal to the sum

$$A = A_T + \frac{\overline{E_b}}{N_0} A_{ISI} + \frac{N_J}{N_0} A_I \tag{2.75}$$

where A_T is the receiver thermal noise covariance matrix normalized to unity noise power density (its elements are a function of the impulse response of the receiver filters), A_{ISI} is the non-symmetrical covariance matrix of the future intersymbol in-

terference*, N_J is the effective interference power density (co-channel or adjacent channel) in the bandwidth of interest, N_0 is the thermal noise power density and A_I is the covariance matrix of the interference signal whose diagonal elements represent the interference signal power (in the bandwidth of interest) per diversity branch relative to the thermal noise power and the off-diagonal elements are proportional to the correlation between the interference on the various diversity branches.

The short-term average bit error rate is then found by performing the averaging over the statistics of ρ, i.e.,

$$\overline{P_e} = \frac{1}{2} \int_0^\infty e^{-x} f(x/\overline{E}_b/N_0)\, dx = \frac{1}{2} F(1/\overline{E}_b/N_0) \qquad (2.76)$$

where $f(x/\overline{E}_b/N_0)$ is the probability density function of the effective SNR, ρ, conditional on a fixed value of the average SNR per bit, $\overline{E}_b/N_0$ and $F(s/\overline{E}_b/N_0)$ is its Laplace transform, i.e.,

$$F(s/\overline{E}_b/N_0) = \int_0^\infty f(x/\overline{E}_b/N_0) e^{-sx}\, dx \quad .$$

The Laplace transform of the conditional pdf for ρ can be found analytically by noting that the random variable α_i is Rayleigh distributed and hence $|\alpha_i|^2$ has an exponential pdf whose Laplace transform is

* The past ISI is assumed to be cancelled by the backward equalizer in the MD-918.

$$F_i(s) = (1 + \lambda_i s)^{-1} .$$

Since the $|\alpha_i|^2$ are independent, the Laplace transform of the conditional pdf for ρ is

$$F(s/\overline{E}_b/N_0) = \sum_{i=1}^{N} (1 + \frac{\overline{E_b}}{N_0} \lambda_i s)^{-1} . \qquad (2.77)$$

The short-term average bit error rate can then be found from (2.76) and (2.77) for a given value of $\overline{E_b}/N_0$ provided the eigenvalues λ_i can be found.

The eigenvalues λ_i are evaluated in the TROPO program (subroutine MDTS) by making certain simplifying assumptions in order to reduce the computational load. In general, one must find N = IxK eigenvalues of the NxN SNR matrix $A^{-1}C$. For large explicit diversity (e.g., for 2S/2F/2A K = 8) and a three-tap forward equalizer (I=3) a rather large matrix results (24x24 in this example). To avoid unnecessary computations, use is made of the fact that the matrix has a redundant block structure whenever two or more of the explicit diversity branches are uncorrelated. Furthermore if two or more uncorrelated explicit diversity branches have equal average received power and equal delay spreads, they will have identical implicit diversity eigenvalues $\lambda_i \overline{E}_b/N_0$. The block structure of the SNR matrix $A^{-1}C$ will vary from one diversity configuration to another and hence so will the eigenvalues.

When only one antenna is used to transmit and two spaced antennas are used to receive (DIVTYP=0) there are four possible diversity configurations depending on whether frequency and/or angle diversity are used in conjunction with space diversity. The possible diversity configurations are: dual space (2S), dual space/dual frequency (2S/2F), dual space/dual angle (2S/2A), and dual space/dual angle/dual frequency diversity (2S/2A/2F). If the antennas are spaced far enough apart and the frequency diversity separation is greater than the sum of the bandwidth and the coherence bandwidth of the troposcatter channel, then the space diversity and frequency diversity channels are uncorrelated. The angle diversity channels are correlated, however, because the two receive antenna beams overlap. Thermal noise is uncorrelated on all explicit diversities. Thus, in the absence of any interfering signal (co-channel or adjacent), the SNR matrix for these four diversity configurations have the following block structure:

For 2S:

$$A^{-1}C = \begin{bmatrix} C_{11} & 0 \\ 0 & C_{22} \end{bmatrix}$$

For 2S/2F:

$$A^{-1}C = \begin{bmatrix} C_{11} & 0 & 0 & 0 \\ 0 & C_{12} & 0 & 0 \\ 0 & 0 & C_{21} & 0 \\ 0 & 0 & 0 & C_{22} \end{bmatrix}$$

For 2S/2A:

$$A^{-1}C = \begin{bmatrix} C_{11}(A_{11}) & C_{11}(A_{12}) & 0 & 0 \\ C_{11}(A_{12}) & C_{11}(A_{22}) & 0 & 0 \\ 0 & 0 & C_{22}(A_{11}) & C_{22}(A_{12}) \\ 0 & 0 & C_{22}(A_{12}) & C_{22}(A_{22}) \end{bmatrix}$$

For 2S/2A/2F:

$$A^{-1}C=\begin{bmatrix} C_{11}(A_{11}) & C_{11}(A_{12}) & 0 & 0 & 0 & 0 & 0 & 0 \\ C_{11}(A_{12}) & C_{11}(A_{22}) & 0 & 0 & 0 & 0 & 0 & 0 \\ 0 & 0 & C_{12}(A_{11}) & C_{12}(A_{12}) & 0 & 0 & 0 & 0 \\ 0 & 0 & C_{12}(A_{12}) & C_{12}(A_{22}) & 0 & 0 & 0 & 0 \\ 0 & 0 & 0 & 0 & C_{21}(A_{11}) & C_{21}(A_{12}) & 0 & 0 \\ 0 & 0 & 0 & 0 & C_{21}(A_{12}) & C_{21}(A_{22}) & 0 & 0 \\ 0 & 0 & 0 & 0 & 0 & 0 & C_{22}(A_{11}) & C_{22}(A_{12}) \\ 0 & 0 & 0 & 0 & 0 & 0 & C_{22}(A_{12}) & C_{22}(A_{22}) \end{bmatrix}$$

where $C_{ij}(A_{11})$ and $C_{ij}(A_{22})$ are 3x3 SNR covariance matrices for the three equalizer taps corresponding to the lower beam (A_{11}) and upper beam (A_{22}) of the i'th space diversity receiving antenna at the j'th frequency diversity. $C_{ij}(A_{12})$ is a 3x3 matrix whose elements are proportional to the cross-correlation between the signals on the three taps in the upper and lower beams of the ith space diversity antenna at the jth frequency diversity.

Since the average signal-to-noise ratio, E_b/N_0, is identical for the two space diversities and/or the two frequency diversities, the redundant block structures of the SNR matrix $A^{-1}C$ show that 2S and 2S/2F have 3 distinct eigenvalues (one for each tap) while 2S/2A and 2S/2A/2F have 6 distinct eigenvalues (3 for the lower beam taps and 3 for the upper beam taps).

The block structures shown above apply only in the absence of any interfering signal. When a co-channel or adjacent channel interferer is present, the interference on the two spaced antennas is correlated so that in general the SNR matrix will not have the simple structure indicated above. Because of the com-

plexity involved in analyzing all possible diversity configurations in the presence of interference, we have concentrated on modelling the effects of the interference on 2S/2F diversity configurations only. The SNR matrix structure for this diversity configuration is in this case

$$A^{-1}C = \begin{bmatrix} C_1(S_{11}) & C_1(S_{12}) & 0 & 0 \\ C_1(S_{12}) & C_1(S_{22}) & 0 & 0 \\ 0 & 0 & C_2(S_{11}) & C_2(S_{12}) \\ 0 & 0 & C_2(S_{12}) & C_2(S_{22}) \end{bmatrix}$$

where $C_j(S_{11})$ and $C_j(S_{22})$ are 3x3 SNR covariance matrices for the three taps corresponding to the space diversity antennas 1 and 2, respectively, at the jth frequency. $C_j(S_{12})$ is a 3x3 matrix whose elements are proportional to the cross correlation between the taps for Antenna 1 and the taps for Antenna 2. The interference is assumed to be uncorrelated at the two frequency diversities. The number of distinct eigenvalues for the 2S/2F diversity configuration in the presence of an interfering signal is 6.

When only one antenna is used to transmit and receive (DIVTYP=1), there are three possible diversity configurations: dual angle (2A), dual frequency (2F) and dual frequency/dual angle diversity (2F/2A). The SNR matrix structure for these three diversity configurations is (assuming no interference)

For 2A:

$$A^{-1}C = \begin{bmatrix} C_1(A_{11}) & C_1(A_{12}) \\ C_1(A_{12}) & C_1(A_{22}) \end{bmatrix}$$

For 2F:

$$A^{-1}C = \begin{bmatrix} C_1(A_{11}) & 0 \\ 0 & C_2(A_{11}) \end{bmatrix}$$

For 2F/2A:

$$A^{-1}C = \begin{bmatrix} C_1(A_{11}) & C_1(A_{12}) & 0 & 0 \\ C_1(A_{12}) & C_1(A_{22}) & 0 & 0 \\ 0 & 0 & C_2(A_{11}) & C_2(A_{12}) \\ 0 & 0 & C_2(A_{12}) & C_2(A_{22}) \end{bmatrix}$$

where $C_j(A_{11})$ and $C_j(A_{22})$ are 3x3 SNR matrices for the taps of the lower and upper beams, respectively, at the jth frequency diversity and $C_j(A_{12})$ is a 3x3 cross-correlation matrix for the

taps of the lower and upper beams. These block structures indicate that there are 3 district eigenvalues for 2F and 6 distinct eigenvalues for 2A and 2F/2A.

Finally when two antennas are used to transmit the same information on orthogonal polarizations, and both polarizations are received on two spaced antennas (DIVTYP=2), there are two possible diversity configurations: dual space/dual polarization (2S/2P) and dual space/dual polarization/dual angle (2S/2P/2A). In the 2S/2P case there are four paths, two of which (paths 1 and 4 are called the parellel paths (see Figure 2-6), and two of which (paths 2 and 3) cross each other. Analysis of this diversity configuration has shown that only the crossing paths are correlated. The block structure of the SNR matrix for 2S/2P and 2S/2P/2A, assuming no interference, is:

For 2S/2P:

$$A^{-1}C = \begin{bmatrix} C_{11} & 0 & 0 & 0 \\ 0 & C_{22} & C_{23} & 0 \\ 0 & C_{23} & C_{33} & 0 \\ 0 & 0 & 0 & C_{44} \end{bmatrix}$$

For 2S/2P/2A:

$$A^{-1}C = \begin{bmatrix} C_{11}(A_1) & 0 & 0 & 0 & 0 & 0 & 0 & 0 \\ 0 & C_{22}(A_1) & C_{23}(A_1) & 0 & 0 & 0 & 0 & 0 \\ 0 & C_{23}(A_1) & C_{33}(A_1) & 0 & 0 & 0 & 0 & 0 \\ 0 & 0 & 0 & C_{44}(A_1) & 0 & 0 & 0 & 0 \\ 0 & 0 & 0 & 0 & C_{11}(A_2) & 0 & 0 & 0 \\ 0 & 0 & 0 & 0 & 0 & C_{22}(A_2) & C_{23}(A_2) & 0 \\ 0 & 0 & 0 & 0 & 0 & C_{23}(A_2) & C_{33}(A_2) & 0 \\ 0 & 0 & 0 & 0 & 0 & 0 & 0 & C_{44}(A_2) \end{bmatrix}$$

where the diagonal "elements" are 3x3 SNR matrices for the taps of each explicit diversity path and the off diagnonal 'elements' are 3x3 cross correlation matrices for the taps of the crossing paths. The number of distinct eiginvalues for 2S/2P is 9 (paths 1 and 4 have identical eigenvalues) while 2S/2P/2A has 18 distinct eigenvalues.

2.8.1.2 Short Term Average Bit Error Rate, Mixed-Mode Propagation

When a specular component due to diffraction is introduced, the average bit error rate is calculated as follows. Let $\underline{q}_i$ be a vector whose elements represent samples of the signal component of the received signal. The signal vector $\underline{q}_i$ has the general form

$$\underline{q}_i = \{q(t_0 - iT - k\tau)\}_{k=-K_1}^{K_2} \qquad (2.78)$$

where τ is the tap spacing on the AFE filter, T is the source symbol interval, t_0 is the sampling time and the subscript i denotes the ith transmitted symbol. The number of equalizer taps is $K = K_1 + K_2 + 1$. The function q(t) is defined in terms of the impulse responses of the transmit filter, $f_T(t)$, the receive filter $f_R(t)$, and the channel impulse response, h(t). We have

$$q(t) = \bar{E}_b^{1/2} \int_{-\infty}^{\infty} f(t-t')h(t')dt', \quad f(t) = \int_{-\infty}^{\infty} f_T(t')f_R(t-t')dt' \tag{2.79}$$

If a_D and a_s are the fraction of received power in the diffraction and scatter components and Δ is the relative delay of the scatter component for mixed mode propagation, then

$$h(t) = \sqrt{a_D}\ \delta(t) + \sqrt{a_s}\ h_s(t-\Delta) \tag{2-80a}$$

and

$$q(t) = \sqrt{a_D}\ \bar{E}_b^{1/2} + \sqrt{a_s}\ \bar{E}_b^{1/2} \int_{-\infty}^{\infty} f(t-t')\ h_s(t'-\Delta)dt' \tag{2-80b}$$

which reduces to the scatter case when $a_D = 0$ and $\Delta = 0$.

To find the performance for mixed mode propagation one computes the matrices A and C as before but now they include the effects of the specular component through the fixed term in q(t). Say we had computed the matrices for the scatter only case; call these A_s and C_s. In this calculation we choose a sampling time

t_0 corresponding to the respective energies in the diffraction and scatter components.* If t_0 is the best sampling time when no scatter is present, a reasonable choice of sampling time would be

$$t_0 = t_{0D} - a_s \Delta \tag{2.81}$$

It is useful to define the scatter component of q(t) as

$$q_s(t) = \int_{-\infty}^{\infty} f(t-t')\, h_s(t'-\Delta)dt' \tag{2.82}$$

and the scatter signal vector

$$\underline{q}_{s_i} = \{q_s(t_0-iT-k\tau\}_{k=-K_1}^{K_2} \tag{2.83}$$

The matrices A_s and C_s are then

$$A_s = A_0 + \frac{\gamma^2 a_s \bar{E}_b}{N_0} \sum_{i \varepsilon I_b} \overline{\underline{q}_{s_i} \underline{q}'_{s_i}} \tag{2.84}$$

$$C_s = \overline{\underline{q}_{s_0} \underline{q}'_{s_0}} \tag{2.85}$$

* NOTE: The selection of an appropriate sampling time reflects the operation of a symbol time tracker system under mixed mode conditions.

Because of the specular component, the combined noise matrix A is given by

$$A = A_s + \frac{\gamma^2 a_D \ \overline{E}_b}{N_0} \sum_{i \in I_b} \underline{f}_i \ \underline{f}_i' \equiv A_s + A_D \qquad (2.86)$$

where

$$\underline{f}_i = \{f(t_0 - iT - k\tau)\}_{k=-K_1}^{K_2} \qquad (2.87)$$

and A_D is the ISI matrix due to diffraction.

The signal-to-noise ratio at the equalizer output is then

$$\rho = \frac{\overline{E}_b}{N_0} \left(\sqrt{a}_D \ \underline{f}_0 + \sqrt{a}_s \ \underline{q}_{s_0}\right)' A^{-1} \left(\sqrt{a}_D \ \underline{f}_0 + \sqrt{a}_s \ \underline{q}_{s_0}\right) \qquad (2.88)$$

In order to determine the bit-error-rate statistics, one converts the above quadratic form into a quadratic form of uncorrelated variables. The transformation which accomplishes this is given by

$$\underline{z} = M'\underline{x} = T'B^{-1}\underline{x} \qquad (2.89)$$

where

$$B = A^{1/2}$$

$$\underline{x} = \sqrt{a}_D \underline{f}_0 + \sqrt{a}_s \underline{q}_{s_0} \tag{2.90}$$

and M is the modal matrix for

$$\mathcal{M} = AM\Gamma \tag{2.91}$$

i.e.,

$$\Gamma = \{\Gamma_{ij}\} = \{\lambda_i \delta_{ij}\} \tag{2.92}$$

With this transformation, one obtains

$$\rho = \frac{\overline{E}_b}{N_0} \underline{z}'\underline{z} = \frac{\overline{E}_b}{N_0} \sum_{k=1}^{K} |z_k|^2 \tag{2.93}$$

The variates z_i are uncorrelated complex Gaussian with moments

$$\overline{\underline{z}} = \sqrt{a_D}\, M'\underline{f}_0 = \sqrt{a_D}\, T'B^{-1}\underline{f}_0 \tag{2.94}$$

$$\overline{|z_i - \overline{z}_i|^2} = a_s \lambda_i \tag{2.95}$$

The Laplace transform of the probability density function (pdf) for the signal-to-noise ρ in (2.88) is the product of Laplace transforms of each pdf for the component SNR ρ_i where

$$\rho_k = \frac{\overline{E}_b}{N_0} |z_k|^2 \tag{2.96}$$

The Laplace transform for each component is

$$\overline{e^{-s\rho_k}} = \frac{1}{2\pi\lambda_k} \int e^{-s\rho_k - |z_k - \overline{z}_k|^2/\lambda_k} dz_k \tag{2.97}$$

Completing the square and performing the indicated integration over the real and imaginary parts of z_k gives the result

$$\overline{e^{-s\rho_k}} = e^{-su_k/(1+sv_k)} (1+sv_k)^{-1} \tag{2.98a}$$

where

$$u_k = \overline{z}_k^2 \overline{E}_b/N_0 \tag{2.98b}$$

$$v_k = a_s \lambda_k \overline{E}_b/N_0 \tag{2.98c}$$

The Laplace transform for the SNR ρ is the product

$$\overline{e^{-s\rho}} = e^{-\sum_{k=1}^{K} su_k/(1+sv_k)} \prod_{\ell=1}^{K} (1+sv_\ell)^{-1} \qquad (2.99)$$

With this result one can obtain the average bit error rate. We assume a modem bit error rate characteristic of the form

$$P_e = 1/2\ e^{-\rho} \qquad (2.100)$$

The average bit error rate is related to the Laplace transform (2.99) by

$$\overline{P}_e = \frac{1}{2}\ \overline{e^{-s\rho}}\Big|_{s=1} = \frac{1}{2}\ e^{-\sum_{k=1}^{K} u_k/(1+v_k)} \prod_{\ell=1}^{K} (1+v_\ell)^{-1} \qquad (2.101)$$

Note that the average BER due to scatter alone is the product term in (2.101) so that we can write the average BER for mixed mode conditions as a weighted form of the scatter average BER, i.e.

$$\overline{P}_e = e^{-\sum_{k=1}^{K} u_k/(1+v_k)}\ \overline{P}_s\ ,\ \overline{P_s} = 1/2 \prod_{\ell=1}^{K} (1+v_\ell)^{-1} \qquad (2.102)$$

and note the following energy relations

$$\sum_{k=1}^{K} u_k < a_D \overline{E}_b / N_0 \qquad (2.103)$$

$$\sum_{k=1}^{K} v_k < a_s \overline{E}_b / N_0 \qquad (2.104)$$

2.8.1.3 Fade Outage Probability, Troposcatter Propagation

The fade outage probability is defined as the probability that the instantaneous bit error rate exceeds a threshold value p given that the short term average SNR per bit $\overline{E}_b/N_0 = \gamma$, i.e., it is given by the conditional cumulative distribution

$$P_0(p/\gamma) = \text{prob}\{P_e > p/E_b/N_0 = \gamma\} \quad . \qquad (2.105a)$$

however since the instantaneous bit error rate exceeds the threshold p when the effective SNR is below a threshold value, i.e., $\rho < r$, the outage probability is also given by

$$P_0(r/\gamma) = \text{prob}\ \{\rho < r/\overline{E}_b/N_0 = \gamma\} \qquad (2.105b)$$

or by

$$P_0(r/\gamma) = \int_0^r f(x/\overline{E}_b/N_0 = \gamma)dx \qquad (2.105c)$$

where the threshold SNR, r, is found from

$$p = \frac{1}{2} e^{-r}$$

i.e.,

$$r = \ell n(1/2p) \quad . \tag{2.106}$$

Evaluation of the outage probability requires that the conditional pdf of ρ, i.e., $f(x/E_b/N_0)$ be determined. The conditional pdf $f(x/E_b/N_0)$ can be found from its Laplace transform $F(s/E_b/N_0)$, i.e., Equation (2.77), using partial fraction expression techniques [Monsen, 1977]. For example if all of the K explicit diversity branches are uncorrelated (eg., 2S, 2S/2F, 2F), then we can write

$$F(s/\overline{E}_b/N_0) = \prod_{i=1}^{I} \left(1 + \frac{\overline{E}_b}{N_0} \lambda_i s\right)^{-K} = \sum_{j=1}^{K} \sum_{i=1}^{I} A_{ij} \left(1 + \frac{\overline{E}_b}{N_0} \lambda_i s\right)^{-j} \tag{2.107}$$

where the A_{ij} are the partial fraction expansion coefficients (calculated in subroutine PDFCON)*. The pdf corresponding to (2.107) is then given by

$$f(x/\overline{E}_b/N_0) = \sum_{j=1}^{K} \sum_{i=1}^{I} A_{ij} \frac{U_i(U_i x)^{j-1}}{(j-1)!} e^{-U_i x} \qquad (2.108)$$

where

$$U_i = \frac{N_0/\overline{E}_b}{\lambda_i} \qquad (2.109)$$

Substituting (2.108) in (2.106) and integrating we get the desired expression for the outage probability

$$P_0(r/\overline{E}_b/N_0 = \gamma) = 1 - \sum_{i=1}^{I} \sum_{j=1}^{K} A_{ij} e^{-U_i r} \sum_{n=1}^{j} \frac{(U_i r)^n}{n!} \qquad (2.110)$$

where use has been made of the fact that the partial fraction expansion coefficients must add up to unity.

* NOTE: Depending on the diversity configuration, some of the explicit diversity branches will be correlated so that (2.107) will have a similar form but the values of I and K will differ.

2.8.1.4 Fade Outage Probability, Mixed Mode Propagation

The fade outage probability is defined as the probability that the BER is greater than a threshold p_t which is equivalent to the probability that the SNR ρ is less than a threshold r where

$$r = -\ln(2p_t) \tag{2.111}$$

Thus the outage probability is defined in terms of the inverse Laplace transform,

$$P_0(r) = \frac{1}{2\pi j} \int_0^r dx \int_{-j\infty+\sigma}^{j\infty+\sigma} e^{sx}\, e^{\overline{-s\rho}}\, ds \quad . \tag{2.112}$$

Since integration is equivalent to division by s in the transform domain, we have

$$P_0(r) = \frac{1}{2\pi j} \int_{-j\infty+\sigma}^{j\infty+\sigma} e^{sr}\, e^{\overline{-s\rho}}\, ds/s \quad . \tag{2.113}$$

One can find the outage probability from (2.99) and (2.113) directly by expanding the exponential in (2.99) in a series and performing partial fraction expansions. For asymptotic results we deduce the following. For small r (large s in the transform domain) we have

$$P_0(r) \doteq e^{-\sum_{k=1}^{K} u_k/v_k}\, Q_0(r) \qquad r << \overline{E}_b/N_0 \tag{2.114a}$$

where $Q_0(r)$ is the outage probability due to scatter alone, viz.,

$$Q_0(r) = \frac{1}{2\pi j} \int_{-j\infty+\sigma}^{j\infty+\sigma} e^{sr} \prod_{k=1}^{K} (1+sv_k)^{-1} \, ds/s \qquad (2.114b)$$

For large r (small s in the transform domain) we have

$$P_0(r) \doteq Q_0(r - a_D \bar{E}_b/N_0) \qquad r > \bar{E}_b/N_0 \qquad (2.115)$$

For purposes of numerical integration over the parameter $\bar{E}_b/N_0$ to obtain the average fade outage probability corresponding to a long interval such as a year, one can approximate $P_0(r)$ by the piece-wise function

$$p_0(r) \doteq \begin{cases} e^{-\sum_{k=1}^{K} u_k/v_k} Q_0(r) & r \leq r_m \qquad (2.116a) \\ Q_0(r - a_D \bar{E}_b/N_0) & r > r_m \qquad (2.116b) \end{cases}$$

where r_m satisfies the relation

$$e^{-\sum_{k=1}^{K} u_k/v_k} Q_0(r_m) = Q_0(r_m - a_D \bar{E}_b/N_0) \qquad (2.117)$$

The approximation is appropriate since the outage probability averaged over long term fading of the diffraction and scatter component will be dominated by the small r and strong scatter (v_k generally large) case for which the approximation (2.116a) is good.

2.8.1.5 Fade Outage Per Call Minute

The fade outage per call minute is defined as the probability of one or more outages of duration less than 5 seconds in a one minute interval [Kirk and Osterholz, 1976]. Mathematically this can be expressed as

$$P_{CM} = 1 - (1-P_0)^{12} \qquad (2.118)$$

where $1-P_0$ is the probability of no outages in a time interval of 5 seconds. Since typical troposcatter fading rates are in the order of 1 Hz and the data rates of interest are in the order of 1 Mb/sec, a good measure of P_0 is given by the outage probability defined in Equation (2.110).

2.8.1.6 1000-Bit Block Error Probability

At a particular instant of time, the probability of a 1000-bit block error is given by

$$P_b = 1 - [1 - P_e(\rho)]^{1000}$$

$$= \sum_{n=1}^{1000} a_n (-1)^{n+1} P_e^{\,n}, \quad a_n = \frac{1000!}{n!(1000-n)!}$$

where P_e is the instantaneous bit error rate, i.e., $P_e = .5 \exp(-\rho)$ where ρ is the effective SNR.

If the 1000-bit block duration is much less than the fade duration (data rate much greater than the fade rate), then the average 1000-bit block error probability is given by the average over the short-term statistics of ρ, i.e.,

$$\overline{P}_b = \sum_{n=1}^{1000} a_n (-1)^{n+1} \int_0^{\infty} \left(\frac{1}{2}\right)^n e^{-nx} f\left(x/\overline{E}_b/N_0\right) dx$$

$$= - \sum_{n=1}^{1000} a_n \left(-\frac{1}{2}\right)^n F\left(n/\overline{E}_b/N_0\right)$$

where $F\left(n/\overline{E}_b/N_0\right)$ is given by Equation (2.77). All 1000 terms in this expression must be evaluated, even for large $\overline{E}_b/N_0$, in order to determine the average 1000-bit block error probability correctly. An upper bound can be obtained as follows.

An upper bound to the instantaneous block error probability is

$$P_b < \begin{cases} 1 & , \rho < \rho_b \\ 1000\ P_e(\rho) & , \rho > \rho_b \end{cases}$$

where $P_e(\rho_b) = .001$ or $\rho_b = 6.2$ (7.9 dB).

Averaging over the short-term fading statistics of ρ, we find the desired upper bound for the average 1000-bit block error probability, i.e.,

$$\overline{P}_b < \int_0^{\rho_b} f(x/\overline{E}_b/N_0)dx + 500 \int_{\rho_b}^{\infty} e^{-x} f(x/\overline{E}_b/N_0)dx$$

$$= \int_0^{\rho_b} f(x/\overline{E}_b/N_0)dx + 500 \int_0^{\infty} e^{-x} f(x/\overline{E}_b/N_0)dx$$

$$- 500 \int_0^{\rho_b} e^{-x} f(x/\overline{E}_b/N_0)dx \qquad (2.119)$$

For large $\overline{E}_b/N_0$, (2.119) is upper bounded by the second term which is equal to 1000 times the average bit error rate, i.e.,

$$\overline{P_b} < 500\ F(1/\overline{E}_b/N_0) = 1000\ \overline{P_e} \qquad (2.120)$$

where $F(s/E_b/N_0)$ is the Laplace transform of the conditional pdf of ρ, defined in Equation (2.77). This upper bound (Equation (2.120)) is used in TROPO to estimate the average 1000-bit block error probability. A tighter upper bound can be obtained by evaluating all three terms in (2.119), but it requires a numerical integration over the conditional probability density function of the detection SNR and it is not currently done for computational reasons.

2.8.2 Long-Term Performance

2.8.2.1 Troposcatter Propagation

The bit error rate and outage probabilities defined in the previous section are short-term performance measures valid over a period of time for which the average SNR per bit (averaged over the Rayleigh fading) is nearly constant. For troposcatter propagation this is the case for time periods of up to an hour. The long-term performance can be found by averaging over the long-term variations in $\bar{E}_b/N_0$. In troposcatter propagation these variations over a year are well described by the lognormal pdf (Gaussian if the SNR is expressed in dB)

$$g(\Gamma) = \frac{1}{\sqrt{2\pi}\,\sigma} e^{-(\Gamma-m)^2/2\sigma^2} \qquad (2.121)$$

where $\Gamma = 10 \log \bar{E}_b/N_0$, m is the yearly median of the average SNR per bit in dB (coded ASNR in subroutine MDTS) and σ is the standard deviation of the average SNR in dB (coded STSNR in MDTS).

The yearly average fade outage probability for troposcatter propagation (coded BOUT(.,.) in MDTS) is then*

$$P_0(r) = \int_{-\infty}^{\infty} d\Gamma \int_0^r dx\, f(x/10 \log \bar{E}_b/N_0 = \Gamma) g(\Gamma)$$

$$= \int_{-\infty}^{\infty} P_0(r/\Gamma)\, g(\Gamma) d\Gamma, \quad r = \ell n(1/2p) \qquad (2.122)$$

---

* This calculation assumes that the multipath distribution can be approximated by its yearly median value.

where $P_0(r/\Gamma)$ is the short term fade outage probability assuming a threshold error rate p and short-term average SNR per bit Γ in dB, and $g(\Gamma)$ is the long term pdf of Γ defined above in Equation (2.121).

In practice the calculation of the above integral (2.122) is difficult because each value of Γ requires a different partial fraction expansion solution to obtain $f(x/\Gamma)$. Fortunately, the conditional (short-term) fade outage probability $P_0(r/\Gamma)$ is a very steep function of Γ relative to the pdf $g(\Gamma)$ so that a relatively simple numerical integration routine should approximate $P_0(r)$, for the error rate thresholds p of interest, quite well. Of particular interest are the error rate threshold values $p = 10^{-3}$, 10^{-4} and 10^{-5} (coded BER(.)).

The numerical procedure used to estimate the yearly average fade outage probability $P_0(r)$, yearly average fade outage per call minute, and yearly average 1000 bit block error probability (coded BOUT(.,.), POUT(.,.), and ABE(.) in MDTS) is as follows. First find the value of Γ which results in a short-term average error rate $\overline{P_e}$ equal to or smaller than the threshold p. Call this value Γ_0. When $\Gamma = \Gamma_0$ the instantaneous BER, P_e, is most of the time much smaller than the average BER. Hence non-negligible values of $f(x/\Gamma)$ must occur when Γ is smaller than Γ_0. Then let the SNR decrease in steps of Δ dB, i.e.,

$$\Gamma_{i+1} = \Gamma_i - \Delta \quad i = 0, 1, 2, \ldots \tag{2.123}$$

and find the corresponding short-term fade outage probability $P_0(r/\Gamma_i)$, fade outage per call minute $P_{CM}(\Gamma_i)$ and 1000 bit block error probability $\overline{P}_b(\Gamma_i)$using the relationships given in Section 2.8.1. This involves finding for each Γ_i the eigenvalues λ_i corresponding to the diversity configurations of interest, finding

the partial fraction expansion coefficients to invert the Laplace transform $F(s/\Gamma_i)$, determining the pdf $f(x/\Gamma_i)$ and obtaining the conditional fade outage probability $P_0(r/\Gamma_i)$ for the threshold error rates of interest. The values of $P_0(r/\Gamma_i)$ should initially be small and increase toward unity. After $P_0(r/\Gamma_i)$ exceeds a threshold the procedure can be terminated and the yearly average fade outage probability approximated by

$$P_0(r) = \sum_{i=0}^{M} g(\Gamma_i)\, P_0(r/\Gamma_i) / \sum_{i=0}^{\infty} g(\Gamma_i) \quad . \tag{2.124}$$

Similar relationships hold for the yearly average fade outage per call minute and yearly average 1000 bit block error probability.

2.8.2.2 Mixed Mode Propagation

The long term average fade outage probability of the MD-918 where mixed-mode propagation takes place is obtained by averaging the short-term fade outage probability over the yearly distribution of the troposcatter and diffraction components of the received signal. If we assume that the long-term fading of the troposcatter and diffraction signal components is independent, the yearly average fade outage probability for a given SNR threshold r is given by

$$P_0(r) = \int_{-\infty}^{\infty}\int P_0(r/\Gamma_S,\Gamma_D)\, g(\Gamma_S)\, g(\Gamma_D) d\Gamma_S\, d\Gamma_D \tag{2.125}$$

where

$$\Gamma_S = 10 \log a_S \overline{E}_b/N_0$$

$$\Gamma_D = 10 \log a_D \overline{E}_b/N_0$$

$$g(\Gamma_S) = \frac{1}{\sqrt{2\pi}\ \sigma_S} e^{-(\Gamma_S - M_S)^2/2\sigma_S^2}$$

$$g(\Gamma_D) = \frac{1}{\sqrt{2\pi}\ \sigma_D} e^{-(\Gamma_D - M_D)^2/2\sigma_D^2}$$

and M_S (coded ASNR) is the yearly median of the troposcatter component of the received SNR in dB, σ_S (coded STSNR) is its standard deviation, M_D (coded ADSNR) is the yearly median of the diffraction component of the received SNR in dB and σ_D (coded SDSNR) is its standard deviation.

2.9 AN/TRC-170 AND DAR MODEM PERFORMANCE

The AN/TRC-170 and DAR Modem performance is calculated by setting MODPAT=2. The modem performance calculations assume pure troposcatter propagation. The regular output consists of:

(i) the most significant implicit diversity eigenvalues,

(ii) the short term average (over the Rayleigh fading) bit error rate (ABER), fade outage per call minute and fade outage probability for received average SNR = -6 to +28 (dB) in 2 dB steps,

(iii) the yearly average fade outage and fade-outage per call minute probabilities

The theoretical analysis of the model used to approximate the performance of the AN/TRC-170 and DAR modems is given in Appendices A through E. The DAR and TRC-170 modems use QPSK modulation with a transmitter time gating technique and an adaptive matched filter receiver. The DAR modem is assumed to use a single frequency to transmit the data while the AN/TRC-170 uses a second frequency to transmit data during the off-time of the other frequency. Figure 2-13 shows the gated transmitted waveforms for the DAR and TRC-170 modems. In the following sections 2.9.1-5 we describe the general flow and the subroutine dependence of the various computations.

2.9.1 Input Requirements

The main subroutine for the performance computations is subroutine TRC. TRC requires input which i) is shared with other modules of TROPO, ii) depends on previously executed modules of TROPO (propagation, filtering/interference) and iii) is TRC-specific. The latter is useful for specialized applications. Subroutine TRCIN serves to interface TRC with the rest of TROPO and to automatically set most of the TRC-specific input to meet the objectives of the general TROPO user.

According to the present setting of TRCIN the only TRC-specific input which must be defined by the user is:

TRCTYP: = 1 for AN/TRC-170 modem,
= 0 for DAR modem.

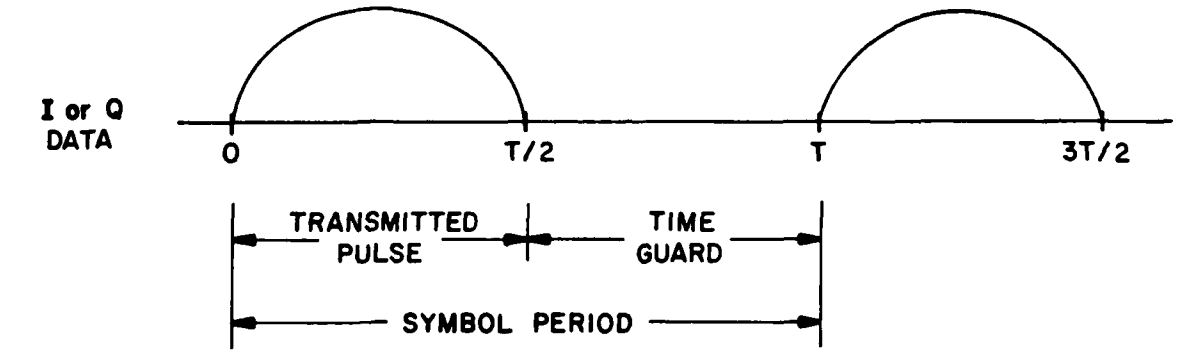

a) DAR MODEM WAVEFORM

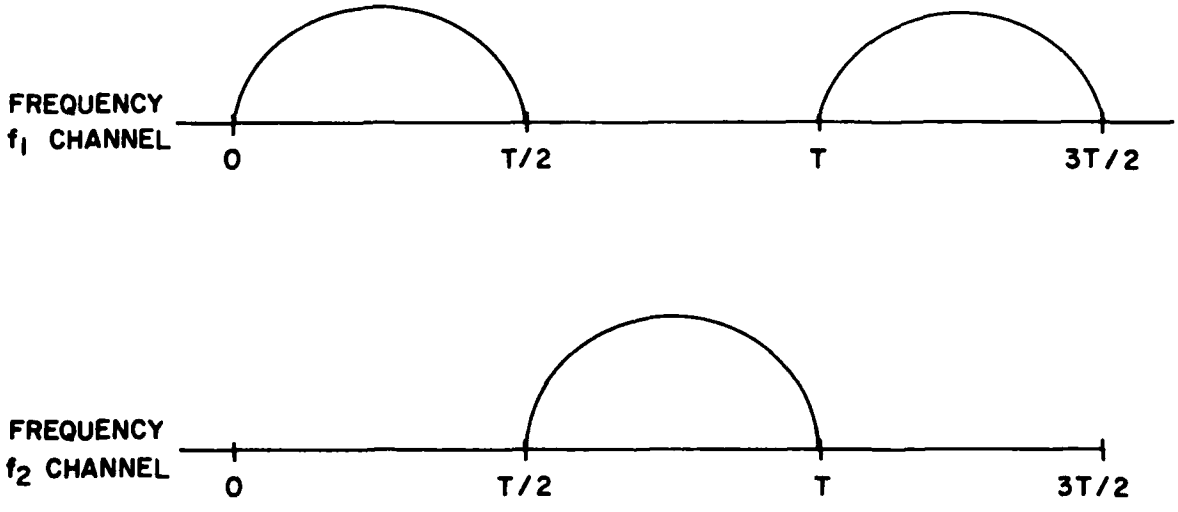

b) TRC-170 MODEM WAVEFORM

Figure 2-13

The shared input data, also user defined, is:

LOUT: output file switch
IBW: filtering switch
DRATE: data rate in bit/sec
NERT: outage threshold switch
BW: bandwidth in MHz

The input taken from the troposcatter propagation module is:

TAU22: 2σ multipath spread of troposcatter signal
ASNR: yearly average SNR in dB
STSNR: yearly standard deviation of SNR in dB

The data rate for which modem performance calculations are allowed must satisfy

$$\frac{BW}{4} < DRATE < BW$$

The input taken from the filtering/interference module (only for IBW >0) is:

TRFILT(•)	:	Tx-Rx filter impulse response
XTRINC	:	step between samples of TRFILT
XTR0	:	time origin of TRFILT
NTR	:	number of points of TRFILT
PEAKAV	:	peak-to-average power ratio of transmitted waveform in dB
SNRJAM	:	noise adjustment for co-channel or adjacent channel interference in dB

SNRBW : noise adjustment for finite bandwidth in dB

SNRF2 : noise adjustment for interference due to 2 frequency transmission (AN/TRC-170 only) in dB

For IBW = 0, TRCIN assumes that the transmitted pulse is rectangular occupying half the symbol interval T, and that the Rx filter is an integrate and dump filter. It then computes the 99 percent transmission bandwidth and the peak-to-average ratio (PEAKAV). After fixing various other TRC parameters, TRCIN calls TRC twice. First to compute the performance for quadruple diversity, which corresponds to a 2S/2F system, and secondly to compute the performance for dual diversity which corresponds to a 2S system. The yearly average fade outage and average fade-outage per call minute probabilities are passed to the SUMPAG file through BOUT(1) and FOUT(1) respectively.

2.9.2 SNR Adjustment

The flow chart of subroutine TRC is given in Figure 2-14. The first essential task is to adjust the average received SNR for degradations due to the peak-to-average transmitted power ratio (PEAKAV), filtering (SNRBW), interference from other systems (SNRJAM) and interference from the 2nd frequency channel (SNRF2) for the AN/TRC-170 system. When a 99% bandwidth or FCC 19311 bandwidth constraint is specified, i.e., IBW >0, these parameters are computed in dB in subroutine FUNJAM. When IBW = 0 (no bandwidth constraint) only PEAKAV (computed in TRCIN) is taken into account. After converting the degradation parameters to decimal form the SNR loss is:

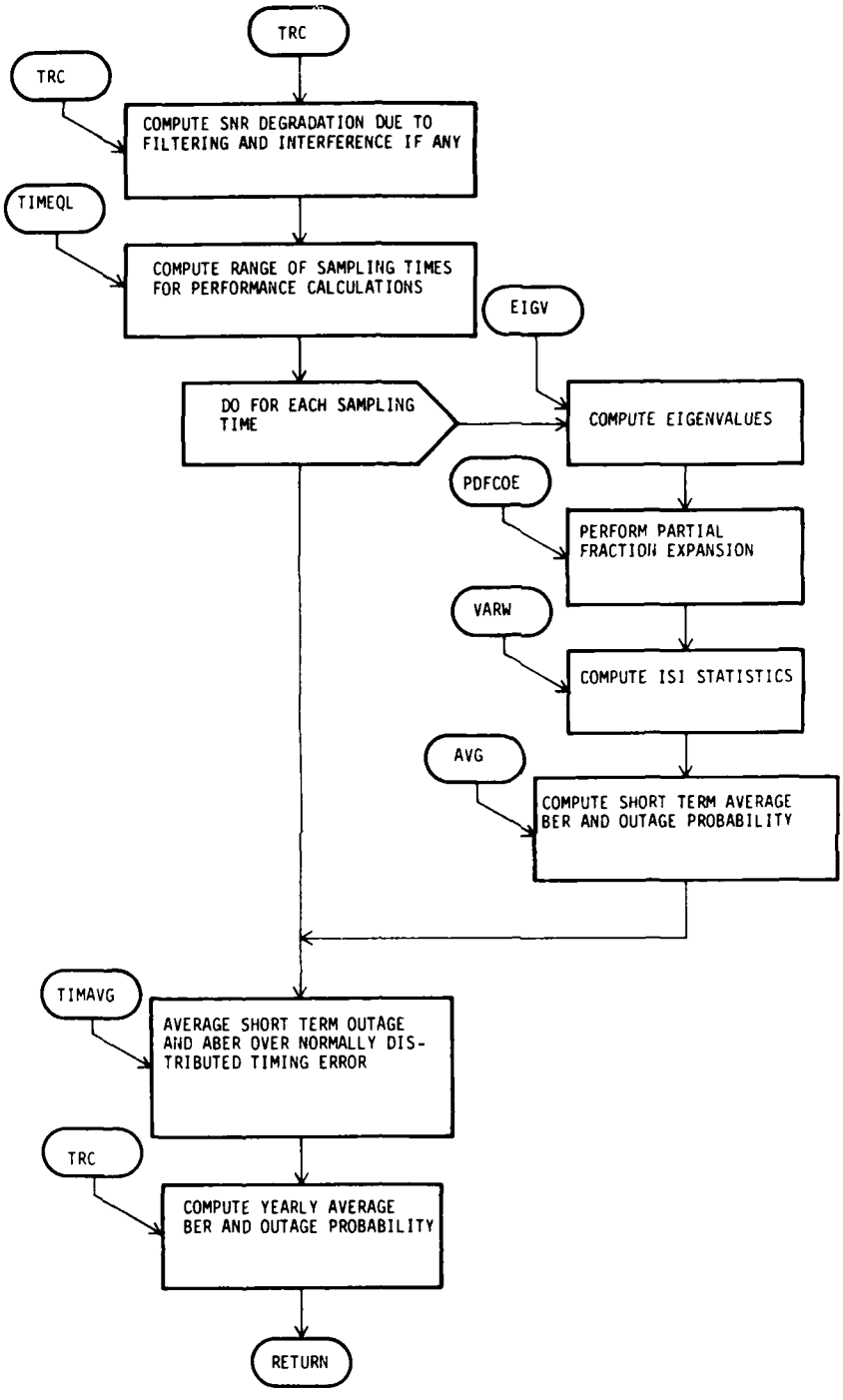

Figure 2-14 Flow Chart for AN/TRC-170-DAR Modem Performance Calculations

```
IF IBW =   0          SNRLOS = PEAKAV
IF IBW >   0
   TRCTYP =   0       SNRLOS = PEAKAV*SNRJAM*SNRBW
   TRCTYP =   1       SNRLOS = PEAKAV*SNRJAM*SNRBW*(1+SNR*SNRF2)
```

The SNRLOS is printed out in dB in the short term performance table. The actual detection SNR on which the performance is based is:

$$\text{Detection SNR} = \text{SNR}_0/\text{SNRLOS}$$

where

$$\text{SNR}_0 = \overline{E}_b/N_0$$

The computation of the SNR degradation due to co-channel or adjacent channel interference assumes that the interference power is the same on all diversity ports and that it is uncorrelated.

2.9.3 The Sampling Time

The sampling time refers to the parameter t_0 of the final report, which adjusts the sequence of sampling and decision instants over the received waveform. Its code name is T0. We have found that even for moderate multipath spreads relative to the symbol interval, i.e., $2\sigma/T > .3$, the performance is affected very much by the selection of t_0. The effect is more prominent in the 2S/2F system than in the 2S system and becomes stronger as the multipath spread increases. A switch IOTIME is used to indicate whether one or more different sampling times considered in the performance calculations are taken into account. With the presently set value IOTIME = 2, an estimate of the average sampling time is computed, on the basis of an early-late technique

reported in [Unkauf, et al., 1979] for the phase error estimator circuit. This is done in subroutine TIMEQL and the estimate is stored in TEQL. TEQL is the solution of f(x) = 0 where:

$$f(x) = \iint R_h(u+x)\, R_h(v+v)\, J(u,v)\, du dv$$

$$J(u,v) = \left[\int_0^{T/2} p(t-u)\, p(t-v)\, dt \right]^2 - \left[\int_{T/2}^{T} p(t-u)\, p(t-v)\, dt \right]^2$$

where p(t) is the impulse response of the cascade of the transmitter and receiver filters, i.e.,

$$p(t) = p_t(t) * p_r(t)$$

and $R_h(t)$ is the power per unit delay multipath profile of the troposcatter signal. The sampling time t_0 is assumed to be distributed normally around TEQL with standard deviation TDEV=0.05T. The short term performance is then computed for 7 values of t_0: TEQL-3*TDEV,..., TEQL+3*TDEV and finally averaged with respect to t_0. The values of t_0 are stored in array T0T0(·). It should be noted that since the signal and ISI statistics depend on t_0 this approach implies that essentially the computational requirements increase 7-fold.

2.9.4 Statistics of Detection Variables

If the transmitted information sequence in one frequency channel of the system is $S_k = a_k + jb_k$, a_k, $b_k = \pm 1$, the detection variable in the in-phase channel and for the mth symbol is given by

$$\tilde{a}_m = a_m \bar{E}_b^{1/2} \gamma + \bar{E}_b^{1/2} \sum_{k=\pm 1} (\alpha_k a_{m-k} + \beta_k b_{m-k}) + n_d$$

The signal gain γ and the ISI weights α_k, β_k fluctuate ramdomly over intervals larger than the coherence time (~.1 sec for the tropospheric scatter channel). Their joint statistics are required to determine the short-term performance. The effective detection noise n_d has power denisty $\gamma N_d/2$, where N_d is the adjusted thermal noise density N_0 discussed in Section 2.9.2. The average received signal energy per bit $\bar{E}_b/N_0$ fluctuates over intervals larger than ~1 hour. Its statistics are required to determine the long-term or yearly system performance. It is assumed that $\bar{E}_b/N_0$ has a log-normal distribution. The mean ASNR and the standard deviation STSNR are calculated in the propagation module and passed to TRC. After the short-term performance has been obtained, the computation of the yearly average performance is the same as with the MD-918 modem (Section 2.8.2). In the remainder of this section we describe the specification of the joint statistics of γ, $\alpha_{\pm 1}$ and $\beta_{\pm 1}$ and in Section 2.9.5 we describe how these statistics are employed to compute the short term performance.

The random variables γ, $\alpha_{\pm 1}$, $\beta_{\pm 1}$ are assumed independent and moreover $\alpha_{\pm 1}$, $\beta_{\pm 1}$ are assumed normal. The probability density function of the signal gain has the form,

$$\text{pdf}(\gamma) = \sum_{i=1}^{D} \sum_{j=1}^{N'} A_{ij}(\underline{\lambda})\, G_i(\gamma, \lambda_j) \ .$$

where D (coded NDIVS) is the number of the independent diversity channels. The parameters λ_j (coded VEIGV($\cdot$)) are the eigenvalues of the covariance matrix V (coded V($\cdot$,$\cdot$) of dimension NxN with elements defined as

$$V_{m,n} = \frac{T}{N} \int p\left(\frac{mT}{N} - u\right)\, p\left(\frac{nT}{N} - u\right)\, R_h(u + t_0)\, du \ .$$

where N (coded NV) is an empirically determined parameter to approximate the non-diversity signal gain as a sum (presently N = 18). The eigenvalues are computed in the subroutine EIGV, p(t) is on the transmitter-receiver pulse computed in the function TXPULS, $R_h(t)$ is the multipath profile computed in the function PROFIL according to the approximation:

$$R_h(t) = b^2 t e^{-bt}, \ b = \sqrt{2/\sigma} \ .$$

The normalized multipath spread σ/T (coded SIGMA) is computed in subroutine TRCIN given 2σ (coded TAU22) and the data rate (coded DRATE). As a general rule the time variable t, in TRC is always normalized with respect to the symbol interval T:

T = 2/DRATE :single frequency DAR

T = 4/DRATE :two-frequencies AN/TRC-170

Once V has been set up, the eigenvalues are computed by invoking the subroutines ELMES and HQR. The sum of the eigenvalues is upper bounded by 1:

$$\sum_{i-1}^{N} \lambda < 1$$

The eigenvalues are ordered in decreasing order, the first N' (coded NEIGEN) are preserved to approximate pdf(γ) and the rest neglected. Presently N' is chosen so that:

$$N' > 3$$

$$\lambda_{N+1} < 0.05\ \lambda_1 = 0.05\ \lambda_{max}$$

Finally the first N' eigenvalues are compensated to preserve the sum value:

$$\lambda_j \text{ replaced by } \lambda_j \left(\sum_{k=1}^{N} \lambda_k\right) / \left(\sum_{k=1}^{N'} \lambda_k\right)$$

which is equal to the average signal gain.

Coming back to the pdf(γ) we note that the function $G_i(x,\lambda)$ is the ith order gamma density with parameter γ:

$$G_i(x,\lambda) = \frac{1}{\lambda^i (i-1)!}\, x^{i-1}\, e^{-x/\lambda}, \quad x>0$$

The coefficients $A_{ij}(\underline{\lambda})$ are the partial fraction expansion coefficients of the Laplace transform of pdf(γ)

$$PDF(s) = \prod_{j=1}^{N'} \frac{1}{(1+\lambda_j s)^D} = \sum_{i=1}^{D} \sum_{j=1}^{N'} A_{ij}(\underline{\lambda})\, \frac{1}{(1+\lambda_j s)^i}$$

The coefficient A_{ij} can be obtained by the formula:

$$A_{D-i,j} = \frac{1}{\lambda_j^{\,i}\, i!}\, \frac{d^i}{ds^i} \prod_{k(+j)=1}^{N'} \frac{1}{(1+\lambda_k s)^D} \qquad s=-1/\lambda_j$$

This computation is done in subroutine PDFCOE and the coefficient stored in array COEFF(1). After the eigenvalue, and the partial fraction expansion coefficients have been specified pdf(γ) is computed from the function PDF.

Regarding the ISI weights $\alpha_{\pm 1}$, $\beta_{\pm 1}$ the Gaussian model requires that their mean and variance be known. The mean turns out to be zero. The variance is,

$$\mathrm{var}(\alpha_k) = \mathrm{var}(\beta_k) \simeq \frac{D}{2} \iint R_h(u+t_0)\, R_h(v+t_0)\, I^2(u,v-kt)\, du\,dv$$

where,

$$I(x,y) = \int_0^T p(t-x)\ p(t-y)\ dt$$

The variances are computed in the function VARW. The integral I is computed in the function P2INT. The larger of the variances is stored in VARAIS and the smaller in VARBIS.

If the computation of the statistics of γ should fail for some reason (e.g., filter impulse response not specified correctly), the short-term modem performance computations are skipped and the performance is set to the value 10. Therefore an average bit error rate of 10 in the output should be interpreted as a flag which indicates that the AN/TRC-170 modem parameters have not been specified properly.

2.9.5 Short Term Modem Performance

The instantaneous bit error rate P_e of the system, including ISI effects, is given by [from Appendix A]

$$P_e(\gamma,\underline{\gamma}_I) = \frac{1}{2} \cdot \frac{1}{16} \sum_{\ell=1}^{16} \mathrm{erfc}\left[(\bar{E}_b\gamma/N_d)^{1/2}(1 + \underline{\gamma}_I\underline{S}_I(\ell)/\gamma)\right] .$$

where erfc(•) is the complimentary error function:

$$\mathrm{erfc}(x) = \frac{2}{\sqrt{\pi}} \int_x^\infty e^{-u^2}\ du$$

$\underline{\gamma}_I$ is the vector of the ISI weights:

$$\underline{\gamma}_I = (\alpha_1, \beta_1, \alpha_{-1}, B_{-1})^T$$

$\underline{S}$ is the vector of the symbols which are adjacent to the currently detected mth symbol:

$$\underline{S}_I = (a_{m-1}, b_{m-1}, a_{m+1}, b_{m+1})^T$$

The index ℓ in $\underline{S}_I(\ell)$ indicates one out of the 16 possible ISI symbol combinations:

ℓ	$\underline{S}_I$			
1	1	1	1	1
2	1	1	1	-1
3	1	1	-1	1
.				
.				
.				
16	-1	-1	-1	-1

The performance measures we are interested in are the average bit error rate P_{avg}:

$$P_{avg} = \int_0^\infty [\iiint P_e(\gamma, \gamma_I)\ \mathrm{pdf}(\gamma, \gamma_I) d\underline{\gamma}_I] d\gamma$$

and the fade outage probability P_{out} for a bit error rate threshold p_t:

$$P_{out} = \iiint_{\Gamma} \text{pdf}(\gamma, \underline{\gamma}_I)\, d\gamma d\underline{\gamma}_I$$

$$\Gamma = \{(\gamma, \underline{\gamma}_I) : P_e(\gamma, \underline{\gamma}_I) > p_t\} .$$

For both P_{avg} and P_{out} we break the computation into two steps. First we compute the conditional performance for a fixed value of the signal gain. Since $\underline{\gamma}_I$ was assumed independent of γ this amounts to:

$$P_{avg}(\gamma) = \iint P_e(\gamma, \underline{\gamma}_I)\, \text{pdf}(\underline{\gamma}_I)\, d\underline{\gamma}_I$$

$$P_{out}(\gamma) = \iint_{\Gamma(\gamma)} \text{pdf}(\underline{\gamma}_I)\, d\underline{\gamma}_I$$

$$\Gamma(\gamma) = \{(\underline{\gamma}_I) : P_e(\gamma, \underline{\gamma}_I) > p_t\} .$$

The short term performance then is computed by averaging with respect to the signal gain:

$$P_{avg} = \int_0^{\infty} P_{avg}(\gamma)\, \text{pdf}(\gamma)\, d\gamma$$

$$P_{out} = \int_0^{\infty} P_{out}(\gamma)\, \text{pdf}(\gamma)\, d\gamma .$$

The second step is straight forward and is performed in the subroutine AVG. When AVG is called from TRC it is provided with one of the subroutines PAVERG or POUTAG, which compute correspondingly $P_{avg}(\gamma)$ and P_{out}. P_{avg} is stored in the array PAVG $(\cdot,\cdot)$, where the first argument stands for the received average SNR and the second argument stands for the sampling time. Recalling our previous discussion, the computation of short term performance for different sampling times is required in order to average out effects of timing jitter. On the other hand the computation of the short term performance versus various SNR's, besides being informative in itself is required for averaging over the long term fluctuations of the SNR to find the yearly performance. The outage probability P_{out} is stored in the array POUT $(\cdot,\cdot,\cdot)$, where the first two arguments have the same significance as in PAVG $(\cdot,\cdot)$ and the third argument indicates the bit error rate threshold P_t. Currently the program is set up to compute outage probabilities for the instantaneous bit error rate thresholds 10^{-3}, 10^{-4}, 10^{-5}.

To complete the exposition of the computational procedure we need to describe how the conditional performance $P_{avg}(\gamma)$ and $P_{out}(\gamma)$ is obtained. A review of the relevant formulas indicates that this computation is very inefficient if done in a straightforward manner because of the dimensionality of the computations. After considerable theoretical manipulations, contained in the final report, we have reduced the required computations so that presently the calculation proceeds in the following way:

i. Conditional average probability of error $P_{avg}(\gamma)$ is computed in the subroutine PAVERG and stored in AVGISI. It is given by

$$2P_{avg}(\gamma) = \sqrt{\gamma}\, \exp[-\gamma y(\overline{E}_b/N_d)] + \operatorname{erfc}[\gamma/\sigma_I\sqrt{2}]$$

where

$$y = \frac{\gamma}{2(\overline{E}_b/N_d)\ \sigma_I^2 + \gamma}$$

and

$$\sigma_I^2 = \mathrm{var}(\alpha_1) + \mathrm{var}(\beta_1) + \mathrm{var}(\alpha_{-1}) + \mathrm{var}(\beta_{-1}) \ .$$

The parameter σ_I^2 is stored in VARISI.

ii. Conditional fade outage probability. A tight upper bound of $P_{out}(\gamma)$ is computed in the subroutine POUTAG and stored in OUTISI. For $\gamma \leq \gamma_{min}$ $P_{out}(\gamma)=1$. The parameter $\gamma_{min} \cdot \overline{E}_b/N_0$ is the solution of the equation

$$\frac{1}{2}\,\mathrm{erfc}(\sqrt{x}) = p_t \ .$$

It is coded on RSNMIN(•) where the argument indicates the threshold p_t. RSNMIN(•) has been computed outside the program and passed by a DATA statement to TRC. For $\gamma > \gamma_{min}$ we have

$$P_{out}(\gamma) \lesssim 1 - \sum_{i=1}^{K} g_1\big((i-1)\delta_L,\ i\delta_L\big) \cdot \sum_{j=1}^{K=1} g_1\big((j-1)\delta_L, j\delta_L\big)$$

$$\cdot \sum_{k=1}^{K-i-j} g_{-1}\big((k-1)\delta_L,\ k\delta_L\big) \cdot \sum_{\ell=1}^{K-i-j-k} g_{-1}\big((\ell-1)\delta_L, \ell\delta_L\big) \ .$$

The function $g_i(u,v)$ is defined as:

$$g_i(u,v) = \text{erfc}\left[\frac{u}{(2\ \text{var}(\alpha_i))^{1/2}}\right] - \text{erfc}\left[\frac{v}{(2\ \text{var}(\alpha_i))^{1/2}}\right]$$

and it is stored in the array DA(•) for the index $i = \pm 1$, which yields the largest var (α_i), and in the array DB(•) for the other index. The parameter K (coded KISI) is presently set to 6.

The parameter δ_L is defined as:

$$\delta_L = \frac{1}{K}\ \alpha_L(\overline{E}_b/N_d,\ \gamma)$$

$$\alpha_L(\overline{E}_b/N_0,\ \gamma) = \gamma \cdot \alpha_L(\gamma \cdot \overline{E}_b/N_d,\ 1)$$

where $\alpha_L(\rho,\ 1)$ is the solution of the equation:

$$8 \cdot f_1(x) = p_t$$

$$f_1(x) = \frac{1}{2} \cdot \frac{1}{16}[\exp[-\rho(1-x)^2] + \exp[-\rho(1+x)^2]]$$

The function $\alpha_L(\rho,1)$ has been computed for 30 ρ-points and for the 3 thresholds of interest and is passed by a DATA statement to TRC coded as UPISIM(,). For a particular ρ, $\alpha_L(\rho,1)$ is obtained by interpolation in the array UPISIM. The parameter $\alpha_L(E_b/N_d, \gamma)$ is coded as UPISI. The parameter δ_L is not coded directly. Instead for the largest var(α_i), i = ±1, the parameter $\delta_L/(2 \text{ var}(\alpha_i))^{1/2}$ is stored in XA and for the smaller var(α_i) the previous parameter is stored in XB.

2.10 TROPOSCATTER CHANNEL SIMULATOR SETTINGS

TROPO also calculates the settings of a tapped delay line troposcatter channel simulator so as to reproduce the same power per unit delay profiles and correlation per unit delay calculated or a dual diversity path.

The troposcatter channel simulator is assumed to be a dual diversity simulator with N-taps per diversity and tap spacing T. The number of taps, N, and tap spacing, T, can be arbitrarily specified. The impulse response of each simulator diversity channel is given by

$$h_k(t) = \sum_{i=1}^{N} W_{ki}\,\delta(t-iT), \quad k=1,2$$

where the simulator tap gains W_{ki} are determined as follows.

The total received power for the kth diversity channel is equal to the sum of the mean squared tap gains, i.e.,

$$P_k = \int_{-\infty}^{\infty} \overline{|h_k(t)|^2}\,dt = \sum_{i=1}^{N} \overline{|W_{ki}|^2} \ .$$

The received power can also be expressed in terms of the integral of the power per unit delay profile calculated by TROPO as

$$P_k = \sum_{n=1}^{NDEL} Q_k(n\tau)$$

where $Q_k(.)$ is the power per unit delay profile calculated for the kth diversity channel, NDEL is the number of delay cells (less than 100) and τ is 'width' of each delay cell.

The mean-squared tap gains for the kth diversity channel are calculated as

$$\overline{|W_{ki}|^2} = \sum_{j=J1}^{J2} \alpha_j Q_k(j\tau), \qquad i=1,\ldots,N$$

where

$$\alpha_j = 1 - \frac{|j-J0|}{T_\tau+1}$$

$$J0 = \left\lfloor i\,\frac{T}{\tau} + 1 \right\rfloor$$

$$J1 = \left\lfloor (i-1)\,\frac{T}{\tau} + 1 \right\rfloor$$

$$J2 = \left\lfloor (i+1)\,\frac{T}{\tau} + 1 \right\rfloor$$

and where $\lfloor . \rfloor$ denotes integer part of the quantity inside the brackets. The tap gains are then normalized so that the target tap gain is unity (0 dB).

The correlation between the gains on the two diversity channels is determined from the relationship

$$W_{1i} W^{*}_{2i} = \sum_{j=J1}^{J2} \alpha_j \, Q_{12}(j\tau)$$

where $Q_{12}(j\tau)$ is the correlation per unit delay profile calculated by TROPO for the path specified and J1 and J2 are defined above.

SECTION 2
REFERENCES

Chadwick, R.B. and Moran K.P. (1980), "Long term measurements of C_n^2 in the boundary layer", Radio Science, V15, pp. 355-362.

CCIR (1978), "Attenuation by atmospheric gases", Report No. 719.

Dougherty, H.T. and Maloney, L.J. (1964), "Application of diffraction by convex surfaces to irregular terrain situations", J. NBS, V68D, pp. 239-249.

Dougherty, H.T. and Wilkerson (1967), "Determination of antenna height for protection against microwave fading", Radio Science, V2, pp. 161-165.

Fried, D.L. (1967), "Optical heterodyne detection of an atmospherically distorted wave front", Proc. IEEE, V55, pp. 55-67.

Gossard, E.E. (1977), "Refractive index variance and its height distribution in different air masses", Radio Science, V12, pp. 89-105.

Kirk, K.W. and Osterholz, J.L. (1976), "DCS Digital Transmission System Performance", DCEC TR-12-76.

Liebe, H.J. (1969), "Calculated tropospheric dispersion and absorption due to the 22-GHz water vapor line", IEEE Trans. Antennas and Propagation, V AP-17, pp. 621-627.

Military Handbook, "Facility Design for Tropospheric Scatter (Transhorizon Microwave System Design)", MIL-HDBK-417, November 1977.

Millington, G., Hewitt, R., and Immirzi, F.S. (1962), "Double knife-edge diffraction in field strength predictions", Proc. IEEE V-109, pp. 419-429.

Monsen, P. (1977), "Theoretical and presumed performance of a DFE modem on a fading multipath channel", IEEE Trans. Communications, V-COM-25, No. 10, pp. 1144-1152.

Parl, S. (1979) "New formulas for tropospheric scatter loss", Radio Science, V14, No. 1, pp. 49-57.

Rice, P.L., Longley, A.G., Norton, A.K., and Barsis, A.P. (1967), "Transmission Loss Predictions for Tropospheric Communication Circuits", Revised NBS Technical Note 101, National Bureau of Standards, Washington, DC.

Röttger, J. (1980), "Reflection and scattering of VHF radar signals from atmospheric refractivity structures", Radio Science, V15, No. 2, pp. 259-275.

Sherwood, A. and Suyemoto, I. (1977), "Multipath measurements over troposcatter paths", Technical Report ESD-TR-77-252, Electronic Systems Division, Air Force Systems Command, US Air Force, Hanscom Air Force Base, Bedford, MA.

Tatarskii, V.I. (1971), "The Effects of the Turbulent Atmosphere on Wave Propagation", pp. 472, National Technical Information Service, Springfield, VA.

Unkauf, M., Davis, P., Alsmeyer, C. (1979), "Digital Transmission System", Final Technical Report, RADC-TR-59-250.

Van Vleck, J.H. (1947), "The absorption of microwaves by oxygen", Phys. Rev., V71, pp. 425-433.

SECTION 3
ANALYTICAL PREDICTIONS FOR SPACE AND FREQUENCY DIVERSITY

In this section, we derive some analytical expressions for the frequency and space correlation coefficients for troposcatter propagation. In particular, we are interested in determining the minimum frequency separation required for frequency diversity operation and the minimum antenna spatial separation for space diversity operation.

3.1 FREQUENCY DIVERSITY ON WIDEBAND TROPOSCATTER LINKS

Assume two transmitted frequencies f_1 and f_2, and let the signal bandwidth be W. The transmitted signals are

$$x_i(t) = x_0(t)\, e^{j2\pi f_i t} \qquad i=1,2 \tag{3.1}$$

where $x_0(t)$ is the baseband signal translated to a convenient RF center frequency f_0, such as $f_0 = (f_1+f_2)/2$. The received waveforms are

$$y_i(t) = \int_0^\infty h(\tau)\, x_i(t-\tau)d\tau \ . \tag{3.2}$$

where $h(\tau)$ is the impulse response of the troposcatter channel which is a randomly varying function.

At the receiver, these are translated to a common frequency which can be taken to be f_0. After frequency translation, each received waveform can be written as

$$z_i(t) = e^{-j2\pi(f_i-f_0)t} y_i(t) \quad . \tag{3.3}$$

We are looking for the correlation between $z_1(t)$ and $z_2(t)$. Assuming the uncorrelated scatterer model for $h(\tau)$ we get

$$\rho(f_1-f_2) = E[z_1(t)z_2^*(t)] = \int_0^\infty Q(\tau)e^{-j2\pi\tau(f_1-f_2)}\overline{|x_0(t-\tau|^2}d\tau \quad . \tag{3.4}$$

where

$$E[h(\tau_1)h^*(\tau_2)] = Q(\tau_1)\delta(\tau_1-\tau_2) \quad .$$

If we assume that the average received power is unity, i.e., $|x_0|^2=1$, then the frequency correlation coefficient

$$\rho(\delta f) = \int_0^\infty Q(\tau)e^{-j2\pi\tau\delta f}d\tau \quad , \tag{3.5}$$

$$\delta f = f_1 - f_2 \quad . \tag{3.6}$$

For narrowband signaling ρ is the Fourier transform of the delay power spectrum $Q(\tau)$. For wideband signaling, we need to look at the correlation at each delay cell of width 1/W. Consider such a cell at delay τ_0,

$$\rho(\tau_0, \delta f) = \int_{\tau_0 - .5/W}^{\tau_0 + .5/W} Q(\tau) e^{-j2\pi\tau\delta f} d\tau \ . \qquad (3.7)$$

If the bandwidth is so wide that $Q(\tau)$ is essentially constant over the delay interval, $\tau_0 \pm .5/W$ (as is the case when three or more delay cells of width 1/W contribute), then

$$\rho(\tau_0, \delta f) \sim Q(\tau_0) e^{-j2\pi\tau_0\delta f} \frac{\sin\pi\delta f/W}{\pi\delta f} \ . \qquad (3.8)$$

In this case, decorrelation is achieved when

$$\delta f \sim W \ . \qquad (3.9)$$

We can conclude that as long as the uncorrelated scatterer model is valid and the bandwidth is wide enough to make implicit diversity significant, then adjacent frequency bands will be uncorrelated without additional separation.

Thus, the frequency separation f_1-f_2 required for uncorrelated frequency diversity operation is

$$f_1 - f_2 = W + B_c \qquad (3.10)$$

where W is the bandwidth and B_c is the frequency separation for which ρ is 0.5 (coherence bandwidth). Both f_1-f_2 and B_c are calculated by the TROPO program and printed by SUMPAG.OUT.

3.2 SPACE DIVERSITY CORRELATION FOR TROPO LINKS WITH NO COUPLING LOSS

The troposcatter propagation model developed for the TROPO program also calculates the correlation of two horizontally spaced diversity antennas by numerical integration of the three dimensional integration defined in Eq. (3.13) below. Quad space diversity is a special case and is discussed in Section 4. In this section, we derive some analytical approximations to this integral. These can be used to obtain estimates of the space diversity correlation for a given antenna spacing and operating frequency. The analytical approximations assume broadbeam antennas.

Let L be the horizontal antenna spacing in the plane perpendicular to the great circle plane*. The path length difference to a point (α, β, y) in the common volume is

$$\delta_R = \sqrt{R_{0R}^2 + (y+L/2)^2} - \sqrt{R_{0R}^2 + (y-L/2)^2} \qquad (3.11)$$

where R_{0R} is the distance from the mid-point between the antennas to the point (α, ρ, y) in the common volume. For large R_{0R} we have

$$\delta_R \simeq \frac{yL}{R_{0R}} = \frac{yL}{d_0} \frac{\sin\theta_1}{\sin\alpha}$$

* NOTE: Vertical antenna spacings can be treated similarly but this case is not currently considered in TROPO.

where $\Theta_1 = \alpha+\beta$ is the scattering angle and d_0 is the length of the straight line connecting transmitter and receiver. The phase difference is

$$\delta_\Phi = \frac{2\pi}{\lambda}\,\delta_R = k_\Phi y \ ,$$

where

$$k_\Phi = \frac{2\pi L}{\lambda d_0}\,\frac{\sin\Theta_1}{\sin\alpha} \ .$$

If the antenna spacing is much smaller than the path length, as is always the case, then the power received on each of the two spaced antennas is clearly the same because the two receiving antennas have the same common volume. If y_i is the signal received on antenna No. i, then the average received signal power (for unit transmitted power) is given by

$$\overline{|y_i|^2} = \frac{(m-3)}{4(m-1)(m-2)}\,\sigma_n^2 r_0^{3-m}\,k^{2-m}\,\Theta^{-m}/d \qquad (3.12)$$

where m is the wavenumber spectrum slope, σ_n is the rms fluctuation in the refractive index, d is the great circle distance between the transmitter and receiver, $k = 2\pi f/c$ is the wavenumber and Θ is the minimum scattering angle on the great circle plane. The correlation between the signals received on antennas 1 and 2 is proportional to $\overline{y_1 y_2^*}$

$$y_1 y_2^* = C \iiint \frac{1}{R_R^2 R_T^2} \left[2\sin(\theta/2)\right]^{-m} e^{jk_\phi y} d^3r \qquad (3.13)$$

where C is a constant proportional to $\sigma_n^2 r_0^{3-m}$. Integrating first in the y-direction (perpendicular to the great circle plane), we have that

$$I_1 \triangleq \int_{-\infty}^{\infty} dy \left(2\sin\frac{\theta}{2}\right)^{-m} \frac{1}{R_T^2 R_R^2} e^{jk_\phi y}$$

$$\simeq \frac{R_0^m}{R_{0T}^2 R_{0R}^2} \int_{-\infty}^{\infty} dy \left[\left(2R_0 \sin\frac{\theta_1}{2}\right)^2 + y^2\right]^{-\frac{m}{2}} jk_\phi y$$

$$= \frac{2\sqrt{\pi}}{\Gamma\left(\frac{m}{2}\right)} \frac{R_0^m}{R_{0T}^2 R_{0R}^2} \left(\frac{k}{2A_0 R_0}\right)^{\frac{m-1}{2}} \frac{K_{m-1}}{2}\left(A_0 R_0 k_\phi\right) \qquad (3.14)$$

where $K_\nu(x)$ is the modified Bessel function of order ν, R_0 is given by

$$R_0 = \frac{R_{0T} R_{0R}}{R_{0T} + R_{0R}} \qquad (3.15)$$

and

$$A_0 = 2\sin\frac{\theta_1}{2} \simeq \theta_1 \ .$$

Replacing A_0 by Θ_1 (small angle approximation) (3.14) becomes

$$I_1 = B\left(\frac{1}{2}, \frac{m-1}{2}\right) \frac{R_0}{R_{0T}^2 R_{0R}^2} \Theta_1^{1-m} f_\nu (\Theta_1 R_0 k_\Phi) \qquad (3.16)$$

where $B(\frac{1}{2}, \frac{m-1}{2})$ is the Beta function, $\nu = (m-1)/2$ and

$$f_\nu(x) = \frac{2}{\Gamma(\nu)} \left(\frac{x}{2}\right)^\nu K_\nu(x) \ .$$

We now integrate along the great circle plane, using the transmitter and receiver elevation angles α and β as coordinates and the approximation

$$\Theta_1 R_0 k_\Phi \sim (\Theta_1)\left(d_0 \frac{\alpha\beta}{\Theta_1^2}\right)\left(\frac{2\pi L}{\lambda d_0} \frac{\Theta_1}{\alpha}\right)$$

$$= \frac{2\pi L}{\lambda} \beta \ .$$

Returning to the original integral (3.13), we have

$$\overline{y_1 y_2^*} = CB\left(\frac{1}{2}, \frac{m-1}{2}\right) \int_{\alpha_0}^{\pi/2} d\alpha \int_{\beta_0}^{\pi/2} d\beta \left[(R_{0T}+R_{0R})\Theta_1^m\right]^{-1} f_\nu \left(\frac{2\pi L}{\lambda}\beta\right) \ . \qquad (3.17)$$

where α_0 and β_0 are the elevation angles of the bottom of the common volume. In the limit as L approaches zero (3.17) reduces to (3.12). This integral cannot be expressed simply. To get an idea of the result we need to investigate the form of $f_\nu(x)$, where the particular value of ν of interest is (m=11/3)

$$\nu = \frac{1}{2}\left(\frac{11}{3} - 1\right) = \frac{4}{3} .$$

When x<.75 we can use the following approximation

$$f_{\frac{4}{3}}(x) \sim \frac{1+3x}{1+3x-1.5x^2} \qquad (3.18a)$$

and when x > .75 we can use

$$f_{\frac{4}{3}}(x) \sim 1.114\left(1 + \frac{0.764}{x+a}\right)e^{-x}\, x^{5/6} . \qquad (3.18b)$$

For continuity, we choose the constant a = 0.083.

Integrating (3.17) over α we get

$$\rho(L) = \frac{\overline{y_1 y_2^*}}{|y_1|^2} = (m-2)\theta_0^{m-2} \int_0^\infty dx(\theta_0+x)^{1-m}\, f_\nu\left[\frac{2\pi L}{\lambda}(\beta_0+x)\right] \qquad (3.19)$$

where we have expressed β as $\beta=\beta_0+x$. When m = 11/3, (3.19) becomes

$$\rho(L) = \frac{5}{3}\,\phi_0^{5/3} \int_{\phi_0 A}^{\infty} dt\,(\phi_0 B+t)^{-8/3} f_{4/3}(t) \qquad (3.20)$$

where

$$\phi_0 = \frac{2\pi L}{\lambda}\,\Theta_0$$

$$A = \frac{1}{2}\,(1+S)$$

$$B = \frac{1}{2}\,(1-S)$$

$$S = \frac{1}{\Theta_0}\,(\beta_0-\alpha_0)$$

$$\simeq \frac{1}{\Theta_0}\left(\Theta_{er} - \Theta_{et} + \frac{2(h_R-h_T)}{d}\right) . \qquad (3.20)$$

where Θ_{et} and Θ_{er} are the horizon elevation angles at the transmitter and receiver, and h_T and h_R are the transmitter and receiver heights above sea level.

The minimum horizontal spacing required for space diversity reception can be determined by finding the value of L for which ρ = .5. Equation (3.20) shows that this value depends on the frequency (or wavelength λ), the scattering angle Θ_0 and the link asymmetry factor S. A similar expression could be derived for vertical antenna spacings.

SECTION 4
ENGINEERING GUIDELINES FOR 2S/2P QUAD DIVERSITY SYSTEMS

Troposcatter communications systems employ diversity to combat fading introduced by the propagation medium. In most cases, it is necessary to use fourth order (quadruple) diversity or higher in order to achieve the desired performance (availability). Quadruple diversity systems may use a combination of space and frequency, space and polarization or space and angle diversity. However, in order to make efficient use of the RF spectrum, most quad diversity systems used on the DCS are implemented by transmitting a single frequency on two orthogonal polarizations and using two antennas at each end of the link, i.e., space/polarization diversity. Such a configuration is often referred to as dual-space/dual-polarization (2S/2P) or quadruple space diversity with polarization marking. Because the multipath fading characteristics of the troposcatter signal are independent of the polarization, no diversity benefit is achieved from use of the two polarizations alone. Quadruple diversity is achieved by employing two different antennas to transmit each polarization separately, and using orthogonal probes (feed-horns) to receive both polarizations with two separate antennas. Decorrelation between the four signals is achieved solely from having the proper spacing between the two transmit and two receive antennas.

In this section we discuss the dependence of the correlation between the various paths on the antenna spacing and antenna size (beamwidth). The discussion is limited to horizontal antenna spacings only as two of the four diversity signals may exhibit a high degree of correlation for some antenna spacings. When the antennas are spaced vertically at each end of the link, the correlation between all four signals decreases as the antenna spacings increases. Engineering guidelines for selecting the

horizontal spacing of the antennas at each end of the link given the symmetry of the link are then developed.

4.1 PATH CROSS-CORRELATIONS

In a 2S/2P diversity configuration with two horizontally spaced antennas at each end of the link there are two transmitted signals and four received signals as shown in Figure 4-1. The four received signals give rise to six cross-correlations among them. The correlations between the various possible pairs of signals are referred to as the correlation between convergent paths (ρ_{12} and ρ_{34}), correlation between divergent paths (ρ_{13} and ρ_{24}), correlation between parallel paths (ρ_{14}) and correlation between crossing paths (ρ_{23}). In this section we establish the relationship between the various cross correlations and the horizontal spacing of the transmit and receive antennas.

From the graphical representation of the four quad space diversity signals in Figure 4-1 one may be tempted to conclude that decorrelation occurs as a result of spatial separation of the common volumes for each path. However this is misleading because typical separations between the centers of the common volumes are in the order of tens of meters while the common volumes are a few kilometers wide at mid path. Thus the majority of scatterers are common to all diversity paths. In fact decorrelation results from path length differences from each scatterer in the common volume to each transmitting and receiving antenna, as explained in Section 3.

The phase difference concept can be used to calculate the correlation between the various troposcatter diversity receiver signals for a given link configuration. The details of the calculation are given in Section 3.2 of this report. We have used this model to calculate the cross-correlation between each pair

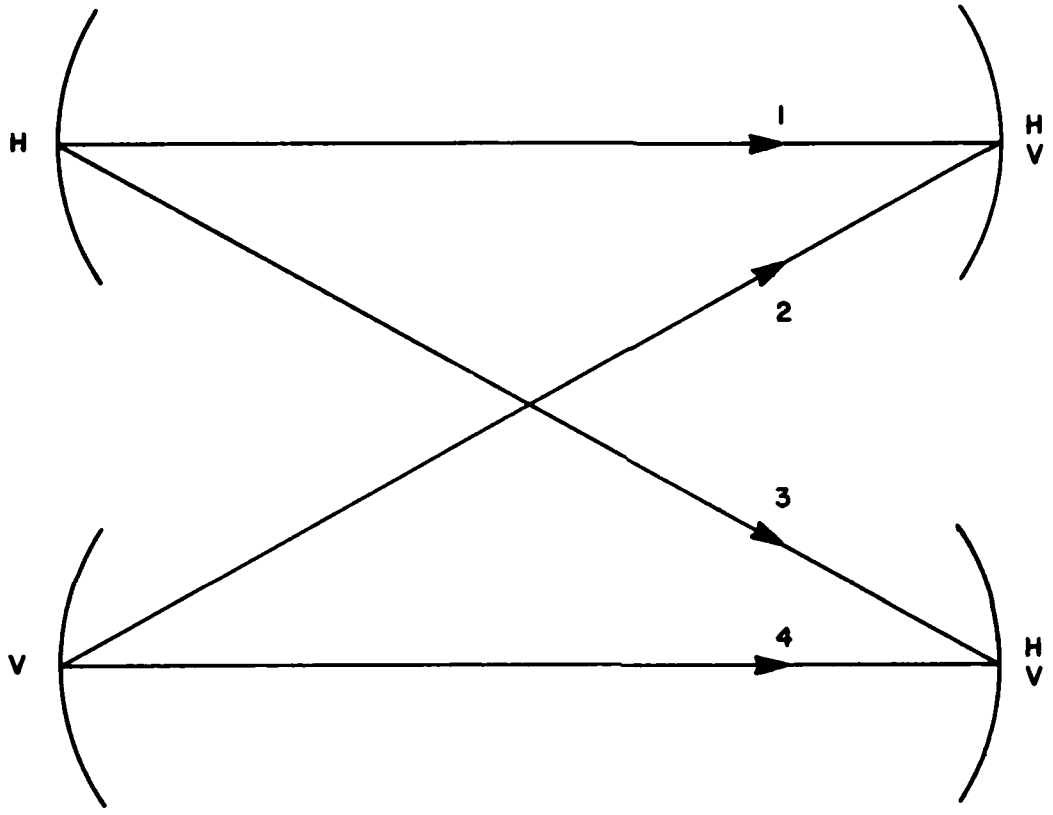

Figure 4-1 Antenna Configuration for Dual Space/Dual Polarization (quad space) Diversity Links with two horizontally spaced antennas at each end of the link (top view).

of paths by numerical integration of Equations (3.12) and (3.13) including the effects of finite antenna beamwidth. The link geometry and system parameters assumed are:

Frequency:	875 MHz
Wavelength:	1.124 ft.
Great Circle Path Length:	191.4 smi
Transmit and Receive Site Elevations:	2099.7 and 2253.9 ft
Transmit and Receive Horizon Elevation Angles above Horizontal (θ_t and θ_r):	0.41° and -0.41°
Transmit and Receive Antenna Diameters:	65.6 ft.
Scattering Angle (θ_0):	2.08 degrees
Transmitter Take-Off Angle Above Slant Path (α_0):	1.44 degrees
Receiver Take-off Angle Above Slant Path: β_0):	0.64 degrees
Path Asymmetry Factor (α_0/β_0):	2.253.

The correlation between the various pairs of paths is plotted in Figure 4-2 as a function of the horizontal center-to-center spacing between the two receive antennas for two transmit antenna horizontal spacings: 100 ft (solid lines) and 200 ft (dashed lines). From these curves it can be seen that for the above link geometry, the convergent and parallel paths are uncorrelated ($\rho_{12} \simeq \rho_{34} \simeq \rho_{14} = 0$) for transmit and receive antenna center-to-center spacings greater than the antenna diameter. The correlation between the divergent paths (ρ_{13} and ρ_{24}) increases as the receive antenna spacing decreases and becomes greater than 0.1 when the receive antenna spacing is smaller than 110 ft (100 λ). Finally, the correlation between the crossing paths is seen to be quite significant for a wide range of receive antenna

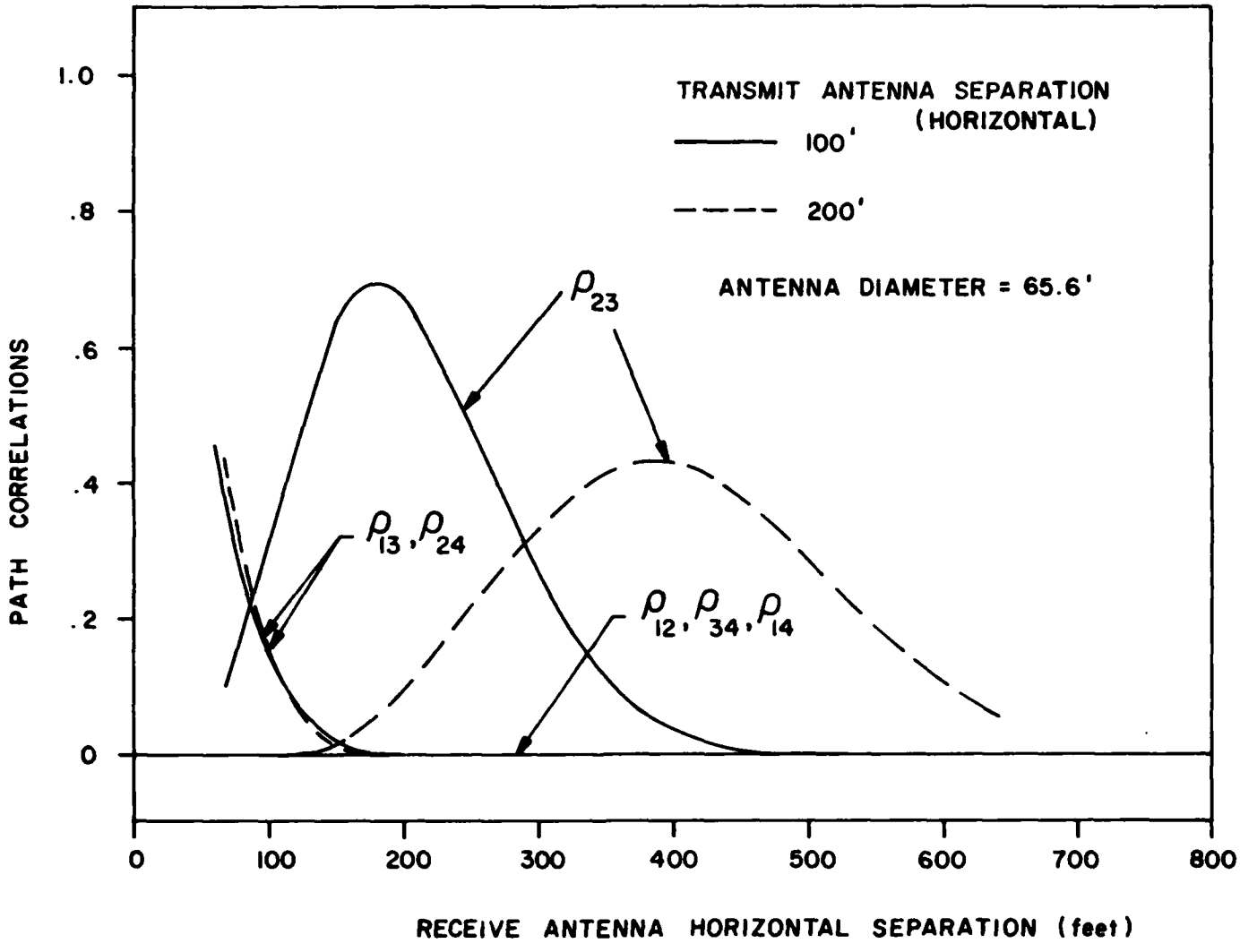

Figure 4-2 Correlation coefficients for 2S/2P diversity paths as a function of receive antenna spacing.

spacings and is maximum at a particular receive antenna spacing. The receive antenna separation for which the correlation between the crossing paths is maximum varies with transmit antenna spacing and its maximum value increases as the transmit antenna spacing decreases.

The effect of antenna beamwidth is shown in Figure 4-3 where we have plotted the correlation between crossing paths, ρ_{23}, as a function of the receive antenna horizontal separation for various antenna diameters, namely 32.8, 65.2 and 131 ft and two transmit antenna horizontal separations, 100 ft (solid lines) and 200 ft (dashed lines). These curves show that the correlation between crossing paths increases as the antenna diameter increases (smaller beamwidth).

4.2 LINK PERFORMANCE AND PATH CORRELATION

The overall performance of a troposcatter link employing a 2S/2P diversity configuration will be suboptimum whenever the antenna spacings at both ends of the link are such that one or more pairs of paths are highly correlated resulting in the loss of one or more diversities. From a link design point of view one is interested in determining what the penalty paid is as a result of the loss in diversity. This will, of course, depend on the performance measure used.

To illustrate the effects of loss of diversity let us use as a performance measure the average signal-to-noise ratio required to achieve a short-term average bit error rate of 10^{-4}.* The penalty paid is the difference in SNR required when all diversities are uncorrelated and the SNR required when two or more

* Another performance measure is the average SNR required to achieve an outage probability of 10^{-4}. The analysis is more complicated though. However, the penalty due to loss of diversity should not differ much.

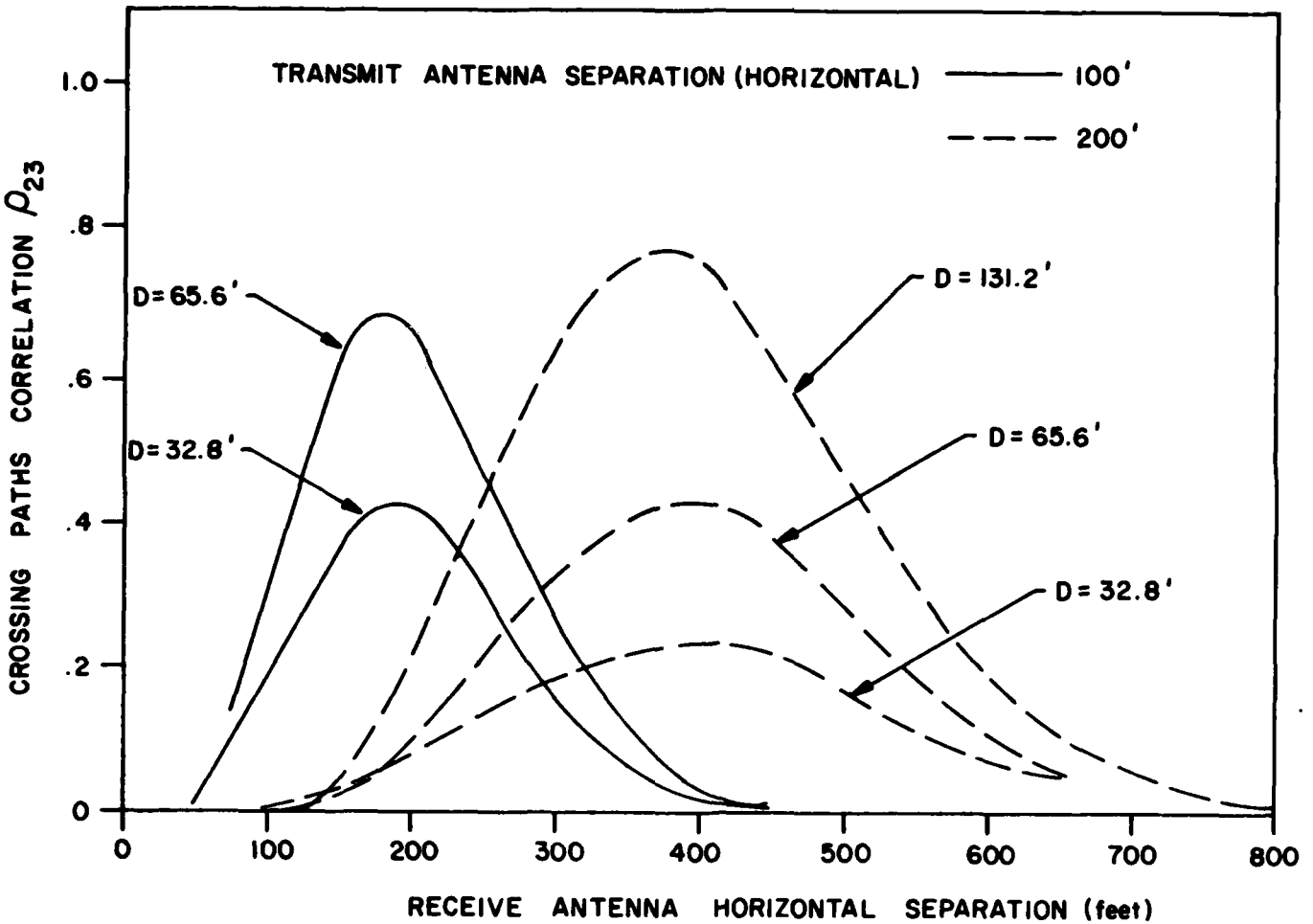

Figure 4-3 Correlation coefficient for crossing paths in 2S/2P diversity links as a function of receive antenna spacing for various antenna diameters (beamwidths).

diversities are correlated. Since we are interested in determining the effects of diversity correlation, let us assume that the data rate is low enough so that delay spread effects (ISI) are negligible. Then, the average bit error rate for a BPSK or QPSK modem with maximal ratio combining (e.g., MD-918) is bounded by (see Section 2.8)

$$\overline{P_e} = \frac{1}{2} \prod_{i=1}^{4} \left(1 + \frac{E_b}{N_0} \lambda_i\right)^{-1} \qquad (4.1)$$

where E_b/N_0 is the average SNR (short-term) and the λ_i are the eigenvalues of the normalized SNR covariance matrix

$$C = \begin{bmatrix} 1 & \rho_{12} & \rho_{13} & \rho_{14} \\ \rho_{12} & 1 & \rho_{23} & \rho_{24} \\ \rho_{13} & \rho_{23} & 1 & \rho_{34} \\ \rho_{14} & \rho_{24} & \rho_{34} & 1 \end{bmatrix} \qquad (4.2)$$

The correlation coefficients of Figures 4-2 and 4-3 can be used to calculate the eigenvalues of C as a function of antenna separation. Once this is done we can find the E_b/N_0 required to achieve an average bit error rate of 10^{-4} by an iterative procedure. This has been done and the results are shown in Figure 4-4 for horizontal transmit antenna spacings at 100 ft and 200 ft and two antenna sizes: 65.6 ft and 131.2 ft. The required SNR is seen to be greatest at those horizontal antenna spacings which result in high correlation between the cross paths (large ρ_{23}). When the receive antenna horizontal spacing is sufficiently large, the required SNR is the same as for uncorrelated quad diversity (e.g., 2S/2F) and is equal to 8.7 dB.

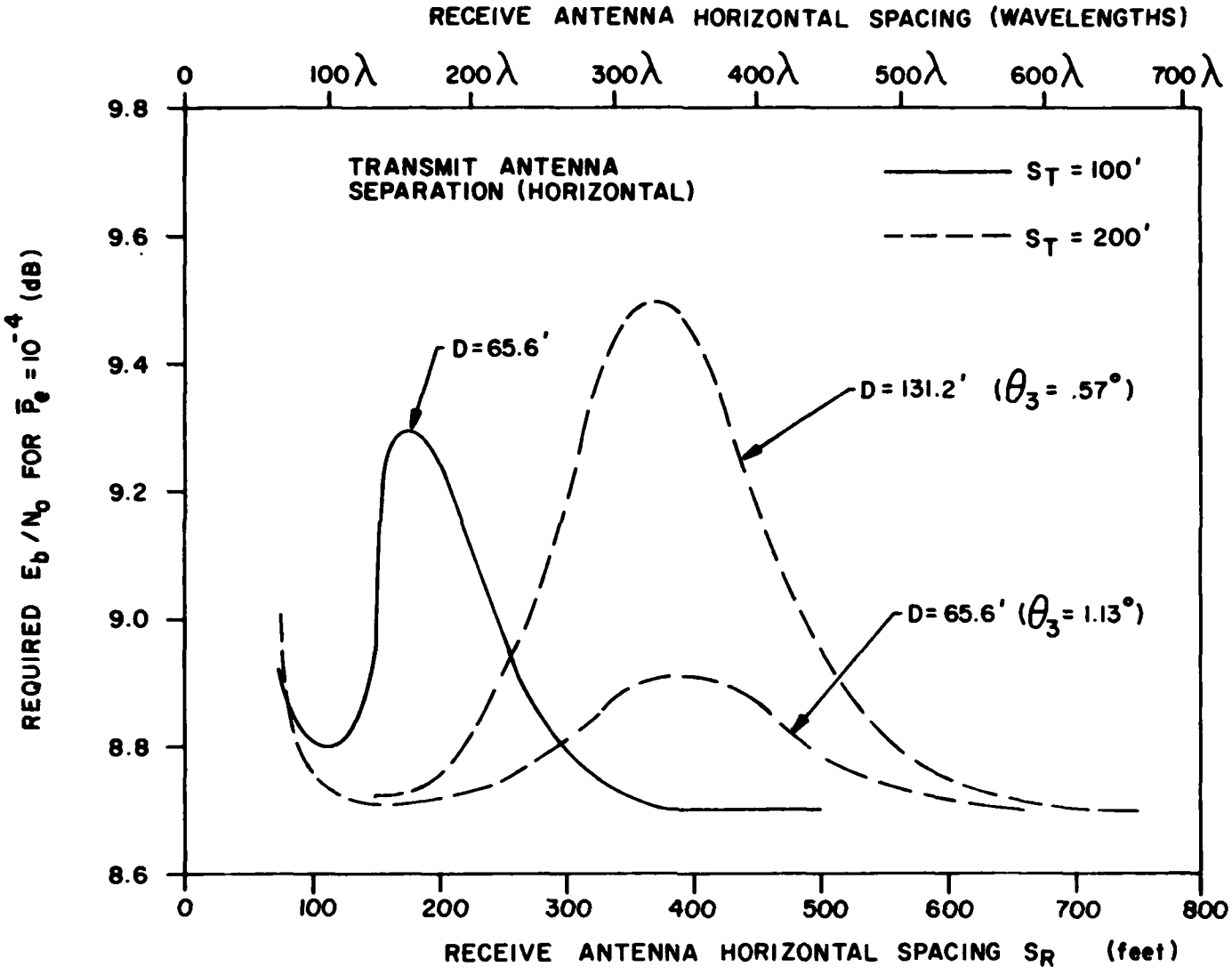

Figure 4-4 Required SNR as a function of receive antenna spacing for various transmit antenna spacings and antenna sizes.

4.3 DEVELOPMENT OF GUIDELINES

In order to develop some guidelines for selecting the transmit and receive horizontal antenna separations it is necessary to establish a relationship between the link geometry and the antenna separations which result in maximum correlation between the crossing paths (and thus poorer performance). Having established this relationship, we can then develop some guidelines so as to avoid antenna spacings which result in poor performance.

The troposcatter signal is a fading signal and can be represented as the sum of a number of phasors with random amplitudes and phases, that is

$$y_2 = \sum_{n=1}^{N} A_n e^{i\Phi_n} \quad .$$

Each phasor represents the fraction of the received signal scattered by an element in the scattering volume. The larger the scattering volume (or the larger the antenna beamwidth), the greater the number of phasors, N. The amplitudes and phases of the phasors can be assumed to be uncorrelated because they represent energy scattered from different portions of the scattering volume separated by distances greater than the correlation distance of the turbulence. The amplitudes are not identically distributed, however, because the scattering angle changes from one portion of the scattering volume to another. The phases can be assumed to be independent and uniformly distributed. Thus the received power via path 2 can be written as

$$E(|y_2|^2) = \sum_{n=1}^{N} E(A_n^2) \quad . \qquad (4.3a)$$

Similarly the troposcatter signal received via path 3 can be written as

$$y_3 = \sum_{n=1}^{N} B_n e^{i\Psi_n}$$

where we have denoted the amplitudes and phases of the signal scattered by the nth element in the scattering volume by different symbols to emphasize the fact that they are different from those for path 2. The received power via path 3 is then

$$E(|y_3|^2) = \sum_{n=1}^{N} E(B_n^2) \quad . \tag{4.4}$$

Now the correlation between the signals received via paths 2 and 3 is defined as

$$\rho_{23} = \frac{E(y_2 y_3^*)}{\sqrt{E(|y_2|^2)\ E(|y_3|^2)}} \tag{4.5}$$

where

$$E(y_2 y_3^*) = \sum_{n=1}^{N} \sum_{m=1}^{N} E(A_n B_m e^{i(\Phi_n - \Psi_m)}) \quad . \tag{4.6}$$

However, since the transmitted signal via paths 2 and 3 is identical, except for the polarization, and the signal scattered by an element in the scattering volume is independent of the polarization, then only that fraction of the energy received via paths

2 and 3 that is scattered by the same element in the scattering volume is correlated. Hence (4.6) reduces to

$$E(y_2 y_3^*) = \sum_{n=1}^{N} E(A_n B_n) E(e^{i(\phi_n - \psi_n)}) \tag{4.7}$$

where it has been assumed that the amplitudes and phases are uncorrelated. In fact the phase difference $\delta_n = \phi_n - \psi_n$ is strictly due to path length differences arising from antenna spacing (see Section 3.2) and may be assumed to be nearly deterministic.

The correlation coefficient then becomes

$$\rho_{23} = \frac{\sum_n E(A_n B_n) e^{i\delta_n}}{\sqrt{\sum_n E(A_n^2) \sum_n E(B_n^2)}} \tag{4.8}$$

where δ_n are the phase differences caused by the antenna separations.

At this point, one is tempted to conclude the decorrelation between the two paths is strictly due to the fact that the correlated scatter from each element in the scattering volume is added incoherently when the δ_n are not zero and that high correlation occurs only when the antenna separation is zero because the δ_n are all zero. However there is one other case in which high correlation occurs with non-zero antenna spacing, as shown in the following. When we displace the antennas horizontally at the transmit and receive ends about the great circle plane (perhaps with different separations), the phase differences exhibit a certain symmetry so that

$$E(y_2 y_3^*) = \sum_{n=1}^{2M} E(A_n B_n)\cos\delta_n$$

$$< \sum_{n=1}^{2M} E(A_n B_n) \qquad (4.9)$$

where $M = N/2$ and $\delta_{M+n} = -\delta_n$.

Furthermore, from Schwartz's inequality we know that

$$\left| \sum_{n=1}^{M} E(A_n B_n) \right| < \left[\sum_{n=1}^{M} E(A_n^2) \sum_{n=1}^{M} E(B_n^2) \right]^{1/2} \qquad (4.10)$$

with equality resulting when B_n is equal to A_n. Physically, the amplitude of the signal scattered in the direction of path 3 by the nth element in the scattering volume, i.e., B_n, is equal to the amplitude of the signal scattered by the same element in the direction of path 2, i.e., A_n, when the two scattering angles are identical. When the scattering angles are not the same, B_n is proportional to A_n. Let us denote the proportionality constant by the symbol β_n and let us define $E(A_n^2) = \gamma_n^2$. Then, β_n^2 represents the ratio of the power scattered by the nth element in the direction of path 3 to the power scattered in the direction of path 2. It is unity when the scattering angle is the same in both directions. The inequality in (4.9) can then be rewritten as

$$E(y_2 y_3^*) = \sum_{n=1}^{2M} \beta_n \gamma_n^2 \cos\delta_n < \sum_{n=1}^{2M} \beta_n \gamma_n^2$$

and

$$\rho_{23} = \frac{\sum_{n=1}^{M} \beta_n \gamma_n^2 \cos \delta_n}{\sum_{n=1}^{M} \gamma_n^2 \sum_{n=1}^{M} \beta_n^2 \gamma_n^2} \qquad (4.11)$$

Clearly high correlation ($\rho_{23} \sim 1$) results when all the δ_n are zero (never the case for non-zero antenna spacing) or when the following is true.

1. $\gamma_i >> \gamma_n$ for all n, $n \neq i$

2. $\beta_i \sim 1$

and

3. $\delta_i = 0$. (4.12)

The first constraint says that one of the elements in the scattering volume must scatter significantly more power (in the direction of path 2) than the others (especially true for narrow beam antennas). This is the element in the scattering volume for which the scattering angle is the smallest. The second constraint says that the power scattered by this same element in the direction of path 3 must be of the same order of magnitude as the power scattered in the direction of path 2. The third constraint says that given that there is one main scatterer i the phase difference between paths 2 and 3 (through the scatterer) must be zero. Thus, constraints 2 and 3 are satisfied when the same element in the scattering volume scatters a greater amount of power

in the direction of paths 2 and 3 than any other elements in the scattering volume. In other words, if most of the power received via paths 2 and 3 is scattered from different portions of the scattering volume, then paths 2 and 3 are uncorrelated.

Two cases, one of high correlation and one of low correlation, are illustrated in Figure 4-5. Since most of the received energy is scattered in the lower portion of the scattering volume we need only consider scattering elements on the lowest horizontal plane. Of them, the scattering element that contributes the most is that which subtends the smallest scattering angle. The projection of the ray path to and from this element onto a horizontal plane is a straight line. The solid lines in Figure 4-5(b) represent a situation in which the troposcatter signals received via the crossing paths are scattered by the same element in the scattering volume (element 1) and are therefore correlated. The dashed lines represent a case which they are scattered by different elements (2 and 3 respectively) and are thus uncorrelated.

The combination of transmit and receive horizontal antenna separations which result in high correlation cross paths are related to the link geometry by

$$\frac{S_T}{S_R} = \frac{d_T}{d_R} = \frac{\alpha_R}{\alpha_T} = \frac{1}{s} \qquad (4.13)$$

where S_T and S_R are the transmit and receive antenna separations, d_T and d_R are the distances from the transmit and receive antennas to the scattering volume, α_T and α_R are the take-off angles of the transmit and receive antennas measured from the slant path (straight line connecting transmit and receive sites). The ratio $s = \alpha_T/\alpha_R$ is defined as the link asymmetry factor which is equal to unity when the center of the scattering volume is half-

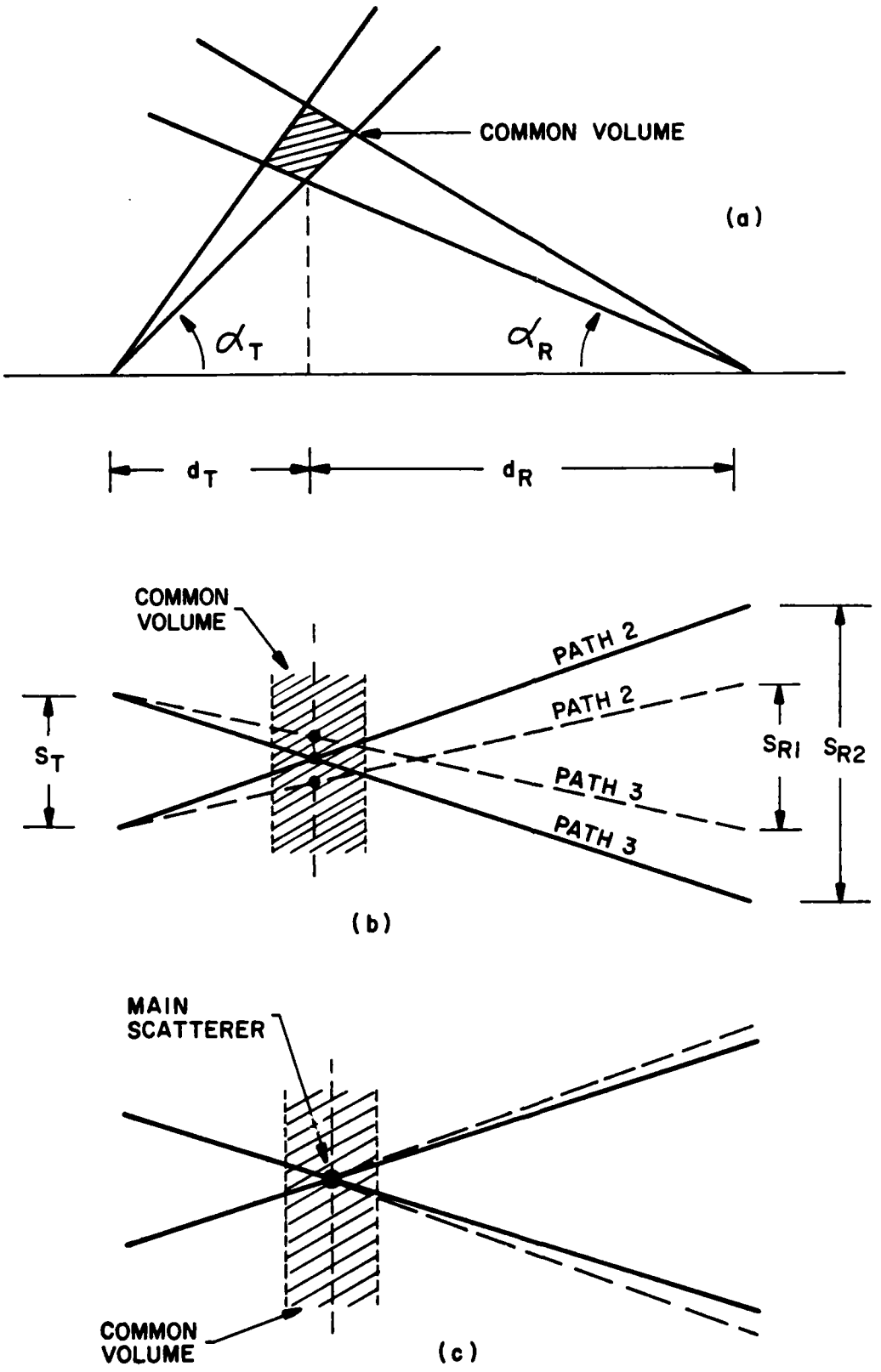

Figure 4-5 Geometrical description of antenna separations which result in high correlation cross paths (solid line in b) and low correlation cross paths (dashed line in b)

way between transmitter and receiver. If the link asymmetry factor is unity high correlation between the crossing paths results when the transmit and receive horizontal antenna separations are identical. Now let us determine if the cross path correlations calculated in Section 4.1 and shown graphically in Figures 4-2 and 4-3 support the theory developed in this section.

The correlations plotted in Figures 4-2 and 4-3 correspond to a link whose asymmetry factor is

$$s = \frac{\alpha_T}{\alpha_R} = 2.25 \ . \qquad (4.14)$$

Thus, from (4.13) we see that high correlation crossing paths should result when

$$S_R = 2.25 \ S_T \ . \qquad (4.15)$$

If S_T = 100 ft, then the crossing paths correlation ρ_{23} should be maximum when S_R = 225 ft., and S_R = 450 ft. when S_T = 200 ft. From Figure 4-3 we see that the correlation between the crossing paths ρ_{23} is indeed rather high at these distances but not quite maximum. The maximum occurs at receiver separations slightly smaller than those predicted by (4.13). The reason for the discrepancy is that in selecting the scattering element which produces the strongest contribution to the received signal we assumed that the antenna gain patterns were constant within their main lobe when in fact they are not. Thus the element which contributes the most to the received signal is one for which its ray path projection onto a horizontal plane is not a straight line but which subtends a small angle as shown by the solid lines in

Figure 4-5(c). The higher antenna gain at the azimuth take-off angle of this ray path more than makes up for the loss of scattered power due to a greater scattering angle.

In the next section the results shown above for high correlation cross paths are used with Figures 4-2 and 4-3 to determine horizontal antenna spacing criteria to minimize the cross paths correlation.

4.4 SUMMARY AND CONCLUSIONS

Up to this point in Section 4.0, we have shown that suboptimum performance of 2S/2P quad diversity systems results when the horizontal separations between the two transmit and two receive antennas are such that the crossing paths are highly correlated. Decorrelation between the crossing paths (to maximize modem performance) is achieved when the horizontal separation between the receive antennas is selected such that

$$S_R > 2 \frac{\alpha_T}{\alpha_R} S_T \qquad \text{if } \frac{\alpha_T}{\alpha_R} > 1 \tag{4.16a}$$

$$S_T > 2 \frac{\alpha_R}{\alpha_T} S_R \qquad \text{if } \frac{\alpha_T}{\alpha_R} < 1 \tag{4.16b}$$

From (4.16) we can see that the only link parameter needed to select the optimum horizontal antenna separations, S_T and S_R, is the link asymmetry factor $s = \alpha_T/\alpha_R$. This parameter is calculated by TROPO and printed out in SUMPAG.OUT. Furthermore, it should be clear that we have used the subscript T to designate one end of the link and R to designate the othe end of the link independent of which end of the link is transmitting or receiving. Thus, the antenna spacings selected according to (4.16) will optimize communications in both directions by the laws of reciprocity.

Now let us consider how one may go about optimizing the horizontal antenna separations S_T and S_R. Let us assume the path asymmetry factor is greater than unity, i.e., $\alpha_T/\alpha_R > 1$. Then the center-to-center antenna separation for the end of the link designated by the subscript T should be at least equal to twice the antenna diameter, i.e., $S_T >$ 2DIAMETER. The center-to-center antenna spacing at the other end of the link should be selected according to (4.16a), i.e., $S_R > 2s\ S_T$ where s is the path asymmetry factor. If the path asymmetry factor is less than unity, i.e., $\alpha_T/\alpha_R < 1$, then select $S_R >$ 2 DIAMETER and $S_T > 2s\ S_R$. Finally if the path asymmetry factor is unity either procedure will apply.

The horizontal antenna separations which result in optimum performance are independent of frequency and antenna size (at least to first order). The reason is that the conditions for decorrelation apply to all antenna beamwidths (i.e., all frequencies for fixed antenna size or all antenna sizes for fixed frequency). However the penalty (increase in required SNR or higher outage probability for fixed SNR) when (4.16) is not satisfied is greater for smaller beamwidths (i.e., greater penalty for larger antennas at the same RF frequency or greater penalty at higher frequencies for the same antenna size).

As a final comment, it should be pointed out that the guidelines of Section 4.3 apply only to quad space diversity configurations where the antennas are spaced horizontally. When the antennas are spaced vertically, the correlation between all diversity ports decreases as the antenna spacing increases. The present version of TROPO does not calculate correlation coefficients for vertically spaced antennas. However, an estimate of the vertical spacings required to achieve decorrelation of the four signals can be obtained from the correlation curves of Figure 4-2 for divergent paths (ρ_{13}). From these curves one many conclude that spacings between 100 and 200 wavelengths should suffice to achieve decorrelation.

SECTION 5
SERVICE PROBABILITY IN CALCULATION OF FADE OUTAGE PROBABILITY

DCEC TR12-76 [Kirk and Osterholz, 1976] specifies a maximum allowable probability of a fade outage below a 1×10^{-4} BER threshold during any digital voice user call minute of 7.5×10^{-4} as the criterion for troposcatter link performance. A fade outage is defined as the event where the short-term (instantaneous) bit error rate is greater than 10^{-4} over the entire year. In this section we develop a method for the incorporation of service probability concepts into the calculation of this outage probability criterion. A summary of the results is provided in the last section.

5.1 OUTAGE PROBABILITY COMPUTATION

Outage probability calculations must consider both the short term (~ 1 sec) complex Gaussian fading statistics of the troposcatter signal and the long term (~ 1 hour) variation in the short term statistics. In addition, service probability introduces the concept of prediction error into the calculation of the long term statistics. Thus, one must consider three layers of random processes. To illustrate, consider the following approach for the calculatin of outage probability.

Within a particular hour, the outage probability is a function of the mean signal-to-noise ratio, the rms multipath spread, and the rms Doppler spread, i.e.,

$$p_0 = p_0(x, s_m, s_D) \qquad (5.1)$$

where

p_0 = fade outage probability per call minute
x = mean SNR (E_b/N_0)
s_m = rms multipath spread
s_D = rms Doppler spread.

The statistical quantities x, s_m, and s_D are short term statistics which reflect the complex Gaussian fading and are frequently characterized by the Rayleigh fading envelope. In order to determine the fade outage for the entire year one must consider the variations in the parameters x, s_m, and s_D over the year. The yearly statistics on x have been studied extensively and a prediction method (NBS Technical Note 101 [Rice, et al., 1967]) exists for computation of the probability distribution of x. Very little data and no theoretical models are available for assessing the yearly variation of multipath and Doppler spread.

Fortunately, with respect to the MD-918 modem, the outage probability p_0 is not a sharp function of either s_m or s_D over the range of expected values of these parameters. The MD-918 modem utilizes a Decision-Feedback Equalizer which compensates for multipath over a range of multipath spread from zero to s_m = T where T is the QPSK symbol period. Over this range, the outage probability does not change dramatically particularly in the weak SNR region where the major contribution to the average outage probability occurs. Also because the fade outage is specified over a range of time from 0.2 to 5.0 seconds, the dependence on Doppler spread in the weak SNR region is also not strong. Thus, we can replace s_m and s_D in (5.1) with their yearly averages to obtain a one dimensional functional dependence for outage probability.

$$p_1(x) \equiv p_0(x, E(s_m), E(s_D)) \qquad (5.2)$$

The expected value notation E(.) is used to denote yearly averages. The fade outage probability at any instant p_f can be computed for the MD-918 modem as a function of the mean SNR x and the mean rms multipath spread $E(s_m)$. It is necessary to relate the instantaneous fade outage probability to the fade outage probability per call-minute. The normalization to one minute suggests that variations in the rms Doppler spread s_D exist and that the temporal statistics of fading are not well understood. Fortunately it appears that the outage probability is not a sharp function of the Doppler statistics [Gadoury, 1983] and the tropo-scatter frequency of operation. A brief argument supporting that view and a proposal of an engineering measure of fade outage per call-minute is presented next.

Lower frequency systems (~ 1 GHz) would have virtually all the fade outages occurring in the DCEC12-76 Range II 0.2 to 5 second period. A reasonable measurement procedure for these systems would be to measure the error rate for 5 seconds and if the error rate exceeds 10^{-4} declare a fade outage. If 12 successive 5 second periods pass without a fade outage, no fade outage in a call-minute occurred. One or more fade outages out of the 12 samples would result in a single fade outage for the call minute. The fade outage per call minute $p_1(x)$ in terms of the instantaneous probability of fade outage $p_f(x)$ is then

$$p_1(x) = \left(1 - p_f(x)\right)^{12} \qquad (5.3)$$

This result is independent of the rms Doppler spread s_D. As one increases the frequency of operation infrequent events will occur where the fade outage is less than 0.2 seconds (counting these would increase p_1 unfairly) and infrequent events where two fade outages occur in 5 seconds (omitting the second

outage decreases p_1 unfairly). A mathematical model to acurately reflect these effects as a function of s_D, is beyond the scope of this effort and would be suspect in any case because of the limited data on s_D variations. Because these two effects tend to cancel each other, an approach independent of s_D is suggested; i.e., use (3) for all frequencies of operation. This approach has the further advantage that averaging p_1 over s_D is not required. Since only limited statistical information on s_D has been collected, gross errors in this averaging procedure are avoided. To find p_1, it is sufficient to average over the mean SNR distribution. We now redirect our attention to the probability density function for that averaging operation and the subsequent calculation of fade outage per call-minute for a specified service probability.

Experimental data shows that the distribution of the mean SNR x in dB is well approximated by the Normal probability density function

$$f_\xi(x|u,s) = \frac{1}{s\sqrt{2\pi}} e^{-(x-u)^2/2s^2} dx \qquad (5.4)$$

where

$$E(\xi) = u \qquad (5.5)$$

$$E[(\xi-u)^2] = s^2 \qquad (5.6)$$

We use a standard notation of representing random variables by Greek letters and a particular value of the random process by English letters. Thus, ξ is the random process for the mean SNR and

$$f_{\xi}(x|u,s)dx = \text{prob } (x < \xi < x + dx) \quad . \tag{5.7}$$

The average outage probability p is found by integration over this density, i.e.,

$$p(u,s) = \int_{-\infty}^{\infty} p_1(x)\, f_{\xi}(x|u,s)dx \quad . \tag{5.8}$$

In the absence of prediction error, the problem is solved and (5.8) is the calculated value of fade outage probability used as the DCS criterion. Prediction error is modeled by assigning probability distributions on the long term parameters, yearly average SNR u, and yearly SNR standard deviation s. A service probability t is achieved if with respect to these distributions a value of outage probability p_t is not exceeded 100% of the time. The mathematical statement is as follows. Let the joint density on the prediction yearly average and standard deviation be

$$f_{\mu,\sigma}(u,s)duds = \text{prob } (u < \mu < u + du,\ s < \sigma < s + ds) \tag{5.9}$$

For a particular yearly average SNR u and yearly standard deviation s, the yearly outage probability is given by the functional relationship defined by the integration procedure in (5.8). If p_t is not exceeded 100t% of the time, we must have

$$t = \int_{p(u,s) < p_t} \int f_{\mu,\sigma}(u,s)\, du\, ds \qquad (5.10)$$

For a 95% service probability, the fade outage probability to be used in the DCEC 12-76 criterion is $p_{0.95}$ calculated from (5.10). Note this answer is not the same as using a 95% service probability distribution for the mean SNR x in place of (5.4) in the yearly average integration (Eq. (5.8)) to find outage probability. This latter approach is far too pessimistic as the 95% service probability distribution for mean SNR has more weight at small SNR values to reflect large prediction error in this region. The larger weight assigned to small SNR values in (5.8) causes a much larger outage probability for service probability values near unity than the exact method given by (5.10).

5.2 PREDICTION ERROR STATISTICS

It remains to determine the prediction density $f_{\mu,\sigma}(u,s)$ and to find p_t through Equation (5.9). A reasonable model for the prediction error consistent with NSB Technical Note 101 is to assume independent Normal distributed errors on the yearly mean SNR and its standard deviation*, i.e.,

$$f_{\mu,\sigma}(u,s) = f_{\mu}(u|u_o,s_u)\, f_{\sigma}(s|s_o,s_s) \qquad (5.11)$$

$$f_{\mu}(u|u_o,s_u) = \frac{1}{s_u\sqrt{2\pi}}\, e^{-(u-u_o)^2/2s_u^2}, \quad -\infty < u < \infty \qquad (5.12)$$

$$f_{\sigma}(s|s_0,s_s) = \frac{1}{s_s\sqrt{2\pi}}\, e^{-(s-s_0)^2/2s_s^2}, \quad -\infty < s < \infty \qquad (5.13)$$

Since we have just defined means and standard deviations of other means and standard deviations, we briefly stop here to clarify these parameters in terms of NBS Technical Note 101 calculations.

u_0 = yearly average of hourly SNR computed for a 50% service probability.

s_0 = standard deviation of hourly SNR for a 50% service probability.

* Although the standard deviation s can never be less than zero it is convenient to use a normal distribution over the $[-\infty, \infty]$ range to represent s. The prediction error s_s is normally much less than s_s which makes this assignment reasonable.

μ = random variable which reflects prediction error in computation of u_0 the yearly average of hourly SNR.

σ = random variable which reflects prediction error in computation of s_0 the standard deviation of hourly SNR.

s_u = rms prediction error for u_0.

s_s = rms prediction error for s.

The quantities u_0, s_0, and s_u can be obtained directly from the Technical Note 101 calculation using a 50% and 95% service probability calculation. Let SNR(y,t) represent the signal-to-noise ratio exceeded 100y% of the time for a service probability t. Then

$$u_0 = SNR(0.5,\ 0.5) \tag{5.14}$$

$$s_0 = \frac{SNR(0.5,0.5) - SNR(0.999,0.5)}{3.09} \tag{5.15}$$

as there are 3.09 standard deviations in the normal distribution to the 99.9% value. The prediction standard deviations s_u for the yearly average is

$$s_u = \frac{SNR(0.5,0.5) - SNR(0.5,0.95)}{1.6} \tag{5.16}$$

as there are 1.6 standard deviations to the 95% value. The prediction error used by NSB Technical Note 101 for this parameter is $\sqrt{12.73}/1.6 = 2.2$ dB. A reasonable procedure to obtain the rms prediction error s_s for the SNR standard deviation is to compute a standard deviation for the 95% service probability distribution, subtract the 50% standard deviation and normalize by 1.6 standard deviations, i.e.,

$$s_s = \frac{1}{1.6}\left[\frac{SNR(0.5,0.95) - SNR(0.999,0.95)}{3.09} - s_0\right] \quad . \qquad (5.17)$$

For values of standard deviation s_0 in the range of 5 to 10 dB, the parameter s_s is about one fourth the value of s_0. Thus, s_s is typically about the same as s_u or a little less.

These calculations are graphically depicted in terms of the slopes and values of the SNR distributions in Figure 5-1.

With this model of the prediction error, we can proceed to compute the outage probability p_t not exceeded 100t% of the time. Consider first the single integration calculations which result from (5.10) when either s_u or s_s is zero.

CASE 1: No prediction error in standard deviation, $s_s = 0$

$$t = \int_{p(u,s_0)<p_t} f_\mu(u|u_0,s_u)du = \frac{1}{s_u\sqrt{2\pi}} \int_{u_0-u_t}^{\infty} e^{-(u-u_0)^2/2s_u^2}\, du \qquad (5.18)$$

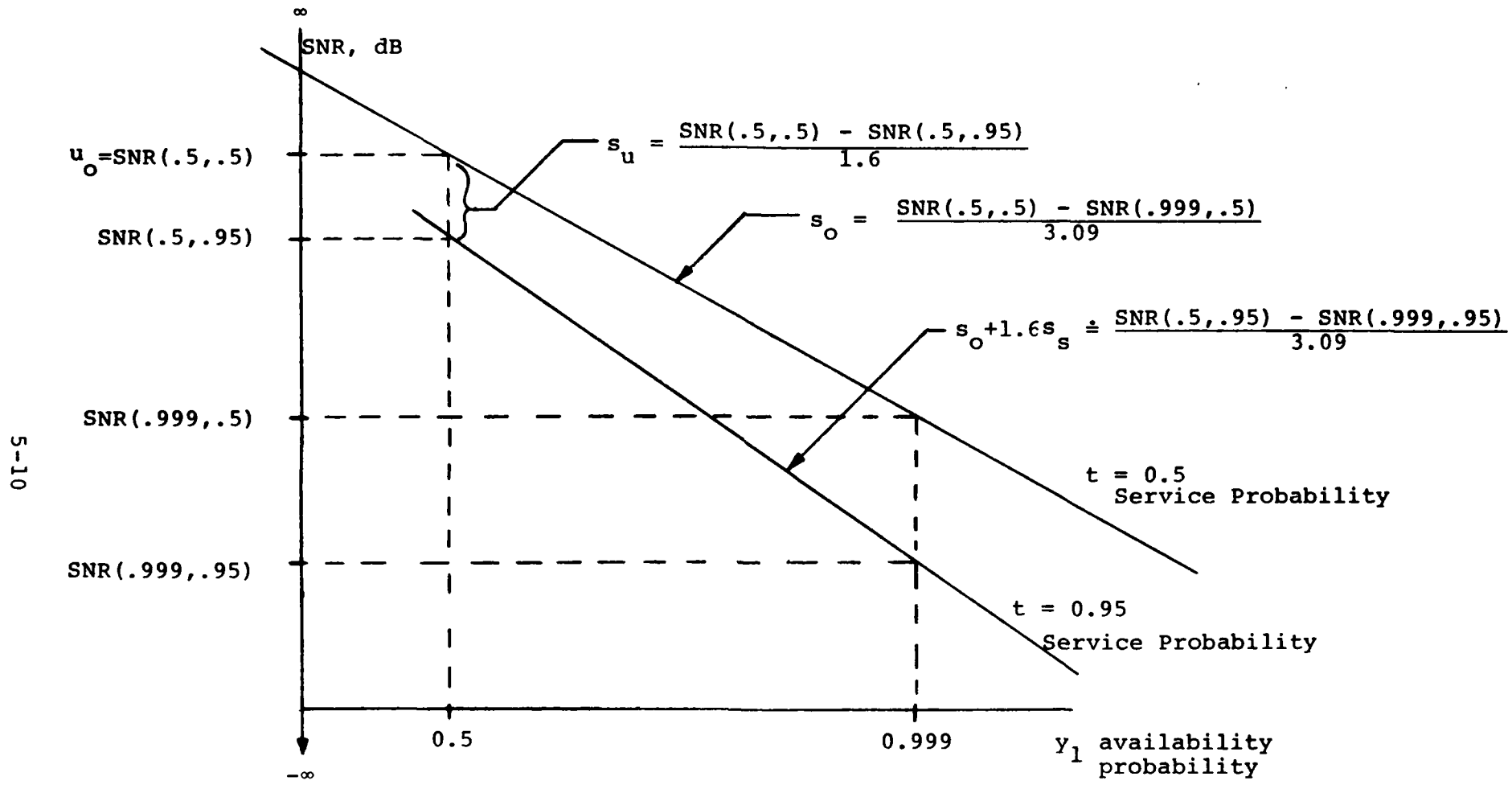

Figure 5-1 Prediction Error Calculations from SNR Distribution

where $u_0 - u_t$ is the SNR exceeded 100t% of the time and

$$p_t = p(u_0 - u_t, s_0) \tag{5.19}$$

$$t = 1 - \frac{1}{\sqrt{2\pi}} \int_{\frac{u_t}{s_u}}^{\infty} e^{-v^2/2}\, dv \equiv 1 - \Phi(u_t/s_u) \tag{5.20}$$

where

$$\Phi(x) = \frac{1}{\sqrt{2\pi}} \int_{x}^{\infty} e^{-y^2/2}\, dy \quad . \tag{5.21}$$

So the outage probability is found by inverting the unit normal function $\Phi(\cdot)$ to find u_t and then computing $p(u - u_t, s_0)$.

CASE 2: No prediction error in median, $s_u = 0$

$$t = \int_{p(u_0,s)<p_t} f_\sigma(s|s_0,s_s)ds = \frac{1}{s_s\sqrt{2\pi}} \int_{-\infty}^{s_0+s_t} e^{-(s-s_0)^2/2s_s^2}\, ds \tag{5.22}$$

where $s_0 + s_t$ is the standard deviation not exceeded 100t% of the time and

$$p_t = p(u_0, s_0 + s_t) \tag{5.23}$$

$$t = \frac{1}{\sqrt{2\pi}} \int_{-\infty}^{s_t/s_s} e^{-v^2/2}\, dv = 1 - \Phi(s_t/s_s) \quad . \tag{5.24}$$

Again, an inversion of the unit normal function to find s_0 and use of (5.8) realizes the outage probability p_t.

5.3 OUTAGE PROBABILITY WITH SERVICE PROBABILITY t

For the general problem where neither s_u or s_s are zero, consider the two-dimensional u,s space shown in Figure 5-2. Rather than find a point on a line as in the previous single integration cases, we now need to find the curve $p(u,s) = p_t$ this would be to draw families of curves of the form

$$p(u, s) = \text{constant}$$

and then by integration of the area to the left of each curve find the service probability. This process would be continued until a constant was selected which gave a service probability close to the desired value t. That constant is then p_t. Because the integration has to be done numerically, we look for an approximate solution which can be calculated without performing a series of numerical integrations in the space of Figure 5-2.

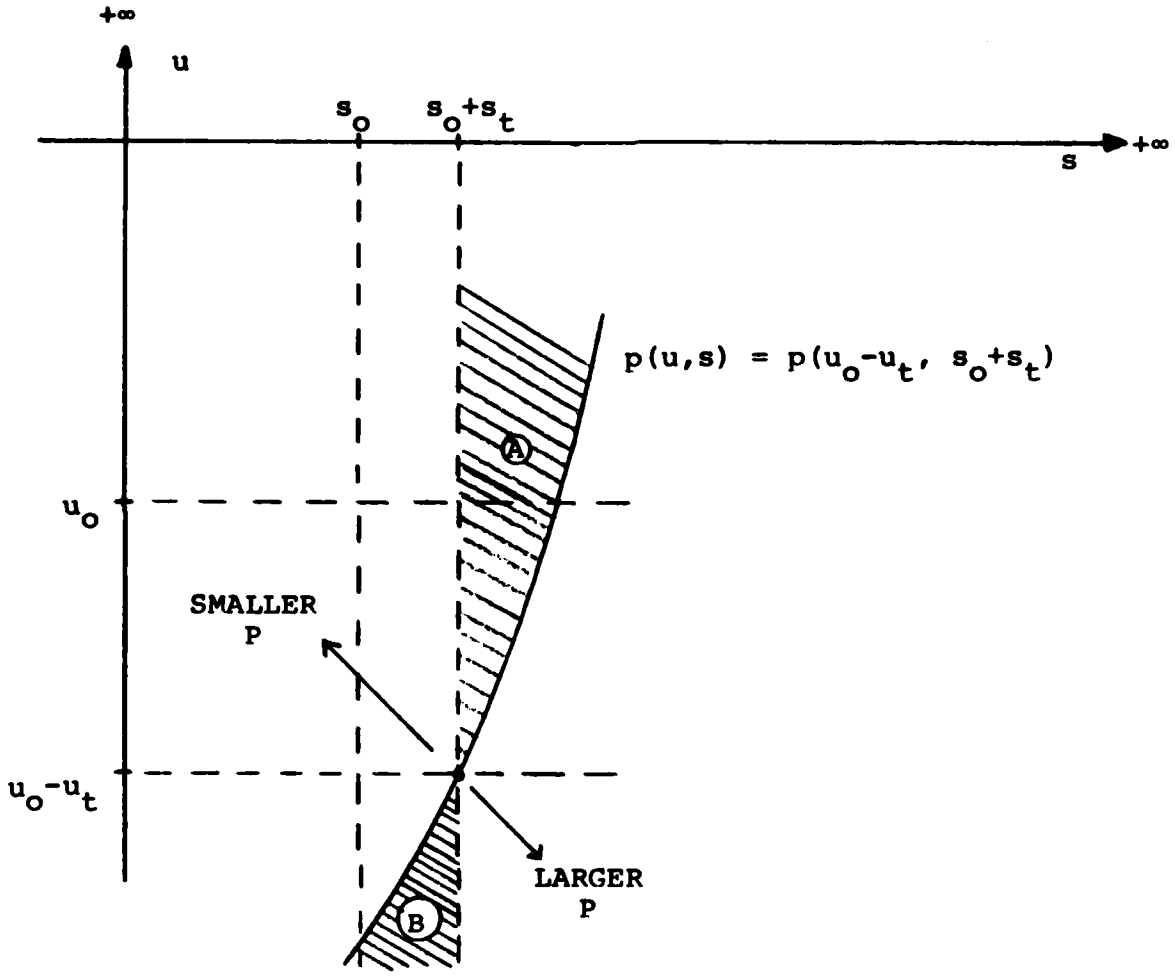

Figure 5-2 Two-dimensional Mean and Standard Deviation Prediction Error Space

Consider the function

$$\hat{p} = p(u_0 - u_t,\ s_0 + s_t) \tag{5.25}$$

which has a service probability

$$\hat{t} = \int\limits_{p(u,s)<\hat{p}} \int f_{\mu,\sigma}(u,s)\ du\,ds \quad . \tag{5.26}$$

The region of integration can be seen from Figure 5-2 and we have

$$\hat{t} = \frac{1}{s_u s_s\ 2\pi} \int_{-\infty}^{\infty} e^{-(u-u_0)^2/2s_u} du \int_{-\infty}^{p(u,s)=\hat{p}} e^{-(s-s_0)^2/2s_s}\ ds \tag{5.27}$$

Our choice of the function (5.25) as the approximate solution is motivated by the fact that small changes in the standard deviation s result in large changes in the average SNR u, i.e., the outage probability for the year is much more sensitive to the yearly distribution standard deviation in dB than to its mean value in dB. Thus, the curve of (5.25) shown in Figure 5-2 is very steep and probably close to linear over the range of interest. Since we found in Case 2 that (c.f., Eq. (5.22))

$$\int_{-\infty}^{\infty} f_\mu(u|u_0,s_u)\ du \int_{-\infty}^{s_0+s_t} f_\sigma(s|s_0,s_s)\ ds = t \quad , \tag{5.28}$$

the function shown in Figure 5-2 will give a result close to t if the probability of region A approximately cancels the probability of region B. If the curve is steep and approximately linear, the value $\hat{p}$ given by (5.25) is an approximate upper bound to p_t. To show this, we first normalize the problem.

For convenience, we define the zero mean, unit variance Normal density function

$$n(t) = \frac{1}{\sqrt{2\pi}} e^{-z^2/2} \tag{5.29}$$

and change variables

$$y = \frac{u - u_0}{s_u} \quad , \quad z = \frac{s - s_0}{s_s}$$

to obtain

$$\hat{t} = \int_{-\infty}^{\infty} n(y)dy \int_{-\infty}^{g(y)} n(z)dz \tag{5.30}$$

where g(y) is the critical value of z which satisfies the relation

$$p(u_0 + ys_u,\ s_0 + g(y)s_s) = \hat{p} = p(u_0 - u_t,\ s_0 + s_t) \quad . \tag{5.31}$$

Because the slope of g(y) at $y = -u_t/u_0$ is small compared to unity and also a slowly changing function of y, a Taylor series expansion of g(y) is suggested. g(y) can then be approximated by the linear function

$$g(y) \doteq a\left(\frac{s_u}{s_s}\right)\left(y + \frac{u_t}{s_u}\right) + \frac{s_t}{s_s} \qquad (5.32)$$

and the slope parameter $a << 1$ which reflects the sensitivity to the standard deviation. In the definitions of s_u and s_s, we indicated that typical values of these parameters are on the order of 2 dB with s_s about equal to s_u or a little less. Thus, the slope $a(s_u/s_s) << 1$ if $a << 1$. It is also convenient to define the normalized distribution values

$$t \equiv 1 - \frac{1}{\sqrt{2\pi}} \int_{y_t}^{\infty} e^{-v^2/2}\, dv \quad , \quad y_t = \frac{s_t}{s_s} = \frac{u_t}{s_u}$$

so that (5.32) becomes

$$g(y) \doteq a\,\frac{s_u}{s_s}\,(y + y_t) + y_t \quad , \quad a << 1 \quad . \qquad (5.33)$$

The error in this approximation is $\hat{t} - t$ which is found from (5.30) and (5.20) to be

$$\hat{t} - t = \int_{-\infty}^{\infty} n(y)dy \int_{-\infty}^{g(y)} n(z)dz - \int_{-\infty}^{\infty} n(y)dy \int_{-\infty}^{y_t} n(z)dz \qquad (5.34)$$

or more concisely

$$\hat{t} - t = \int_{-\infty}^{\infty} n(y)dy \int_{y_t}^{g(y)} n(z)dz = \Phi(y_t) - \overline{\Phi[g(y)]} \qquad (5.35)$$

where the overbar denotes an average with respect to the unit normal distribution.

A graphic illustration of these functions for t = 0.95 is given in Figure 5-3. It is easiest to proceed by making a Taylor series exansion of the second term in (5.35) about $y = -y_t$. To first order,

$$\hat{t} - t \doteq \Phi(y_t) - \Phi(y_t) + \frac{e^{-z_t^2/2}}{\sqrt{2\pi}} \overline{(y + y_t)}\, g'(y)\Big|_{y=-y_t}$$

$$\hat{t} - t \doteq a \frac{s_u}{s_s} y_t\, e^{-y_t^2/2}/\sqrt{2\pi} \approx a \frac{s_u}{s_s} y_t^2 (1 - t) \qquad (5.36)$$

which establishes that $\hat{p}$ is an approximate upper bound and it is tight when the slope $a(s_u/s_s)$ is much less than unity. Unfortunately, it is not possible to establish that $\hat{p}$ is an absolute upper bound because the second derivative of g(y) is negative which results in a negative error in (5.36) when the expansion is carried out to second order. The second order term tends to reduce the approximation error but it is not possible to show that the error remains positive for all values of the prediction statistics.

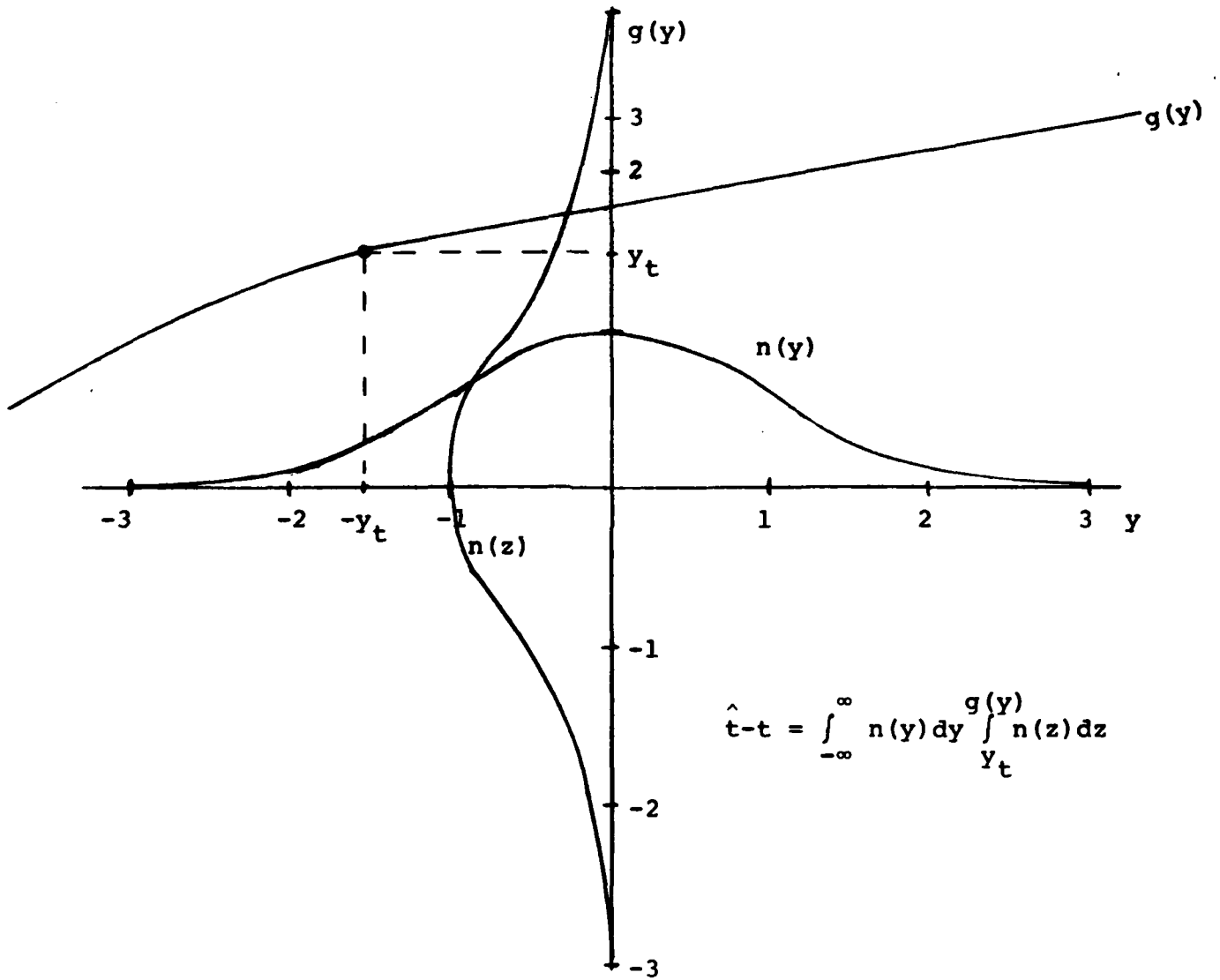

Figure 5-3 Calculation of Approximation Error

5.4 SUMMARY

The fade outage probability per call minute with a service probability of t can be computed using prediction statistics derived from NBS Technical Note 101 [Rice et al., 1967] and one fade outage calculation. First, the SNR(p,t) distribution for availability p and service probability of 0.5 and t must be computed from Technical Note 101. The prediction statistics are then found from

$$\text{Standard Deviation of SNR, } t = 0.5 = s_0 = \frac{SNR(0.5,0.5) - SNR(0.999,0.5)}{3.09}$$

$$\text{Average SNR, } t = 0.5 = u_0 = SNR(0.5, 0.5)$$

$$\text{Standard deiviation of prediction of SNR mean} = s_u = \frac{SNR(0.5,0.5) - SNR(0.5,t)}{y_t}$$

$$\text{Standard Deviation of prediction of SNR standard dev.} = s_s = \frac{1}{y_t}\left[\frac{SNR(0.5,t) - SNR(0.999,t)}{3.09} - s_0\right]$$

$$\text{Mean SNR exceeded 100t\% of time} = u_0 - u_t = u_0 - y_t s_u$$

$$\text{Standard Deviation of SNR not exceeded 100t\% of time.} = s_0 + s_t = s_0 + y_t s_s$$

where y_t is the unit Normal distribution value satisfying

$$t = 1 - \frac{1}{\sqrt{2\pi}} \int_{y_t}^{\infty} e^{-y^2/2}\, dy = 1 - \Phi(y_t) \quad .$$

For $t = 0.95$, $y_t = 1.6$.

The fade outage probability per call minute $p_1(x)$ as a function of the hourly SNR x in dB must then be calculated from the complex Gaussian short term statistics and modem characteristics. The fade outage probability per call minute with a service probability of t is then given by the integration formula

$$p(t) = \int_{-\infty}^{\infty} p_1(x)\, f_\xi(x|u_o - u_t,\ s_o + s_t)\, dx \qquad (5.37)$$

where $f_\xi(x|u,s)$ is the long term Normal distribution of SNR with mean u dB and standard deviation s dB, i.e.,

$$f_\xi(x|u,s) = \frac{1}{s\sqrt{2\pi}}\, e^{-(x-u)^2/2s^2}$$

and

$p_1(x)$ depends on modem characteristics

x = hourly SNR.

REFERENCES

Kirk, K.W. and J.L. Osterholz, (1976), "DCS Digital Transmission System Performance", DCEC Technical Report TR 12-76, November 1976.

Rice, P.L., A.G. Longley, K.A. Norton, and A.P. Barsis (1967), "Transmission Loss Predictions for Tropospheric Communications Circuits", NBS Technical Note 101, Revised January 1, 1967.

Gadoury, J.B. (1983), "Error Performance Characterization Study of a Digital Troposcatter Modem (MD-918/GRC)", Final Technical Report on Contract DCA100-80-C-0031, GTE Products Corporation, for the Defense Communications Agency.

SECTION 6
MODEL PREDICTIONS

In this section we discuss the predictions of the TROPO models for some selected cases and compare them with measured data for those cases for which there is available data. Section 6.1 discusses RSL predictions, Section 6.2 discusses rms (2σ) delay spread predictions for pure troposcatter propagation, Section 6.3 discusses MD-918 short-term performance predictions and Section 6.4 discusses AN/TRC-170 short-term performance predictions.

6.1 RSL PREDICTIONS

A comparison of the predicted RSL distribution and the RSL distributions measured on four DCS links, which are representative of typical path profiles encountered in the DCS network, has been conducted. The distributions of the measured RSL (vertical bars) are for a period of 2-3 weeks while the predicted distributions are yearly distributions assuming a continental temperate climate for all links except one. The relevant path parameters and measured and predicted RSL distributions for each link are discussed next.

6.1.1 Elmadag-Karatas Link

This is a mixed troposcatter/diffraction path. The path parameters are:

Path Length	: 254.6 statute miles
RF Frequency	: 850 MHz
TX Power	: 10 kW
Line Losses	: 4 dB
Receiver Noise Figure	: 3.5 dB
Transmit Antenna Size	: 60 ft
Receive Antenna Size:	: 120 ft
Transmit Antenna Elevation Above Sea Level (Elmadag)	: 6160 ft
Receive Antenna Elevation Above Sea Level (Karates)	: 80 ft
Number of Obstacles	: 2
Obstacle Elevations Above Sea Level	: 8100 and 8800 ft
Distance From Each Obstacle to Transmitter (Elmadag)	: 137.8 and 190 statute miles

The predicted and measured RSL distributions are shown in Figure 6-1. The measured RSL distribution for the 5, 20, 50, 80 and 95 percentile points is shown as vertical bars. It was measured simultaneously on four collocated receivers. The spread in the data is probably due to differences in the line losses and filters in the four receivers. The predicted RSL for the diffraction signal is stronger than for the troposcatter signal and in better agreement with the measured data. Three predicted RSL distributions for the diffraction signal component are shown.

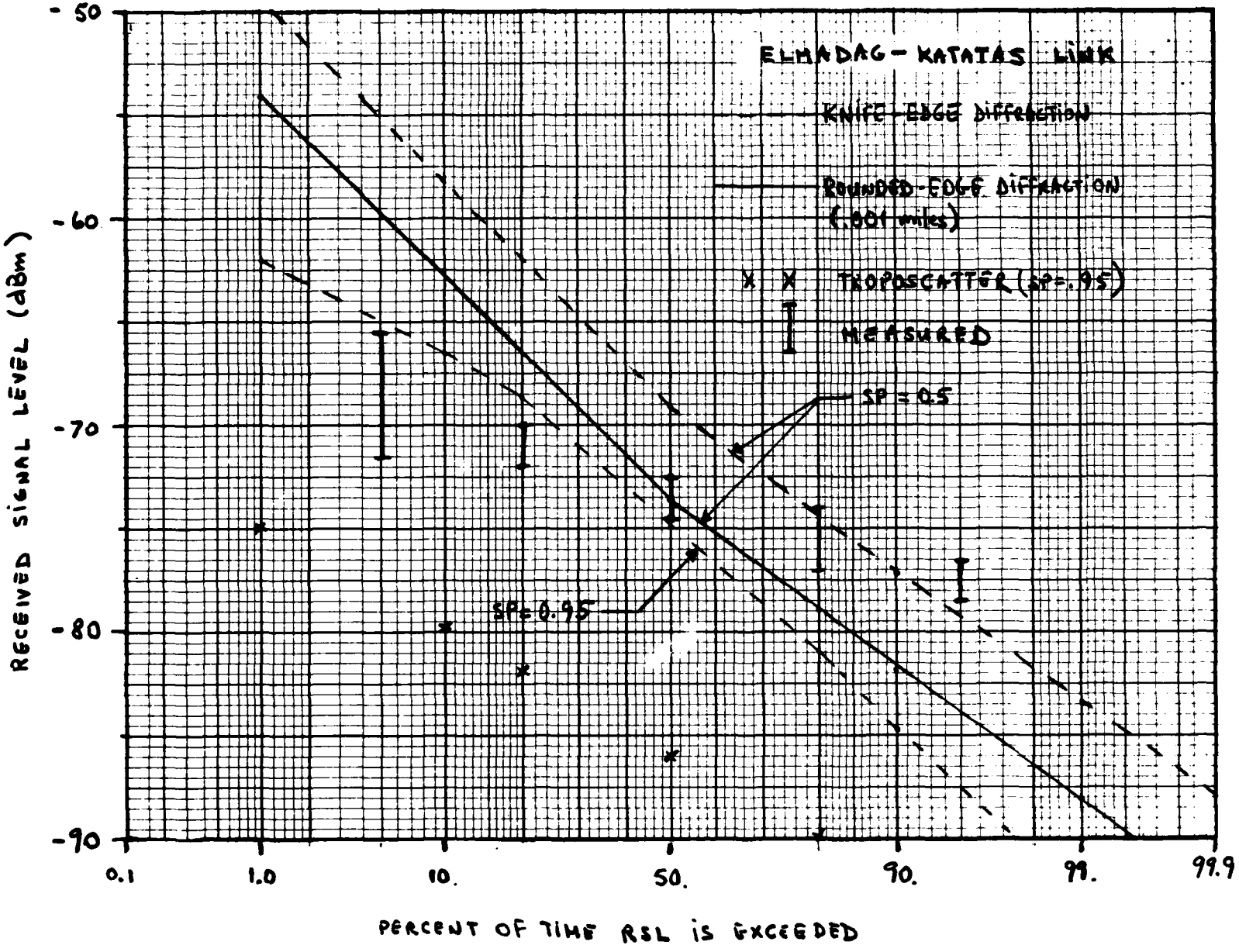

Figure 6-1 Predicted and Measured RSL Distribution for ELMADAG-KATATAS Link

One assumes double knife-edge diffraction with no margin for prediction error (service probability = 0.5). The median of this predicted distribution is 3.5 to 5.5 dB stronger than the median of the measured data. If a margin for prediction error is allowed (service probability = 0.95), the predicted median assuming double knife-edge diffraction is 0.5 to 2.5 dB weaker than the measured median. Better agreement between the predicted and measured medians can be achieved by assuming diffraction by two rounded edges of horizontal extent of .001 miles with no margin for prediction error. The predicted variability about the median is much greater than that measured. This is probably due to the fact that the measured distribution is for a two week period while the predicted distribution is for the whole year.

6.1.2 Sinop-Samsun Link

This is a pure diffraction path. The path parameters are:

Path Length	: 78 statute miles
RF Frequency	: 850 MHz
TX Power	: 10 Watts
Line Losses	: 3 dB
Antenna Sizes (both sites)	: 30 ft
Transmit Antenna Elevation Above Sea Level	: 730 ft
Receive Antenna Elevation Above Sea Level	: 3190 ft
Number of Obstacles	: 2
Obstacle Elevations Above Sea Level	: 3650 and 3950 ft

Distance From Each Obstacle to Transmitter (Sinop)	: 60.5 and 66.5 miles
Receiver Noise Figure	: 4 dB

The predicted and measured RSL distributions are shown in Figure 6-2. If both obstacles are treated as knife edges and no margin for prediction error is allowed (service probability = 0.5), the predicted median is 2.5 to 6.5 dB stronger than the measured median. Closer agreement between the predicted and measured medians can be attained by treating the edges as knife-edges and allowing a margin for prediction error (service probability = 0.95) or by treating the first edge as a knife-edge and the second as a rounded edge with horizontal extent of 0.008 miles with no margin for prediction error. The predicted variability about the median is again greater than the measured variability for the same reasons mentioned earlier.

6.1.3 Elmadag-Sahin Tepesi Link

This is a pure troposcatter path over rough terrain. The path parameters are:

Path Length	: 204 statute miles
RF Frequency	: 800 MHz
TX Power	: 10 kW
Line Losses	: 4 dB
Antenna Sizes (both sites)	: 60 ft
Transmit Antenna Elevation Above Sea Level	: 6160 ft
Receive Antenna Elevation Above Sea Level	: 3060 ft

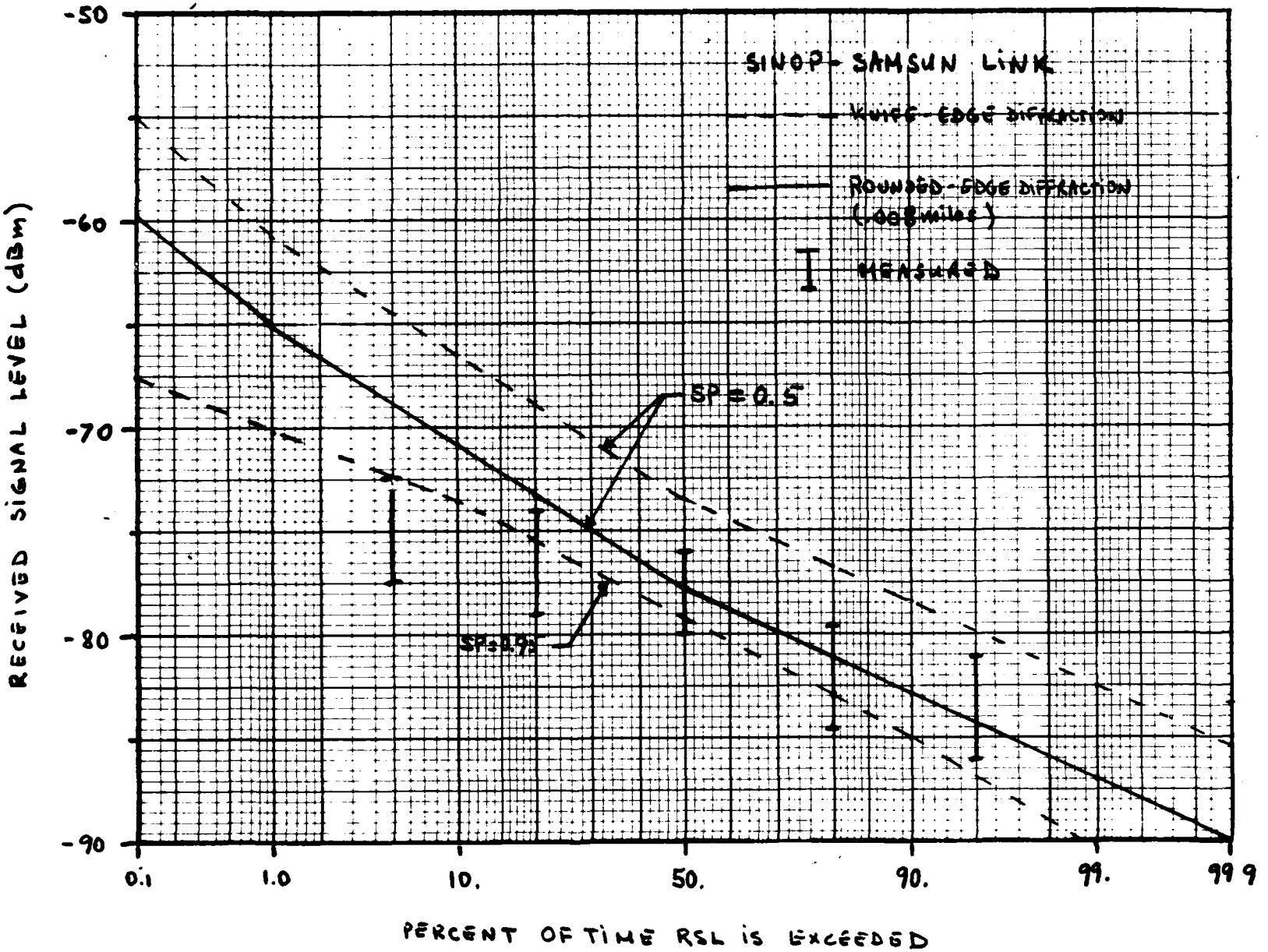

Figure 6-2 Predicted and Measured RSL Distribution for SINOP-SAMSUN Link

Transmitter Horizon Elevation Above Sea Level	: 4000 ft
Receiver Horizon Elevation Above Sea Level	: 3000 ft
Transmitter Horizon Distance	: 40 miles
Receiver Horizon Distance	: 32 miles
Receiver Noise Figure	: 3.5 dB

The predicted and measured RSL distributions are shown in Figure 6-3. The measured distributions on each receiver at each terminal differed substantially probably due to differences in transmission line and filter losses as well as differences in their boresight elevations. The predicted median when no margin for prediction error (service probability = 0.5) is allowed for is about 1.5 dB to 9 dB stronger than the median. Good agreement is achieved when a margin for prediction error is allowed (service probability = 0.95).

6.1.4 Mt. Limbara - Mt. Vergine Link

This is a pure troposcatter path over water. The path parameters are:

Path Length	: 293 statute miles
RF Frequency	: 2.6 GHz
TX Power	: 10 kW
Line Losses	: 4 dB
Antenna Sizes (both sites)	: 60 ft
Transmit Antenna Elevation Above Sea Level	: 4018 ft

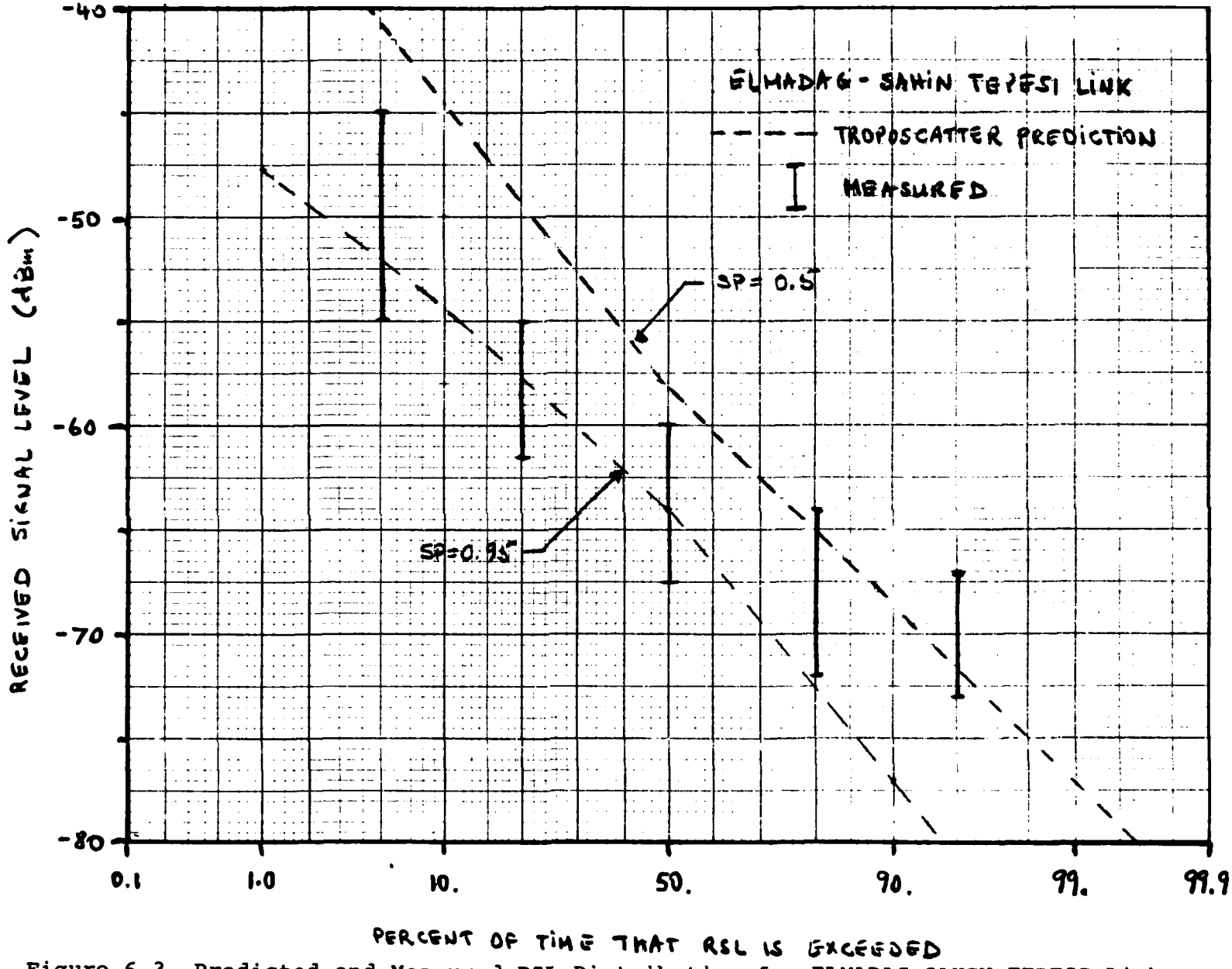

Figure 6-3 Predicted and Measured RSL Distribution for ELMADAG-SAHIN TEPESI Link

Receive Antenna Elevation Above Sea Level	: 4965 ft
Transmitter Horizon Elevation Above Sea Level	: 0 ft
Receive Horizon Elevation Above Sea Level	: 800 ft
Transmitter Horizon Distance	: 85 miles
Receiver Horizon Distance	: 98 miles
Receiver Noise Figure	: 3.5 dB

The predicted and measured RSL distributions are shown in Figure 6-4. The predicted RSL distribution for this link assumes an NBS Technical Note 101 maritime over sea climate. The predicted RLS distribution with no allowance for prediction error (service probability = 0.5) is seen to agree well with the measured distribution. When allowance for prediction error is specified (service probability = 0.95), the predicted RSL distribution is 6 dB weaker than the measured distribution. Note that even though the predicted distribution is for a whole year, it agrees well with the measured 2-week distribution at percentiles higher than 50%.

6.2 TROPOSCATTER DELAY SPREAD PREDICTIONS

TROPO gives predictions of the rms delay spread of the troposcatter signal for median meteorological conditions. Measurements of rms delay spread on two troposcatter paths indicate that the delay spread can vary by a factor of 2-3 in the course of a year [Sherwood, et al., 1977]. Variability in the rms delay spread is caused by variations in the effective earth radius factor (or the mean refractivity gradient) and variations in the

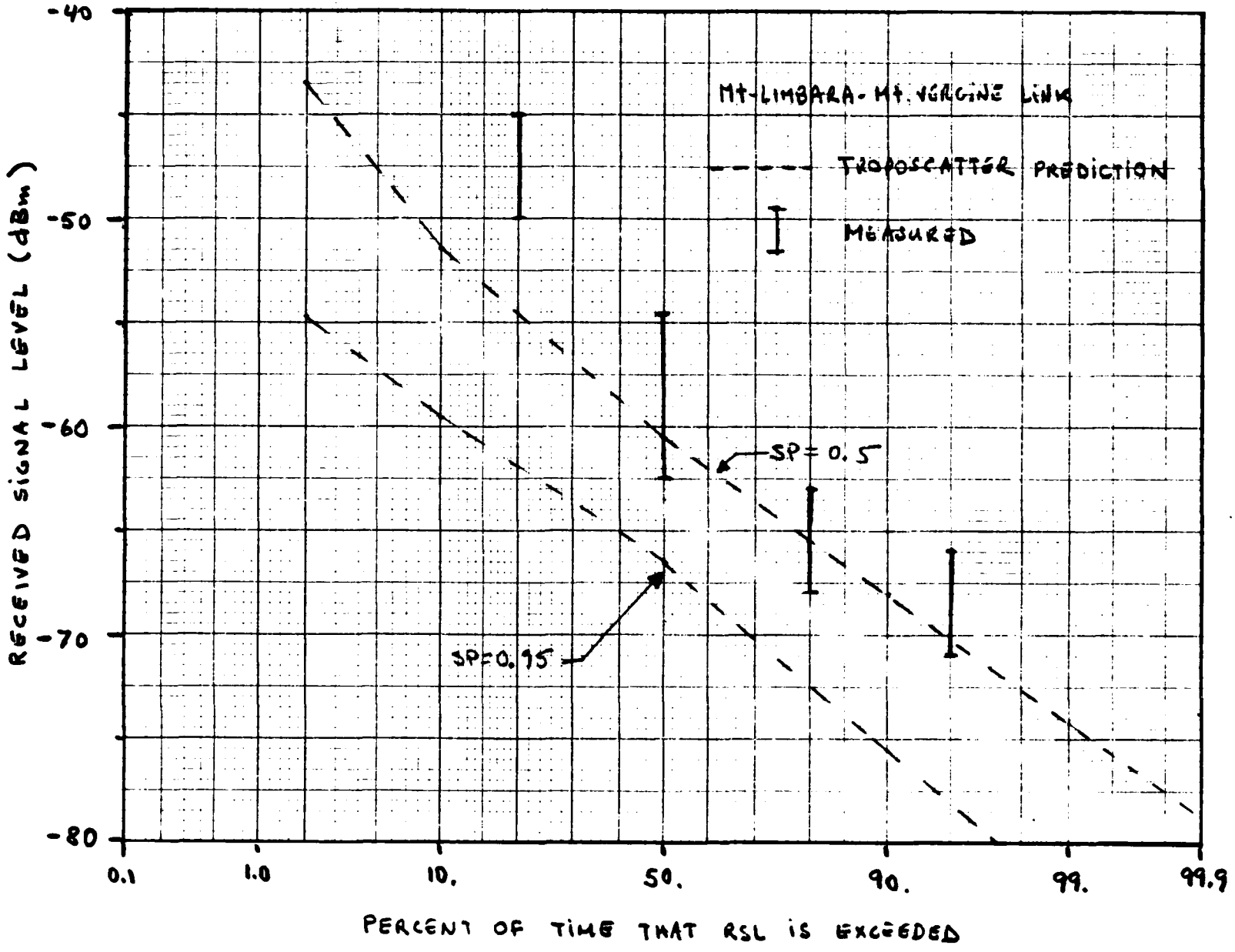

Figure 6-4 Predicted and Measured RSL Distribution for MT. LIMBARA-MT. VERGINE Link

height profile of the structure constant, C_n^2 , of the atmospheric refractive index fluctuations. The delay spreads measured by Sherwood, et al. [1977] indicate that variability in the height profile of the structure constant is the main source of variability in the delay spread. This has been determined by comparing the measured delay spread distribution with that predicted assuming a constant structure constant height profile and a variable effective earth radius factor. Thus in this case, the predicted rms delay spread exceeded 90% of the time would correspond to the effective earth radius factor not exceeded 90% of the time and the predicted rms delay spread exceed 10% of the time would correspond to the effective earth radius factor not exceeded 10% of the time.

The main path parameters which affect the rms multipath spread are the path length, scattering angle (depends on effective earth radius), frequency and antenna diameter. The path parameters of the two links on which the Sherwood, et al. [1977] measurements were made are given in Table 6-1. The distribution of the effective earth radius factor in the vicinity of the measurements for the period during which the measurements were made is shown in Figure 6-5. The predicted rms delay spread based on the measured distribution of the effective earth radius factor is shown in Figures 6-6 and 6-7. These figures also show the rms delay spread measured by Sherwood, et al. [1977]. Good agreement between the predicted median and measured median is found for the paths where 28' (Youngstown-Verona) and 8' antennas were used. However, the measured median for the Ontario Center-Verona path where 15' antennas were used is about 100 nanoseconds while the predicted median is 70 nanoseconds. The reason for the discrepancy is attributed to the prober used in the measurements (RAKE receiver) which had a resolution of 100 nanoseconds making it difficult to measure delay spreads of less than 100 nsec with any accuracy.

TABLE 6-1
PATH PARAMETERS

Link	Ontario Center-Verona	Youngstown-Verona
Path Length	86 Miles	168 Miles
Frequency	4.78 GHz	4.69 GHz
Transmit Antenna Size	8' and 15'	28'
Receive Antenna Size	8' and 15'	28'
Transmitter Take-Off Angle	.80°	1.25°
Receiver Take-Off Angle	.975°	0.75°
Transmitter Power	1 kW	3 kW

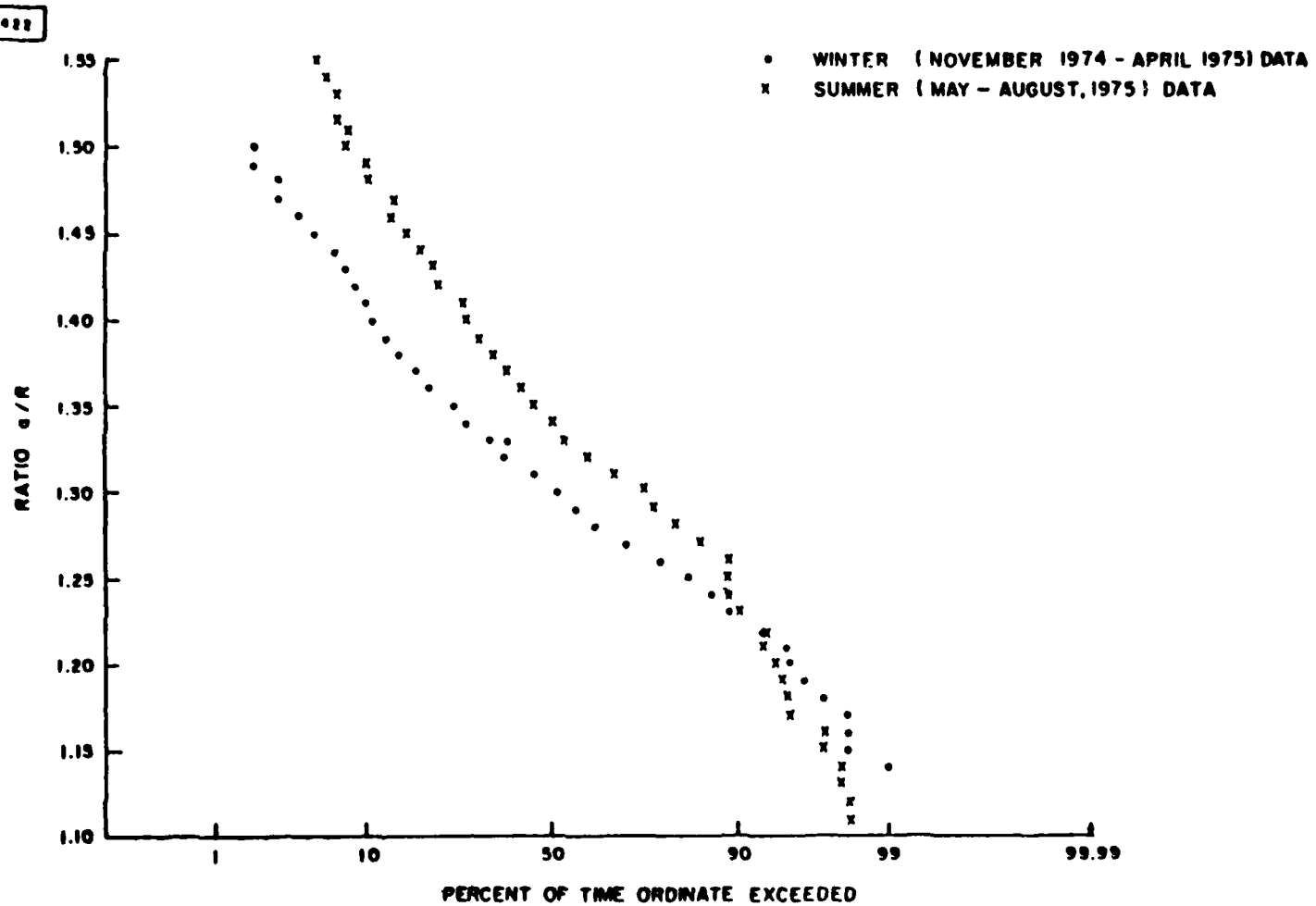

Figure 6-5 Effective Earth Radius Factor a/R Distributions - Winter and Summer Data (Buffalo)

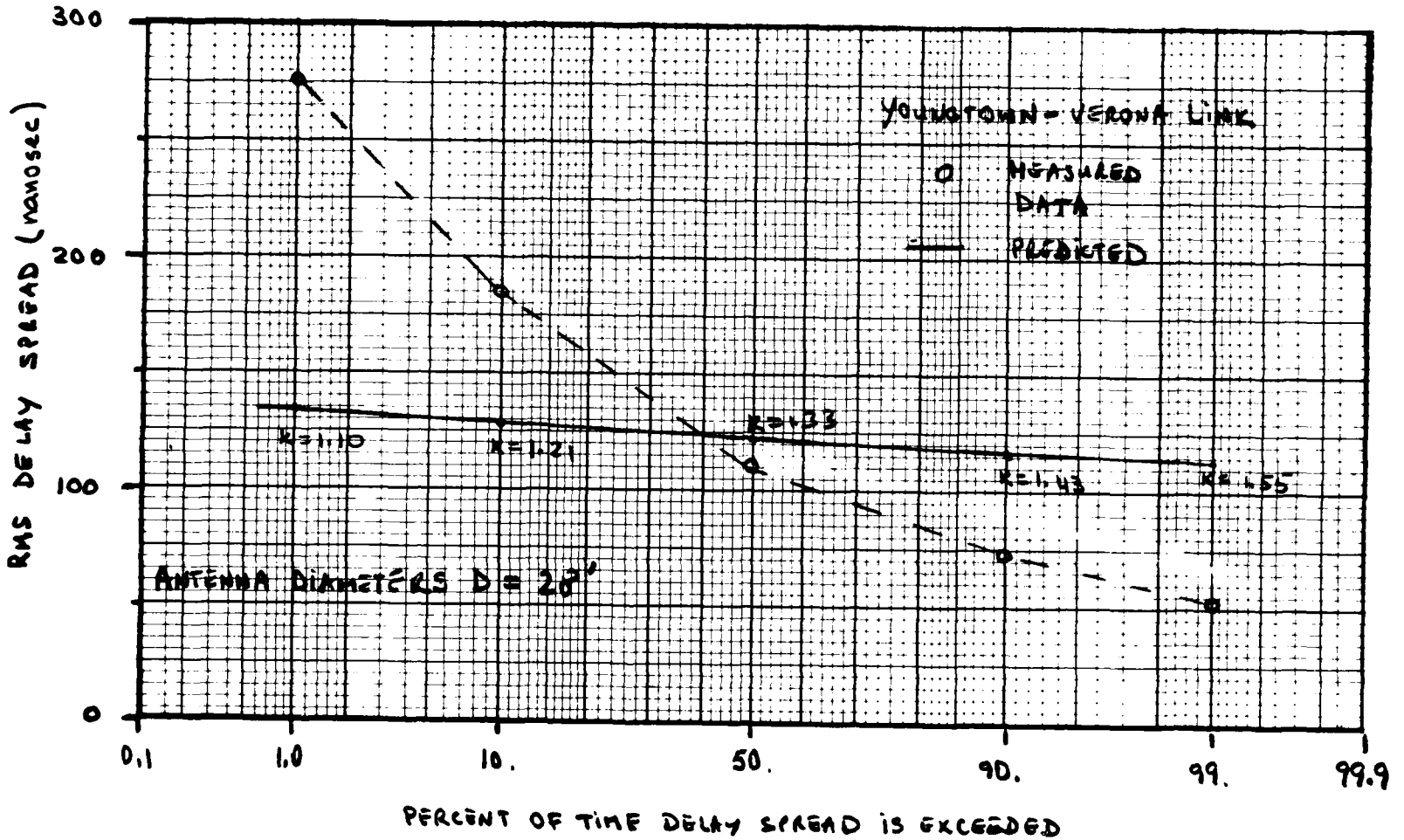

Figure 6-6 Predicted and Measured RMS Delay Spread for YOUNGSTOWN-VERONA Link

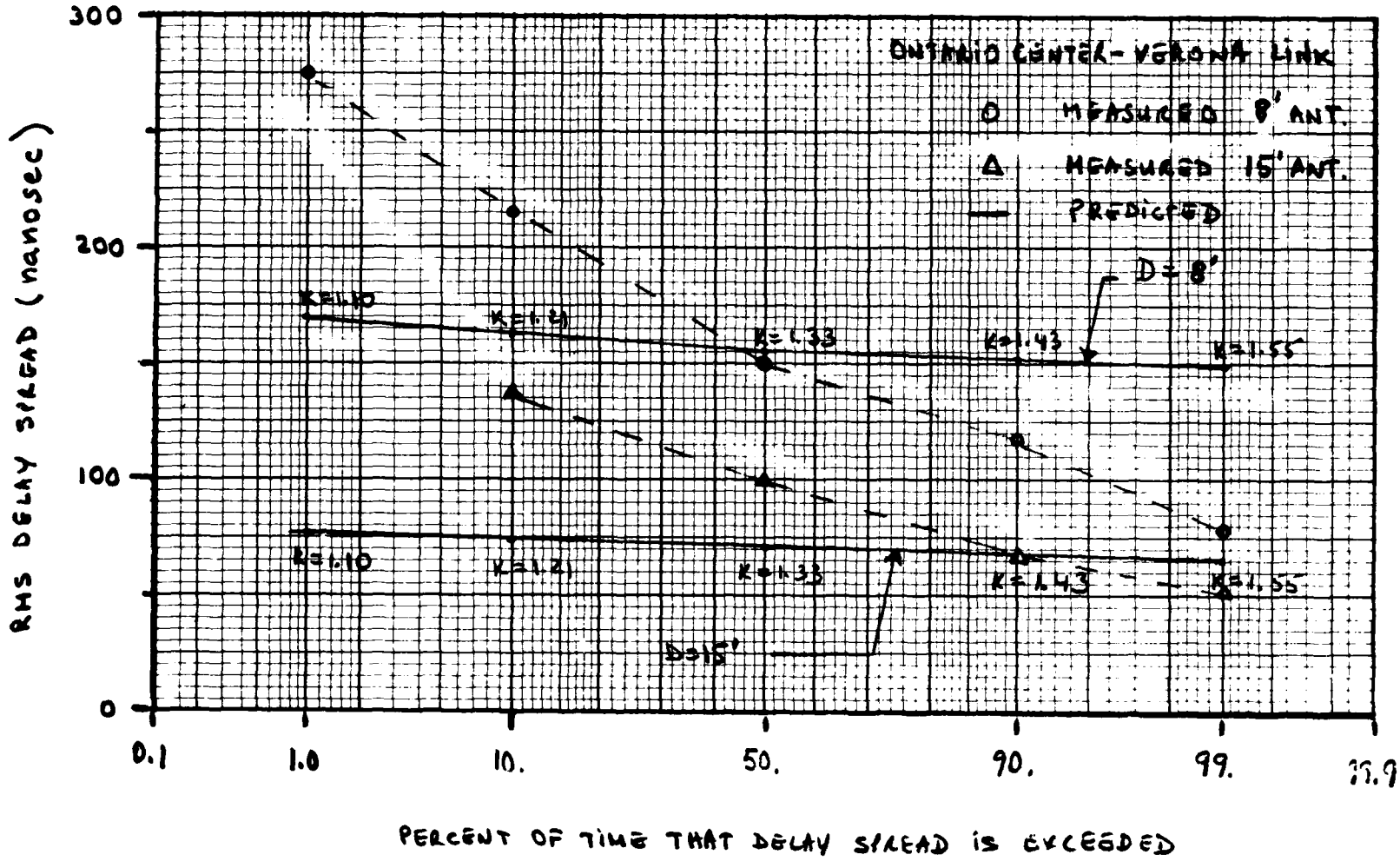

Figure 6-7 Predicted and Measured RMS Delay Spread for ONTARIO CENTER-VERONA Link

The measured variability in delay spread is seen to be much greater than that predicted based on the effective earth radius factor variability only. This leads us to conclude that most of the variability in delay spread is due to variations in the height profile of the structure constant. Unfortunately, such data is not available.

6.3 MD-918 MODEM PERFORMANCE

TROPO calculates the short-term average bit error rate, 100 bit block error probability, fade outage probability and fade outage per call minute performance of the MD-918 modem in the Rayleigh fading (pure troposcatter) and Rician fading (mixed troposcatter/diffraction) channels as a function of the average SNR per bit, $\overline{E}_b/N_0$ or peak SNR per bit, E_p/N_0. Predictions of the average yearly performance are also given for the predicted yearly median of the SNR per bit and its standard deviation.

As an example of the MD-918 modem performance calculations, we show in Figure 6-8 plots of the fade outage probability of the MD-918 in a Rayleigh fading channel (pure troposcatter) as a function of the peak SNR per bit, E_p/N_0, for various rms (2σ) delay spreads of the channel. The outage probability calculation assumes that an outage occurs whenever the (instantaneous) bit error rate is greater than 10^{-4}. Since the MD-918 uses QPSK modulation, this bit error rate threshold will be exceeded when the detection (instantaneous) SNR per bit is less than 8.4 dB. The curves of Figure 6-8 assume a 2S/2F diversity configuration, a data rate of 2.3 Mb/s and a 99% bandwidtn allocation of 3.5 MHz. The transmitter RF filter required to meet this bandwidth constraint is a 2-pole Butterworth filter with 3-dB cut-off frequency (half of 3 dB bandwidth) of 1.69 MHz. The receiver is assumed to have a 4-pole Butterworth filter with 3-dB cut-off frequency of 1.74 MHz. The peak-to-average power ratio the

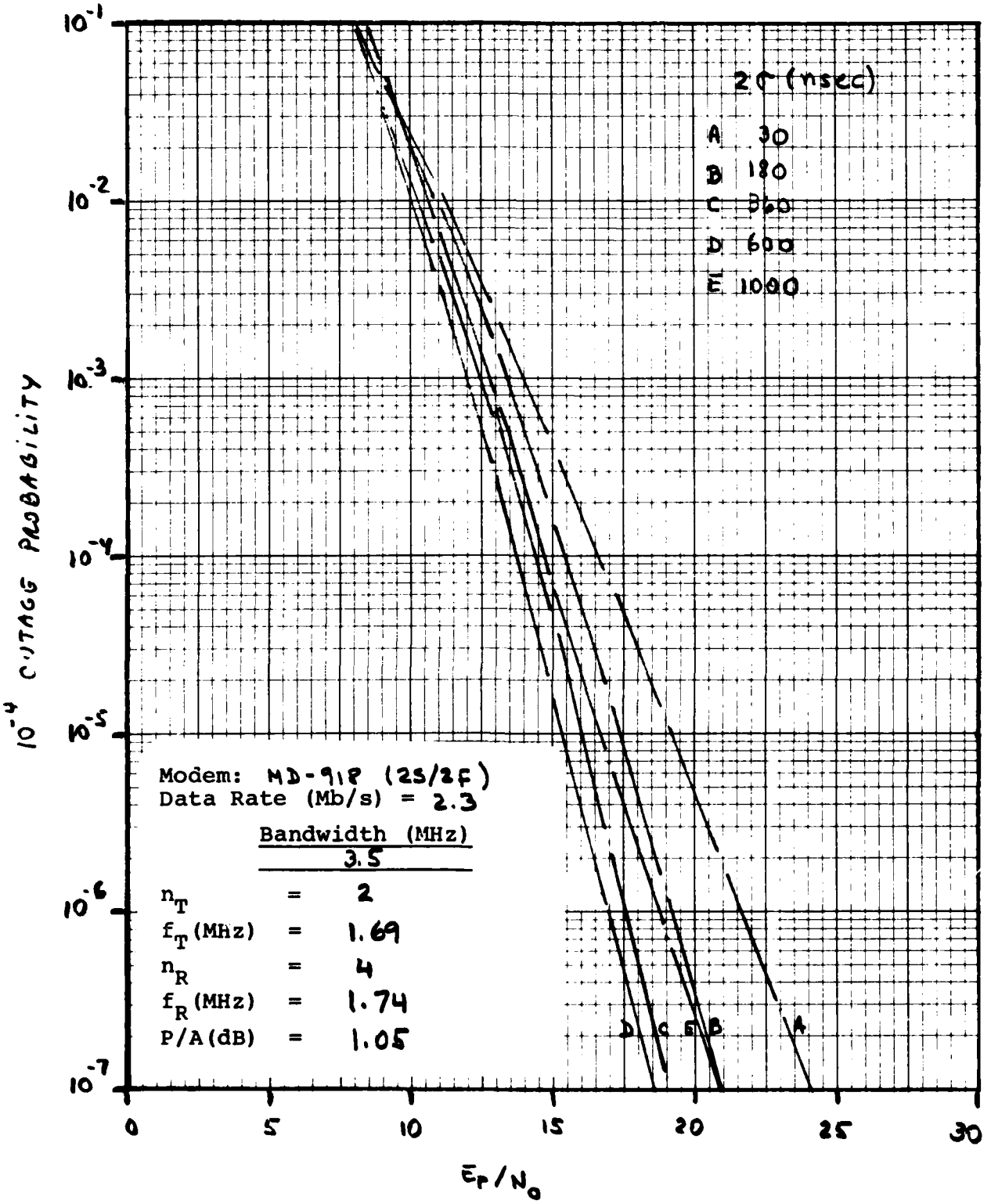

Figure 6-8 Short-term outage probability for the MD-918 modem as a function of the peak SNR per bit

transmitted waveform is 1.05 dB. The peak SNR per bit E_p/N_0 in dB is defined as the average SNR per bit, $\overline{E}_b/N_0$, in dB plus the peak-to-average loss due the transmitter RF filter.

The curves of Figure 6-8 show that the performance improves by 4 dB (at 10^{-7}) as the delay spread increases from 30 nanoseconds to 600 nanoseconds. The reason for the improvement in performance is that as the delay spread increases there is more implicit diversity in the channel. However, as the delay spread increases above 1000 nanoseconds the performance is degraded due to the large amount of intersymbol-interference (ISI) which cannot be removed by the adaptive equalizer. For comparison purposes, an ideal QPSK modem with quad diversity (2S/2F) reception with maximal ratio combining and no ISI degradation and no implicit diversity requires an average SNR per bit, $\overline{E}_b/N_0$, of 17.2 dB to achieve a fade outage probability (relative to a 10^{-4} BER threshold) of 10^{-5}.

The predicted and measured outage probability performance of the MD-918 modem (2S/2F diversity configuration) in the presence of adjacent channel interference is shown in Figure 6-9 as a function of the average SNR per bit, $\overline{E}_b/N_0$, for interference-to-signal power ratio, I/S, of $-\infty$ (no interference), 35 dB and 50 dB. The MD-918 modem data rate is 9.9 Mb/s and the bandwidth allocation is 10.5 MHz. The rms delay spread of the troposcatter channel is 693 nanoseconds. The adjacent channel interference is a QPSK signal and the frequency separation between the interference and desired signal is 21.0 MHz. The solid curves in Figure 6-9 represent the outage probability predicted by TROPO while the dashed curves are those measured under a separate DCA contract using a troposcatter channel simulator [Gadoury, 1983]. Good agreement (to within 1.5 dB) between the measured and predicted performance is seen in all cases.

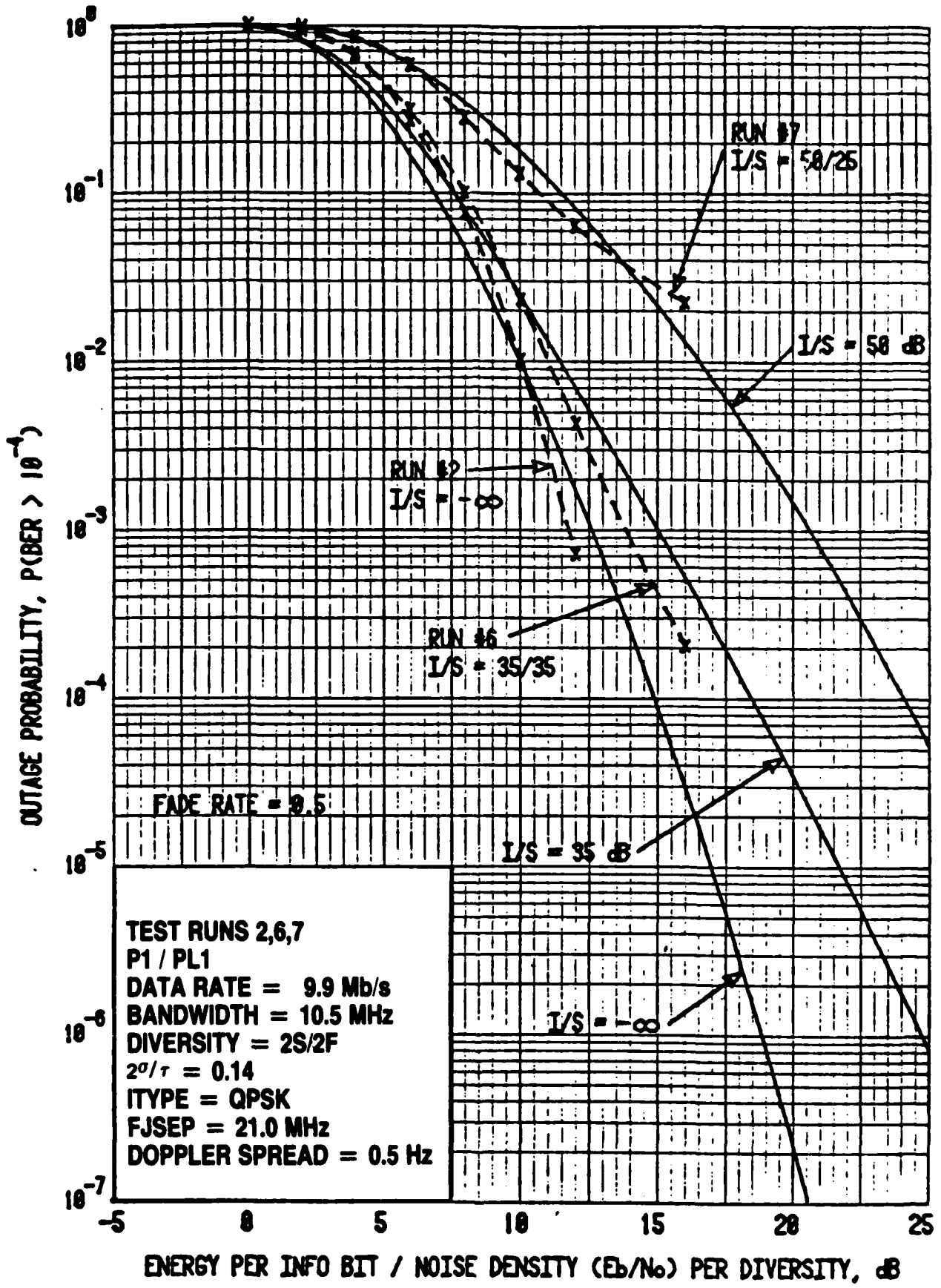

Figure 6-9 Predicted and measured MD-918 modem outage probability with adjacent channel interference as a function of the average SNR per bit for various interference-to-signal ratios (from Gadoury, 1983).

6.4 AN/TRC-170 MODEM PERFORMANCE

TROPO calculates the short-term average bit error rate, fade outage probability and fade outage per call minute performance of the AN/TRC-170 in a Rayleigh fading channel (e.g., troposcatter channel) as a function of the short-term average SNR per bit, $\bar{E}_b/N_0$ or the peak SNR per bit, E_p/N_0. Predictions of the yearly average bit error rate, average fade outage and average fade outage per call minute are also calculated for the predicted yearly median of the SNR per bit and its standard deviation.

The short term fade outage probability of the two-frequency AN/TRC-170 modem, assuming a (instantaneous) bit error rate threshold of 10^{-4}, is shown in Figure 6-10 as a function of the peak SNR per bit, E_p/N_0, for various channel delay spreads. The curves correspond to a 2S/2F configuration of the AN/TRC-170 with a data rate of 2.3 Mb/s and a 99% bandwidth allocation of 3.5 MHz. The transmitter RF filter required (per frequency) to meet the bandwidth constraint is a 2-pole Butterworth filter with 3-dB cut-off frequency of 0.86 MHz. The receiver is assumed to have a 6-pole Butterworth filter (per frequency channel) with 3-dB cut-off frequency of 0.86 MHz. The peak-to-average power ratio of the transmitted waveform is 4.1 dB. The curves show that the performance of the AN/TRC-170 also improves initially as the delay spread of the channel increases due to the greater implicit diversity available. However, the effects of the inter-symbol interference limit the modem performance when the delay spread is greater than 500 nanoseconds. For comparison purposes, we show in Figure 6-11 the performance of a modem which uses only 1-frequency (DAR modem) rather than 2 to transmit the same data rate with the same bandwidth allocation and employs the same waveform and signal processing as the AN/TRC-170. The transmitter filter for this modem is the same as for the 2-frequency AN/TRC-170. However the receiver filter does not have to filter

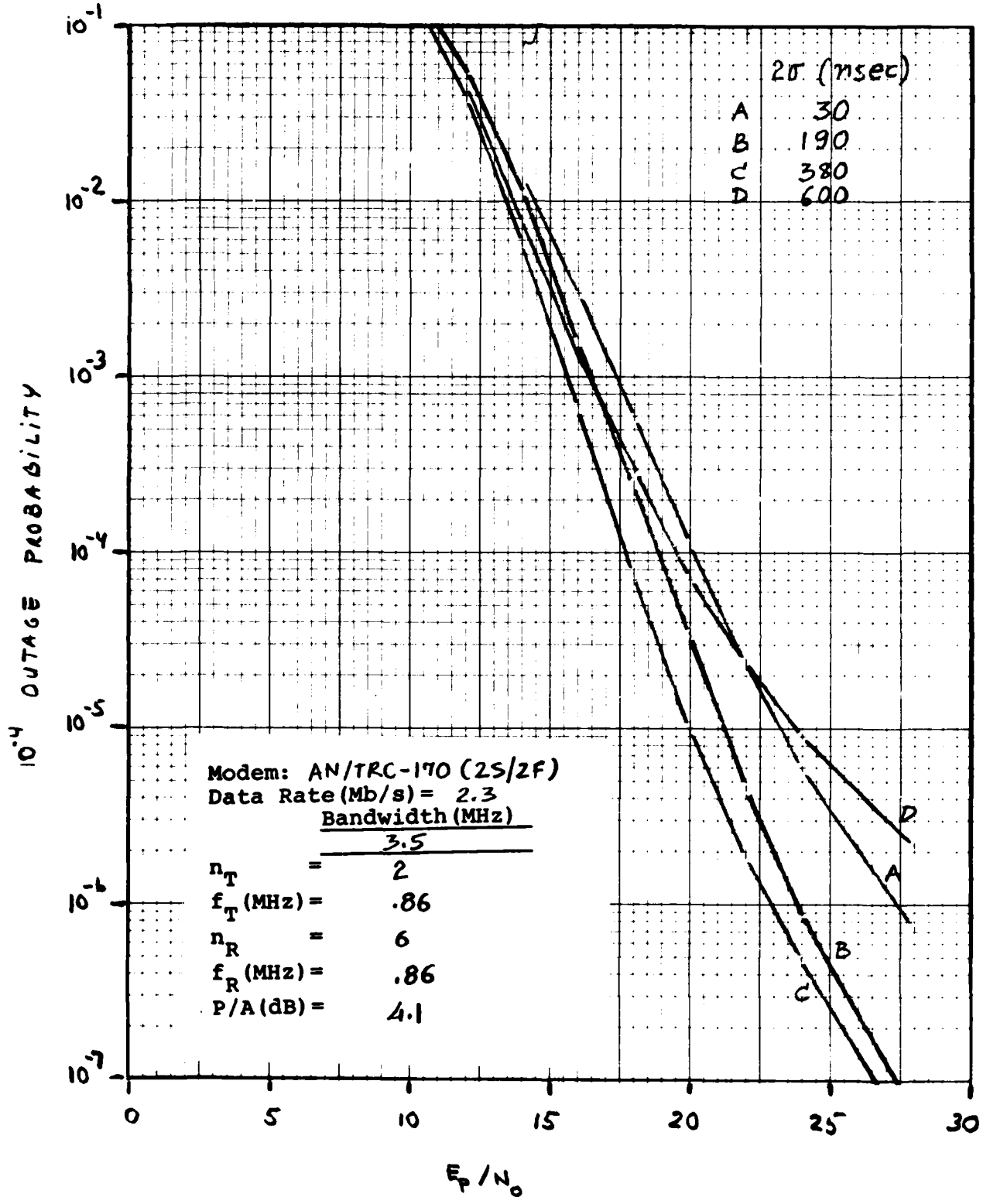

Figure 6-10 Short-term outage probability for the AN/TRC-170 modem as a function of the peak SNR per bit

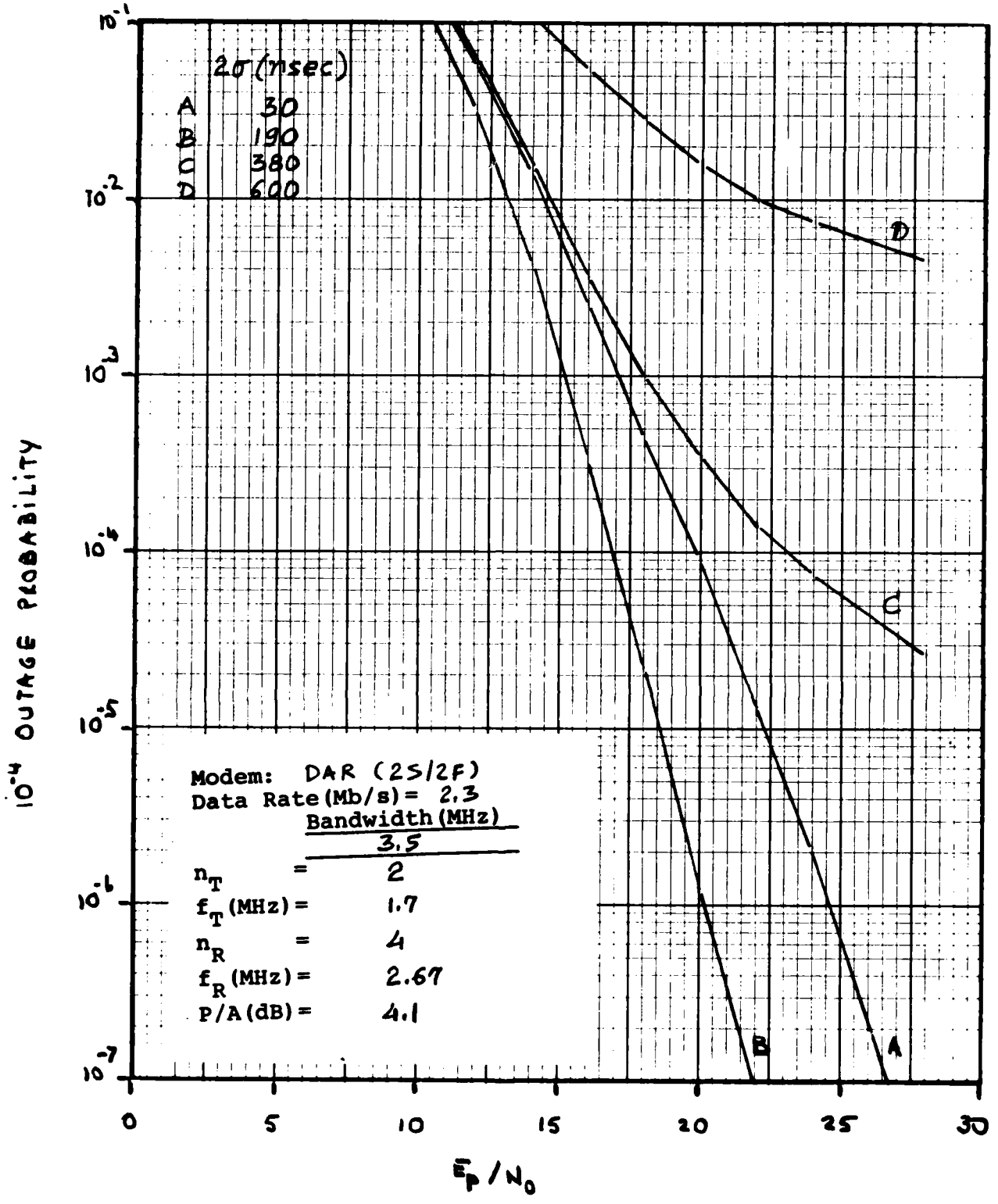

Figure 6-11 Short-term outage probability for a one frequency DAR modem as a function of the peak SNR per bit

out the other frequency and hence is assumed to be a 2-pole Butterworth filter with 3-dB cut-off frequency of 2.67 MHz. The performance of this modem is seen to be better than that of the AN/TRC-170 for channel delay spreads of less than 200 nanoseconds because of greater implicit diversity. However, its performance is severely degraded when the delay spread is 380 nanoseconds or greater.

REFERENCES

Sherwood, A. and L. Suyemoto (1977), "Multipath Measurements over Troposcatter Path", Technical Report, ESD-TR-77-252, Electronic Systems Division, Air Force Systems Command, U.S. Air Force, Hanscom Air Force Base, Bedford, MA.

Gadoury, J.B. (1983), "Error Performance Characterization Study of a Digital Troposcatter Modem (MD-918/GRC)", Final Report on Contract DCA100-80-C-0031, GTE Products Corporation, for the Defense Communications Agency.

APPENDIX A

Performance Analysis Of The AN/TRC-170 Modem On A Fading Multipath Channel

INTRODUCTION

The AN/TRC-170 digital modem [1,2,3] is a decision directed adaptive system for troposcatter communications. Currently the AN/TRC-170 modem accommodates data rates up to 2.3 Mb/s and is primarily used to link tactical air bases with command and control elements.

Figure A-1 illustrates the system concept for BPSK transmission. The transmitted pulse occupies a fraction (usually 1/2) of the symbol interval as a means to reduce the ISI effects due to channel distortion. The received waveform as well as past decisions on the transmitted data are used to derive an estimate (the reference pulse) of the channel pulse at the output of the Adaptive Channel Estimator (ACE). Originally the ACE subsystem employed a recirculating filter with positive feedback gain $K<1$, to reduce the noise in the reference waveform, Figure A-2a. Because of implementation difficulties [3] the recirculating filter was replaced by a 24 tap delay line, Figure A-2b, which is currently in use.

The ACE is followed by an implementation of a classical matched filter. The reference waveform and the received waveform (both at IF) are mixed and the output passes through a low-pass filter to obtain the envelope. This is then integrated over one symbol interval and sampled to form the decision variable. The combination of signals from other diversities may take place before the integrator to reduce system complexity. Assuming that

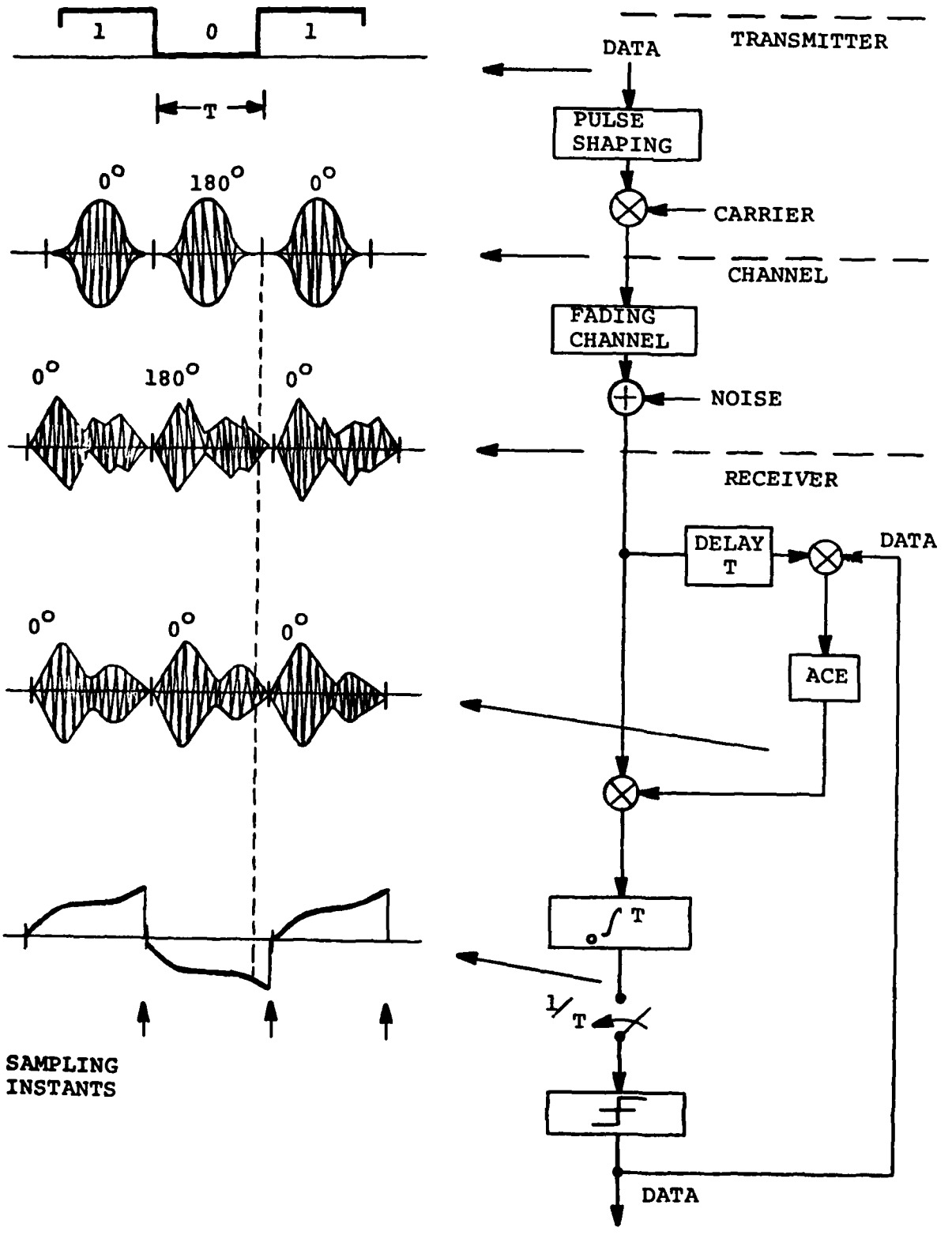

Figure A-1 TRC-170 System Concept for BPSK Transmission

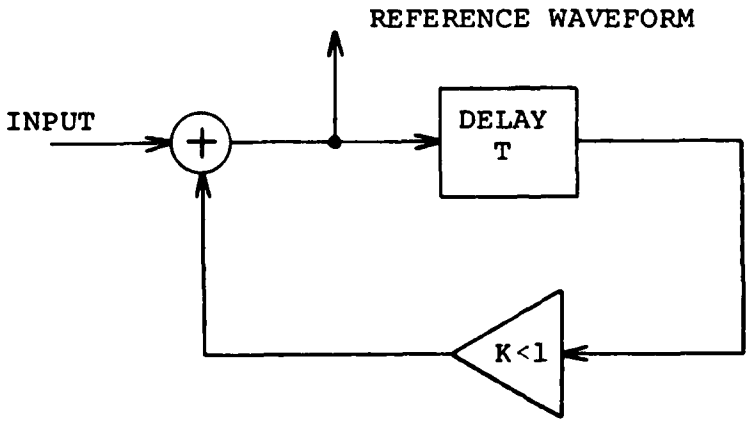

(a)

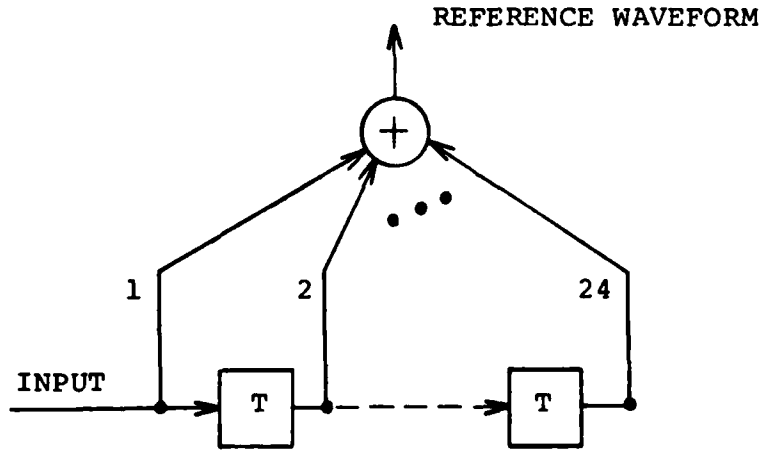

(b)

Figure A-2 Implementation of the Adaptive Channel Estimator (ACE): (a) Recirculating Loop; (b) 24-tap Delay Line

the noise powers at each diversity input are equal and uncorrelated the weighting of the received waveform by the reference waveform and summing corresponds to maximal ratio combining of the diversities.

The necessary modifications of the basic design to accommodate QPSK transmission are shown in Figure A-3. One ACE serves both the I and Q channels. Finally, Figure A-4 shows a modification of the basic design which employs QPSK transmission at 2 frequencies. At the transmitter one of the transmission waveforms is shifted in time by half the symbol interval and added to the other. At the receiver the two waveforms are separated by channelizing filters, aligned in time and processed by separate QPSK modules. The 2 frequency system, which is actually employed in the TRC-170 modem, has twice the complexity of the single frequency system, but it can accommodate twice as high data rates for the same multipath spread tolerance.

Although this system has been extensively documented there has not been published yet an analysis of its performance under multipath fading and ISI conditions. This is the objective of the analysis presented in this section. In the following in Section A.1 we develop a system model that includes ISI effects, and approximate the distribution of the probability of error for a Rayleigh fading channel. In Section A.2 we average over the channel statistics to find the average probability of error (average bit error rate, ABER) as well as the probability that a given error threshold is exceeded (outage probability). Appendicies B-E contain the proofs of some of the mathematical results of the analysis.

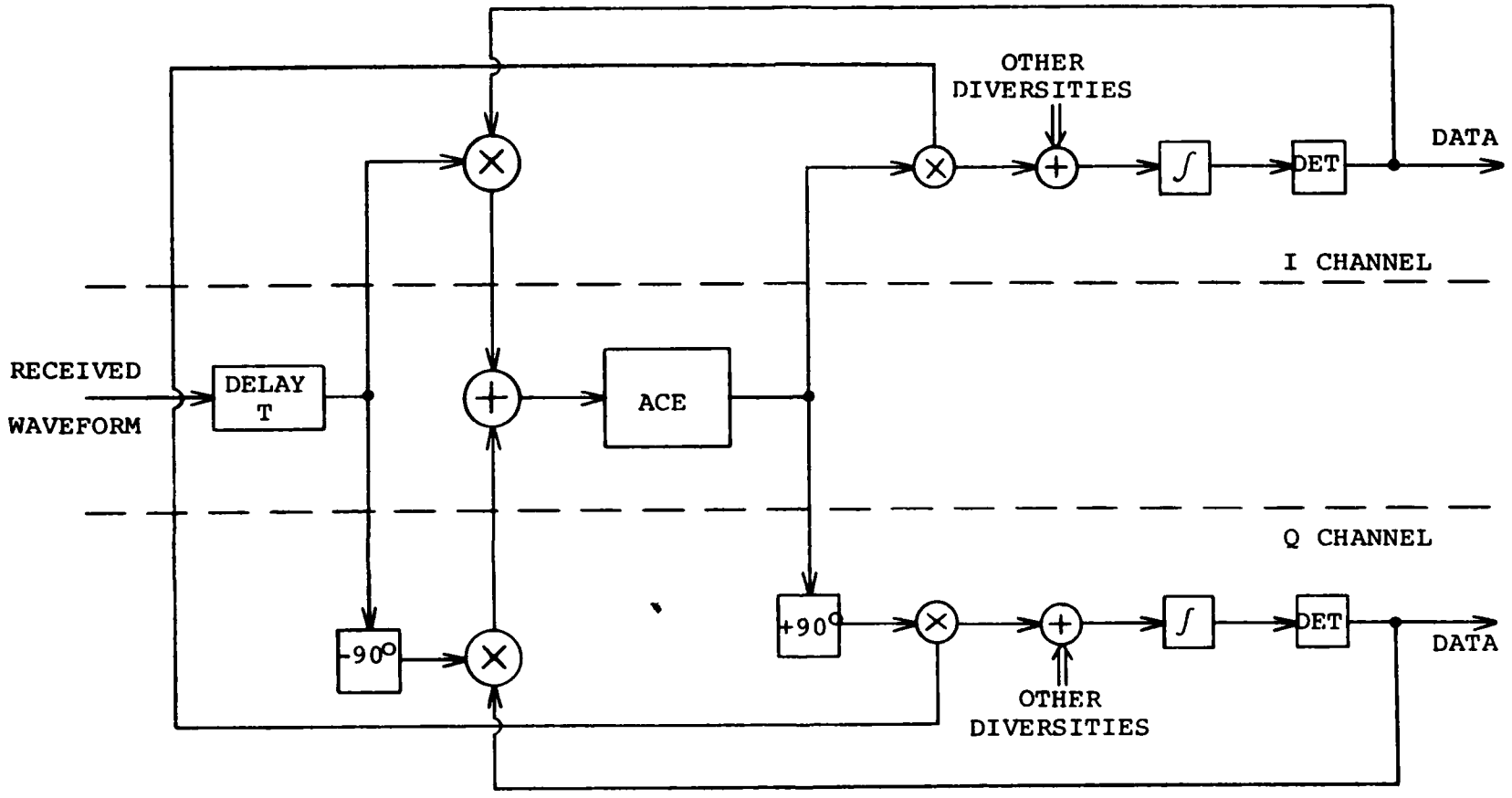

Figure A-3 TRI-170 System Concept for QPSK Transmission

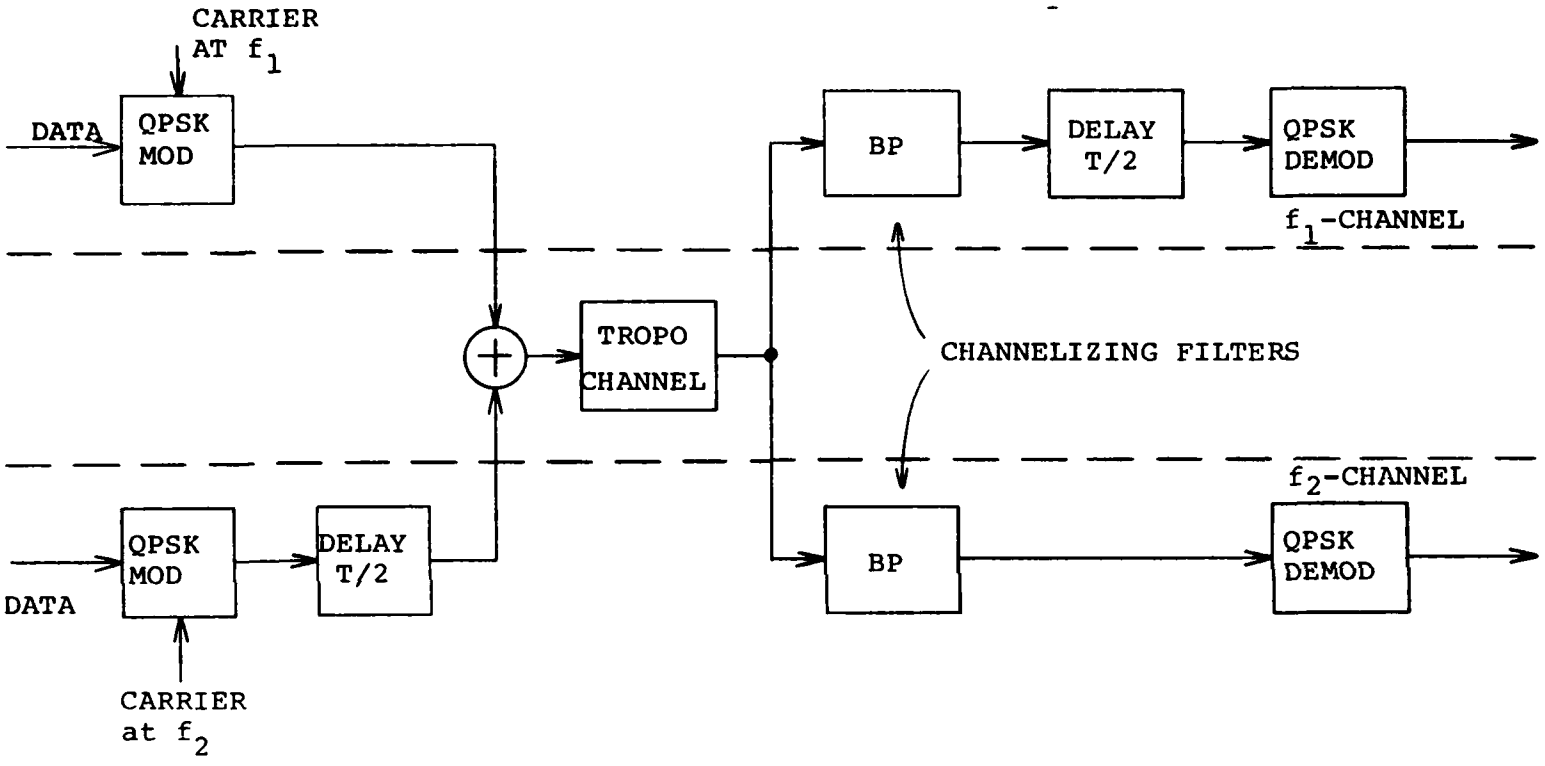

Figure A-4 TRI-170 System Concept for a 2-Frequency Operation

A.1 SYSTEM MODEL

In the following we use complex notations to represent in-phase and quadrature components. Explicit modulation-demodulation operations are not shown. We distinguish between the two frequency channels of the system by using unprimed symbols for the frequency f_1 and primed symbols for the frequency f_2. We assume throughout that the data transmitted at f_1 are independent from the data transmitted at f_2. The transmitted waveform then can be expressed as:

$$s(t) = \sum_k \left(s_k p_T(t-kT) + s_k' p_T'(t-kT)\right) . \qquad (A.1)$$

The data s_k have the form a_k+jb_k, $a_k,b_k=\pm 1$. p_T is the impulse response of the pulse shaping filter at the transmitter, and it is assumed to have unit energy. T is the symbol interval.

The tropospheric channel is modeled as a randomly time varying linear system. The response at time t_1 due to a unit energy impulse applied at time t_1-t is $E_b^{1/2}h(t;t_1)$, where the constant E_b refers to the average attenuation of the signal and $h(t;t_1)$ is a zero mean complex Gaussian random process in the time variable t_1. Generally, the autocorrelation of h is

$$\langle h(t+\tau;t_2)\, h^*(t;t_1)\rangle = R_h(t+\tau,t;t_2,t_1) .$$

We use < > to denote averaging over a known ensemble. Regarding R_h, we assume that the process h is wide sense stationary (WSS) so that:

$$R_h(t+\tau,t;t_2,t_1) = R_h(t+\tau,t;|t_2-t_1|) \ ,$$

and that the channel response associated with path delay $t+\tau$ is uncorrelated with the response associated with path delay t so that:

$$R_h(t+\tau,t;|t_2-t_1|) = \delta(\tau)R_h(t;|t_2-t_1|) \ .$$

The last assumption is referred to as the uncorrelated scattering (US) assumption and the combined model of the fading channel is usually referred to as the WSSUS model.

To consider the effect of the time variations of the channel, let $R_H(f;\Delta t)$ be the Fourier transform of $R_h(t;\Delta t)$ and consider the function $R_H(0;\Delta t)$. The range of Δt over which this function is significant is the coherence time of the channel, i.e., the changes of the channel within that interval are small. Typical coherence times for the troposcatter channel are of the order of 0.1 sec. Therefore, for symbol rates of the order of 500 kHz, typical for applications of the AN/TRC-170 system, we can practically assume that the channel response is constant. In the following we omit for convenience the dependence of the channel on time differences Δt. Finally, we assume that the various diversity channels are independent. Our model for the diversity channels i and j can be summarized:

$$\langle h_i(t+\tau)h_j^*(t)\rangle = \delta_{ij}\delta(\tau)\, R_h(t) \quad . \tag{A.2}$$

$R_h(t)$ is referred to as the multipath intensity profile. It is normalized to unit area and its standard deviation is usually denoted by σ.

If a single pulse is transmitted through the channel, the received power will be spread on the average within the multipath spread interval of length 2σ. Typical multipath spreads for the troposcatter channel are of the order of .1 μsec. The multipath profile can either be computed on the basis of the antenna configuration or given the parameter σ it can be approximated by a gamma function:

$$R_h(t) \approx b^2 te^{-bt}, \quad b=\sqrt{2}/\sigma \quad .$$

We assume that all diversity channels have the same average attenuation, E_b. The ith diversity channel distortion also includes additive complex white Gaussian noise $n_i(t)$ with power density N_0. The noise processes in the various diversity channels are independent but have the same power density. Under these conditions the received waveform at the ith diversity channel is:

$$r_i(t) = E_b^{1/2} s*h_i(t) + N_0^{1/2} n_i(t) \tag{A.3}$$

where * denotes the convolution operation.

The average received energy per symbol per diversity channel is:

$$|s_k|^2 E_b \int \langle |p_T * h_i(t)|^2 \rangle dt = 2E_b \int p_T^2(t)dt \int R_h(\tau)d\tau \ .$$

Therefore, the received SNR per bit and per diversity channel is E_b/N_0.

From now, we consider the group of the subchannels at frequency f_1. The received waveform first passes through a channelizing filter $p_R(t)$ which rejects the portion of the signal transmitted at frequency f_2. The resulting waveform $p_R * r_i$ is then fed to the ACE of the ith diversity. Let us denote the complex random pulse $p_T * h_i * p_R$ by q_i. We usually refer to this pulse as the signal pulse. The waveform $p_R * r_i$ can then be expressed as:

$$r_i * p_R(t) = E_b^{1/2} s_m q_i(t-mT) + E_b^{1/2} \sum_{k \neq 0} s_{m-k} q_i\big(t-(m-k)T\big) + N_0^{1/2} n_i * p_R(t)$$

$$+ E_b^{1/2} \sum_k s_k' p_T' * h_i * p_R(t-kT) \ . \qquad \text{(A.4)}$$

We have singled out the contribution of the mth pulse to consider the detection of the mth symbol. The decision variable for the mth symbol depends on the values of $r_i * p_R$ in the observation interval:

$$t_0 + mT < t < t_0 + (m+1)T \ . \qquad \text{(A.5)}$$

The parameter t_0 adjusts the sampling instants on the received waveform and it will be referred to as the sampling time. Let us denote by $\hat{q}_{I,i}(t)$ the output at the I-channel of the ACE. After mixing the received and the reference waveform, diversity combining, integration over the interval (5) and sampling, the decision variable for the mth bit in the I-channel is:

$$\tilde{a}_m = \sum_{i=1}^{D} R_e\{ \int_{t_0+mT}^{t_0+(m+1)T} r_i^* p_R(t) \hat{q}_{I,i}(t) dt \} \qquad (A.6)$$

where D is the number of the diversity channels.

From Eqs. (A.4) and (A.6) the decision variable $\tilde{a}_m$ can be decomposed into a signal term:

$$E_b^{1/2} Re\{ s_m \sum_{i=1}^{D} \int_{t_0+mT}^{t_0+(m+1)T} q_i(t-mT) \hat{q}_{I,i}^*(t)\, dt \}, \qquad (A.7)$$

an ISI term:

$$E_b^{1/2}\, Re\{ \sum_{k\neq 0} s_{m-k} \sum_{i=1}^{D} \int_{t_0+mT}^{t_0+(m+1)T} q_i(t-mT+kT) \hat{q}_{I,i}^*(t) dt \}, \qquad (A.8)$$

a noise term:

$$N_0^{1/2}\ R_e\Big\{\sum_{i=1}^{D}\int_{t_0+mT}^{t_0+(m+1)T} n_i^* p_R(t)\hat{q}_{I,i}^{**}(t)dt\Big\} \qquad (A.9)$$

and an f_2-interference term:

$$E_b^{1/2}\ \mathrm{Re}\Big\{\sum_k s_k'\sum_{i=1}^{D}\int_{t_0+mT}^{t_0+(m+1)T} p_T'^* h_i^* p_R(t-kT)\hat{q}_{I,i}^{**}(t)dt\Big\}\ . \qquad (A.10)$$

The analysis of the system performance in the next part is largely based on the statistical identification of the above components of the detection variable.

A.2 PERFORMANCE ANALYSIS

For a short interval of time during which the channel response is essentially invariant, the system yields a certain bit error rate (BER), denoted as P_e. We are interested in the channel-average bit error rate (ABER), denoted as P_{avg}:

$$P_{avg} = \langle P_e \rangle_{channel}\ ,$$

as well as the outage probability at a given threshold p_{thr}, denoted as P_{out}:

$$P_{out} = Pr\{P_e > p_{thr}\} .$$

These performance measures require a complete statistical description of the components of the detection variable, which we do in Subsection A.2.1. In Subsection A.2.2, we calculate the BER by averaging over the ISI interference. In Subsection A.2.3, we calculate the ABER, which can be computed exactly. Unfortunately, the exact computation of the outage probability is inefficient. In Subsection A.2.4 we present an algorithm which computes a tight upper bound of the outage probability.

A.2.1 Analysis of the Detection Variable

One major item which affects the signal and distortion components of the detection variable is the reference pulse $\hat{q}_{I,i}$ at the output of the ith ACE. In Appendix E we show that if s_m does not fall in a long burst of same transmitted symbols, then during the mth observation interval $\hat{q}_I$ approximates well the signal pulse q:

$$\hat{q}_I(t) = Gq(t-mT) . \qquad (A.11)$$

G is a constant which scales the entire detection variable and therefore it can be set equal to 1. Eq. (A.11) implies that the reference pulse is free from noise and ISI distortion but it includes the effects of the sampling time jitter as Figure A-5 shows.

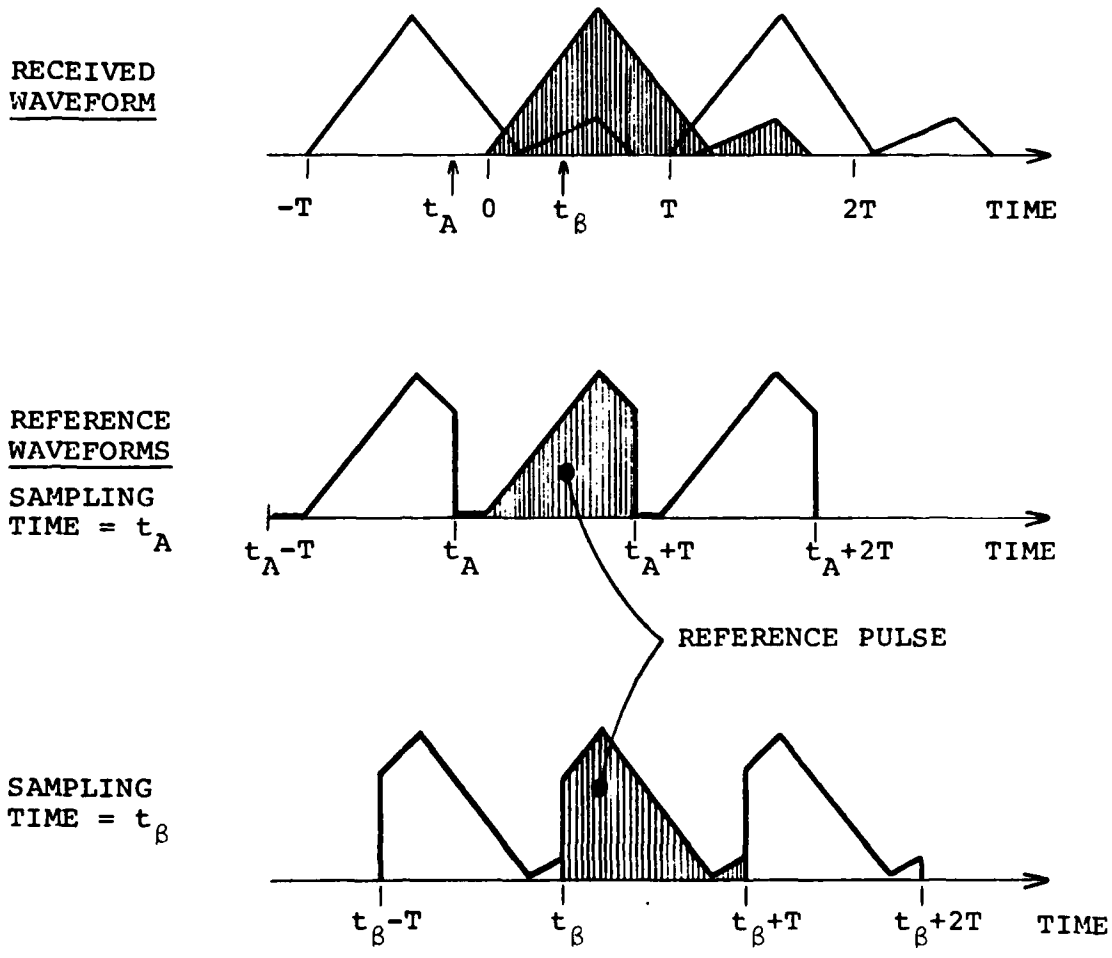

Figure A-5 Effects of the Sampling Time on the Reference Waveform

Next we consider the noise + f_2-interference terms. We take into account the interference by considering the interference signal after IF-filtering as noise-like and this effectively increases the noise power density from N_0 to N_f. In Appendix B we compute the average interference power after IF-filtering and we show that the equivalent noise spectral density is (Eq. (B7)):

$$N_f = N_o \left[1 + \frac{2}{T} \cdot \frac{E_b}{N_o} \cdot \frac{\int S_T(f+\Delta f)\, S_R(f)\, d_f}{\int S_R(f)\, d_f}\right]$$

where $S_a(f) = |P_a(f)|^2$ is the power spectrum corresponding to the filter $p_a(t)$ and $\Delta f = |f_1 - f_2|$ is the frequency separation of the two transmission channels. Regarding the noise we note that since $n_i(t)$ is involved linearly the total noise n_d is a normal, zero mean, random variable. In Appendix B we derive the variance σ_d^2 of the detection noise:

$$\sigma_d^2 = \frac{1}{2} N_f \sum_{i=1}^{D} \int_{t_0}^{t_0+T} \int q_i(v) q_i^*(u) B_{p_r}(v-u)\, dv\, du \qquad (A.12)$$

where $B_x(a)$ denotes the correlation function of $x(t)$ at lag a:

$$B_x(a) = \int x(t)x(t-a)dt \; . \qquad (A.13)$$

We note that if p_R has substantially larger bandwidth than p_T, which corresponds to a large separation of the two frequency subchannels, the function B_{p_r} effectively limits the integral of Eq. (A.12) on the line $u=v$. For analytical reasons, which will

be clear in the following sections, we shall approximate the RX-filter correlation as a δ-function so that Eq. (A.12) yields:

$$\sigma_d^2 \simeq \frac{1}{2} N_d \sum_{i=1}^{D} \int_{t_0}^{t_0+T} |q_i(u)|^2 du \ . \qquad (A.12')$$

The noise spectral density N_d is the compensation to N_f to preserve the same average noise power $\langle \sigma_d^2 \rangle$, the averaging considered over the channel statistics, in Eqs. (A.12) and (A.12'). In Appendix B we show that (Eq. (B18)):

$$N_d = N_f \frac{\int R_h(t) f_2(t) dt}{\int R_h(t) f_1(t) dt}$$

where:

$$f_1(t) = \int_{t_0}^{t_0+} \int p_T^* p_R(u-t) p_T^* p_R(v-t) B_{p_r}(v-u) du dv$$

$$f_2(t) = \int_{t_0}^{t_0+T} [p_T * p_R(u-t)]^2 du$$

We consider now the signal and ISI terms of the decision variable. Substituting the reference pulse from Eq. (11) and changing the variable of integration we obtain in place of Eqs. (A.7) and (A.8):

SIGNAL: $$a_m E_b^{1/2} \sum_{i=1}^{D} \int_{t_0}^{t_0+T} |q_i(t)|^2 dt \qquad (A.7')$$

ISI: $$E_b^{1/2} \, \mathrm{Re}\left\{ \sum_{k\neq 0} s_{m-k} \sum_{i=1}^{D} \int_{t_0}^{t_0+T} q_i(t+kT) q_i^*(t) dt \right\} . \qquad (A.8')$$

We define the random variables:

$$\gamma = \sum_{i=1}^{D} \int_{t_0}^{t_0+T} |q_i(t)|^2 dt \qquad (A.14)$$

$$\alpha_k + j\beta_k = \sum_{i=1}^{D} \int_{t_0}^{t_0+T} q_i(t+kT) q_i^*(t) dt, \quad k=\pm 1, \pm 2, \ldots \qquad (A.15)$$

Substituting γ, α_k, β_k in Eqs. (A.7'), (A.8'), and (A.12') we see that the detection variable $\tilde{a}_m$ can be expressed compactly as:

$$\tilde{a}_m = a_m E_b^{1/2} \gamma + E_b^{1/2} \sum_{k\neq 0} (\alpha_k a_{m-k} - \beta_k b_{m-k}) + n_d \qquad (A.16)$$

where the variance of the noise n_d is $\sigma_d^2 = 1/2 \, N_d \gamma$. To reduce the complexity of the calculations we shall limit the ISI effects to the past pulse s_{m-1} and the future pulse s_{m+1} only. Let us introduce the ISI-signal vector $\underline{s}_I$:

$$\underline{s}_I = (a_{m-1}, b_{m-1}, a_{m+1}, b_{m+1})^T , \qquad (A.17)$$

and the ISI-weight vector $\underline{\gamma}_I$:

$$\underline{\gamma}_I = (\alpha_1, \beta_1, \alpha_{-1}, \beta_{-1})^T . \tag{A.18}$$

Then Eq. (A.16) reduces to:

$$\tilde{a}_m = a_m E_b^{1/2} \gamma + E_b^{1/2} \underline{\gamma}_I^T \underline{s}_I + n_d . \tag{A.16'}$$

We consider now the effects of the random channel variations. Since γ as well as $\underline{\gamma}_I$ depend on the channel response n_i they are random variables with statistics determined by the channel model of Eq. (A.2). We usually refer to γ as the signal gain. Clearly, a complete description of the detection variable requires knowledge of the joint probability density function $\text{pdf}(\gamma, \underline{\gamma}_I)$. This is computationally a very difficult problem and we shall resort to the following simplifications:

1. $$\text{pdf}(\gamma, \underline{\gamma}_I) = \text{pdf}(\gamma)\ \text{pdf}(\alpha_1)\ \text{pdf}(\beta_1)\ \text{pdf}(\alpha_{-1})\ \text{pdf}(\beta_{-1}) . \tag{A.17}$$

2. The r.v's α_k, β_k are normal. (A.18)

In Appendix C we study the distribution of the gain. We show that:

$$\text{pdf}(\gamma) \approx \sum_{i=1}^{D} \sum_{j=1}^{N} A_{ij}(\underline{\lambda})\, G_i(\gamma;\lambda_j), \quad \gamma>0 , \tag{A.19}$$

where the parameter N is determined empirically to approximate the non-diversity gain as a sum:

$$\int_0^T |q(t+t_0)|^2 dt \approx \frac{T}{N} \sum_{j=1}^{N} |q(j\,\frac{T}{N} + t_0)|^2 .$$

The parameters λ_j are the eigenvalues of the covariance matrix V:

$$\begin{aligned} V_{m,n} &= \frac{T}{N} < q(\tfrac{mT}{N} + t_0)q^*(\tfrac{nT}{N} + t_0) > \\ &= \frac{T}{N} \int p_T{}^* p_R(\tfrac{mT}{N} - u)p_T{}^* p_R(\tfrac{nT}{N} - u)R_h(u + t_0)du, \end{aligned} \tag{A.20}$$

the parameters A_{ij} are known functions of the eigenvalues $\underline{\lambda} = (\lambda_1, \ldots, \lambda_N)^T$:

$$A_{D-i,j}(\underline{\lambda}) = \frac{1}{\lambda_j^i\, i!} \frac{d^i}{ds^i} \prod_{k(\neq j)=1}^{N} \frac{1}{(1+\lambda_k s)^D} \Bigg|_{s=-1/\lambda_j}$$

and $G_i(x;\lambda)$ is the ith order gamma density for the r.v. x with parameter λ:

$$G_i(x;\lambda) = \frac{1}{\lambda^i (i-1)!} x^{i-1} e^{-x/\lambda}, \quad x>0 . \tag{A.21}$$

Regarding the ISI weights, the Gaussian model requires that their mean and variance be known. These calculations are done in Appendix D. The mean turns out to be zero. The variance is:

$$\text{var}(\alpha_k) = \text{var}(\beta_k) = \frac{D}{2} \int\int R_h(u+t_0) R_h(v+t_0) I^2(u,v-kT) du dv. \tag{A.22}$$

where the function I(x,y) is a correlation type integral for the pulse $p_T * p_R$:

$$I(x,y) = \int_0^T p_T * p_R(t-x) p_T * p_R(t-y) dt . \tag{A.23}$$

A.2.2 The Bit Error Rate

During an interval when the channel is essentially fixed the BER depends on the transmitted symbols that are adjacent to the current symbol, or in our terminology on the ISI-signal $\underline{s}_I$. Our approach is to determine the BER $P_e(\ell)$ for a general ISI-signal $\underline{s}_I(\ell)$ and then average over all possible ISI-signals:

$$P_e = \sum_{\ell} P_e(\ell) \Pr\{\underline{s}_I(\ell)\} . \tag{A.24}$$

Since we have limited the dimension of $\underline{s}_I$ to 4, Eq. (A.17), and each component, can take independently the values ±1, there are 16 possible vectors $\underline{s}_I$ each one with probability 1/16. On the basis of Eq. (A.16') we see that if the transmitted symbols correspond to $\underline{s}_I(\ell)$ the BER by definition is:

$$P_e(\ell) = 1/2 \Pr\{n_d + E_b^{1/2} \underline{\gamma}_I^T \underline{s}_I(\ell) > E_b^{1/2} \gamma \Big| a_m = -1\}$$

$$+ 1/2 \Pr\{n_d + E_b^{1/2} \underline{\gamma}_I^T \underline{s}_I(\ell) < -E_b^{1/2} \gamma \Big| a_m = 1\} . \quad (A.25)$$

Taking into account that the noise n_d is zero mean normal with variance $\sigma_d^2 = 1/2\, N_d \gamma$, Eq. (A.25) yields:

$$P_e(\ell) = 1/4 \operatorname{erfc}[(E_b/N_d)^{1/2} \gamma^{1/2} (1 - \underline{\gamma}_I^T \underline{s}_I(\ell)/\gamma)]$$

$$+ 1/4 \operatorname{erfc}[(E_b/N_d)^{1/2} \gamma^{1/2} (1+ \underline{\gamma}_I^T \underline{s}_I(\ell)/\gamma)] , \quad (A.26)$$

where erfc(x) is the complimentary error function:

$$\operatorname{erfc}(x) = (2/\pi^{1/2}) \int_x^\infty e^{-u^2} du \quad . \quad (A.27)$$

When we substitute $P_e(\ell)$ from Eq. (A.26) into Eq. (A.24) we note that for every $\underline{s}_I(\ell)$ which yields an ISI term $W = \underline{\gamma}_I^T \underline{s}_I(\ell)$ There is exactly one vector, say $\underline{s}_I(\ell')$ which yields $W'=-W$. There-

fore, the two terms in the r.h.s. of Eq. (A.26) when averaged yield the same result and we have:

$$P_e = \frac{1}{2} \cdot \frac{1}{16} \sum_{\ell=1}^{16} \text{erfc}\left[(E_b/N_d)^{1/2}\ \gamma^{1/2}\ \left(1 + \underline{\gamma}_I^T \underline{s}_I(\ell)/\gamma\right)\right] . \quad \text{(A.28)}$$

This is our final result for the BER. Reflecting on the form of the BER we notice that the ISI manifests through the terms $\underline{\gamma}_I^T \underline{s}_I(\ell)/\gamma$. These terms averaged over the source statistics yield zero because of the PSK modulation. Because of assumption (18) about the distribution of $\underline{\gamma}_I$ the same is true if they are averaged over the channel statistics. Therefore, the average BER has the classical form $\frac{1}{2}\,\text{erfc}(\rho)$, where $\rho = (E_b\gamma/N_d)^{1/2}$ is the received SNR. For large ρ the effect of the negative fluctuations of the ISI terms dominates the effect of the positive ones, the net result being a substantial increase of the BER over the no ISI case.

Regarding the computational implications of the ISI terms we notice that we have to carry out a separate integration for each ISI component in addition to one integration for the signal gain. Since any reasonable analysis of ISI effects must take into account the immediate past and future pulses, we are already burdened with 5-dimensional integrations. Had we not approximated the variance of the filtered noise according to Eq. (12') there would be an additional r.v., strongly correlated with the attenuation, to be averaged out. The thrust of the analysis in the following sections refers to reducing or approximating the required 5-dimensional integrations.

A.2.3 The Average Bit Error Rate

The ABER is a classical performance criterion in digital systems over random channels, mostly because it usually leads to manageable analysis. From the user's point of view, it implies that all the bits are equally significant. This is very reasonable for data transmission but in other systems, as for example, voice transmission employing PCM, it is not meaningful.

By definition, the ABER P_{avg} is:

$$P_{avg} = \int_0^\infty \int \int_{-\infty}^{\infty} \int \int P_e(\gamma, \underline{\gamma}_I) pdf(\gamma, \underline{\gamma}_I) d\gamma d\underline{\gamma}_I \ ,$$

where we write $P_e(\gamma, \underline{\gamma}_I)$ to indicate that we are interested in the dependence of the BER on the signal gain and the ISI-weights. Employing our assumption (A.17) we can separate out the averaging with respect to the gain and express P_{avg} as:

$$P_{avg} = \int_0^\infty P_{avg}(\gamma) pdf(\gamma) d\gamma \ , \qquad (A.29)$$

where:

$$P_{avg}(\gamma) = \int \int_{-\infty}^{\infty} \int \int P_e(\gamma, \underline{\gamma}_I) pdf(\underline{\gamma}_I) d\underline{\gamma}_I \qquad (A.30)$$

is the ISI only averaged BER, which still depends on the gain. The integration for $P_{avg}(\gamma)$ is 4-dimensional and direct evaluation is computationally inefficient. Fortunately based on the symmetry of the PSK signalling and our assumption (A.18) on the distribution of $\underline{\gamma}_I$ we can reduce the computation of $P_{avg}(\gamma)$ to a

single dimensional integral. [illegible] separate the component α_1 of γ_I and [illegible] denote the vector of the remaining [illegible] $\alpha_{m+1}, D_{m+1})^T$ denote the vector of the [illegible] then:

$$P_{avg}(\gamma) = \int_{-\infty}^{\infty} \int \left[\int_{-\infty}^{\infty} P_e \gamma, \gamma_I', \ldots \right] \ldots \gamma_I' \quad . \quad (A.31)$$

From Eq. (A.28) we see that α_1 is involved in P_e through the product $\alpha_1 a_{m-1}$. Since the source symbol a_{m-1} takes the values ± 1, P_e can be decomposed into two parts P_e^+ and P_e^- which differ only in the sign of α_{m-1} and each contains half of the terms of P_e:

$$P_e^+(\gamma, \underline{\gamma}_I'; \alpha_1) = \frac{1}{2} \cdot \frac{1}{16} \sum_{\ell=1}^{8} \operatorname{erfc}\left[(E_b/N_d)^{1/2} \gamma^{1/2} (1+\alpha_1/\gamma + (\underline{\gamma}_I')^T \underline{s}_I'/\gamma)\right] , \quad (A.32)$$

$$P_e^-(\gamma, \underline{\gamma}_I'; \alpha_1) = P_e^+(\gamma, \underline{\gamma}_I'; -\alpha_1) , \quad (A.33)$$

$$P_e(\gamma, \gamma_I) = P_e^+(\gamma, \underline{\gamma}_I'; \alpha_1) + P_e^-(\gamma, \underline{\gamma}_I'; \alpha_1) . \quad (A.34)$$

By assumption (A.18):

$$\begin{aligned} \mathrm{pdf}(\alpha_1) &= [2\pi \mathrm{var}(\alpha_1)]^{-1/2} \exp(-\alpha_1^2 / 2\ \mathrm{var}(\alpha_1)) \\ &= \mathrm{pdf}(-\alpha_1) \quad . \end{aligned} \tag{A.35}$$

Eqs. (A.33) and (A.35) imply:

$$\int_{-\infty}^{\infty} P_e^+(\gamma, \underline{\gamma}_I'; \alpha_1)\mathrm{pdf}(\alpha_1)\, d\alpha_1 = \int_{-\infty}^{\infty} P_e^-(\gamma, \underline{\gamma}_I'; \alpha_1)\mathrm{pdf}(\alpha_1) d\alpha_1 \quad . \tag{A.36}$$

Eqs. (A.34) and (A.36) imply that the integral in brackets in Eq. (A.31) can be expressed only through P_e^+ so that:

$$\begin{aligned} P_{avg}(\gamma) &= \int \int_{-\infty}^{\infty} \int \left[2 \int_{-\infty}^{\infty} P_e^+(\gamma, \underline{\gamma}_I'; \alpha_1)\mathrm{pdf}(\alpha_1) d\alpha_1\right] \mathrm{pdf}(\underline{\gamma}_I') d\underline{\gamma}_I'. \\ &= 2 \int \int_{-\infty}^{\infty} \int \int P_e^+(\gamma, \underline{\gamma}_I'; \alpha_1)\mathrm{pdf}(\underline{\gamma}_I) d\underline{\gamma}_I \quad . \end{aligned} \tag{A.37}$$

By comparing Eqs. (A.37) and (A.30) we see that the net result of these manipulations was to obtain in the integrant of $P_{avg}(\gamma)$ a BER related function, i.e. P_e^+, with half as many terms as P_e but still the dimension of the integral has not been reduced. Nevertheless, if we repeat the same procedure for the remaining ISI weights β_1, α_{-1}, β_{-1} the integral for $P_{avg}(\gamma)$ will involve only the combination $\alpha_1+\beta_1+\alpha_{-1}+\beta_{-1}$ i.e., Eq. (A.37) evolves to:

$$P_{avg}(\gamma) = 16 \int\int_{-\infty}^{\infty}\int\int P_e^+(\gamma;\alpha_1+\beta_1+\alpha_{-1}+\beta_{-1})\,pdf(\underline{\gamma}_I)\,d\underline{\gamma}_I \ , \qquad (A.38)$$

where:

$$P_e^+(\gamma;x) = \frac{1}{2} \cdot \frac{1}{16}\ \mathrm{erfc}\left[(E_b/N_0)^{1/2}\ \gamma^{1/2}\ (1+x/\gamma)\right] \ . \qquad (A.39)$$

Let us denote the sum of the ISI weights by α_I:

$$\alpha_I = \alpha_1 + \beta_1 + \alpha_{-1} + \beta_{-1} \ . \qquad (A.40)$$

Now the 4-dimensional integral of Eq. (A.18) is one way of expressing the average value of $P_e^+(\gamma,\alpha_I)$ with respect to α_I. A much simpler expression is:

$$P_{avg}(\gamma) = 16 \int_{-\infty}^{\infty} P_e^+(\gamma,\alpha_I)\,pdf(\alpha_I)\ d\alpha_I \ , \qquad (A.41)$$

at which point we see that we have eliminated the need for multiple integration. To complete our task we need to specify the distribution of the sum of ISI weights α_I. Since these r.v.'s were assumed independent, zero mean normal, α_I is also zero mean normal with variance:

$$var(\alpha_I) = 2(var(\alpha_1) + var(\alpha_{-1})), \qquad (A.42)$$

because $\mathrm{var}(\alpha_k) = \mathrm{var}(\beta_k)$. Reviewing the above approach we note that it can be applied for any number of interfering symbols. It is only required that we compute for each interfering symbol the variance of the correponding ISI weight, according to Eqs. (A.22) and (A.23), and take it into account in the variance of α_I.

The computation of $P_{avg}(\lambda)$ can be reduced further analytically by employing the exponential approximation to the erfc(x):

$$\mathrm{erfc}(x) \approx \begin{cases} e^{-x^2} & x \geq 0 \\ 2 - e^{-x^2} & x < 0 \end{cases} \quad . \tag{A.43}$$

With this approximation, the integral of Eq. (A.41) yields:

$$P_{avg}(\gamma) = 1/2\left(y^{1/2} \exp[-\gamma y(E_b/N_d)] + \mathrm{erfc}\left[\frac{\gamma}{(2\mathrm{var}(\alpha_I))^{1/2}}\right]\right) \tag{A.44}$$

where:

$$y = \frac{\gamma}{2(E_b/N_d)\mathrm{var}(\alpha_I)+\gamma} \quad . \tag{A.45}$$

Finally, the ABER P_{avg} can be computed numerically from Eq. (A.29) by replacing $P_{avg}(\gamma)$ from Eq. (A.44) and pdf(γ) from Eq. (A.29).

A.2.4 The Outage Probability

It has been observed that the intelligibility of the speech in digital voice channels exhibits a threshold effect, that is if the BER is lower than some level the intelligibility is virtually unimpaired whereas above that level it drops markedly. In [5] it is reported that for the TRC-170 system employing continuously Variable Slope Delta modulation (CVSD) this level lies between BER=10^{-2} and BER=10^{-3}. Under these circumstances a meaningful performance criterion is the outage probability P_{out} at some BER threshold p_{thr}.

Let us denote by Γ the region of the 5-dimensional space $(\gamma, \underline{\gamma}_I)$ in which the BER exceeds p_{thr}:

$$\Gamma = \{(\gamma, \underline{\gamma}_I): P_e(\gamma, \underline{\gamma}_I) > p_{thr}\} \quad . \tag{A.46}$$

By definition P_{out} is:

$$P_{out} = \int \int \int_{\Gamma} \int \int \text{pdf}(\gamma, \underline{\gamma}_I) d\gamma d\underline{\gamma}_I \quad .$$

It is convenient to separate out the averaging with respect to the gain. To that end, we need to consider the intersection $\Gamma(x)$ of the outage region Γ with the hyperplane $\gamma=x$:

$$\Gamma(x) = \{(\underline{\gamma}_I) : P_e(x,\underline{\gamma}_I) > p_{thr}\} , \tag{A.47}$$

and define the ISI-only averaged outage probability:

$$P_{out}(\gamma) = \int \int_{\Gamma(\gamma)} \int \int pdf(\underline{\gamma}_I)d\underline{\gamma}_I . \tag{A.48}$$

P_{out} then can be expressed in a form similar to Eq. (A.29):

$$P_{out} = \int_0^\infty P_{out}(\gamma)pdf(\gamma)d\gamma . \tag{A.49}$$

The difficult part in the computation of P_{out} is the computation which involves the 4-dimensional integral of Eq. (A.48). In fact, the problem here is more difficult than the one we had with the computation of $P_{avg}(\gamma)$ because we have to specify the 4-dimensional region $\Gamma(\gamma)$ by solving the nonlinear equation $P_e(\gamma,\underline{\gamma}_I)=p_{thr}$. A closed form expression for $P_{out}(\gamma)$ cannot be obtained. Instead we developed an efficient algorithm to compute a tight upper bound to $P_{out}(\gamma)$. The integral of Eq. (A.49) is computed then numerically to find P_{out}. Since $pdf(\gamma)>0$, the resulting outage probability is a tight upper bound to the actual one. The balance of this section describes the algorithm for the calculation of $P_{out}(\gamma)$.

We discuss first the specification of the integration region $\Gamma(\gamma)$. To clarify the geometry we show in Figure A-6 the integration space for 2 ISI weights. The outage region Γ extends for $\gamma > 0$ and outside a cone shaped surface where the BER reaches the threshold value. This cone evolves after the point $\gamma = \gamma_{min}$, $\underline{\gamma}_I = 0$ where γ_{min} is the solution of:

$$P_e(\gamma,0) = \frac{1}{2}\,\mathrm{erfc}\left[(E_b/N_d)^{1/2}\gamma^{1/2}\right] = p_{thr}\ , \qquad (A.50)$$

i.e., for $\gamma<\gamma_{min}$ the received signal energy is so small that the BER is always smaller than the threshold even without any ISI penalty. For $\gamma>\gamma_{min}$ the eq. $P_e(\gamma,\underline{\gamma}_I) = p_{thr}$ has solutions for $\underline{\gamma}_I \neq 0$. Considering the plane $\gamma=x$ in Figure A-6, these solutions lie on the heavily drawn curve C(x). For a larger number of ISI weights C(x) evolves to some surface:

$$C(x) = \{\underline{\gamma}_I : P_e(x, \underline{\gamma}_I) = p_{thr}\}\ , \qquad (A.51)$$

to which we refer usually as the outage surface. The physical significance of the outage surface is that regardless of how large the received signal energy is the BER will exceed the threshold whenever the ISI weights result in a point in $\Gamma(\gamma)$ outside $C(\gamma)$. $P_{out}(\gamma)$ measures how frequently this occurs and depends on how confined the distribution of the ISI weights are within the outage surface.

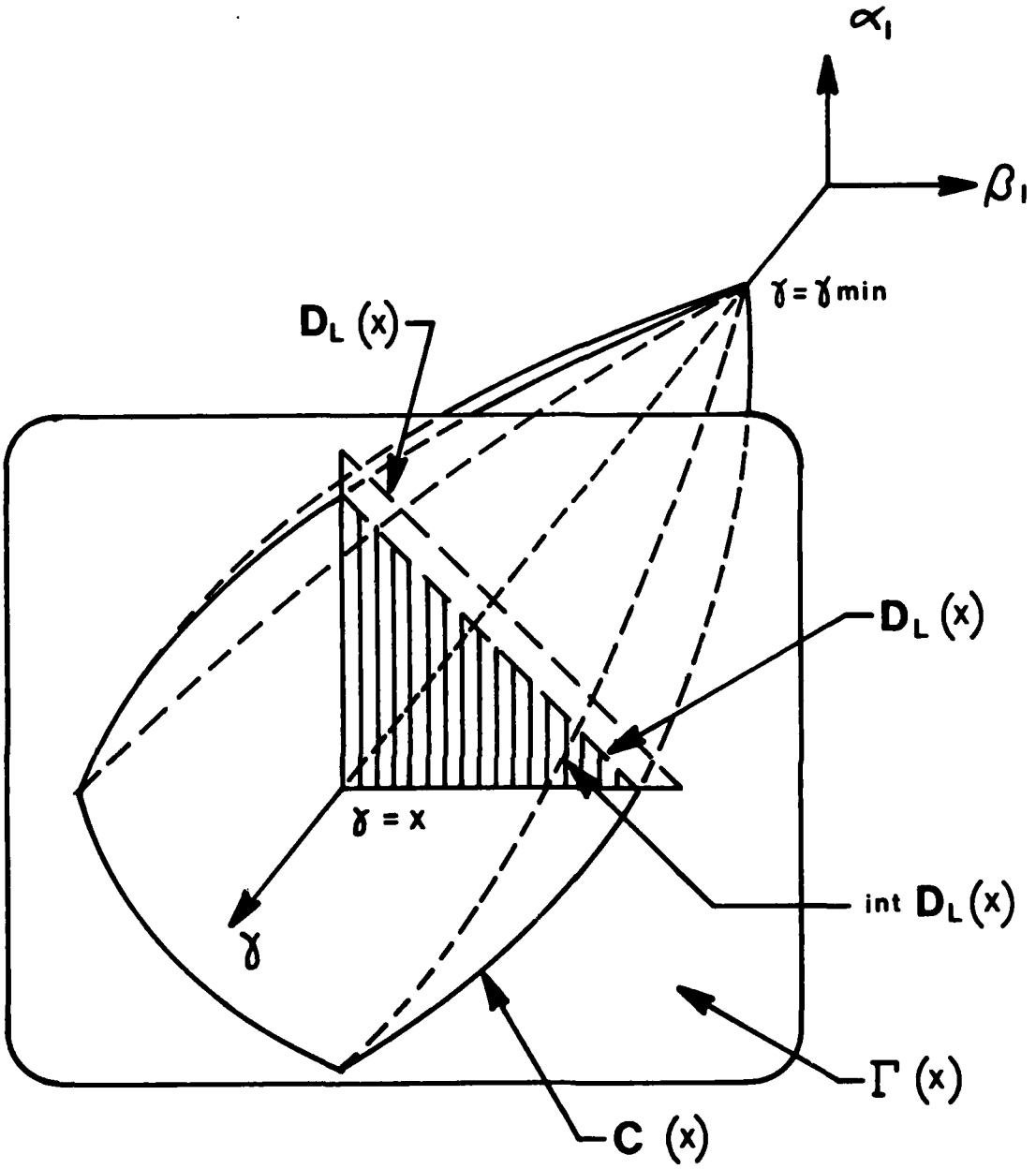

Figure A-6 The Integration Region of P_{out} for 2 ISI Components

We notice in Figure A-6 two dominant characteristics of $C(\underline{\gamma}_I)$. (i) $C(\gamma)$ is symmetric with respect to the γ-axis. This is due to the symmetry of the BER, Eq. (A.28), with respect to the ISI terms, i.e., $P_e(\underline{\gamma}_I)=P_e(-\underline{\gamma}_I)$, so that if some $\underline{\gamma}_I \in C(\gamma)$ it is also true that $(-\underline{\gamma}_I) \in C(\gamma)$. This property is true for every γ and it implies that we need to specify only the restriction of C for $\underline{\gamma}_I > 0$, as shown in Figure A-7. (ii) Consider the restriction of C for $\underline{\gamma}_I > 0$. It can be shown that the surface C is bounded above by the hyperplane D_u, which is tangent to C at the middle point $\alpha_1 = \beta_1 = \alpha_{-1} = \beta_{-1}$, and below by the hyperplane D_L which passes through the points where C cuts the axis. Figure A-6 helps to visualize this situation. For 2 ISI weights the bounding hyperplanes degenerate to the heavy broken lines which enclose the curve C.

We intend to bound $P_{out}(\gamma)$ by replacing the outage surface with the symmetric extension of the hyperplanes D_u and D_L. Clearly D_u will result in a lower bound of the outage probability whereas D_L will result in an upper bound. The computational advantage of this approximation is that the specification of the hyperplanes D_u and D_L requires only one parameter, namely the axis crossing points α_u and α_L respectively:

$$D_u : \quad \alpha_1 + \beta_1 + \alpha_{-1} + \beta_{-1} = \alpha_u \tag{A.52}$$

$$D_L : \quad \alpha_1 + \beta_1 + \alpha_{-1} + \beta_{-1} = \alpha_L \, . \tag{A.53}$$

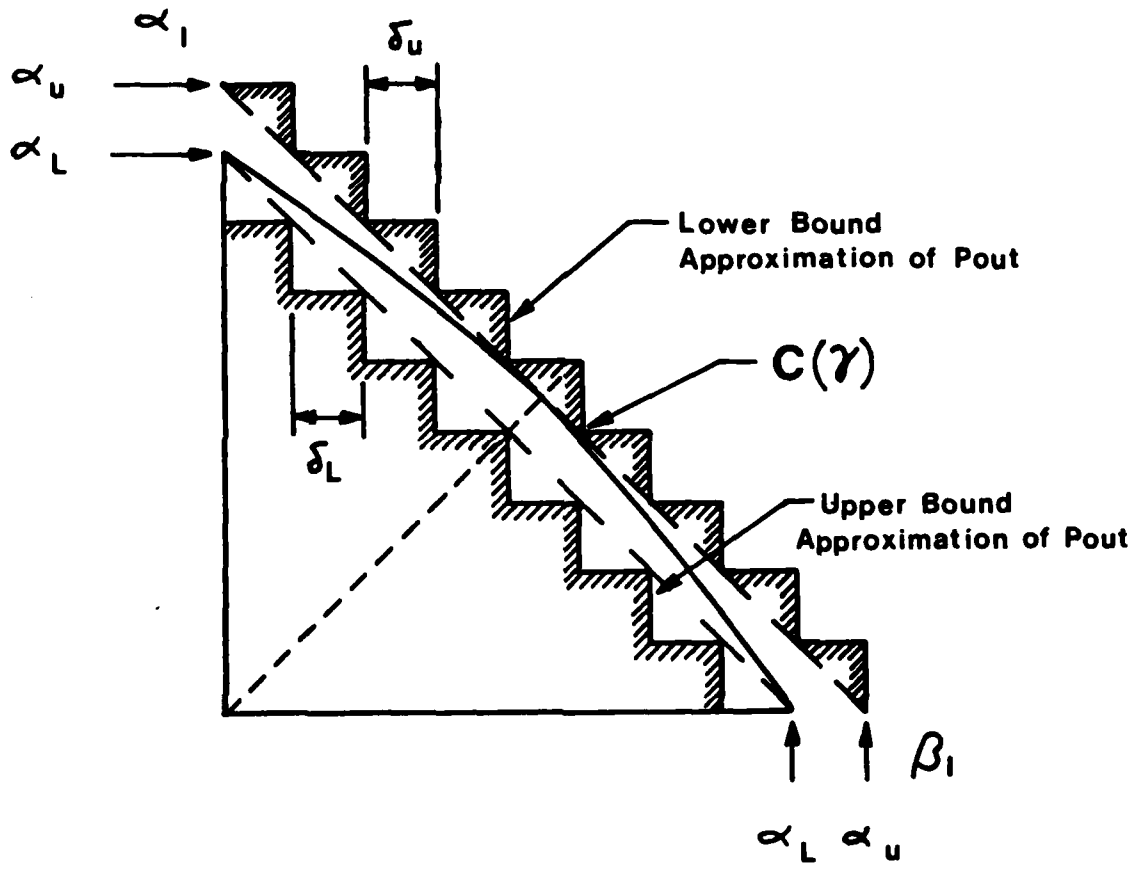

Figure A-7 The Bounds of the Integration Region of P_{out} for 2 ISI Components

It can be shown that α_u, α_L are unique solutions of the nonlinear equations:

$$\alpha_u: \qquad f(x) + 4f(x/2) + 3f(0) = p_{thr} \tag{A.54}$$

$$\alpha_L: \qquad 8f(x) = p_{thr} \tag{A.55}$$

where f(x) is defined as:

$$f(x) = \frac{1}{2} \cdot \frac{1}{16} \left(\exp\left[-\frac{E_b}{N_d}\gamma\left(1 - \frac{x}{\gamma}\right)^2\right] + \exp\left[-\frac{E_b}{N_d}\gamma\left(1 + \frac{x}{\gamma}\right)^2\right]\right) \tag{A.56}$$

The form of f(x) apparently indicates that Eqs. (A.54) and (A.55) have to be solved separately for an E_b/N_0 and any γ. We can avoid this by solving at the outset Eqs. (A.54) and (A.55) with respect to the γ-normalized function f_1 instead of f:

$$f_1(x) = \frac{1}{2} \cdot \frac{1}{16}\left[\exp\left[-\rho(1-x)^2\right] + \exp\left[-\rho(1+x)^2\right]\right] \tag{A.57}$$

and for an array of SNR's ρ. Figure A-8 shows that these solutions increase smoothly with ρ approaching the asymptotic value 1. Let us denote these solutions by $\alpha_u(\rho,1)$, $\alpha_L(\rho,1)$. For a given E_b/N_d and a given γ, $\alpha_L = \alpha_L(E_b/N_d, \gamma)$ can be determined from $\alpha_L(\rho,1)$:

$$\alpha_L(E_b/N_d, \gamma) = \gamma \cdot \alpha_L(\gamma \cdot E_b/N_d, 1) \; . \tag{A.58}$$

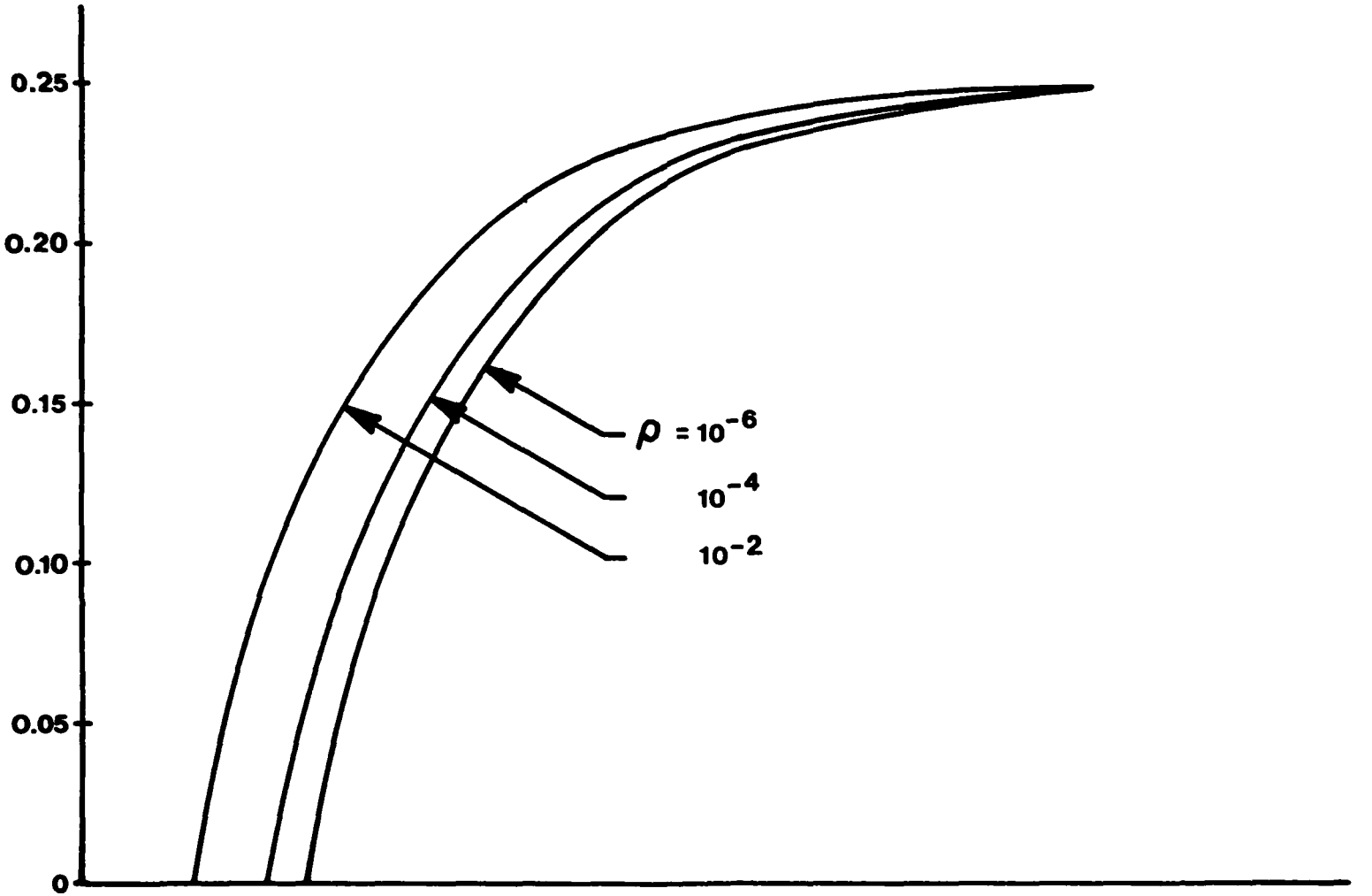

Figure A-8 Normalized Limit of ISI Region for Various Outage Thesholds

The same relation is true for α_u. For any value of ρ the normalized parameter $\alpha_L(\rho,1)$ can be obtained very accurately by interpolation on the appropriate curve of Figure A-8.

Having specified the geometry of the integration region we discuss now the final computation of $P_{out}(\gamma)$. Clearly for $\gamma \leq \gamma_{min}$, $P_{out}(\gamma) = 1$ so we need to consider only the range $\gamma > \gamma_{min}$ where the outage surface develops. The integral of Eq. (A.49) can be made more manageable by the following steps: (i) Employ the previously noticed symmetry of the outage surface and the pdf($\underline{\gamma}_I$) to restrict the integration only for $\underline{\gamma}_I > 0$:

$$P_{out}(\gamma) = 16 \int\int\int\int_{\Gamma(\gamma),\, \underline{\gamma}_I>0} \text{pdf}(\underline{\gamma}_1)\, d\underline{\gamma}_1 \ .$$

(ii) Integrate over the interior of the outage surface, rather than over the exterior:

$$P_{out}(\gamma) = 1 - 16 \int\int\int\int_{\text{int } C(\gamma),\ \underline{\gamma}_I>0} \text{pdf}(\underline{\gamma}_I)\, d\underline{\gamma}_I \ . \qquad \text{(A.48')}$$

(iii) Bound $P_{out}(\gamma)$ by replacing C with the hyperplanes D_L and D_u:

$$P_{out}(\gamma) \leq 1 - 16 \int\int\int\int_{\text{int } D_L(\gamma),\ \underline{\gamma}_I>0} \text{pdf}(\underline{\gamma}_I)\, d\underline{\gamma}_I, \qquad \text{(A.59)}$$

$$P_{out}(\gamma) \geq 1 - 16 \int\int\int\int_{\text{int } D_u(\gamma),\ \underline{\gamma}_I>0} \text{pdf}(\underline{\gamma}_I)\, d\underline{\gamma}_I. \qquad \text{(A.60)}$$

Because of the dimensionality, straightforward numerical integration of Eqs. (A.59), (A.60) is still impractical. One approach we can take is first to ignore the constraint $\gamma_I \geq 0$, in which case the integration is reduced to the single variable α_I, as with P_{avg}, and then compensate for the contribution outside the integration region. A more direct approach is suggested by the fact that since the components of $\underline{\gamma}_I$ are assumed independent if we integrate the pdf($\underline{\gamma}_I$) over a cube $\underline{\gamma}_I' \leq \underline{\gamma}_I \leq \underline{\gamma}_I''$ the result is an easily computed product of terms involving the erfc(•):

$$\int_{\alpha_1'}^{\alpha_1''} \int_{\beta_1'}^{\beta_1''} \int_{\alpha_{-1}'}^{\alpha_{-1}''} \int_{\beta_{-1}'}^{\beta_{-1}''} \text{pdf}(\underline{\gamma}_I)\, d\underline{\gamma}_I =$$

$$= \frac{1}{16}\, g_1(\alpha_1', \alpha_1'')\, g_1(\beta_1', \beta_1'')\, g_{-1}(\alpha_{-1}', \alpha_{-1}'')\, g_{-1}(\beta_{-1}', \beta_{-1}'') \qquad \text{(A.61)}$$

where:

$$g_i(u,v) = \text{erfc}\left[\frac{u}{(2\ \text{var}(\alpha_i))^{1/2}}\right] - \text{erfc}\left[\frac{v}{(2\ \text{var}(\alpha_i))^{1/2}}\right] \qquad \text{(A.62)}$$

Eq. (A.61) reflects the fact: $\text{var}(\alpha_i) = \text{var}(\beta_i)$. We can fill then the interior of either D_u or D_L with a small number of hypercubes and sum over a number of terms like the r.h.s. of Eq. (A.61). This procedure is clarified in Figure A-7. If we choose to partition the intervals $[0, \alpha_u]$, $[0, \alpha_L]$ in K sections, so that the edge of the hypercube has length $\delta_u = \alpha_u/K$ for integration in the int D_u or $\delta_L = \alpha_L/K$ for integration in the int D_L, we obtain in the place of Eqs. (A.59) and (A.60):

$$P_{out}(\gamma) \leq 1 - \sum_{i=1}^{K} g_1((i-1)\delta_L, i\delta_L) \cdot \sum_{j=1}^{K-i} g_1((j-1)\delta_L, j\delta_L)$$

$$\cdot \sum_{k=1}^{K-i-j} g_{-1}((k-1)\delta_L, k\delta_L) \cdot \sum_{\ell=1}^{K-i-j-k} g_{-1}((\ell-1)\delta_L, \ell\delta_L) \qquad \text{(A.63)}$$

$$P_{out}(\gamma) \geq 1 - \sum_{i=1}^{K+1} g_1((i-1)\delta_u, i\delta_u) \cdot \sum_{j=1}^{K+1-j} g_1((j-1)\delta_u, j\delta_u)$$

$$\text{(A.64)}$$

$$\cdot \sum_{k=1}^{K+1-i-j} g_{-1}((k-1)\delta_u, k\delta_u) \cdot \sum_{\ell=1}^{K+1-i-j-k} g_{-1}((\ell-1)\delta_u, \ell\gamma_u)$$

The parameters which depend on γ in the r.h.s. of the above equations are the hypercube lengths δ_L and δ_u. The upper limit of the summations of Eq. (A.60') indicate that we have extended the integration somewhat above D_u to insure that the result is always the lower bound of $P_{out}(\delta)$. Our approximations are illustrated in Figure A-7. In practice we have found that the difference in predicted performance due to the upper and lower bound of $P_{out}(\gamma)$ was negligible. The efficiency of the above procedure is based on the fact that good accuracy is retained with a small partition number K, i.e., K = 6 ÷ 10.

If we desire to include ISI effects from more than 2 symbols we must:

(i) compute additional ISI weight variances according to Eqs. (A.22) and (A.23),

(ii) modify the Eqs. (A.54) and (A.55) for the parameters α_L and α_u,

(iii) augment the product of sums term in the r.h.s. of Eqs. (A.63) and (A.64) by 2 additional summations for each additional interfering symbol.

This concludes our discussion for the outage probability.

REFERENCES

[1] M.G. Unkauf, O.A. Tagliaferri, "An Adaptive Matched Filter Modem For Digital Troposcatter," in Conf. Rec., 1975 IEEE Int. Cont. Communications, pp. (5-15) - (5-19).

[2] M. Unkauf, N. Liskov, R. Curtis, S. Boak, "Advanced Digital Troposcatter Modem Technology," EASCON 77, pp. (35-3A) - (35-3A).

[3] M. Unkauf, P. Davis, C. Alsmeyer, "Digital Transmission System", Final Technical Report, RADC-TR-79-250, Oct. 1979.

[4] P. Monsen, "Theoretical and Measured Performance of a DFE Modem on a Fading Multipath Channel," IEEE Trans. on Communications, Vol. COM-25, No. 10, Oct. 1979 pp. 1144-1153.

[5] Brand E.T., Connor J.W., Sherwood A.R., "AN/TRC-170 Troposcatter Communication System," NATO Conference Proceedings, Brussels, 1980, paper 8.

APPENDIX B:
Detection Noise Statistics For The AN/TRC-170

Here we elaborate on modelling the f_2-interference as independent thermal noise and on the approximation of the detection noise power σ_d^2 as a linear expression of the signal gain γ.

We consider first the average power of the residual f_2-interference term after IF filtering, Eq. (4):

$$2E_b \sum_k \langle |p'*h\ (t-kT)|^2 \rangle = 2E_b \sum_k \int (p'(t-kT-u))^2 R_h(u)\ du \tag{B1}$$

where $p' = p_T'*p_R$ and we have dropped the channel index i. Eq. (B1) indicates that this power is a periodic function of the time with period T. To have a reasonable noise model we consider the time averaged interference power:

$$\sigma_f^2 = \frac{1}{T}\ 2E_b \int_0^T \sum_k \int (p'(t-kT-u))^2 R_h(u)\ du\ dt\ . \tag{B2}$$

If σ_f^2 was the power of a white noise independent from the thermal noise n(t), with spectral density N, filtered by $p_R(t)$, we would have:

$$\sigma_f^2 = N \int S_R(f)\ df\ , \tag{B3}$$

where $S_R(f) = |P_R(f)|^2$ is the power spectrum of $p_R(t)$.

Therefore the f_2-interference can be accounted for by increasing the thermal noise spectral density from N_o to N_f:

$$N_f = N_o + N, \tag{B4}$$

and by Eq. (B3):

$$N_f = N_o \left(1 + \frac{\sigma_f^2}{N_o} \frac{1}{\int S_R(f) d_f}\right) . \tag{B5}$$

We consider now the integral in the right side of Eq. (B2). Carrying out first the integration in the t-variable we obtain:

$$\int_o^T \sum_k \int (p'(t-kT-u))^2 R_h(u)\, du\, dt$$

$$= \int \left[\sum_k \int_o^T (p'(t-kT-u))^2 dt \right] R_h(u)\, du$$

$$= \int \left[\sum_k \int_{-kT}^{T-kT} (p'(t-u))^2 dt \right] R_h(u)\, du$$

$$= \int \left[\int (p'(t-u)^2\, dt \right] R_h(u)\, du$$

$$= \int (p'(t))^2\, dt \int R_h(u)\, du$$

$$= \frac{1}{2} \int \left[S_T(f-\Delta f) + S_T(f+\Delta f) \right] S_R(f) df$$

$$= \int S_T(f+\Delta f)\, S_R(f)\, df \qquad \text{(B6)}$$

where we have used the fact that the multipath profile has been normalized to unit area. Combining the Eqs. (B2), (B5), (B6) we obtain the equivalent noise spectral density to account for f_2-interference effects:

$$N_f = N_o \left[1 + \frac{2}{T} \cdot \frac{E_b}{N_o} \cdot \frac{\int S_T(f+\Delta f)\, S_R(f)\, df}{\int S_R(f)\, df} \right] . \qquad \text{(B7)}$$

A more sensitive approach would be to compute the power of the interference after the correlation filter, term (10), but this leads to a complicated analysis similar to the one for the ISI variance.

We proceed now to the variance of the detection noise. This is given by the term (9) with the spectral density N_o replaced by N_f and the reference pulse $\hat{q}$ replaced by the signal pulse q according to Eq. (11):

$$n_d = N_f^{1/2} \, \mathrm{Re}\{z\} \qquad \text{(B8)}$$

$$z = \sum_{i=d}^{D} \int_{t_o}^{t_o+T} n_i * p_R(u-mT)\, q_i^*(u)\, du \qquad \text{(B9)}$$

For a fixed channel we compute the variance $\langle|z|^2\rangle$ with respect to the noise statistics:

$$\langle|z|^2\rangle = \left\langle \sum_{i,j=1}^{D} \int_{t_o}^{t_o+T} \int q_i^*(u)\, q_j(v)\, p_R{*}n_i(u-mT)\, p_R{*}n_j^*(v-mT)\,dudv \right\rangle$$

$$= \sum_{i,j=1}^{D} \int_{t_o}^{t_o+T} \int q_i^*(u) q_j(v) \int\int p_R(u-mT-u_1)\, p_R(v-mT-v_1)$$

$$\langle n_i(u_1) n_j^*(v_1)\rangle\, dudvdu_1dv_1$$

$$= \sum_{i=1}^{D} \int_{t_o}^{t_o+T} \int q_j^*(u) q_i(v) \int p_R(u-t)\, p_R(v-t)\, dt$$

$$= \sum_{i=1}^{D} \int_{t_o}^{t_o+T} \int q_i(v) q_i^*(u)\, \mathrm{cor}(p_R)\,(v-u)\, dudv \qquad \text{(B10)}$$

By symmetry the variance of Re {z{ is $\langle|z|^2\rangle/2$ and by combining Eqs. (B9), (B10) we obtain the result of (Eq. 12):

$$\sigma_d^2 = \langle n_d^2\rangle = \frac{1}{2} N_f \sum_{i=1}^{D} \int_{t_o}^{t_o+T} \int q_i(v) q_i^*(u)\, \mathrm{cor}(p_R)\,(v-u)\, dudv$$

(B11)

To make the performance analysis manageable it is desirable to replace the summation term in σ_d^2 by the limiting case when the receiver filter bandwidth becomes much larger than the transmitter bandwidth so that $cor(p_R)(t) \sim cor(p_R)(o)\ \delta(t)$. In this case:

$$\sigma_d^2 \simeq \frac{1}{2} N_d \sum_{i=1}^{D} \int_{t_o}^{t_o+T} [q_i(u)]^2 du = \frac{1}{2} N_d \gamma \quad . \tag{B12}$$

The effective spectral density N_d is fixed to preserve the same average power with respect to the channel statistics:

$$N_d = 2 \frac{\langle \sigma_d^2 \rangle}{\langle \gamma \rangle} \tag{B13}$$

We compute $\langle \sigma_d^2 \rangle$ and $\langle \gamma \rangle$. Let $p = p_T * p_R$. Then:

$$\frac{2}{N_f} \langle \sigma_d^2 \rangle = \sum_{i=1}^{D} \int_{t_o}^{t_o+T} \int \langle q_i(v) q_i^*(u) \rangle\ cor(p_R)(v-u)\ dudv$$

$$= \sum_{i=1}^{D} \int_{t_o}^{t_o+T} \int \left[\int p(v-t)p(u-t)R_h(t)dt \right] cor(p_R)(v-u)dudv$$

$$= D \int R_h(t)\ f_2(t)\ dt \tag{B14}$$

where

$$f_2(t) = \int_{t_o}^{t_o+T} \int p(v-t)p(u-t)cor(p_R)(v-u)\ dudv \tag{B15}$$

Similarly:

$$\langle \gamma \rangle = D \int R_h(t)\, f_1(t)\, dt \tag{B16}$$

where:

$$f_1(t) = \int_{t_o}^{t_o+T} p^2(u-t)\, du \tag{B17}$$

Combining Eqs. (B13), (B14), (B16) we obtain:

$$N_d = N_f \frac{\int R_h(t)\, f_2(t)\, dt}{\int R_h(t)\, f_1(t)\, dt} \tag{B18}$$

where the function $f_1(t)$, $f_2(t)$ are given in Eqs. (B17), (B15). N_d is the effective thermal noise spectral density for the performance analysis.

APPENDIX C:
Distribution of the Signal Gain For the AN/TRC-170

Here we approximate the distribution of the signal gain with the distribution of an inner product of complex normal random variables.

The signal gain is defined in Eq. (14). Since the response of different channels are independent we can concentrate first on the non-diversity case:

$$\gamma = \int_{t_o}^{t_o+T} |q(t)|^2 \, dt = \int_{o}^{T} |q(t+t_o)|^2 \, dt \qquad (C1)$$

The signal pulse q is the convolution of the random channel response h with the combined transmitter-receiver filter $p = p_t * p_R$ and h is a complex normal process. Hence q is also a complex normal process. Our problem then is to find the distribution of the magnitude squared of a normal process integrated over a finite interval. Generally the distribution of an integral of a process leads to an involved analysis. The notable exception is when the process is normal when the integral, as a linear operation, possesses also a normal distribution. One rough approximation we can make at this point is to compute the first two moments of γ and then fit a chi-square distribution. A more sensitive approximation is to replace the stochastic integral of Eq. (C1) with a sum of random variables:

$$\gamma \approx \frac{T}{N} \sum_{j=1}^{N} \left| q\left(j \frac{T}{N} + t_o\right) \right|^2 \qquad (C2)$$

The passage from Eq. (C1) to Eq. (C2) has the formal appearance of a numerical approximation to an integral. Intuitively we expect that if N is large enough the approximation will be satisfactory. We are performing nevertheless a stochastic approximation, for which we are not aware of any well developed theory, and the issues involved are much more subtle than in the case of a numerical integration. We develop first the distribution of the stochastic sum of Eq. (C2) and we will return to the question of the validity of our approximation and the required number of points N.

Let us define the (Nx1) normal, zero mean, random vector $\underline{q}$:

$$(\underline{q})_j = \left(\frac{T}{N}\right)^{1/2} q\left(j\,\frac{T}{N} + t_o\right) \tag{C3}$$

so that in vector notation:

$$\gamma = \underline{q}'\,\underline{q} \tag{C4}$$

where by $\underline{q}'$ we denote the conjugate transpose of $\underline{q}$.

Let V be the covariance matrix of $\underline{q}$:

$$V = \langle \underline{q}\,\underline{q}' \rangle \quad , \tag{C5}$$

and carrying out the indicated averaging with respect to the channel statistics:

$$\begin{aligned} V_{m,n} &= \frac{T}{N} \langle q\left(m\,\frac{T}{N} + t_o\right) q^*\left(n\,\frac{T}{N} + t_o\right) \rangle \\ &= \frac{T}{N} \int p_T{}^* p_R\left(m\,\frac{T}{N} - u\right) p_T{}^* p_R\left(n\,\frac{T}{N} - u\right) R_h(u+t_o)\, du \ . \end{aligned} \tag{C6}$$

V is a symmetric positive definite matrix. There exists a unique ortho normal matrix, say M, which diagonalizes V:

$$V = M' \Lambda M \quad , \tag{C7}$$

$$M'M = I \quad . \tag{C8}$$

The diagonal matrix Λ in Eq. (C7) is the matrix of the positive eigenvalues λ_n, n = 1,N, of V:

$$\Lambda_{m,n} = \lambda_n \delta_{mn} \quad , \tag{C9}$$

and the matrix I in Eq. (C8) is the unity matrix. Eq. (C8) implies that the linear transformation induced by M on $\underline{q}$ preserves the inner product $\underline{q}'\underline{q}$:

$$(M\underline{q})' (M\underline{q}) = \underline{q}' (M'M) \underline{q} = \underline{q}'\underline{q} \quad . \tag{C10}$$

This product is exactly our signal gain and therefore we can replace Eq. (C4) by:

$$\gamma = (M\underline{q})' (M\underline{q}) \tag{C4^1}$$

The usefulness of expressing γ through $(M\underline{q})$ rather than through $\underline{q}$ lies in the fact that $(M\underline{q})$ has a diagonal covariance matrix equal to Λ:

$$\langle (M\underline{q})\ (M\underline{q})' \rangle = M \langle \underline{q}\underline{q}' \rangle\ M' = MVM' = \Lambda \quad , \tag{C11}$$

using Eqs. (C7) and (C8). Since the components of $(M\underline{q})$ are linear combinations of normal random variables, they are normal themselves. The diagonal variance matrix Λ then implies that the components of $(M\underline{q})$ are independent. Hence the distribution of γ can be obtained as the N- fold convolution of the distributions of the random variables $\left|(M\underline{q})_n\right|^2$, n = 1,N.

We compute the distribution of $\left|(M\underline{q})_n\right|^2$. Let

$$z = (M\underline{q})_n = x + jy \tag{C12}$$

For the real, normal, zero mean random variables x and y we know that $\langle x^2 \rangle = \langle y^2 \rangle = \lambda_n/2$, $\langle xy \rangle = 0$. Hence the magnitude $|z|$ has a Rayleigh density:

$$\text{r.v.}|z|: \quad \text{pdf}(u) = \frac{2u}{\lambda_n}\, e^{-u^2/\lambda_n}, \quad u>o, \tag{C13}$$

where by r.v. A: we denote that the probability density function pdf(.) refers to the random variable A. By square-low transformation the desired pdf of $\left|(M\underline{q})_n\right|^2 = |z|^2$ is:

$$\text{r.v.}|z|^2: \quad \text{pdf}(u) = \frac{1}{\lambda_n}\, e^{-u/^2\lambda_n}, \quad u>o \quad , \tag{C14}$$

Now to obtain the pdf of the signal gain by an N-fold convolution is computationaly impractical. A standard method is to resort to

Laplace of Fourier transforms of the pdf so that the convolution leads to products. Employing the Laplace transform, since we deal with positive random variables, let:

$$PDF(s) = \int_0^\infty pdf(u)\, e^{-su}\, du \qquad (C15)$$

Then:

$$\text{r.v.}|z|^2\text{:} \quad PDF(s) = \frac{1}{1+\lambda_n s} \quad . \qquad (C16)$$

Therefore for the non-diversity case the PDF of γ will consist of the product:

$$\text{r.v.}\gamma\text{:} \quad PDF(s) = \prod_{j=1}^{N} \frac{1}{1+\lambda_j s} \quad . \qquad (C17)$$

Reviewing our approach up to this point we see that once we find the eigenvalues of V the pdf of γ can be obtained by our inverse transform of Eq. (C17). The reliability of the method therefore depends substantially on whether the computed eigenvalues converge as the number of points N increases. Many computer experiments confirm that this actually is the case. Actually the pdf of γ is dominated by the few, 3 to 5, largest eigenvalues which stabilize substantially after N = 15. Another direct criterion to judge the reliability of the method is to compare the moments of γ as computed from Eq. (C1) and from Eq. (C17). We have experimented with the first moment:

$$\text{Eq. (C1):} \quad \langle\gamma\rangle = \int_o^T \left[\int \left[p_T * p_R\,(t-u) \right]^2 R_h(u+t_o)\, du \right] dt \,, \tag{C18}$$

$$\text{Eq. (C17):} \quad \langle\gamma\rangle = \sum_{j=1}^{N} \lambda_j \,. \tag{C19}$$

and we have seen that when the eigenvalues stabilize the mean value of the signal gain is also approximated well. Although our experiments indicate that our method can be made very reliable by increasing N, computational considerations call clearly for as small an N as possible. In fact with N=20 we had numerical troubles in some cases in the routines which compute the eigenvalues. Finally N was fixed to 18.

We come now to the diversity case i.e.:

$$\gamma = \sum_{i=1}^{D} \int_o^T \left| q(t+t_o) \right|^2 dt \tag{C20}$$

Since the diversities are assumed independent of each other and with the same statistical properties, the PDF of γ can be obtained by raising the PDF of the non-diversity case to the power D:

$$\text{r.v.}\,\gamma: \quad \text{PDF}(s) = \prod_{j=1}^{N} \frac{1}{(1+\lambda_j s)^D} \,. \tag{C21}$$

Partial fraction expansion on Eq. (C21) yields:

$$\text{PDF}(s) = \sum_{i=1}^{D} \sum_{j=1}^{N} A_{ij} \frac{1}{(1+\lambda_j s)^i} \quad . \tag{C22}$$

The coefficients A_{ij} can be obtained by the formula:

$$A_{D-i,j} = \frac{1}{\lambda_j^{\,i}\, i!} \frac{d^i}{ds^i} \left[\prod_{k(\neq j)=1}^{N} \frac{1}{(1+\lambda_k s)^D} \right] s = -\frac{1}{\lambda_j} \tag{C23}$$

in terms of the eigenvalues, and the inverse Laplace transform of Eq. (C22) yields:

$$\text{r.v.}\gamma : \text{pdf}(u) = \sum_{i=1}^{D} \sum_{j=1}^{N} A_{ij}\; G_i\,(u;\, \lambda_j) \tag{C24}$$

where:

$$G_i(u;\lambda) = \frac{1}{\lambda^i (i-1)!}\; u^{i-1}\; e^{-u/\lambda} \quad , \quad u > 0 \quad . \tag{C25}$$

APPENDIX D

The Statistics of the ISI Weights for the AN/TRC-170

Here we calculate the first and second moments of the ISI weights α_k, β_k, $k \neq 0$ with respect to the channel statistics. Since α_k, β_k were assumed to be normally distributed, these moments describe completely their joint distribution.

In the following we use heavily the decomposition of the complex channel response into real and imaginary parts:

$$h_i(t) = h_{iR}(t) + j\, h_{iI}(t) \ . \tag{D-1}$$

To complement the channel model described by Eq. (2), we assume that the components h_{iR}, h_{iI} are normal, uncorrelated and have equal power, i.e.,

$$\langle h_{iR}(t+\tau)\, h_{jR}(t)\rangle = \langle h_{iI}(t+\tau)\, h_{jI}(t)\rangle = \frac{1}{2}\, \delta_{ij}\delta(\tau)\, R_h(t) \tag{D-2}$$

$$\langle h_{iR}(t+\tau)\, h_{jI}(t)\rangle = 0 \ . \tag{D-3}$$

Now we rewrite the defining equation for the ISI weights, Eq. (15), separating out the channel response:

$$\alpha_k + j\beta_k = \sum_{i=1}^{D} \iint I(u-t_0,\ v-t_0-kT)\, h_i^*(u)\, h_i(v)\, du\, dv \tag{D-4}$$

where $I(x,y)$ is a correlation type integral for the combined transmitter-receiver pulse:

$$I(x,y) = \int_0^T p(t-x)\, p(t-y)\, dt, \qquad \text{(D-5)}$$

$$p(t) = p_T(t) * p_R(t) . \qquad \text{(D-6)}$$

To simplify the calculations we assume throughout that the pulse p(t) is essentially confined within the symbol interval so that:

$$I(x,y) \approx 0 \quad \text{for } |x-y| > T . \qquad \text{(D-7)}$$

This assumption is very reasonable given the time gating of the transmitted pulse in the AN/TRC-170 system.

We consider now the first moments. From Eq. (D-4):

$$\langle \alpha_k \rangle + j\langle \beta_k \rangle = D \int I(u, u-kT)\, R_h(u + t_0)\, du . \qquad \text{(D-8)}$$

Since the right side is real, we have always:

$$\langle \beta_k \rangle = 0 . \qquad \text{(D-9)}$$

Regarding $\langle \alpha_k \rangle$ we see that since $k \neq 0$ the condition of Eq. (D-7) applies so that:

$$\langle \alpha_k \rangle \simeq 0 . \qquad \text{(D-10)}$$

We consider next the moment $\langle \alpha_k\, \alpha_\ell \rangle$. From Eq. (D-4):

$$\langle \alpha_k \alpha_\ell \rangle = \sum_{i,j=1}^{D} \int\int\int\int I(u_1-t_0,\, u_1-t_0-kT)\, I(u_2-t_0,\, v_2-t_0-\ell T) \cdot H_{RR}(u_1,v_1,u_2,v_2)\, du_1\, dv_1\, du_2\, dv_2 \qquad \text{(D-11)}$$

where:

$$H_{RR}(u_1,v_1,u_2,v_2) = \langle \mathrm{Re}\{h_i^*(u_1)h_i(v_1)\}\ \mathrm{Re}\{h_j^*(u_2)h_j(v_2)\rangle \qquad \text{(D-12)}$$

We calculate the function H_{RR} by applying Eqs. (D-1), (D-2), (D-3):

$$\begin{aligned} H_{RR} &= \langle [h_{iR}(u_1)h_{iR}(v_1) + h_{iI}(u_1)h_{iI}(v_1)] \\ &\quad \cdot [h_{jR}(u_2)h_{jR}(v_2) + h_{jI}(u_2)h_{jI}(v_2)]\rangle \\ &= 2\langle h_{iR}(u_1)h_{iR}(v_1)h_{jR}(u_2)h_{jR}(v_2)\rangle \\ &\quad + 2\langle h_{iR}(u_1)h_{iR}(v_1)h_{jI}(u_2)h_{jI}(v_2)\rangle \end{aligned} \qquad \text{(D-13)}$$

At this step, we have used the symmetry of the channel statistics with respect to the real and the imaginary part to equate the moments:

$$h_{iR}(u_1)h_{iR}(v_1)h_{jR}(u_2)h_{jR}(v_2) = h_{iI}(u_1)h_{iI}(u_1)h_{iI}(u_2)h_{iI}(u_2)$$

$$h_{iR}(u_1)h_{iR}(v_1)h_{jI}(u_2)h_{jI}(v_2) = h_{iI}(u_1)h_{iI}(v_1)h_{jR}(u_2)h_{jR}(v_2) \qquad \text{(D-14)}$$

To expand the 4th order moments in the right side of Eq. (D-13) we use the moment theorem for normal random variables:

$$
\begin{aligned}
H_{RR} = \; & 2\left[\tfrac{1}{4} R_h(u_1)R_h(u_2)\ \delta(u_1-v_1)\ \delta(u_2-v_2)\right. \\
& \quad + \tfrac{1}{4} R_h(u_1)R_h(v_1)\ \delta(u_1-u_2)\ \delta(v_1-v_2)\ \delta_{ij} \\
& \quad \left. + \tfrac{1}{4} R_h(u_1)R_h(v_1)\ \delta(u_1-v_2)\ \delta(v_1-u_2)\ \delta_{ij}\right] \\
& + 2\left[\tfrac{1}{4} R_h(u_1)R_h(u_2)\ \delta(u_1-v_1)\ \delta(u_2-v_2)\right] .
\end{aligned}
\tag{D-15}
$$

Combining the 1st and 4th terms in the right side of Eq. (D-15), replacing H_{RR} in Eq. (D-11) and changing variables we obtain

$$
\begin{aligned}
\langle \alpha_k \alpha_\ell \rangle = \int\int R_h(u+t_0)R_h(v+t_0) \times \Big[& D^2\ I(u,u-kT)\ I(v,v-\ell T) \\
& + \tfrac{1}{2} D\ I(u,v-kT)\ I(u,v-\ell T) \\
& + \tfrac{1}{2} D\ I(u,v-kT)\ I(v,u-\ell T)\Big]\, du\, dv .
\end{aligned}
\tag{D-16}
$$

Now we use the approximation of Eq. (D-7) to simplify the integral of Eq. (D-16). Clearly the 1st term within the brackets is always negligible. The 2nd term is negligible whenever $k \neq \ell$

because if $|u-v+kT| < T$ then $|u-v+\ell T| > T$. The simplification of the 3rd term is a bit more involved. First, if both k, ℓ have the same sign, say positive this term is negligible because for $u > v$ the condition $|u-v+kT| > T$ applies and for $u < v$ the condition $|v-u+\ell T| > T$ applies. Now assume that $k > 0$ and $\ell < 0$. Then as before the region $u > v$ yields a negligible contribution. For $u < v$ we are looking at the arguments $|\Delta-kT|$ and $|\Delta-|\ell|T|$ where $\Delta = v-u > 0$. If $k \neq |\ell|$ one of the arguments will be larger than T and the term will be negligible. It remains the case $k = |\ell|$. The requirement $|\Delta-kT| < T$ implies $kT < \Delta < (1+k)T$. If a typical multipath profile extends at most over a symbol interval the product $R_h(u)R_h(u+\Delta)$ will be negligible for $k > 1$. We conclude that all the variances $\langle \alpha_k^2 \rangle$ depend only on the 2nd term and only the cross covariance $\langle \alpha_1 \alpha_{-1} \rangle$ may be significant:

$$\langle \alpha_k^2 \rangle = \mathrm{var}(\alpha_k) \simeq \frac{D}{2} \int\int R_h(u+t_0)\, R_h(v+t_0)\, I^2(u,v-kT)\, du dv \qquad \text{(D-17)}$$

$$\langle \alpha_1 \alpha_{-1} \rangle \simeq \frac{D}{2} \int\int R_h(u+t_0)\, R_h(v+t_0)\, I(u,v-T)\, I(v,u+t)\, du dv \qquad \text{(D-18)}$$

$$\langle \alpha_k \alpha_\ell \rangle \simeq 0 \qquad \text{for } (k,\ell) \neq (1,-1) \qquad \text{(D-19)}$$

We consider next the moment $\langle \beta_k, \beta_\ell \rangle$. Following the previous steps we have:

$$\langle \beta_k, \beta_\ell \rangle = \sum_{i,j=1}^{D} \iiiint I(u_1-t_0,\, v_1-t_0-kT)\, I(u_2-t_0,\, v_2-t_0-\ell T) \cdot H_{II}(u_1,v_1,u_2,v_2)\, du_1 dv_1 du_2 dv_2 \qquad \text{(D-20)}$$

$$H_{II} = \langle \mathrm{Im}\{h_i^*(u_1)h_i(v_1)\}\ \mathrm{Im}\{h_j^*(u_2)h_j(v_2)\}\rangle$$

$$= \langle [h_{iR}(u_1)h_{iI}(v_1) - h_{iI}(u_1)h_{iR}(v_1)]$$

$$\cdot\ [h_{jR}(u_2)h_{jI}(v_2) - h_{jI}(u_2)h_{jR}(v_2)]\rangle$$

$$= 2\langle h_{iR}(u_1)h_{iI}(v_1)h_{jR}(u_2)j_{jI}(v_2)\rangle$$

$$- 2\langle h_{iI}(u_1)h_{iR}(v_1)h_{jR}(u_2)h_{jI}(v_2)\rangle$$

$$= 2 \cdot \tfrac{1}{4} R_h(u_1)\ R_h(v_1)\ \delta(u_1-u_2)\ \delta(v_1-v_2)\ \delta_{ij}$$

$$+ \quad 2 \cdot \tfrac{1}{4} R_h(u_1)\ R_h(v_1)\ \delta(u_1-v_2)\ \delta(v_1-u_2)\ \delta_{ij} \qquad \text{(D-21)}$$

Replacing Eq. (D-21) into Eq. (D-20), we obtain:

$$\langle \beta_k \beta_\ell \rangle = \tfrac{1}{2} D \int\int R_h(u+t_0)\ R_h(v+t_0) \times [I(u,v-kT)\ I(u,v-\ell T)$$

$$- I(u,v-kT)\ I(v,u-\ell T)]\ dudv \qquad \text{(D-22)}$$

Comparing the cross-moments $\langle \alpha_k \alpha_\ell \rangle$, Eq. (D-16), and $\langle \beta_k \beta_\ell \rangle$, Eq. (D-22) we see that the integral of the latter contains the 2nd minus the 3rd term of the former. Following our previous discussion we obtain therefore:

$$\langle \beta_k^2 \rangle = \text{var}(\beta_k) \simeq \frac{D}{2} \iint R_h(u+t_0)\, R_h(v+t_0)\, I^2(u,v-kT)\, du\,dv \qquad \text{(D-23)}$$

$$\langle \beta_1 \beta_{-1} \rangle \simeq -\frac{D}{2} \iint R_h(u+t_0) R_h(v+t_0) I(u,v-T) I(v,u+T)\, du\,dv \qquad \text{(D-24)}$$

$$\langle \beta_k \beta_\ell \rangle \simeq 0 \qquad \text{for } (k,\ \ell) \neq (1,\ -1)\ . \qquad \text{(D-25)}$$

Finally, the cross-moments $\langle \alpha_k\ \beta_\ell \rangle$ can be shown to be always equal to zero because their intergrand contains the moment $H_{RI}(u_1,v_1,u_2,v_2)$:

$$\begin{aligned} H_{RI} &= \langle \text{Re}\{h_i^*(u_1)\ h_i(v_1)\}\ \text{Im}\{h_j^*(u_2)\ h_j(v_2)\} \rangle \\ &= \langle [h_{iR}(u_1)\ h_{iR}(v_1) + h_{iI}(u_1)\ h_{iI}(v_1)] \\ &\quad \cdot [h_{jR}(u_2)\ h_{jI}(v_2) - h_{jI}(u_2)\ h_{jR}(v_2)] \rangle \\ &= 0 \end{aligned} \qquad \text{(D-26)}$$

because all of the moment terms are unbalanced with respect to the real and imaginary components so that Eq. (D-3) applies. Therefore:

$$\langle \alpha_k\ \beta_\ell \rangle = 0\ . \qquad \text{(D-27)}$$

If we relate the above results to the basic simplifications of Eqs. (D-17), (D-18) for the calculation of the system performance we notice that the cross covariances $\langle \alpha_1 \ \alpha_{-1} \rangle$ and $\langle \beta_1 \ \beta_{-1} \rangle$ are not taken into account. We may expect this effect to show up under large multipath spreads, i.e., $2\sigma > T$. Nevertheless a more significant improvement to our model would be to study the cross-covariance of the signal gain γ with the ISI weights and replace the distributions of the ISI weights with distributions that are conditioned on γ.

APPENDIX E

Derivation of the Reference Pulse For The AN/TRC-170

Here we find how the reference pulse of the I-output of the ACE, $\hat{q}_I(t)$, relates to the received waveform under the assumption of correct fed-back symbols. All of the signals involved refer to a particular diversity channel. Since the tapped delay line (TDL)-ACE can be obtained as a special case of the recirculating loop (RL)-ACE we examine first the later. From Figures 2A and 3 we see that during the mth observation interval $t_o + mT > t > t_o + (m+1)\,T$, $\hat{q}_I$ relates to the ACE inputs and its past values by:

$$\begin{aligned}\hat{q}_I(t) &= K\,\hat{q}_I(t-T) + a_{m-1}r^*p_R(t-T) + b_{m-1}r^*p_R(t-T)e^{-j\pi/2} \\ &= K\,\hat{q}_I(t-T) + s^*_{m-1}r^*p_R(t-T) \quad .\end{aligned} \tag{E1}$$

Applying Eq. (E1) for t-T, t-2T,... and taking into account that as $n \to \infty$ $\lim K^n = o$, since $K < 1$, we obtain:

$$\hat{q}_I(t) = \sum_{\ell=1}^{\infty} K^{\ell-1}\, s^*_{m-1}\, r^*p_R(t-\ell T) \quad . \tag{E2}$$

r^*p_R can be gotten from Eq. (4) as:

$$r^*p_R(t) = E_b^{1/2} \sum_k s_k\, q(t-kT) + N_1^{1/2}\, u(t) \quad , \tag{E3}$$

where we have approximated the f_2-interference as noise-like and have accounted for the increase in noise power by increasing the spectral density to $N_1 > N_0$. From Eqs. (E2), E3):

$$\hat{q}_I(t) = E_b^{1/2} \sum_k \sum_{\ell=1}^{\infty} K^{\ell-1} s_k s^*_{m-\ell} q(t-(k+\ell)T) + N_1^{1/2} \sum_{\ell=1}^{\infty} K^{\ell-1} s^*_{m-\ell} u(t-\ell T)$$

and by changing the index k to $j = m-(k+\ell)$ we can express the reference pulse as:

RL-ACE

$$\hat{q}_I(t) = E_b^{1/2} \sum_j B_j(m) q(t-mT+jT) + N_1^{1/2} v(t), \quad \text{(E5)}$$

$$B_j(m) = \sum_{\ell=1}^{\infty} K^{\ell-1} s_{m-\ell-j} s^*_{m-\ell}, \quad \text{(E6)}$$

$$v(t) = \sum_{\ell=1}^{\infty} K^{\ell-1} s^*_{m-\ell} u(t-\ell T), \quad \text{(E7)}$$

For the TDL-ACE the infinite sum of Eq. (E1) is limited to 24 terms and K=1 so that the resulting reference waveform is:

TDL-ACE

$$\hat{q}'_I(t) = E_b^{1/2} \sum_j B'_j q(t-mT+jT) + N_1^{1/2} v'(t), \quad \text{(E5')}$$

$$B'_j(m) = \sum_{\ell=1}^{24} s_{m-\ell-j} s^*_{m-\ell}, \quad \text{(E6')}$$

$$v'(t) = \sum_{\ell=1}^{24} s^*_{m-\ell} u(t-\ell T). \quad \text{(E7')}$$

To evaluate the improvement in the ACE output, Eq. (E5), over the input, Eq. (E3), we note that during the mth observation interval the signal pulse, which ideally should be regenerated by the ACE,

is $q(t - mT)$ and under moderate ISI conditions it is distorted mostly by the adjacent pulses $q(t-mT+T)$, $q(t-mT-T)$ and the noise. Rewritting Eqs. (E3) and (E5) to single out these effects we have:

$$r^* \rho_R(t) = E_b^{1/2} s_m q(t-mT) + E_b^{1/2} \sum_{k=\pm 1} s_{m-k} q(t-mT+kT) + N_1^{1/2} u(t) \tag{E8}$$

$$\hat{q}_I(t) = E_b^{1/2} B_o q(t-mT) + E_b^{1/2} \sum_{j=\pm 1} B_j(M) q(t-mT+jT) + N_1^{1/2} v(t) \; . \tag{E9}$$

The equation for $\hat{q}_I'$ is the primed version of Eq. (E9). We observe that regarding the noise the SNR improves from E_b/N_1 to $(E_b/N_1)\, B_o^2/2$ var (v). From Eqs. (E6), (E6') we see that B_o, B_o' are independent of the data sequence and of m:

$$\begin{aligned} B_o &= 2/1-K \\ B_o^1 &= 2 \cdot 24 \end{aligned} \tag{E10}$$

whereas the output noise variances are:

$$\begin{aligned} \text{var (v)} &= 2/1-k^2 \\ \text{var (v')} &= 2 \cdot 24 \end{aligned} \tag{E11}$$

Therefore the ACE yields an SNR gain:

$$\begin{aligned} &\text{RL-ACE} \quad : \quad \text{SNR gain} = 1+K/1-K = 12.8 \text{ dB } (K=.9) \\ &\text{TDL-ACE} \quad : \quad \text{SNR gain} = \quad 24 \quad = 13.8 \text{ dB} \end{aligned} \tag{E12}$$

so that we can neglect noise effects in the reference pulse. Regarding the ISI effects we have at the input a signal-to-interference-ratio (SIR):

$$SIR_{in} = \frac{1}{2} q^2 (t-mt) \; / \; (q^2(t-mT+T) + q^2(t-mT-T) \qquad \text{(E13)}$$

whereas at the output:

$$SIR_{out} = \frac{1}{2} B_o^2 \, q^2(t-mT) / \langle \left| B_1 q(t-mT+T) + B_{-1} q(t-mT-T) \right|^2 \rangle \qquad \text{(E14)}$$

and similarly for the TDL-ACE. Now Eqs. (E6), (E6') indicate that B_{-1}, B_{-1}' are strongly correlated with B_1^*, $(B_1')^*$ respectively:

$$B_{-1}(m) = s_m \, s_{m-1}^* + K \, B_1^*(m) \qquad \text{(E15)}$$

$$B_{-1}'(m) = s_m \, s_{m-1}^* - s_{m-25}^* \, s_{m-24} + B_1^{*\prime}(m) \; ,$$

and they have the same variance:

$$\text{var}\,(B_1) = \text{var}\,(B_{-1}) = 4/1-K^2 \qquad \text{(E16)}$$

$$\text{var}\,(B_1') = \text{var}\,(B_{-1}') = 4 \cdot 24$$

Therefore Eq. (E14) simplifies:

$$SIR_{out} = SIR_{in} \cdot B_o^2 \; / \; \text{var}\,(B_1) \; . \qquad \text{(E14')}$$

The resulting SIR gain is the same as the SNR gain:

RL-ACE : SIR gain = 1+K/1-K (E17)
TDL-ACE : SIR gain = 24 .

Unfortunately we cannot safely assume that the ISI effects on the reference pulse are always negligible as we did for the noise. The reason is that noise samples separated by a fraction of the symbol interval T are essentially uncorrelated whereas the ISI coefficients $B_{\pm 1}(m)$ are constant within each observation interval and most importantly they are strongly correlated within the memory span of the ACE. In other words if a burst of same symbols happens from $m = m_1-12$ up to $m = m_1+12$ the coefficients $B_{\pm 1}(m)$ will be significant relative to B_o for $m_1 \leq m \leq m + 24$. To take into account these situations in system performance we must:

i) find the distribution of $B_{\pm 1}(m)$ over the memory span of the ACE,

ii) for given values of $B_{\pm 1}(m)$ compute the performance on the basis of the distorted reference pulse:

$$\hat{q_I}(t) = G\left[q(t-mT) + \frac{1}{B_o} \sum_{j=\pm 1} B_j(m)\, q(t-mT+jT) \right] \quad \text{(E18)}$$

where the constant $G = E_b^{1/2} B_o$

iii) average the performance over the distribution of $B_{\pm 1}(m)$

As the analysis of Section A.2.1 indicates, this approach complicates substantially the dependence of the detection variable on the ISI terms and it is not pursued presently. Most of the time the coefficients $B_{\pm 1}(m)$ will be insignificant relative to B_o and the reference pulse will approximate well the signal pulse:

$$\hat{q}_I(t) = G\, q\,(t-mT) \qquad \text{(E19)}$$

The system performance predictions based on the simplified model of Eq. (E19) are optimistic under strong ISI conditions but there are no simple ways to determine theoretically the effects of large multipath spreads on the AN/TRC-170 modem performance.